Decentralized Cooperative Manipulation and Consensus through Object Sensing

Applied to the Aerial Towing Problem

P. van den Bos

Master of Science Thesis

TU Delft Delft University of Technology

Delft Center for Systems and Control

Decentralized Cooperative Manipulation and Consensus through Object Sensing

Applied to the Aerial Towing Problem

Master of Science Thesis

For the degree of Master of Science in Systems and Control at Delft University of Technology

P. van den Bos

March 6, 2018

Faculty of Mechanical, Maritime and Materials Engineering (3mE) · Delft University of Technology

Abstract

With the decrease in sensor and actuator costs decentralized control strategies have become increasingly attractive, aiming to use multiple simpler robots for achieving a global objective. The problem of reaching the global objective generally results in a consensus problem requiring communication amongst the agents. The cooperative manipulation problem, where a payload is manipulated using multiple robots, poses an attractive alternative: By using the payload's motion as the means of communication, the agents can reach consensus without using explicit communication. The advantage being that no additional bandwidth is required as the number of participating agents increases and all to all communication is effectively achieved.

Whereas previous works considered only the translation dynamics this thesis work considers the use of the full rigid body motion as a means of communication, such that the agents reach consensus on the desired wrench and the payload is stabilized at any desired configuration. As a possible application the towing of an payload by multiple Unmanned Aerial Vehicles (UAV) via cables is considered. This brings the additional challenge of underactuation from the perspective of each agent, since only forces can be used to control the full payload's motion.

The result is a decentralized nonlinear control law for the forces applied to a payload such that consensus is reached amongst the agents, the leader's control action is amplified and the payload is stabilized at any desired configuration. Proofs are constructed via Lyapunov arguments and the applicability of the control design to the Aerial Towing Problem (ATP) is validated in simulation.

Contents

List of Figures

List of Tables

Acknowledgements

I would like to express my sincere grattitude towards my supervisor dr.ir. Tamás Kevicky, Associate Professor , Delft Center for Systems and Control for his guidance and support during this thesis work.

Delft, University of Technology
March 6, 2018

P. van den Bos

Chapter 1

Introduction

This thesis considers the merging of three interesting problems: How to cooperatively manipulate a payload using Unmanned Aerial Vehicles (UAV), how to reach consensus amongst the agents and how to accomplish this without explicit communication. Let us start with an example burrowed from [2] which illustrates how these problems can be solved simultaneously: Consider several people moving a heavy table. The transportation task of moving the table is subject to a global objective being the desired position and orientation of the table, which is known to the owner of the table. Suppose that, excluding the owner of the table, each person is wearing a blindfold and during the transportation it is not allowed to communicate in any way. Is it still possible to reach consensus on the desired motion and cooperatively manipulate the payload? As the owner of the table initiates the motion in the desired direction the blindfolded people are able to deduce the desired motion of the payload, and support this motion. Communication is thus still possible through the payload's motion. Although this scenario might appear unconventional when helping your friend move a table, consider the food retrieval observed in ant-colonies. This process has been well studied [3] leading to the conclusion that no explicit communication is used other than sensing the motion of the payload. The image of this thesis is completed by taking it one step further: Consider the transportation of the payload using multiple UAV connected to the payload via cables. This extends the transportation problem to one in the three-dimensional space and makes the payload's motion as a means of communication that much more interesting.

1-1 Aim and Motivation

The UAV have steadily gained popularity over the years, presenting itself as a highly mobile system and is envisioned to become a part of our every day lives. Due to its small size and limited energy storage the manipulation tasks are primarily restricted by the weight of the load. To complement this, the decreasing cost of sensors and actuators fuels the interest in cooperative systems performing high level tasks, thus making the towing of a payload using multiple UAV a viable method to overcome the limitations of any single UAV.

The motivation for decentralized control in general is to create systems that are less prone to failure or where failure of a single agent is less costly. Consider the use of a single high-end robot for transporting a given load, where system failure stops the entire process and part replacement is expensive. This is in direct contrast to the use of multiple simpler robots that cooperatively perform the same task. This reasoning advocates for investigating decentralized control methods and consensus protocols in general.

Given that a task is to be carried out using multiple agents it is generally assumed that the agents can exchange the necessary information required to achieve the global objective. For cooperative manipulation tasks the agents are dynamically coupled and communication must be sufficiently fast to prevent internal loading of the payload (squeezing) and loss of stability. The use of all-to-all communication would bring the control problem back to a centralized control strategy, but as the number of agents increases this type of communication rapidly increases in time-consumption and is deemed infeasible. By using the payload itself as the means of communication, all-to-all communication can be achieved regardless of the number of participating agents.

It can be concluded that the use of the payload's motion is a fast means of communication that scales well for an increasing number of agents, allowing for a fully decentralized implementation. Application to the Aerial Towing Problem (ATP) using multiple UAV is worth investigating, and could pave the way to a small-scale experiment.

1-2 Connection with Existing Literature

Towing of a Payload Using Multiple UAV Control methods for a single UAV are well established [4], [5], where the geometric control law appears to have become the norm. Solutions to the ATP using a single UAV can be found in [6] and centralized approaches to the Cooperative Manipulation Problem (CMP) using multiple UAV has been described in [7], [8] and [9]. A decentralized approach to the cooperative ATP is shown in [10], where the solution is based on formation control and Passivity Based Control (PBC). The major difference between the approach in [10] and the subject of this thesis is that explicit communication is used in [10].

Payload motion as the means of communication during transportation On the subject of decentralized CMP the use of the transported payload as the means of communication has not gone unnoticed. This method of communication has been observed in nature while studying the food retrieval by ants towards their nest [3]. Inspired by these studies on ants in a series of papers [11], [11], [2], [12] the so called Force-Amplifying N-robot Transport System (Force-ANTS) framework is proposed. where a swarm of simple robots is used to manipulate a heavy payload's linear motion in the plane. In the Force-ANTS framework the robots use the payload's acceleration as the means of reaching consensus without using explicit communication. It is shown that the followers amplify the leaders force, allowing for control over the payload velocity. The CMP for the linear motion of a payload is also addressed in [13], as an example case of a general PBC method for distributed systems. In [13] the intend is to make the follower agents compliant to the leader's desired motion, rather than

to amplify the leaders force. The proposed solutions in [12] and [13] consider the translation dynamics in the plane only with the aim of reaching a desired velocity. No extension to control of the rotational motion is presented.

1-3 Thesis Scope and Goals

This thesis work considers a Leader-Follower (LF) type CMP where only some of the agents have access to the desired payload motion. Since the agents, that is the robots, are dynamically coupled through the payload this would require a fast type of communication. The approach given in [2] presents an elegant solution by considering the payload motion as the means of reaching consensus. Furthermore, this method allows the leaders' control effort to be amplified by the follower agents without communication. Considering the results reported in the literature, the following conclusion is drawn:

1. The results reported in the literature that use the payload as the means of communicating the desired motion only consider the linear translation dynamics. The problem of reaching consensus on the desired payload configuration, that is a rotation as well as position, is not addressed.
2. The Force-ANTS framework showed that, not only consensus can be reached, but that the leader control effort can also be amplified without communication. It was shown that this allows the leader to control the linear velocity, but the problem of amplifying the leaders' control effort to reach any desired configuration was not addressed.
3. The reported results assume acceleration or force measurements of the payload to be available. The effect of arbitrary state measurements on the consensus dynamics is not considered.

The extension of the LF based CMP to control the full rigid body motion opens a path to a much wider range of possible applications. A human operator can be considered to control the payload motion, without requiring an interface to the robots. Consider for example a mechanic that can rotate a heavy car into a position that allows for ease of access, without any effort. With the decrease in size and cost of commercially available UAV the aerial CMP could be accomplished using many smaller UAV, and furthermore, allow for a small scale experiment in the near future. It is thus proposed to investigate the aerial CMP of a payload towed by multiple UAV via cables, where consensus is reached on the desired configuration using the payload as the medium of communication.

As a simplification of the problem, the consensus laws will be designed while neglecting the robot dynamics. This results in a more analytic approach while considering a directly actuated rigid body. Subsequently, the effectiveness will be evaluated for the ATP by adding the UAV dynamics to the description. The control law for the UAV will be designed with the aim of controlling the force at the attachment point of the cable. It thus makes sense to consider the directly actuated rigid body to be actuated by forces, rather than wrenches. As the agents apply a force to control the configuration, this brings the challenge of underactuation from the perspective of each agent. With these considerations the goals for this thesis are defined as follows.

1. The presented control laws are to be designed for three requirements:
   (a) The leader control effort is to be amplified by the follower agents.
   (b) The follower agents reach consensus on the applied wrench.
   (c) The payload is to be stabilized at any desired configuration.
2. The research goals are defined for a more abstract setting: The underlying consensus dynamics when agents communicate through the motion of a rigid body is to be investigated. This can be further divided into the following objectives,
   (a) Investigate different methods of attitude representation, and the effect on the consensus dynamics.
   (b) Investigate the effect of underactuation on the consensus dynamics.
   (c) Investigate how consensus can be reached without acceleration measurements.
   (d) Proofs of stability are to be provided, and the convergence rate should be derived wherever possible.
3. The application of the consensus protocols to the ATP is to be investigated. This is further divided into the following objectives,
   (a) Investigate the possibility of using a single leader to control the payload motion.
   (b) Give a recommendation for a small scale experiment.
4. All investigative efforts are to amount to a proposed control law, which is to be validated via simulation.

1-4 Main Assumptions

To emphasize the scope of this thesis, the main simplifications are reviewed in the following.

Neglecting the Robot Dynamics The intention in this thesis work is to apply the consensus problem to the ATP. The constraint free equations of motion of the complete system shows a complicated interaction between the UAV and the payload dynamics. It is therefore chosen to present an academic research into the consensus problem by considering a directly actuated rigid body, where the robot dynamics is neglected. The effectiveness of the proposed consensus laws to the ATP is then verified via simulation, rather than analytic expressions.

Simplified Mathematical Description of the ATP When aiming for a realistic mathematical description of the ATP the increase in complexity appears to know no bounds. A variety of models can be found in the literature, where the main difference is in the modeling of the cables. Cable slackening is modeled in [14] through a switched description, whereas in [15] an elaborate constraint free description is presented where the cables are modeled as a string of bodies. Even for a single UAV the model can become arbitrarily complex, for example by considering effects of rotor flapping or drag [16]. In this thesis work the aim is merely to gap the bridge between abstract consensus problems and the application to a more practical

example. For this purpose it was deemed that a simplistic description of the ATP would suffice. The most important assumptions are given as:

1. The cables are modeled as massless rigid links,
2. The UAV are assumed to be fully actuated.

Constant Reference Signal In this thesis work it is assumed that the desired payload configuration is constant. This allows all solutions to be evaluated by considering the step response, and the performance of different solutions is easily compared.

A Model Based Approach In a futuristic setting, one could imagine attaching a few robots to a payload, instantly allowing it to be transported by any chosen operator. In such a scenario it indicates that the control laws are either independent of the payload parameters, or can adapt to it. Although very interesting, the adaptive approach is outside the scope of this text. Excluding adaptive approaches, it was found that parameter independent approaches tend to aim at stabilizing at a desired configuration, and not a desired velocity. In this thesis there is the additional requirement of amplification of the leader's wrench. This indicates that consensus must be reached before reaching the desired configuration. Exact results for convergence during motion imply that the parameters of the payload must be known. This thesis thus considers a model based approach, and assumes that the payload parameters are known to the agents.

Global Sensing Capabilities As the payload is the means of communication it can be imagined that the agent's sensing capabilities effects the underlying communication topology. The effect of local sensing brings an additional challenge, and forms the main focus in [17]. However, the consideration of local versus global sensing is only meaningful if the solutions are model independent. Disregarding the consensus problem, consider that in order to cancel the gravitational wrench acting on the payload, that the attitude and grasping matrix must be known to all agents. Thus, assuming these are available, global measurements can then be obtained from local measurements through forward kinematics. It is therefore concluded that an investigation into local measurements is only meaningful after investigating an adaptive control approach, or otherwise remove the parameter dependency. For this reason the agents are assumed to have global measurements of the payload state.

1-5 Thesis Structure

This chapter introduced the problem of cooperative manipulation while reaching consensus without communication. This led to the definition of the research goals for this thesis work, and the main assumptions where defined. The remainder of this thesis is structured as follows.

Chapter 2 considers the simplest case, with respect to the subsequent chapters. The agent dynamics is neglected, it is assumed that the agents can measure the acceleration of the payload, and a minimal attitude representation is used. Firstly, the agents are considered to

apply a wrench at the payload Center of Gravity (CoG), which is referred to as full actuation. Subsequently, the proposed solution is extended to the case where the followers apply a force at the attachment point, referred to as the underactuated case. The efficacy of the proposed control laws is shown in simulation.

Chapter 3 aims for a global system description by using the rotation matrix directly for control. Otherwise, the same assumptions hold: The agent dynamics is neglected, and acceleration measurements are assumed to be available. With the introduction of the rotation matrix, a significant increase in complexity is found, despite the simplified scenario. For this reason the chapter begins with the fully actuated case and the synchronization of the agents without a leader. Subsequently the leader is added to the problem, after which the proposed solution is extended to the underactuated case. The proposed solutions are simulated and the chapter concludes with a discussion on the results.

Chapter 4 relaxes the assumption of requiring acceleration measurements, and aims to reconstruct the desired payload configuration through an observer. Still, the robot dynamics are neglected and a minimal attitude representation is again used. The fully actuated case is considered first, after which the more complicated underactuated case is considered. The control laws are validated through simulations.

Chapter 5 introduces the robot dynamics by considering the ATP where multiple UAV are towing the payload via cables. A downside of this approach is that at least three leaders are required to control the payload motion. The chapter begins with the review of a centralized approach taken from the literature. A decentralized approximation is proposed such that the agents no longer require the full system state. Subsequently the proposed solution is extended to the case where the agents have to reach consensus on the desired configuration, i.e. the follower UAV are introduced. The solution presented in Chapter 4 is applied to the ATP and the effectiveness is shown via simulation results.

Chapter 6 considers an alternative for the leader design. The aim is to remove the requirement of three leaders, by considering a single leader attached to the payload via three extendable cables. The computation of the desired cable lengths introduces the inverse kinematics problem, for which a solution is proposed. The control law is then designed for the case where a single UAV is towing the payload. Subsequently, the follower UAV are added to the system. The follower UAV are still connected via a single cable each, and use the control law of the previous chapter. Simulation results of the proposed solutions are presented.

Chapter 7 finalizes this thesis work with conclusions and a discussion on the found results. It includes a recommendation for a small scale experiment, and recommendations for future research.

Chapter 2

Payload Acceleration Measurements as a Means of Communication: Modified Rodrigues Parameters

This chapter considers the case that all agents have access to the payload acceleration, and the agent dynamics is neglected. With the use of Modified Rodrigues Parameters (MRPs) it is shown that the agents can directly exchange information on the desired configuration. A decoupling strategy is pursued with the aim to isolate the consensus dynamics from the payload dynamics. Although this allows for a straightforward analysis of the consensus dynamics, the boundedness of the payload state can not be guaranteed. For the fully actuated case this problem is resolved by introducing a small coupling gain, resulting in global convergence to the desired equilibrium. For the underactuated case this problem was not resolved. Despite the global convergence of the estimation errors, the payload state is only proven to converge locally. Via simulations it is shown that the proposed solution can handle large angular rotations.

In the following section the MRPs are introduced. Section 2-2 considers the fully actuated case, and presents a globally stabilizing solution. In Section 2-3 the more complicated underactuated case is considered. Section 2-4 validates the proposed solution through simulation results. This chapter finalizes with a discussion and conclusion on the proposed solution in Section 2-5.

2-1 Modified Rodrigues Parameters for Attitude Control

This chapter considers the use of MRPs as a parameterization of the rotation matrix. There are in fact many representations to choose from, and it often appears that the chosen representation is simply a matter of taste. The main motivation for considering the MRPs in this thesis is that they form a minimal attitude representation allowing for an additive tracking

error. By comparison, the additive and nonlinear form of the applied torque to a rigid body are respectively given as,

$$\tau = \Xi(\sigma)^T(\sigma - \sigma_{\text{des}}), \qquad \text{and} \qquad \tau = \frac{\left(1-\|\sigma_{\text{des}}\|^2\right)\sigma - \left(1-\|\sigma\|^2\right)\sigma_{\text{des}} + 2\tilde{\sigma}\sigma_{\text{des}}}{1+\|\sigma\|^2\|\sigma_{\text{des}}\|^2 + 2\sigma_{\text{des}}^T\sigma}, \tag{2-1}$$

where σ denotes the payload MRPs, σ_{des} denotes the reference MRPs and $\Xi(\sigma)$ denotes the kinematic matrix given in (A-28). The nonlinear form should be seen as the proper use of MRPs for attitude control, as it corresponds to the MRPs that describes the rotation required to go from σ to σ_{des}. The additive form does not enjoy such an interpretation, but tends to reduce the mathematical complexity. Nevertheless, both these laws have been applied in the literature to control and consensus problems (see [18] for the additive form and, amongst many others, [19] for the nonlinear form), and the additive form is considered in this thesis work.

Any minimal attitude representation allows for an additive tracking error, thus leaving a number of parameterizations to choose from [20]. The most popular of which are the Euler angles, Classical Rodrigues Parameters (CRPs) and Modified Rodrigues Parameters (MRPs). Of these representations the MRPs have the largest reach, as they allow to describe rotations up to angles of ± 360 deg, whereas this is limited for the Euler angles to ± 90 deg about the second rotating axis, and up to ± 180 deg in any direction for the CRPs. Furthermore, the MRPs allow for a singularity free kinematic description and show a large region of approximately linear behavior.

The Singularity of Modified Rodrigues Parameters The use of MRPs for representing the payload attitude has several implications that require further clarification. The MRPs are radially unbounded and the kinematic description is singularity free. However, the mapping from the payload attitude to the corresponding MRPs shows a division by zero type singularity for angles of ± 360 deg, for which the MRPs would go to infinity. Supposing that it can be shown that all signals remain bounded, then it is still possible to speak of global convergence if the following assumption holds:

Assumption 2-1.1. *Considering the use of MRPs as the attitude representation, it is assumed that neither the initial payload attitude nor the desired payload attitude is chosen at the singular rotation $\theta = \pm 360$ deg, where θ is the angle of rotation associated with the rotation matrix.*

For the fully actuated system, discussed in the following section, it can be shown that all signals remain bounded and converge to the desired equilibrium. For the attitude to reach the singular point it would mean that the MRPs tend to infinity. This directly leads to the conclusion that the singular point is not reached [21].

From a practical point of view Assumption 2-1.1 holds little value. It is not advisable to put the reference near the singularity, e.g. 359 deg, where the MRPs are very large and known to be numerically unstable [20]. Only without control saturation- and sampling time limits would it be possible to stabilize the payload at 359 deg. A more practical assumption would be that neither the initial attitude nor the desired payload attitude is chosen

outside ± 180 deg. Since any static payload configuration can be described using an angle of $|\theta| \leq 180$ deg, this covers all initial and desired payload attitudes. Reaching the singularity would then indicate an overshoot over 180 deg. Should the attitude still reach the singular configuration, then it is argued in [21] that *any* control action results in leaving the singularity.

Finally there should be made a distinction between the payload configuration and the payload configuration space. The payload configuration refers to any static configuration whereas the configuration space refers to the nonlinear manifold on which the motion evolves. The MRPs can be used for rotations up to ± 360 deg and are thus not able to globally map the configuration space to the parameterized space. However, any *static* payload configuration can be described using an angle of $|\theta| \leq 180$ deg, and is thus well covered by the parameterized space.

To summarize the above considerations regarding the use of MRPs for converging to any static payload attitude: Theoretically, global convergence results can be obtained if all signals remain bounded and Assumption 2-1.1 holds. In practice, a well tuned control law is able to stay well away from the singularity due to the large range of the MRPs.

2-2 Jacobian Transposed Control Approach for the Fully Actuated Case

This section considers the Cooperative Manipulation Problem (CMP) of a payload that is rigidly grasped by multiple robots. It is assumed that the robot dynamics can be neglected, and that they are well approximated as a controlled wrench at the attachment point. This scenario will be referred to as the fully actuated case, indicating that the participating agents, i.e. the robots, can apply both a force and a torque to the payload. A single leader is used to control the desired payload configuration, and an arbitrary number of follower agents are to amplify the leader's control effort. It is assumed that the full state and the accelerations of the payload Center of Gravity (CoG) are available to all agents. Furthermore, it is assumed that the agents apply a wrench at the payload CoG. This last assumption is relaxed at the end of this section.

In the following a separation strategy is proposed that aims to isolate the consensus problem from the payload dynamics. It is shown that with acceleration measurements, and a minimal attitude representation, the resulting consensus dynamics is of first order with all to all communication. However, due to the nonlinearity of the payload dynamics the separation theorem for linear systems does not apply. This is resolved by introducing a small coupling between the consensus- and payload dynamics, such that global convergence to the desired equilibrium is achieved.

The remainder of this section is structured as follows. The payload dynamics assuming full actuation is introduced in Subsection 2-2-1. In Subsection 2-2-2 the agent control laws for the applied wrench is presented, which leads to a simplification of the payload dynamics. Subsequently, the objective of the CMP is defined in Subsection 2-2-3, followed by the proposed solution in Subsection 2-2-4. This section concludes with a discussion and final remarks in Subsection 2-2-5.

2-2-1 Payload Dynamics Assuming Full Actuation

The payload is modeled as a rigid body upon which the agents apply a wrench at the payload CoG. Let the state of a rigid body be represented in terms of the twist $\nu = \begin{bmatrix}\Omega^T & v^T\end{bmatrix}^T \in \mathbb{R}^6$, where Ω and v denote the angular- and linear velocity, and the configuration coordinates $q = \begin{bmatrix}\sigma^T & r^T\end{bmatrix}^T \in \mathbb{R}^6$, where $\sigma \in \mathbb{R}^3$ and $r \in \mathbb{R}^3$ denote the payload MRPs and position respectively. Let the subscript o refer to the payload, such that the payload equations of motion are given as

$$\begin{aligned} M_o\dot{\nu}_o &= -C_o(\nu_o) - G_o + \sum w \\ \dot{q}_o &= J_o(q_o)\,\nu_o \end{aligned} \tag{2-2}$$

where $M_o \in \mathbb{R}^{6\times6}$ represents the mass tensor, $C_o(\nu_o) \in \mathbb{R}^6$ the Coriolis terms, $G_o \in \mathbb{R}^6$ the (gravitational) potential terms, $J_o(q_o) \in \mathbb{R}^{6\times6}$ the payload kinematic jacobian, and $w \in \mathbb{R}^6$ denotes a wrench, such that $\sum w$ denotes the total wrench acting at the payload CoG. The explicit expressions for M_o, $C_o(\nu_o)$, G_o and $J_o(q_o)$ can be found in Appendix A-4-2.

2-2-2 Agent Control Laws and Reduced Payload Dynamics

It is assumed that a single leader and n_f-follower agents are participating in the CMP. Assuming an even distribution of the weight over all agents, let the leader wrench, denoted by w_l, be given as

$$w_l = \tfrac{1}{n_f+1}\left(C_o(\nu_o) + G_o\right) - M_o\left(\zeta_l\nu_o + K_l J_o(q_o)^T e_l\right) \tag{2-3}$$

where the subscript l refers to the leader, $\zeta_l \in \mathbb{R}^{6\times6}$ and $K_l \in \mathbb{R}^{6\times6}$ are diagonal, positive definite gain matrices, and e_l is the leader tracking error, for which the kinematics is given as

$$e_l = q_o - q_{\text{des}}, \qquad \dot{e}_l = \dot{q}_o = J_o(q_o)\,\nu_o \tag{2-4}$$

where q_{des} is the desired configuration. The above shows that the desired configuration, as known to the leader, is assumed to be constant. The follower control law shows an identical structure,

$$w_i = \tfrac{1}{n_f+1}\left(C_o(\nu_o) + G_o\right) - M_o\left(\zeta_i\nu_o + K_i J_o(q_o)^T e_i\right), \qquad i \in \{1,\dots,n_f\} \tag{2-5}$$

where the subscript i refers to the i^{th}-agent, $\zeta_i \in \mathbb{R}^{6\times6}$ and $K_i \in \mathbb{R}^{6\times6}$ are diagonal positive definite matrices, and e_i is the i^{th}-agent's estimate of the leader's tracking error e_l. For the proposed control law it must hold that $K_* J_o(q_o) = J_o(q_o) K_*$, i.e. these matrices must commute. From the definition of $J_o(q_o)$ given in (A-34) it then follows that, for the leader as well as the follower agents, the feedback gain K_* is further restricted as

$$K_* = \begin{bmatrix} k_{\sigma,*} I_{3\times3} & 0 \\ 0 & K_{r,*} \end{bmatrix} \tag{2-6}$$

where $K_{r,*} > 0$ is a diagonal 3×3 matrix and $k_{\sigma,*} > 0$ is a scalar. Substitution of the leader and follower wrenches, (2-3) and (2-5) respectively, into the dynamics (2-2) allows for

a reduction of the equations of motion,

$$\begin{aligned} \dot{\nu}_o &= -\zeta_{\text{sum}}\nu_o - J_o(q_o)^T\left(K_l e_l + K_i \sum_{i=1}^{n_f} e_i\right) \\ \dot{e}_l &= J_o(q_o)\,\nu_o \end{aligned} \tag{2-7}$$

where $\zeta_{\text{sum}} = \zeta_l + \sum_{i=1}^{n_f} \zeta_i$, i.e. the sum of all control gains, and it was used that the matrices K_* and $J_o(q_o)$ commute.

2-2-3 Mathematical Objective for the Cooperative Manipulation Problem

Note from the reduced dynamics (2-7) that if the follower estimates of the tracking error e_i converge to that of the leader e_l, that the leader control action is effectively amplified. The problem of reaching consensus amongst the agents is then already covered. What remains is for the payload to converge to the desired configuration q_{des}. The objectives can thus be summarized as:

Objectives 2-2.1. *Consider the CMP described by the reduced description* (2-7)*. The convergence of the system to the desired equilibrium follows if the*

$$\begin{aligned} &\textit{estimation error:} && \Delta e_i = e_i - e_l, \quad i \in \{1,\ldots,n_f\}, \\ &\textit{and tracking error:} && e_l = q_o - q_{des} \end{aligned} \tag{2-8}$$

converge to zero.

2-2-4 Proposed Consensus Law for the Fully Actuated Case

To meet the objectives 2-2.1 the following solution is proposed:

Proposition 2-2.1. *Consider the fully actuated CMP to be described by the reduced payload dynamics given in* (2-7)*. Let the followers update their estimate of the tracking error e_i as*

$$\dot{e}_i = (\epsilon_i + 1)\,\dot{q}_o - \Gamma_i\left(K_{sum} e_i - y\right) \tag{2-9}$$

where $K_{sum} = K_l + \sum_{i=1}^{n_f} K_i \in \mathbb{R}^6$ is the sum of the leader and follower feedback gains, $\Gamma_i \in \mathbb{R}^6$ is the i^{th}-agent's observer gain, $\epsilon \in \mathbb{R}$ is a small scalar constant, and y is the measurement given as

$$y = J_o(q_o)^{-T}\left(\dot{\nu}_o + \zeta_{sum}\nu_o\right) \tag{2-10}$$

with $\zeta_{sum} = \zeta_l + \sum_{i=1}^{n_f} \zeta_i$ is the sum of the damping gains. Then, there exist arbitrarily small constants $\epsilon_i > 0$ such that the Objectives 2-2.1 are globally achieved.

The above makes use of the inverse of the transpose of $J_o(q_o)$. From the definition of $J_o(q_o)$ (A-34) and the MRPs kinematics in (A-34) it can be seen that the inverse exists for all bounded configuration states.

Underlying Consensus Dynamics

Due to the explicit definition of the measurement y the underlying consensus law is not directly apparent from the Proposition 2-2.1. Therefore, before constructing the proof, the underlying consensus dynamics will be revealed.

From the reduced dynamics (2-7) it can be seen that the measurement y gives access to the weighted sum of the tracking errors,

$$y = K_l e_l + \sum_{i=1}^{n_f} K_i e_i. \tag{2-11}$$

Substitution of the above equation into the update law for (2-9) reveals the interaction between the agents,

$$\dot{\hat{e}}_i = (1+\epsilon_i)\,\dot{q}_o - \Gamma_i \left(K_l\left(\hat{e}_i - e_l\right) + \sum_{j=1}^{n_f} K_j\left(\hat{e}_i - \hat{e}_j\right)\right). \tag{2-12}$$

The above dynamics can be written in terms of the i^{th}-estimation error, $\Delta e_i = \hat{e}_i - e_l$, by combining the leader error kinematics (2-4) with the above equation to obtain,

$$\Delta\dot{e}_i = -\Gamma_i \left(K_l \Delta e_i + \sum_{j=1}^{n_f} K_j\left(\Delta e_i - \Delta e_j\right)\right) + \epsilon_i \dot{q}_o. \tag{2-13}$$

The equation above shows that, for $\epsilon_i = 0$, the underlying consensus dynamics is reflected in the estimation error, and shows weighted, all-to-all communication.

Proof of Convergence of the Estimation Error

The approach is to decouple the proof, according to the Objectives 2-2.1, by first showing that the estimation errors $\Delta e_i = \hat{e}_i - e_l$ of all agents converge. In the following it will be assumed that $\epsilon_i = 0$. To this end, consider the Lyapunov candidate given as

$$V_\Delta = \tfrac{1}{2} \sum_{i=1}^{n_f} \Delta e_i^T K_i \Gamma_i^{-1} \Delta e_i \tag{2-14}$$

where $K_i\Gamma_i^{-1}$ is a multiplication of two diagonal matrices, and thus symmetric. Taking the time derivative of V_Δ and substitution of the estimation error dynamics (2-13) gives

$$\dot{V}_\Delta = -\sum_{i=1}^{n_f} \Delta e_i^T K_i K_l \Delta e_i - \Delta e^T L_w^{(e)} \Delta e, \qquad \{\epsilon_i = 0\}. \tag{2-15}$$

where $\Delta e = \begin{bmatrix}\Delta e_1^T & \Delta e_2^T & \dots & \Delta e_{n_f}^T\end{bmatrix}^T \in \mathbb{R}^{6n_f}$ is the stacking of all local estimation errors as a single vector and $L_w^{(e)}$ is the weighted Laplacian matrix for the complete graph as given in Definition A-1.4 by substituting $a_i = K_i$ in the definition. From Definition A-1.4 it holds that $L_w^{(e)} \geq 0$. It follows directly that the estimation errors Δe remain bounded and globally converge to the origin for $\epsilon_i = 0$. For deriving the convergence rate, consider that $e_q^T L_w^{(e)} e_q \geq 0$, such that (2-15) can be written as,

$$\dot{V}_\Delta \quad \leq \quad -\sum_{i=1}^{n_f} \Delta e_i^T K_l K_i \Delta e_i \leq -k_{l,\min} \sum_{i=1}^{n_f} \Delta e_i^T K_i \Delta e_i \tag{2-16}$$

where $k_{l,\min}$ denotes the smallest scalar value on the diagonal of K_l. Similarly, let $\gamma_{\min}$ denote the smallest scalar value on the diagonal of all observer gain matrices Γ_i, and rewrite the above equation as,

$$\dot{V}_\Delta \quad \leq \quad -2k_{l,\min}\gamma_{\min} \sum_{i=1}^{n_f} \left(\tfrac{1}{2\gamma_{\min}} \Delta e_i^T K_i \Delta e_i \right) \leq -2k_{l,\min}\gamma_{\min} V_\Delta \tag{2-17}$$

where the last inequality was obtained using V_Δ as given in (2-14). From Lemma A-5.3 it then follows that the convergence rate towards the leader is lower bounded as $\alpha = 2k_{\min}\gamma_{e,\min}$.

Proof of Asymptotic Convergence of the Payload Tracking Error

Consider expressing the reduced payload dynamics (2-7) in terms of the estimation errors $\Delta e_i = e_i - e_l$,

$$\dot{\nu}_o \quad = \quad -\zeta_{\text{sum}}\nu_o - J_o\left(q_o\right)^T K_{\text{sum}} e_l - J_o\left(q_o\right)^T \sum_{i=1}^{n_f} K_i \Delta e_i \tag{2-18}$$

where $\zeta_{\text{sum}} = \zeta_l + \sum_{i=1}^{n_f} \zeta_i$ and $K_{\text{sum}} = K_l + \sum_{i=1}^{n_f} K_i$. The proof of convergence of the estimation error assumed $\epsilon_i = 0$, allowing for the consensus dynamics to be separated, as can be seen from (2-13). However, the separation theorem generally does not hold for nonlinear systems. Therefore, to meet the objectives 2-2.1 let $\epsilon_i = \Gamma_i \epsilon$ where $\epsilon > 0$ is taken arbitrarily small, and consider the Lyapunov candidate given as,

$$V \quad = \quad V_e + \tfrac{1}{\epsilon} V_\Delta \quad \begin{cases} V_e \quad = \quad \tfrac{1}{2}\nu_o^T \nu_o + \tfrac{1}{2} e_l^T K_{\text{sum}} e_l \\ V_\Delta \quad = \quad \tfrac{1}{2\epsilon} \sum_{i=1}^{n_f} \Delta e_i^T K_i \Gamma_i^{-1} \Delta e_i \end{cases} \tag{2-19}$$

where $\epsilon > 0$ is taken arbitrarily small and V_Δ was proposed in (2-14). Taking the time derivative and using (2-13) then gives,

$$\dot{V} \quad = \quad \dot{V}_e + \sum_{i=1}^{n_f} \Delta e_i^T K_i J_o\left(q_o\right) \nu_o - \tfrac{1}{\epsilon} \left(\sum_{i=1}^{n_f} \Delta e_i^T K_i K_l \Delta e_i + \Delta e^T L_w^{(e)} \Delta e \right). \tag{2-20}$$

where the last term was given in (2-15). The expression for $\dot{V}_e$ is obtained from (2-18), resulting in,

$$\dot{V} \quad = \quad -\nu_o^T \zeta_{\text{sum}} \nu_o - \tfrac{1}{\epsilon} \left(\sum_{i=1}^{n_f} \Delta e_i^T K_i K_l \Delta e_i + \Delta e^T L_w^{(e)} \Delta e \right) \leq 0. \tag{2-21}$$

This shows that all signals ν_o, e_l and Δe_i remain bounded. Since q_{des} is constant, and $e_l = q_o - q_{\text{des}}$ is bounded, it follows that q_o is bounded. From this it follows that also $\dot{\nu}_o$, $\dot{e}_l = \dot{q}_o = J_o(q_o)\,\nu_o$ and $\dot{e}_i$ remain bounded. It then follows that $\ddot{V}$ is bounded, and thus $\dot{V}$ is continuously differentiable and has a finite limit, which allows the use of Barbalat's Lemma A-5.2. Thus $\lim_{t\to\infty} \dot{V} = 0$, and it follows from LaSalle's invariance principle and the payload dynamics (2-18) that $\lim_{t\to\infty} e_l = 0$ since $J_o(q_o)$ is invertible. This shows that the payload globally, asymptotically converges to the desired configuration, and completes the proof.

2-2-5 Remarks and Extensions on the Proposed Solution

A few remarks on the proposed consensus law, followed by the interpretation of the coupling gain:

- The requirement was for the followers to amplify the leaders control action. From the payload dynamics (2-7) it can be seen that the leader's control action is indeed amplified if $e_i = e_l$. The idea is that the consensus dynamics is made faster then the desired payload dynamics, which can be achieved through the observer gain Γ, resulting in the amplification of the leader wrench.

- The assumption of having a single leader is non-restrictive: Multiple leaders would appear to the followers as a single wrench appearing at the payload CoG. The resulting problem has an identical structure, where the leader gain is simply changed to the sum of the leader gains.

- Note that the update law (2-9) requires knowledge on the control gains used by all other agents, since $K_{\text{sum}} = K_l + \sum_{i=1}^{n_f} K_i$. This is required to obtain a Laplacian matrix with a zero-row sum in (2-13).

Extension of a Wrench at the Payload CoG to a Wrench at the Attachment Points For the fully actuated system the case where the agents apply a wrench at the payload CoG can be directly extended to the case of grasping the payload at the attachment points. Considering the case of full actuation, the mapping between the wrench at the attachment point, and the wrench at the payload CoG is given as

$$w_i = \begin{bmatrix} I_{3\times3} & \tilde{p}_i R^T \\ 0 & I_{3\times3} \end{bmatrix} \times w_{p_i} \quad \leftrightarrow \quad \begin{bmatrix} I_{3\times3} & -\tilde{p}_i R^T \\ 0 & I_{3\times3} \end{bmatrix} \times w_i = w_{p_i} \tag{2-22}$$

where w_{p_i} is the wrench at the i^{th}attachment point, w_i is the wrench at the payload CoG, p_i is the position of the attachment point on the payload, the tilde operator is given in Definition A-2.1, and $R_o \in SO(3)$ is the payload rotation matrix. This mapping is always invertible and can thus be thought of as implicitly being applied to all results presented in this thesis work that consider full actuation at the attachment points.

The Effect of the Coupling Gain Clearly, the design was for $\epsilon = 0$, and then to separate the consensus- and payload dynamics. As the proof did not allow this, the addition of the coupling gain was introduced. The intention was to illustrate that ϵ can be made arbitrarily small, and effectively allows for a decoupling of the proof. Nevertheless, even non-negligible ϵ has a clear interpretation, and could be advocated for:

- The effect of ϵ is that it injects damping into the payload motion. It can thus be seen as a trade-off between injecting more damping and amplifying the leader control action.
- It was shown that the estimation error converges globally, and independent of the payload motion. And yet, this does not prove that the MRPs do not escape to infinity before the estimation error converges. From the simulations it was found that the MRPs are well behaved, and ϵ was set to zero. However, one simulation does not cover all possible situations. It might be that for a poorly tuned observer the gain $\epsilon > 0$ becomes critical to ensure the stability of the payload motion while the estimation error converges.

2-3 Jacobian Transposed Control Approach for the Underactuated Case

The aim of this thesis is to propose a consensus law that is applicable to the Aerial Towing Problem (ATP) using multiple Unmanned Aerial Vehicles (UAV)s. For the ATP the assumption of full actuation is not realistic, even when the UAV dynamics are neglected. It is thus desired to design the consensus law for the case that the agents can apply only forces at the attachment points, rather than a wrench. From the perspective of the agents, this gives the problem of underactuation. The proposed solution is to assume identical observer gains and use the generalized inverse of the adjoint matrices [22]. Similar as before, it is assumed that the agents have access to the payload state and accelerations.

The effect of the underactuation is that the consensus dynamics is described by a state dependent Laplacian matrix. As was done for the fully actuated case the proposed strategy is to separate the consensus- from the payload dynamics. This allows global convergence of the consensus dynamics to be derived, despite the complexity of the Laplacian matrix. However, due to the nonlinearity of the payload dynamics the separation theorem for linear systems does not apply, and stability of the payload dynamics is only locally guaranteed.

The remainder of this section is structured similar to the previous. The payload dynamics for the underactuated case is introduced in Subsection 2-3-1. In Subsection 2-3-2 the agent control laws are presented, leading to a simplification of the payload dynamics. Subsequently, the mathematical objective of the CMP is defined in Subsection 2-3-3, followed by the proposed solution in Subsection 2-3-4. This section concludes with a discussion and final remarks in Subsection 2-3-5.

2-3-1 Payload Dynamics Assuming Underactuation

Consider the case were n_f-agents are able to apply a force at the attachment point, and a single leader applies a wrench at the payload CoG. Following the notation given in Subsection

2-2-1, let the payload equations of motion be given as

$$\begin{aligned} M_o\dot{\nu}_o &= -C_o(\nu_o) - G_o + w_l + \sum_{i=1}^{n_f} J_{p_i}(q_o)^T F_{p_i} \\ \dot{q}_o &= J_o(q_o)\,\nu_o \end{aligned} \tag{2-23}$$

where $w_l \in \mathbb{R}^6$ denotes the leader wrench at the payload CoG, $F_{p_i} \in \mathbb{R}^3$ denotes the i^{th}-agent's force applied at the attachment point on the payload, and $J_{p_i}(q_o)^T \in \mathbb{R}^{6\times 3}$ denotes the jacobian transposed of the velocity at the attachment point,

$$J_{p_i}(q_o)^T = \begin{bmatrix} \tilde{p}_i R_o^T \\ I_{3\times 3} \end{bmatrix} \tag{2-24}$$

where p_i represents the position of the i^{th}-attachment point given in the body fixed frame, $R_o \in SO(3)$ is the rotation matrix (A-26) and the tilde operator is given in Definition A-2.1.

2-3-2 Agent Control Laws and Reduced Payload Dynamics

As it is assumed that the leader still applies a wrench at the CoG, the leader control law is taken the same as for the fully actuated case (2-3), with the error kinematics given by (2-3) and the gain matrices $K_* > 0$, $\zeta_* > 0$ are assumed to be diagonal matrices, with K_* having the structure given in (2-6).

The proposed method for dealing with the underactuation is to use the generalized inverse of the collection of $J_{p_i}(R_o)^T$ matrices (2-24), given as

$$J_{p_i}(R_o)^\dagger = J_{p_i}(R_o) \times \left(\sum_{i=1}^{n_f} J_{p_i}(R_o)^T J_{p_i}(R_o) \right)^{-1} \tag{2-25}$$

where $J_{p_i}(R_o)^\dagger$ denotes the generalized inverse. The agents compute the applied force at the attachment point F_{p_i} as,

$$\begin{aligned} F_{p_i} &= n_f J_{p_i}(R_o)^\dagger w_i \\ &= n_f J_{p_i}(R_o)^\dagger \left(\tfrac{1}{n_f+1} \left(C_o(\nu_o) + G_o \right) - M_o \left(\zeta \nu_o + K J_o(q_o)^T e_i \right) \right) \end{aligned} \tag{2-26}$$

where w_i is computed according to (2-5), and n_f is the number of follower agents. The agents are assumed to use identical feedback gains $\zeta_i = \zeta$ and $K_i = K$, but this assumption is relaxed in Subsection 2-3-5.

Substitution of the leader and follower control laws, (2-3) and (2-26) respectively, into the payload dynamics (2-23), simplifies the payload dynamics as,

$$\begin{aligned} \dot{\nu}_o &= -\zeta_{\text{sum}} \nu_o - K_l J_o(q_o)^T e_l - \sum_{i=1}^{n_f} W_i(q_o)\, K J_o(q_o)^T e_i \\ \dot{e}_l &= J_o(q_o)\,\nu_o \end{aligned} \tag{2-27}$$

where

$$W_i(q_o) = n_f M^{-1} J_{p_i}(q_o)^T J_{p_i}(q_o)^\dagger M. \tag{2-28}$$

Note from the definition of the generalized inverse (2-25) that if $w_i = w_j$ for all i, j that the generalized inverse drops from the problem completely, since $\sum_{i=1}^{n_f} W_i(q_o) = n_f I$. This property is further emphasized by the control objectives stated in the following.

2-3-3 Mathematical Objective for the Cooperative Manipulation Problem

As a means to eliminate the problem of underactuation, consider the following decoupling of the objectives:

Objectives 2-3.1. *Considering the CMP and the system dynamics given in* (2-27)*. The convergence of the system to the desired equilibrium follows if the*

$$\begin{aligned} &\textit{disagreement:} && \delta e_i, = e_i - \tfrac{1}{n_f} \sum_{j=1}^{n_f} e_j, \\ &\textit{mean estimation error:} && \Delta\bar{e} = \tfrac{1}{n_f} \sum_{i=1}^{n_f} (e_i) - e_l, \\ &\textit{and tracking error:} && e_l = q_o - q_{des} \end{aligned} \tag{2-29}$$

all converge to the origin.

Before proceeding with the proposed control law and the proof, consider that the local estimation error $\Delta e_i = e_i - e_l$ can be expressed in terms of the disagreement and mean estimation error as $\Delta e_i = \delta e_i + \Delta\bar{e}$. Furthermore, the disagreement variable can be related to the Laplacian matrix for the complete graph as,

$$\delta e = \tfrac{1}{n_f} (L \otimes I_{6\times 6}) e \tag{2-30}$$

where L is given in Definition A-1.3, and δe denotes the stacking of the local variables into a vector, $\delta e = \begin{bmatrix} \delta e_1^T & \delta e_2^T & \dots & \delta e_{n_f}^T \end{bmatrix}^T$ and similarly for e.

2-3-4 Proposed Consensus Law for the Underactuated Case

Except for the use of the generalized inverse, the control law for the underactuated case is similar to the fully actuated case, but instead the control gains are identical for all agents:

Proposition 2-3.1. *Consider the underactuated CMP as described by the reduced payload dynamics given in* (2-27)*. Let the followers update their local estimate of the tracking error* e_i *as*

$$\dot{e}_i = J_o(q_o)\nu_o - \Gamma(K_{sum}e_i - y) \tag{2-31}$$

where $K_{sum} = K_l + n_f K$ *is the sum of the leader and follower feedback gains,* Γ *is the agent observer gain, and* y *is the measurement given as*

$$y = -J_o(q_o)^{-T}(\dot{\nu}_o + \zeta_{sum}\nu_o) \tag{2-32}$$

with $\zeta_{sum} = \zeta_l + n_f\zeta$*. Then, considering the Objectives 2-3.1, the disagreement and estimation error dynamics converge globally to the origin, while the payload tracking error is shown to locally converge to the desired equilibrium.*

Underlying Consensus Dynamics

The underlying consensus dynamics can be obtained by substitution of the measurement y into the proposed update law. From the reduced equations of motion (2-27) it can be seen that y in Proposition 2-3.1 is given as

$$y = K_l e_l + \sum_{i=1}^{n_f} J_o(q_o)^{-T} W_i(q_o) J_o(q_o)^T K e_i. \tag{2-33}$$

Consider the estimation error $\Delta e_i = e_i - e_l$, such that substitution of the expression above into (2-31) gives,

$$\Delta\dot{e}_i = -\Gamma K_l \Delta e_i - \Gamma \sum_{j=1}^{n_f} \underbrace{J_o(q_o)^{-T} W_j(q_o) J_o(q_o)^T}_{\text{state dependent weights}} K(\Delta e_i - \Delta e_j) \tag{2-34}$$

where it was used that $\sum_{i=1}^{n_f} W_i(q_o) = n_f I$. This shows that the estimation errors are still coupled as in (2-13), but now through state dependent weighting matrices. This would result in a non-symmetric, state dependent, weighted Laplacian matrix. Furthermore, the weights are rank deficient- and non-symmetric matrices. This motivates the use of the decoupled objectives and an identical observer gain Γ.

Proof of Global Convergence of the Disagreement Dynamics

The disagreement dynamics of the follower agents can be obtained from the local update law (2-31), consider stacking all the update laws into a single vector,

$$\dot{e} = -n_f \Gamma K e + \mathbf{1}_{n_f} \otimes (\dot{q}_o + \Gamma y) \tag{2-35}$$

where $e = \begin{bmatrix} e_1^T & e_2^T & \dots & e_{n_f}^T \end{bmatrix}^T \in \mathbb{R}^{6n_f}$, and $\epsilon_i(q_o) = 0$. Left multiplication with the Laplacian matrix L gives the disagreement vector,

$$\delta\dot{e} = (L \otimes I_{6\times 6})\dot{e} = -n_f (L \otimes (\Gamma K)) e = -n_f \left(I_{n_f \times n_f} \otimes (\Gamma K)\right) \delta e. \tag{2-36}$$

Note that the measurements y and the payload velocity $\dot{q}_o$ have dropped, since $\mathbf{1}_{n_f} \in \mathbf{null}\{L\}$ for the complete graph. From the above equation it can be seen that the disagreement dynamics of all the agents is decoupled, since $I_{n_f \times n_f} \otimes (\Gamma K_q)$ is block diagonal. The disagreement dynamics is then finally obtained as,

$$\delta \dot{e}_i = -n_f \Gamma K \delta e_i \tag{2-37}$$

From the above it can be seen that the disagreement globally converges to the origin, independent of the payload motion. The convergence rate towards the agreement set is bounded as $\alpha \geq n_f \gamma_{\min} k_{\min}$ where $\gamma_{\min}, k_{\min}$ are the minimum scalar entries of the diagonal matrices Γ and K respectively.

Proof of Global Convergence of the Mean Estimation Error Dynamics

Following the decoupling of the Objectives 2-3.1, let the estimation error dynamics (2-34) be written in terms of the mean estimation error and the disagreement vector as,

$$\Delta \dot{\bar{e}} = -\Gamma K_l \Delta \bar{e} - \Gamma \sum_{j=1}^{n_f} J_o(q_o)^{-T} W_j(q_o) J_o(q_o)^T K (\delta e_i - \delta e_j). \tag{2-38}$$

Consider the Lyapunov candidate given as,

$$V_\Delta = \tfrac{1}{2} \Delta \bar{e}^T \Delta \bar{e}. \tag{2-39}$$

Taking the time derivative of the expression above gives,

$$\dot{V}_\Delta = -\Delta \bar{e}^T \Gamma K_l \Delta \bar{e} + \Delta \bar{e}^T \Lambda_a(q_o) \delta e \tag{2-40}$$

with

$$\Lambda_a(q_o) = -\Gamma J_o(q_o)^{-T} \left[\times \left(W_1(q_o) J_o(q_o)^T K \right) \quad \dots \left(W_{n_f}(q_o) J_o(q_o)^T K \right) \right] \tag{2-41}$$

From the proof of the disagreement dynamics it was concluded that δe is bounded and converges to zero. The matrix $\Lambda_a(q_o)$ is in fact bounded for any q_o. This can be seen from the definition of $J_o(q_o)$ in (A-34) and the MRPs and the kinematics in (B-29). Even though $J_o(q_o)$ can become very large, the inverse will then decrease just as fast, due to the division by $\left(1 + \left(\sigma_o^T \sigma_o\right)\right)^2$ seen in (B-29). Furthermore the matrices $W_i(q_o)$ are bounded, as they only depend on the rotation matrix, which is bounded. Since $\Lambda_a(q_o)$ is bounded, and δe exponentially decreases, this shows that $\dot{V}_\Delta$ has a finite limit. Furthermore $\ddot{V}_\Delta$ is bounded, since $\Delta \dot{\bar{e}}$ is bounded as can be seen from (2-38). Barbalat's Lemma A-5.2 can thus be applied to conclude that $\lim_{t \to \infty} \dot{V}_\Delta = 0$. LaSalle's invariance theorem is then applicable to conclude that $\lim_{t \to \infty} \Delta \bar{e} = 0$ from (2-38). The conclusion is that the estimation error dynamics, as given in the Objectives 2-3.1, globally converges.

Proof of Local Convergence of the Payload Tracking Error

The payload dynamics (2-27) written in terms of δe and $\Delta \bar{e}$ results in

$$\dot{\nu}_o = -\zeta_{\text{sum}} \nu_o - K_{\text{sum}} J_o(q_o)^T e_l + \Lambda_b(q_o) \Delta \bar{e} + \Lambda_c(q_o) \delta e \tag{2-42}$$

where the expressions for $\Lambda_b \in \mathbb{R}^{6\times 6}$ and $\Lambda_c \in \mathbb{R}^{6\times 6n_f}$ are given as

$$\begin{aligned} \Lambda_b(q_o) &= J_o(q_o)^T \sum_{i=1}^{n_f} K_i \\ \Lambda_c(q_o) &= \begin{bmatrix} W_1(q_o) K J_o(q_o)^T & \dots & W_{n_f}(q_o) K J_o(q_o)^T \end{bmatrix} \end{aligned} \tag{2-43}$$

Linearizing the payload dynamics (2-42) about the desired equilibrium state gives,

$$\begin{bmatrix} \dot{\nu}_o \\ \dot{e}_l \end{bmatrix} \approx \begin{bmatrix} -\zeta_{\text{sum}} & -K_{\text{sum}} J_o(q_{\text{des}})^T \\ J_o(q_{\text{des}}) & 0 \end{bmatrix} \begin{bmatrix} \nu_o \\ e_l \end{bmatrix} - \begin{bmatrix} \Lambda_b(q_{\text{des}}) & \Lambda_c(q_{\text{des}}) \\ 0 & 0 \end{bmatrix} \begin{bmatrix} \Delta e \\ \delta e \end{bmatrix} \tag{2-44}$$

where the equilibrium state was taken as q_{des} for the payload configuration and as the origin for ν_o, $\Delta\bar{e}$ and δe_i. For the linearized system the separation theorem can be used. Since it was shown that $\lim_{t\to\infty} \Delta\bar{e} = 0$ and $\lim_{t\to\infty} \delta e_i = 0$, the separation theorem for linear systems allows the stability of (2-44) to be assessed considering that $\Delta\bar{e} = 0$ and $\delta e_i = 0$. Local asymptotic stability follows from the Lyapunov candidate given as

$$V_o = \tfrac{1}{2}\nu_o^T \nu_o + \tfrac{1}{2} e_l^T K_{\text{sum}} e_l, \quad \rightarrow \quad \dot{V}_o = -\nu_o^T \zeta_{\text{sum}} \nu_o, \tag{2-45}$$

which shows that $\lim_{t\to\infty} \nu_o = 0$. It then follows from LaSalle's invariance principle and (2-44) that $\lim_{t\to\infty} e_l = 0$, since $J_o(q_o)$ is invertible, completing the proof.

2-3-5 Remarks and Extensions

the following contains some final remarks on the the proposed solution to the underactuated CMP:

Distribution of the Control Effort over the Agents using The Weighted Generalized Inverse The use of identical control gains $K_i = K$ can be relaxed by using a weighted generalized inverse,

$$J_{p_i}(q_o)^{\dagger} = A_i J_{p_i}(q_o) \times \left(\sum_{j=1}^{n_f} J_{p_j}(q_o)^T A_j J_{p_j}(q_o) \right)^{-1} \tag{2-46}$$

where A_i is a weighting matrix that can be used to distribute the control effort amongst the agents. The above weighted generalized inverse can be used for the control action of the agents (2-26) and Proposition 2-3.1 remains unchanged. The assumption on identical observer gains is however restrictive for the chosen approach.

The leader as a wrench at the CoG The leader is still represented as a wrench at the payload CoG, denoted by w_l, rather than a force. As the final objective is to apply the control laws to the aerial towing problem this might seem like an odd choice. However, from the perspective of the follower agents the leader always appears as a wrench acting at the payload CoG. Thus, if the leader can only use a force, this means that multiple leaders will be needed to control the wrench at the CoG. But for the consensus problem there is no difference.

Motivation for Assuming Identical Observer Gains The use of identical observer gains allowed the generalized inverse to be eliminated from the problem. In effect, it is avoided to consider the Laplacian matrix associated with the consensus dynamics given in (2-34). This shows that the elements of the adjacency matrix would be constructed from,

$$J_o\left(q_o\right)^{-T} W_j\left(q_o\right) J_o\left(q_o\right)^T = n_f J_o\left(q_o\right)^{-T} M^{-1} J_{p_i}\left(q_o\right)^T J_{p_i}\left(q_o\right)^{\dagger} M J_o\left(q_o\right)^T \tag{2-47}$$

which is a challenging task. Note that the problem is, primarily, that the above matrices can not be used directly for a Laplacian matrix, because it would result in a non-symmetric matrix. Furthermore, these matrices would not be used in a Lyapunov candidate, as these give rise to complicated time derivatives.

Challenge with Kinematics and Matrix Weights A reduction of the problem is achieved by assuming that the attachment points of the agents are placed symmetrically on the payload, as was proposed in [11]. This allows the generalized inverse to become state independent. However, as can be seen from (2-47), the jacobian matrices are still not able to cancel, as these generally do not commute with arbitrary matrices.

2-4 Simulation Results Assuming Acceleration Measurements and MRPs

This section presents the simulation results for the underactuated case, i.e. Proposition 2-3.1 where a single leader controls a wrench at the payload CoG and $n_f = 10$ agents control the force at their corresponding attachment point. The purpose of the simulation is to show that the objectives 2-3.1 are achieved, even for large angles of rotation. The simulation setting is very similar for all chapters, and a short description can be found in Appendix C. The observer gain for the reconstruction of the desired position was taken as $\Gamma_r = 6.32 \times I_{3\times 3}$, and for the desired attitude as $\Gamma_\sigma = 0.40$.

The simulation results for the underactuated case, i.e. Proposition 2-3.1, are shown in Figure 2-1 and Figure 2-2 for the attitude and translation dynamics respectively.

Payload Tracking Error Dynamics From Figure 2-1a and Figure 2-2a it can be seen that the payload velocities converge to zero, and that the payload configuration depicted Figure 2-1b and Figure 2-2b converges to the reference. The colored dashed lines shown in Figure 2-1b and Figure 2-2b correspond to the case were the leader controls the payload without any followers, and is used as a benchmark for evaluating the performance. It can be seen that the addition of the followers results in a delay in the step response. This delay is expected, since the follower agents need time to estimate the desired payload attitude.

Amplification of the Leader Control Effort The leader control effort is shown in Figure 2-1c and Figure 2-2c, and Figure 2-1d and Figure 2-2d show the leader tracking error. The colored dashed lines correspond to the benchmark. It can be seen that the leader control effort is indeed lowered by a factor of approximately the total number of agents, in this case $1 + n_f = 11$. The leader control effort is thus amplified, without a significant reduction in performance.

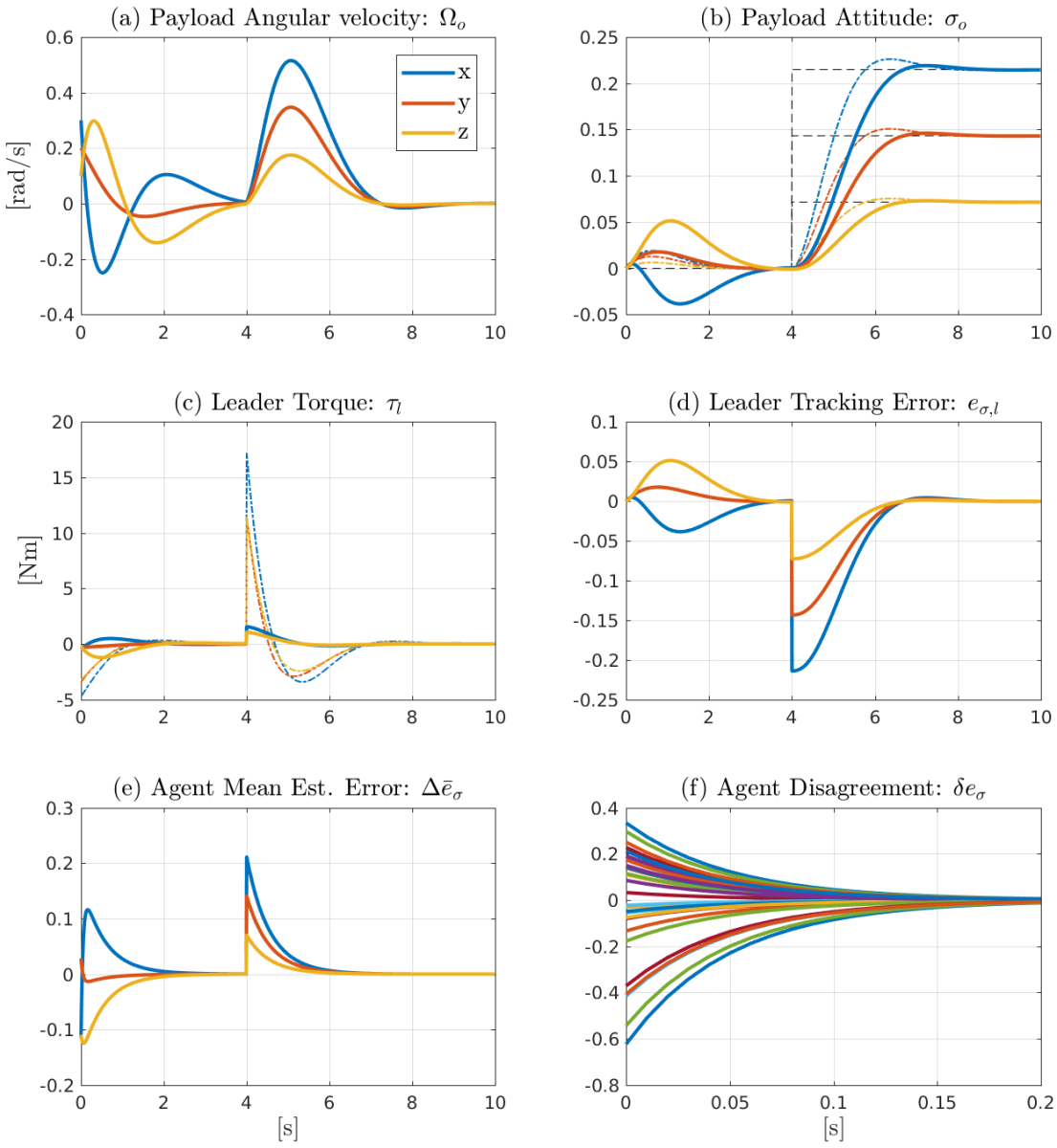

Figure 2-1: Simulation results of the attitude dynamics for the underactuated CMP (Proposition 2-3.1): From left to right and top to bottom the plots show, (a) the payload angular velocity, (b) the payload MRPs, (c) the torque applied by the leader, (d) the leader tracking error, (e) the mean of the agent's estimation errors, and (f) the disagreement of the agent's estimation errors. The three colors, blue red and yellow, represent the x, y and z directions of the corresponding three dimensional vectors. The black dashed line in the attitude plot shows the leader reference MRPs. It can be seen that the leader applies a reference step to the desired payload attitude at $t = 4$[s], corresponding to a $\theta = 60\,\text{deg}$ rotation about the $\epsilon = [3 \quad 2 \quad 1]^T$ axis. The colored dashed lines in the payload attitude and leader torque plot show the simulation result for the case that the leader is controlling the payload alone.

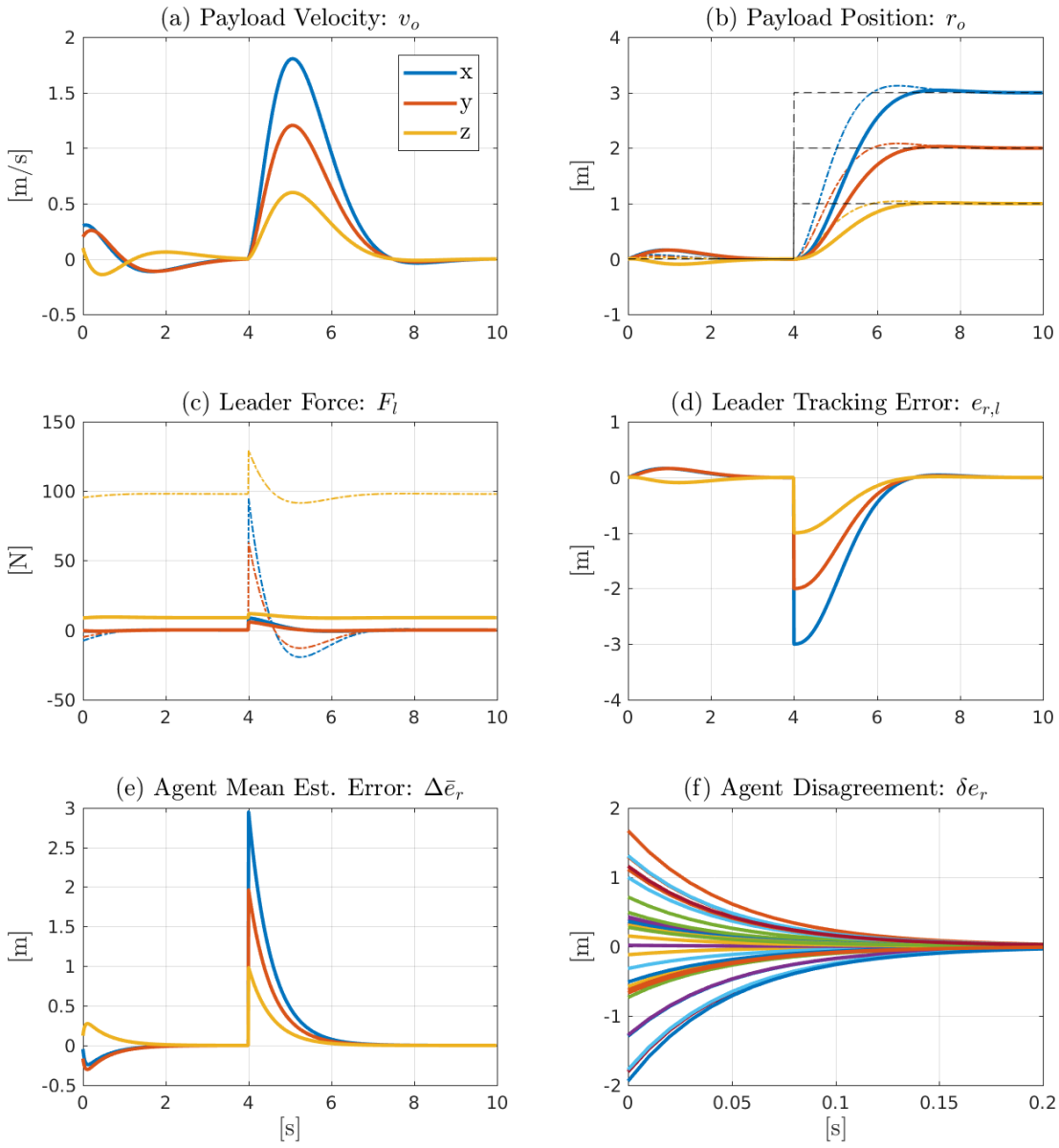

Figure 2-2: Simulation results of the translation dynamics for the underactuated CMP (Proposition 2-3.1): From left to right and top to bottom the plots show, (a) the payload linear velocity, (b) the payload position, (c) the force applied by the leader, (d) the leader tracking error, (e) the mean of the agent's estimation errors, and (f) the disagreement of the agent's estimation errors. The three colors, blue red and yellow, represent the x, y and z directions of the corresponding three dimensional vectors. The black dashed line in the position plot shows the leader's desired position, changing from the origin to $r_{\text{des}} = [3 \quad 2 \quad 1]^T$ at $t = 4$[s]. The colored dashed lines in the position and force plot show the simulation result for the case that the leader is controlling the payload alone.

Consensus Dynamics of the Estimation Errors The mean estimation errors are shown in Figure 2-1e and Figure 2-2e. From these it can be concluded that the delay in the step response of the payload attitude is indeed caused by the estimation dynamics. The disagreement dynamics can be seen to converge much faster to the origin, as was derived in Subsection 2-3-4, having little effect on the performance. Note that the agents are initialized with a very large estimation error ranging $\pm 180\,\text{deg}$, and that the leader step response corresponds to a large rotation of $60\,\text{deg}$. These results clearly show that the control and consensus law in Proposition 2-3.1 allows for large angular rotations, despite the proof of local convergence.

2-5 Conclusion

In this chapter the CMP of the payload was addressed for both the fully actuated and underactuated case. It was assumed that the agents have access to the payload accelerations and full state. The dynamics of the agents were neglected, resulting in a directly actuated rigid body. For the fully actuated case a consensus law was proposed that allowed for individual control and observer gains. It was shown that global convergence of the consensus dynamics can be achieved by separating the consensus dynamics from the payload dynamics, resulting in weighted all to all communication. However, it could not be shown that the payload state remains bounded in the time that the estimation errors converge. By introducing a small coupling gain global convergence of both the consensus and payload dynamics was achieved. For the underactuated case it was proposed to use the generalized inverse of the adjoint matrices to compute the desired force at the agent attachment points. It was shown that the consensus dynamics between the agents was governed by a state dependent weighted Laplacian matrix. By assuming identical observer gains for all follower agents the consensus dynamics could be separated from the payload motion. Although global convergence of the estimation errors was derived, the stability of the payload motion could only be guaranteed locally.
Simulation results of the proposed solutions showed that the control and consensus laws allow for large reference step commands and is able to recover from large initial estimation errors. It was verified that the leader control effort is indeed amplified and that consensus on the desired payload configuration is reached.

Chapter 3

Payload Acceleration Measurements as a Means of Communication: Geometric Control

The field of Geometric control concerns itself with globally defined control laws for systems that evolve on a nonlinear manifold which can not be globally defined using the Euclidean space [23]. This is of special interest for controlling mechanical systems as the rotational motion of a body evolves on $SO(3)$ rather than $\mathbb{R}^n$ [24]. When speaking of geometric control this indicates the mathematical characterization of a configuration and motion using group theory and differential geometry. In practice however, geometric attitude control indicates that the control law is defined using the rotation matrix, rather than a parameterization thereof. Since the rotation matrix is globally defined, this will also hold for the control law, allowing for a global system analysis. When using a parameterization of the rotation matrix, e.g. Euler angles, quaternions, Classical Rodrigues Parameters (CRPs) or Modified Rodrigues Parameters (MRPs), the configuration space can not globally, or unambiguously, be defined. Considering the aim of this thesis, geometric control will simply refer to the control law using the rotation matrix directly for control, rather than the mathematical framework upon which it is build.

This chapter explores the use of geometric control, and considering the discussion above, one would expect that global convergence will be shown. Unfortunately this was not achieved. The presented consensus laws will be shown to be globally stable, but the proof of convergence depends on a region of attraction. Through simulations it is illustrated that there is a strong incentive that the proposed solutions result in global convergence to the desired equilibrium. Despite the dependence on the convergence region, the proposed consensus laws are still considered as interesting results, if only to motivate further research in this direction. Regarding the previous chapter the same assumptions hold: The agent dynamics are neglected, and acceleration measurements are assumed to be available. In addition it is assumed that the observer gains of the agents are identical.

The following section gives a short review on geometric control applied to consensus problems as a comparison to the proposed solutions in this chapter. Section 3-2 considers the fully actuated case and the synchronization of the agents without a leader. Subsequently, in Section 3-3, the leader is added to the problem. The dependency on the found convergence region is discussed in Section 3-5. In Section 3-4 the proposed solution is extended to the underactuated case. Section 3-6 presents simulation results, and the chapter concludes with a discussion in Section 3-7.

3-1 Comparison with the Literature on Geometric Cooperative Control

Nonlinear attitude control and consensus problems have been brought together in the literature resulting in what can be described as the attitude synchronization of rigid bodies. The focus of these results is partly on the properties of the chosen communication topology, which is of lesser interest for this thesis work. Using the payload as the means of communication tends to remove most communication problems. Furthermore, the problem of synchronizing multiple rigid bodies is, in several ways, different from the subject considered in this thesis. Firstly, the reviewed results considered the control of multiple bodies which are only virtually coupled. Secondly, in the approaches on attitude consensus there is not the element of amplification of the leader control action, simply because it does not apply. Nevertheless, it will be shown that the consensus problem and the proposed solutions have a strong similarity to the proposed consensus laws in this chapter. Disregarding advances in describing the communication topology allows many of the consensus laws used for attitude control to be captured by two structures, as discussed in the following.

Coupling the Kinematics of Multiple Agents Through the Dynamics The most general approach to the attitude synchronization of multiple rigid bodies is to let the motion of the rigid bodies themselves take part in the consensus dynamics. In a nutshell: The i^{th}-agent receives the attitudes of his neighbors, and uses the relative attitude error directly as a torque to control his own attitude. Although different parameterizations are assumed in the literature (such as MRPs in [19] and [25], or quaternions in [26], [27], [28] and [29]) these control laws can equivalently be represented using rotation matrices. Considering the attitude dynamics given in Appendix A-4-1, let the i^{th}-agent torque be taken such that the attitude dynamics of the i^{th}-agent is given as,

$$\begin{aligned} \mathcal{I}_i\dot{\Omega}_i &= -\tilde{\Omega}_i\mathcal{I}_i\Omega_i - \zeta_i\Omega_i - \sum_{i=1}^{n_{\text{tot}}} a_{ij}\mathbb{P}_a\left\{R_i^TR_j\right\}^V \\ \dot{R}_i &= R_i\tilde{\Omega}_i \end{aligned} \tag{3-1}$$

where a_{ij} are the elements of the adjacency matrix for a symmetric graph Laplacian, $\zeta_i > 0$ are the damping matrices, and the index i references the i^{th}-agent. This illustrates that the motion is coupled to the attitude of the other agents through the information on the relative attitudes $R_i^TR_j \in SO(3)$. Synchronization is then directly proven by considering the

Lyapunov candidate given as,

$$V = \frac{k_R}{2}\text{tr}\left\{[R_i]_{\text{vec}}^T (L \otimes I_{3\times 3}) [R_i]_{\text{vec}}\right\} + \sum_{i=1}^{n_{\text{tot}}} \frac{1}{2}\Omega_i^T \mathcal{I}_i \Omega_i, \quad \rightarrow \quad \dot{V} = -\sum_{i=1}^{n_{\text{tot}}} \zeta_{\text{sum}} \Omega_i^T \mathcal{I}_i \Omega_i \tag{3-2}$$

where L is the symmetric Laplacian matrix associated with the chosen communication topology. and proof of convergence follows from LaSalles's invariance principle. It must be noted that the purpose of the consensus law given in (3-1) is to reach consensus on the attitude R_i, but this is done indirectly through the angular acceleration $\dot{\Omega}_i$.

Coupling the Kinematics of Multiple Agents Directly The coupling of the attitude kinematics directly is considered in [30], [31], [32], [33], [34]. By assuming that the angular velocity is directly controlled a purely kinematic consensus law results. The consensus law proposed in [31] is taken as,

$$\dot{R}_i = R_i \sum_{i=1}^{n_{\text{tot}}} a_{ij} \mathbb{P}_a \left\{R_i^T R_j\right\} \tag{3-3}$$

where a_{ij} are the elements of the adjacency matrix for a symmetric graph Laplacian, $\mathbb{P}_a\{\cdot\}$ is the a-symmetric operator given in Definition A-2.2 and $R_i \in SO(3)$ is the i^{th}-agent's rotation matrix. The proof of convergence is derived from the simple Lyapunov candidate,

$$V = \sum_{i=1}^{n_{\text{tot}}} \frac{1}{2}\text{tr}\{I - R_i\} \tag{3-4}$$

from which can be derived that the agents converge to the agreement set if initially all rotation matrices are positive definite $R_i > 0$. This is equivalent to the existence a reference frame such that all the agent's orientations are within an angular displacement of $\theta = \pm\frac{1}{2}\pi$ of said reference frame. The convergence region is thus not global, but it can be shown to be invariant.

Comparison of the Literature with the Cooperative Manipulation Problem (CMP) The main difference with the approaches considered in the literature is that the agents are not allowed to communicate in this thesis work. As a result of this restriction the i^{th}-agent does not have access to the rotation matrix of the j^{th}-agent, and is thus unable to compute the relative attitude error $R_i^T R_j \in SO(3)$ as is the case in (3-3) and (3-1).

3-2 Follower Synchronization Assuming Full Actuation

Although the leader driven geometric control approach discussed in this chapter is incomplete, since global converge could not be shown, it is still deemed to be an interesting approach. To motivate further research in this direction it is shown that the autonomous system, that is without a leader, is globally asymptotically converging. It is assumed that multiple robots rigidly grasp the payload, which is referred to as the fully actuated case. Similar to the previous chapter, it is assumed that the full state and the accelerations of the payload Center of Gravity (CoG) are available to all agents, and the robot dynamics are neglected.

The remainder of this section is structured as follows. The payload dynamics is introduced

in Subsection 3-2-1. In Subsection 3-2-2 the follower control laws for the applied wrench is presented, allowing the payload dynamics to be simplified. The objective of the consensus law is defined subsequently in Subsection 3-2-3 followed by the proposed solution in Subsection 3-2-4.

3-2-1 Globally Defined Payload Dynamics

Let the state of a rigid body be represented in terms of the angular velocity $\Omega \in \mathbb{R}^3$, the linear velocity $v \in \mathbb{R}^3$, the attitude $R \in SO(3)$ and the position $r \in \mathbb{R}^3$. The payload equations of motion are then given by the payload dynamics,

$$\begin{aligned} \mathcal{I}_o \dot{\Omega}_o &= -\tilde{\Omega}_o \mathcal{I}_o \Omega_o + \sum \tau \\ m_o \dot{v}_o &= m_o g \bar{b}_3 + \sum F, \end{aligned} \tag{3-5}$$

and the payload kinematics

$$\begin{aligned} \dot{R}_o &= R_o \tilde{\Omega}_o \\ \dot{r}_o &= v_o, \end{aligned} \tag{3-6}$$

where m and $\mathcal{I}$ represent the mass and inertia respectively, $\sum F$ and $\sum \tau$ respectively represent the sum of the forces and torques acting on the payload CoG, g denotes the constant gravitational acceleration, $\bar{b}_3 = \begin{bmatrix} 0 & 0 & 1 \end{bmatrix}^T$ denotes the third basis vector, the tilde operator $\{\tilde{\cdot}\}$ is given in (A-10), and finally the subscript o denotes the reference to the payload.

3-2-2 Agent Control Laws and Reduced Payload Dynamics

As discussed in section 2-2-5, for the fully actuated case the problem can be simplified by assuming that the agents apply a wrench at the payload CoG, without loss of generality. The control structure of the agents is taken as a typical geometric control law,

$$\begin{aligned} \tau_i &= -\mathcal{I}_o \left(\zeta_i \Omega_o + k_i \mathbb{P}_a \left\{ R_{\text{des},i}^T R_i \right\}^V \right) + \tfrac{1}{n_f} \tilde{\Omega}_o \mathcal{I}_o \Omega_o \\ F_i &= -m_o \left(\beta_i v_o + K_i \left(r_i - r_{\text{des},i} \right) \right) - \tfrac{1}{n_f} m_o g \bar{b}_3 \end{aligned} \tag{3-7}$$

where the payload dynamics is canceled, and the matrices $\zeta_i \in \mathbb{R}^{3\times3}$, $\beta_i \in \mathbb{R}^{3\times3}$ and $K_i \in \mathbb{R}^{3\times3}$ are positive definite, diagonal matrices, $k_i \in \mathbb{R}$ is a positive scalar, $\mathbb{P}_a\{\cdot\}$ is the a-symmetric operator given in Definition A-2.2, and the superscript V denotes the untilde-operator given in Definition A-2.1. The agents use their local estimate of the desired configuration $\{r_{\text{des},i}, R_{\text{des},i}\}$ and these are the variables on which consensus must be reached. Substitution of the control law (3-7) into the payload dynamics given in (3-5) results in the reduced equations of motion,

$$\begin{aligned} \dot{\Omega}_o &= -\zeta_{\text{sum}} \Omega_o - \sum_{i=1}^{n_f} k_i \mathbb{P}_a \{E_i\}^V \\ \dot{v}_o &= -\beta_{\text{sum}} v_o - \sum_{i=1}^{n_f} K_i e_{r,i}. \end{aligned} \tag{3-8}$$

where $e_{r,i} = r_o - r_{\text{des},i}$ and $E_i = R_{\text{des},i}^T R_o$ are the local position and attitude tracking errors respectively, $\zeta_{\text{sum}} = \sum_{i=1}^{n_f} \zeta_i$ and $\beta_{\text{sum}} = \sum_{i=1}^{n_f} \beta_i$ are the sum of the control gains in (3-7).

3-2-3 Mathematical Objective for Agent Synchronization

In the absence of a leader, it is desired for the agents to synchronize, that is to reach consensus on the tracking errors. Naturally, the payload should stabilize at the desired configuration.

Objectives 3-2.1. *Consider the CMP without a leader described by the reduced description* (3-8)*. The stability of the system follows if, considering the translation, the*

$$\begin{aligned} &\textit{disagreement:} && \delta e_i = e_i - \tfrac{1}{n_f}\sum_{j=1}^{n_f} e_j, \\ &\textit{and tracking error:} && e_i = q_o - q_{i,des} \end{aligned} \tag{3-9}$$

converge to zero for all $i \in \{1, \ldots, n_f\}$*, and considering the attitude, if the*

$$\begin{aligned} &\textit{disagreement:} && E_{ij} = E_i^T E_j, \\ &\textit{and tracking error:} && E_i = R_{des,i}^T R_o \end{aligned} \tag{3-10}$$

converge to the identity matrix for all $i, j \in \{1, \ldots, n_f\}$*.*

3-2-4 Proposed Synchronization Law for the Fully Actuated Case

In the absence of a leader the following update law is proposed to meet the Objectives 3-2.1:

Proposition 3-2.1 (Desired Attitude Synchronization Assuming Full Actuation)**.** *Consider the CMP of the payload using n_f-agents, and no leader, resulting in the reduced payload dynamics given in* (3-8)*. Let the agents update the estimate of the desired payload configuration as*

$$\begin{aligned} \dot{E}_i &= E_i\tilde{\Omega}_o - \gamma E_i\left(k_{sum}\mathbb{P}_a\left\{E_i\right\} - \tilde{y}_R\right) \\ \dot{e}_{r,i} &= v_o - \Gamma\left(K_{sum}e_i - y_r\right) \end{aligned} \tag{3-11}$$

where $\gamma_i = \gamma \in \mathbb{R}$ and $\Gamma_i = \Gamma \in \mathbb{R}^{3\times3}$ are positive definite observer gains, which are assumed identical for all agents, additionally Γ is assumed to be a diagonal matrix, $E_i \in SO(3)$ and $e_{r,i} \in \mathbb{R}^3$ denote the attitude and position tracking error estimates respectively, $k_{sum} = \sum_{i=1}^{n_f} k_i \in \mathbb{R}$ and $K_{sum} = \sum_{i=1}^{n_f} K_i \in \mathbb{R}^{3\times3}$ are the sum of the control gains in (3-7)*, the tilde operator $\tilde{(\cdot)}$ is given in Definition A-2.1, and the measurements y_R and y_r are given as*

$$\begin{aligned} y_R &= -\dot{\Omega}_o - \zeta_{sum}\Omega_o \\ y_r &= -\dot{v}_o - \beta_{sum}v_o \end{aligned} \tag{3-12}$$

where $\zeta_{sum} = \sum_{i=1}^{n_f} \zeta_i$ and $\beta_{sum} = \sum_{i=1}^{n_f} \beta_i$. Then, the Objectives 3-2.1 are almost globally achieved.

The term *almost global* convergence is sometimes used for geometric control, and refers to the different possible equilibria [5]. In the following it will be shown that $\lim_{t\to\infty} \mathbb{P}_a\left\{E_i\right\} = 0$, which holds for $\theta_i = c\pi$ and any integer c, where θ_i is the angle associated with $E_i \in SO(3)$. This situation can be compared to the upward and downwards equilibria of a simple pendulum. Instability of the equilibria $\theta_i = \pm\pi$ is shown in [35] for a comparable problem by substitution of quaternions into the rotation matrix, and linearizing about the undesired equilibria. In the following, this derivation is omitted and the desired attitude R_{des} is said to be an *almost* globally stable equilibrium of the attitude dynamics.

Underlying Consensus Dynamics The consensus dynamics can be revealed by eliminating the measurement y from the update law in Proposition 3-2.1. The reduced equations of motion (3-8) motivate the choice for the measurements y (3-12) as these reduce to $y_R = \sum_i k_i\mathbb{P}_a\left\{E_i\right\}^V$ and $y_r = \sum_i K_i e_i$. This gives the consensus law (3-11) as

$$\begin{aligned} \dot{E}_i &= E_i\tilde{\Omega}_o - \sum_{j=1}^{n_f} \gamma k_j E_i\left(\mathbb{P}_a\left\{E_i\right\} - \mathbb{P}_a\left\{E_j\right\}\right) \\ \dot{e}_{r,i} &= v_o - \sum_{j=1}^{n_f} \Gamma K_j\left(e_{r,i} - e_{r,j}\right). \end{aligned} \tag{3-13}$$

The interpretation of the above equations as a consensus law is discussed at the end of this section, but they clearly illustrate the connection to both the other agents and payload motion. In comparison with the literature it can be seen as a combination of (3-1) and (3-3).

Proof of Synchronization for the Translation Dynamics

Considering the translation dynamics, the situation is very similar to that considered in Section 2-2. However, the absence of a leader allows the payload motion to be directly coupled with the consensus dynamics. For the translation dynamics consider the following Lyapunov candidate,

$$V = \tfrac{1}{2} v_o^T \Gamma^{-1} v_o + \sum_{i=1}^{n_f} e_{r,i}^T K_i \Gamma^{-1} e_{r,i} \tag{3-14}$$

Taking the time derivative of the expression above, and substitution of the system dynamics (3-8) and the consensus law (3-13) gives

$$\dot{V} = -v_o^T \zeta_{\text{sum}} \Gamma^{-1} v_o - \sum_{i=1}^{n_f} e_{r,i} K_i \sum_{j=1}^{n_f} K_j \left(e_{r,i} - e_{r,j} \right) \tag{3-15}$$

The above equation can be rewritten as

$$\dot{V} = -v_o^T \zeta_{\text{sum}} \Gamma^{-1} v_o - e_r^T L_w^{(e)} e_r \tag{3-16}$$

where $L_w^{(e)}$ is the weighted Laplacian matrix for the complete graph as given in Definition A-1.4, where $a_i = K_i \in \mathbb{R}^{3\times 3}$ in the definition. Considering that the feedback gains $K > 0$ and observer gains $\Gamma > 0$ are positive definite diagonal matrices, it holds that $L_w^{(e)}$ is a symmetric matrix, and from Definition A-1.4 it follows that $L_w^{(e)} \geq 0$. Furthermore it holds that $e_r^T L_w^{(e)} e_r = 0$ iff $e_{r,i} \in \mathbb{A}$, where $\mathbb{A}$ is the agreement set given in Definition A-1.1. It then follows from (3-16) that the agent's estimates of the tracking error converges to the agreement set $\lim_{t\to\infty} e_{r,i} \in \mathbb{A}$, and that the payload velocity $\lim_{t\to\infty} v_o = 0$. From LaSalle's invariance principle and the payload dynamics (3-8) it then follows that the tracking error converges to zero asymptotically $\lim_{t\to\infty} r_o = r_{\text{des}}$ where $\lim_{t\to\infty} r_{\text{des},i} = r_{\text{des}}$.

Proof of Synchronization for the Attitude Dynamics

For ease of exposition the proof for the attitude dynamics is broken into a few steps. To this end let the Lyapunov candidate for the attitude dynamics be given as,

$$V = \tfrac{1}{2} \left\| \Omega_o \right\|^2 + \sum_{i=1}^{n_f} k_i V_{E,i}, \tag{3-17}$$

and begin by considering the terms $V_{E,i}$ given as

$$V_{E,i} = \tfrac{1}{2} \text{tr} \left\{ I - E_i \right\}. \tag{3-18}$$

Taking the time derivative of the above equation, and substitution of the proposed consensus law (3-2.1), gives

$$\dot{V}_{E,i} = -\tfrac{1}{2} \text{tr} \left\{ E_i \left(\tilde{\Omega}_o + \gamma \sum_{j=1}^{n_f} k_j \mathbb{P}_a \left\{ E_j - E_i \right\} \right) \right\} \tag{3-19}$$

Note that the above equation shows the product of the rotation matrix $E_i \in SO(3)$ with a skew symmetric matrix, since $\tilde{\Omega}_o \in so(3)$ and $\mathbb{P}_a \left\{ \cdot \right\} \in so(3)$, see Definition A-2.2. The above

expression is thus of the form $\text{tr}\{E_i\tilde{\omega}\}$ where $\tilde{\omega} \in so(3)$, which allows the use of Lemma A-2.7, resulting in,

$$\dot{V}_{E,i} = \left(\mathbb{P}_a\{E_i\}^V\right)^T \left(\Omega_o + \gamma \sum_{j=1}^{n_f} k_j \left(\mathbb{P}_a\{E_j\}^V - \mathbb{P}_a\{E_i\}^V\right)\right) \tag{3-20}$$

Returning to the original Lyapunov candidate for the attitude dynamics,

$$V = \tfrac{1}{2}\|\Omega_o\|^2 + \sum_{i=1}^{n_f} k_i V_{E,i} \tag{3-21}$$

taking the time derivative, substituting the attitude dynamics (3-8) and the expression for $\dot{V}_{E,i}$ (3-20), gives

$$\begin{aligned} \dot{V} &= -\Omega_o^T \zeta_{\text{sum}} \Omega_o - \sum_{i=1}^{n_f} k_i \Omega_o^T \mathbb{P}_a\{E_i\}^V + \sum_{i=1}^{n_f} k_i \dot{V}_{E,i} \\ &= -\Omega_o^T \zeta_{\text{sum}} \Omega_o + \sum_{i=1}^{n_f}\sum_{j=1}^{n_f} \gamma k_i k_j \left(\mathbb{P}_a\{E_i\}^V\right)^T \left(\mathbb{P}_a\{E_j\}^V - \mathbb{P}_a\{E_i\}^V\right) \end{aligned} \tag{3-22}$$

The summation can be rewritten using the weighted Laplacian matrix for the complete graph resulting in,

$$\dot{V} = -\Omega_o^T \zeta_{\text{sum}} \Omega_o - \gamma \left[k_i \mathbb{P}_a\{E_i\}^V\right]_{\text{vec}}^T \left(L_w^{(E)} \otimes I_{3\times 3}\right) \left[k_i \mathbb{P}_a\{E_i\}^V\right]_{\text{vec}} \leq 0 \tag{3-23}$$

where $L_w^{(E)}$ is the weighted Laplacian matrix as given in Definition A-1.4, where $a_i = k_i \in \mathbb{R}$ in the definition. The first term in $\dot{V}$ shows that the angular velocities Ω_o converge to zero, and the second term is only zero if $\mathbb{P}_a\{E_i\}^V \in \mathbb{A}$ as follows from the Definition A-1.4 for $L_w^{(E)}$. From LaSalle's invariance theorem and the attitude dynamics (3-8) it follows that $\lim_{t\to\infty} \sum_{i=1}^{n_f} \mathbb{P}_a\{E_i\} = 0$. This implies that $\theta_i = c\pi$ with c any integer. The undesired equilibria can be evaluated using quaternions, as was done in [35]. This is omitted here, resulting in almost global convergence to the desired equilibrium, thus completing the proof.

3-3 Leader Driven Geometric Control and Full Actuation

The previously discussed method for pose synchronization resulted in the payload stabilizing at a configuration which depends on the initial values of the participating agents. This section discusses the adding of a leader agent as a means of controlling the agreement variable, that is the final desired configuration. The system is shown to be globally Lyapunov stable and it is shown that if the agent's attitude tracking errors $E_i \in SO(3)$ are within an angular displacement of $\pm\frac{1}{2}\pi$ that exponential convergence is achieved. However, the introduction of the leader complicates the dynamics, and a proof for global asymptotic stability is proposed as future work.

Other than adding the leader, the scenario under consideration is the same as the previous section. Most importantly, the agents use identical observer gains, have access to the

payload acceleration and velocity measurements, and apply a wrench to the payload.

The remainder of this section is structured as follows. The controlled payload dynamics is given in Subsection 3-3-1. The objective of the consensus law is defined in Subsection 3-3-2, followed by the proposed solution in Subsection 3-3-3.

3-3-1 Agent Control Laws and Reduced Payload Dynamics

The system description, that is the payload dynamics, the control law for the applied wrench, and the consensus law, follow the same structure as for the synchronization problem. The leader control law is the same as that of the followers, with the exception of having direct access to the actual desired payload configuration, rather than a local estimate. Following the steps outlined in Subsection 3-2-2 this leads to the reduced payload dynamics given as,

$$\begin{aligned} \dot{\Omega}_o &= -\zeta_{\text{sum}}\Omega_o - k_l \mathbb{P}_a \left\{E_l\right\}^V - \sum_{i=1}^{n_f} k_i \mathbb{P}_a \left\{E_i\right\}^V \\ \dot{v}_o &= -\beta_{\text{sum}} v_o - K_l e_{r,l} - \sum_{i=1}^{n_f} K_i e_{r,i}. \end{aligned} \tag{3-24}$$

where $e_{r,l}$ and E_l are the leader position and attitude tracking errors. As it is assumed that the desired payload configuration is constant the following kinematic relations for the leader tracking error are derived,

$$\begin{aligned} E_l &= R_{\text{des}}^T R_o, & \dot{E}_l &= E_l \tilde{\Omega}_o \\ e_{r,l} &= r_o - r_{\text{des}}, & \dot{e}_{r,l} &= v_o. \end{aligned} \tag{3-25}$$

3-3-2 Mathematical Objective for the Cooperative Manipulation Problem

The objective for the translation dynamics is omitted in the following, as it shows an identical structure to that posed in the previous chapter, see Objectives 2-2.1. Considering the attitude dynamics, the objectives are posed as follows:

Objectives 3-3.1. *Consider the CMP without a leader described by the reduced description* (3-8)*. Regarding the attitude dynamics, the convergence to the desired equilibrium follows if the*

$$\begin{aligned} &\textit{disagreement:} && E_{ij} = E_i^T E_j, \quad \forall j \in \{1, \ldots, n_f\} \\ &i^{th}\textit{-estimation error:} && E_{il} = E_i^T E_l \\ &\textit{and tracking error:} && E_l = R_{des}^T R_o \end{aligned} \tag{3-26}$$

all converge to the identity matrix, for any i^{th}-agent.

3-3-3 Proposed Geometric Consensus Law Assuming Full Actuation

As mentioned in the introduction, the proof for globally achieving the Objectives 3-3.1 was not found. Nevertheless, the following proposition shows promising results:

Proposition 3-3.1 (Geometric Consensus Law)**.** *Consider adding a leader to the CMP of the payload as described in Proposition 3-2.1, such that the payload dynamics are obtained as* (3-24)*. Let the agents update the estimate of the desired payload configuration as*

$$\begin{aligned} \dot{E}_i &= E_i\tilde{\Omega}_o - \gamma E_i\left(k_{sum}\mathbb{P}_a\left\{E_i\right\} - \tilde{y}_R\right) \\ \dot{e}_{r,i} &= v_o - \Gamma_i\left(K_{sum}e_{r,i} - y_r\right) \end{aligned} \tag{3-27}$$

where the measurements y_R and y_r are as given in Proposition 3-2.1, $\gamma > 0$ and $\Gamma_i > 0$ are the observer gains, with $\Gamma_i \in \mathbb{R}^{3\times 3}$ a diagonal matrix, $\{e_{r,i}, E_i\} \in SE(3)$ denotes the estimated configuration tracking error, $k_{sum} = k_l + \sum_{i=1}^{n_f} k_i$ and $K_{sum} = K_l + \sum_{i=1}^{n_f} K_i$ are the sum of the control gains in (3-24)*, and the tilde operator $\tilde{(\cdot)}$ is given in Definition A-2.1.*

Then, system state remains bounded. The Objectives 3-3.1 are guaranteed to be achieved if $|\theta_i| < \frac{1}{2}\pi$ and $|\theta_l| < \frac{1}{2}\pi$, where θ_* denotes the angle of rotation associated with E_*. Furthermore, within that region a bound on the convergence rate can be derived.
Regarding the translation dynamics, the equivalent Objectives posed in 2-2.1 are globally achieved.

A subtle difference with the proposed consensus law, in comparison with the synchronization law, is that for the translation dynamics it is allowed to use individual gains $\gamma_{r,i}$. This has more to do with the method for constructing the proof than the effect of adding a leader. By choosing the observer gains as identical, the proof is constructed using a single Lyapunov function. In the following the proof is decoupled, which allows individual observer gains for the translation dynamics. For the attitude dynamics none of these considerations apply, as we are forced by the nonlinearity of the problem to use identical gains.

The Underlying Consensus Law

The reduced equations of motion (3-24) motivate the choice for the measurements y given in (3-12) as these are equivalent to $y_R = k_l\mathbb{P}_a\left\{E_l\right\}^V + \sum_i k_i\mathbb{P}_a\left\{E_i\right\}^V$ and $y_r = K_l e_{r,l} + \sum_i K_i e_{r,i}$. This shows that the consensus law (3-27) is equivalent to

$$\dot{E}_i = E_i\tilde{\Omega}_o - \gamma E_i\left(k_l\left(\mathbb{P}_a\left\{E_i\right\} - \mathbb{P}_a\left\{E_l\right\}\right) + \sum_{j=1}^{n_f} k_j\left(\mathbb{P}_a\left\{E_i\right\} - \mathbb{P}_a\left\{E_j\right\}\right)\right) \tag{3-28}$$

and,

$$\dot{e}_{r,i} = v_o - \Gamma_i\left(K_l\left(e_{r,i} - e_{r,l}\right) + \sum_{j=1}^{n_f} K_j\left(e_{r,i} - e_{r,j}\right)\right). \tag{3-29}$$

From the above consensus dynamics it can be seen that each agent has direct access to the leader's desired configuration. For the translation tracking error the payload velocity can be eliminated by considering the estimation error dynamics $\Delta e_{r,i} = e_{r,i} - e_{pos,l}$, resulting in

$$\Delta \dot{e}_{r,i} = -\Gamma_i \left(K_l \Delta e_{r,i} + \sum_{j=1}^{n_f} K_j \left(\Delta e_{r,i} - \Delta e_{r,j} \right) \right). \tag{3-30}$$

For the attitude consensus law no such simplification can be done, and the description given in (3-28) must suffice.

Proof of Convergence for the Translation Dynamics

The structure of the consensus- and payload dynamics concerning the payload translation can be seen as a sub-case of the situation considered in Section 2-2. The estimation error was shown to converge via the Lyapunov candidate given as

$$V_\Delta = \sum_{i=1}^{n_f} \tfrac{1}{2} \Delta e_{r,i}^T K_i \Gamma_i^{-1} \Delta e_{r,i}, \tag{3-31}$$

and exponential convergence to the origin follows from the time derivative,

$$\dot{V}_\Delta = -\Delta e_r^T L_w^{(e)} \Delta e_r - \sum_{i=1}^{n_f} \Delta e_{r,i}^T K_i K_l \Delta e_{r,i} \tag{3-32}$$

where $\Delta e_r = \begin{bmatrix} \Delta e_{r,1}^T & \dots & \Delta e_{r,n_f}^T \end{bmatrix}^T$ denotes the stacking of all the estimation errors into a single vector, $L_w^{(e)}$ the weighted Laplacian matrix as given in Definition A-1.4, by taking $a_i = K_i$ in the definition. As the system is linear the separation theorem applies, and the payload can be shown to converge to the desired position, by assuming the consensus dynamics to have converged already.

Proof of Convergence for the Attitude Dynamics

The proof of Proposition 3-3.1 regarding the attitude dynamics is constructed in several steps. Firstly it is shown that all signals remain bounded. Subsequently, the proof of convergence for the attitude dynamics is broken down in three steps, according to the posed Objectives 3-3.1. It is emphasized that the proof holds for a region given as $|\theta_i| < \frac{1}{2}\pi, \forall i$ and $|\theta_l| < \frac{1}{2}\pi$, which denote the angle of rotation associated with $E_i \in SO(3)$ and $E_l \in SO(3)$ respectively. This restriction will be further discussed in Section 3-5.

Proof of Stability of the Attitude Dynamics

Boundedness can be shown using the identity $\mathbb{P}_a \{E\}^V = \sin(\theta)\,\epsilon$ for any $E \in SO(3)$, where ϵ and θ are the axis and angle of rotation associated with $E \in SO(3)$, see Lemma A-5.1. It follows that $\|\mathbb{P}_a \{E\}\| \leq 1$, which can be used to show boundedness of the payload angular velocity Ω_o.

To this end, consider the Lyapunov candidate given as

$$V = \tfrac{1}{2}\Omega_o^T\Omega_o. \tag{3-33}$$

Taking the time derivative, and substituting the reduced dynamics (3-24), gives

$$\dot{V} = -\Omega_o^T\zeta_{\text{sum}}\Omega_o - \Omega_o^T\left(k_l\mathbb{P}_a\left\{E_l\right\}^V + \sum_{i=1}^{n_f} k_i\mathbb{P}_a\left\{E_i\right\}^V\right). \tag{3-34}$$

Using $\|\mathbb{P}_a\left\{E_*\right\}\| \leq 1$ this gives,

$$\dot{V} \leq -c_{\min}\Omega_o^T\Omega_o + k_{\text{sum}}\|\Omega_o\| \quad = \begin{cases} < 0 & \text{if} \quad \|\Omega_o\| > k_{\text{sum}}/c_{\min} \\ \\ \geq 0 & \text{otherwise} \end{cases} \tag{3-35}$$

where $c_{\min} > 0$ is the minimal scalar entry on the diagonal of ζ_{sum}. From Lemma A-5.1 it follows that Ω_o is a bounded signal. All other dynamic variables are rotation matrices confined to $SO(3)$, and are thus inherently bounded.

Proof of Synchronization of the Agents

In the following it will be shown that the agents synchronize, i.e. converge to the agreement set, if $|\theta_i| < \pm\frac{1}{2}\pi$, where θ_i is the angle of rotation associated with $E_i \in SO(3)$. The attitude consensus law given in Proposition 3-3.1 is restated here for convenience,

$$\dot{E}_i = E_i\tilde{\Omega}_o - \gamma k_{\text{sum}}E_i\mathbb{P}_a\left\{E_i\right\} + \gamma E_i\tilde{y}_R \tag{3-36}$$

where $\gamma, k_{\text{sum}} > 0$. Consider the Lyapunov candidate

$$V_\delta = \text{tr}\left\{[I - E_i]_{\text{vec}}^T\left(L \otimes I\right)[I - E_i]_{\text{vec}}\right\} \quad \begin{cases} = 0 \quad \text{if} \quad E_i \in \mathcal{A} \\ \\ \geq 0 \quad \text{otherwise} \end{cases} \tag{3-37}$$

where $[I - E_i]_{\text{vec}}$ denotes the stacking of the matrices $I - E_i$ for $i = 1, \ldots, n_f$ where $I = I_{3\times 3}$ denotes the 3×3 identity matrix, unless otherwise noted, $L \in \mathbb{R}^{n_f \times n_f}$ denotes the Laplacian matrix for the complete graph (A-1.3). The above Lyapunov function is based on the basic Lyapunov function given in (A-22), with the addition of the Laplacian matrix for the complete graph to penalize the disagreement. Before taking the time derivative the above expression can be further simplified: Since $\mathbf{1}_n \in \textbf{null}\{L\}$ it also holds that $[I]_{\text{vec}} \in \textbf{null}\{L \otimes I\}$. Therefore the Lyapunov function given above simplifies to

$$V_\delta = \text{tr}\left\{[E_i]_{\text{vec}}^T\left(L \otimes I\right)[E_i]_{\text{vec}}\right\} \tag{3-38}$$

Taking the time derivative, and substitution of (3-36) gives

$$\dot{V}_\delta \quad = \quad \text{tr}\left\{-\gamma k_{\text{sum}}\left[E_i\right]_{\text{vec}}^T\left(L \otimes I\right)\left[E_i\mathbb{P}_a\left\{E_i\right\}\right]_{\text{vec}} + \left[E_i\right]_{\text{vec}}^T\left(L \otimes I\right)\left[E_i\left(\tilde{\Omega}_o + \gamma\tilde{y}_R\right)\right]_{\text{vec}}\right\} \tag{3-39}$$

This can be rewritten as

$$\dot{V}_\delta = \mathrm{tr}\left\{-\gamma k_{\mathrm{sum}} \left[E_i\right]_{\mathrm{vec}}^T (L \otimes I) \left[E_i \mathbb{P}_a \left\{E_i\right\}\right]_{\mathrm{vec}} + \underbrace{\left[E_i\right]_{\mathrm{vec}}^T (L \otimes I) \left[E_i\right]_{\mathrm{vec}}}_{\text{symmetric}} \left(\tilde{\Omega}_o + \gamma \tilde{y}_R\right)\right\} \tag{3-40}$$

The last term is a symmetric matrix multiplied by a skew-symmetric matrix $\tilde{y}_R = -\tilde{y}_R^T$, since the tilde operator produces a skew symmetric matrix, see Definition A-10, and $\left[E_i\right]_{\mathrm{vec}}^T (L \otimes I) \left[E_i\right]_{\mathrm{vec}}$ is symmetric since $L = L^T$. This allows the use of Lemma A-2.1 to show that the last term drops from the equation. What remains is the first term,

$$\dot{V}_\delta = -\gamma k_{\mathrm{sum}} \mathrm{tr}\left\{\left[E_i\right]_{\mathrm{vec}}^T (L \otimes I) \left[E_i \mathbb{P}_a \left\{E_i\right\}\right]_{\mathrm{vec}}\right\}. \tag{3-41}$$

The asymmetric operator $\mathbb{P}_a\left\{\cdot\right\}$ can be expanded using Definition A-2.2, resulting in

$$\dot{V}_\delta = -\tfrac{\gamma k_{\mathrm{sum}}}{2} \mathrm{tr}\left\{\left[E_i\right]_{\mathrm{vec}}^T (L \otimes I) \left[E_i^2 - I\right]_{\mathrm{vec}}\right\}. \tag{3-42}$$

where the orthonormality property of the rotation matrix was used $E_i E_i^T = I$. Further simplification is achieved using $\left[I\right]_{\mathrm{vec}} = \left(\mathbf{1}_{n_f} \otimes I\right) \in \mathbf{null}\{L \otimes I\}$,

$$\dot{V}_\delta = -\tfrac{\gamma k_{\mathrm{sum}}}{2} \mathrm{tr}\left\{\left[E_i\right]_{\mathrm{vec}}^T (L \otimes I) \left[E_i^2\right]_{\mathrm{vec}}\right\}. \tag{3-43}$$

The E_i^2 term forms an obstruction at this point. Begin by adding $\left[E_i E_i^T\right]_{\mathrm{vec}} = \left[I\right]_{\mathrm{vec}}$ to the right-side, which is allowed as it lies in the null space of $L \otimes I$,

$$\dot{V}_\delta = -\tfrac{\gamma k_{\mathrm{sum}}}{2} \mathrm{tr}\left\{\left[E_i\right]_{\mathrm{vec}}^T (L \otimes I) \left[E_i \left(E_i + E_i^T\right)\right]_{\mathrm{vec}}\right\}. \tag{3-44}$$

Using the definition of $\mathbb{P}_s\left\{E_i\right\} = \frac{1}{2}\left(E_i + E_i^T\right)$, Definition A-2.2, rewrite the above equation as,

$$\dot{V}_\delta = -\gamma k_{\mathrm{sum}} \mathrm{tr}\left\{\left[E_i\right]_{\mathrm{vec}}^T (L \otimes I) \left[E_i\right]_{\mathrm{diag}} \left[\mathbb{P}_s \left\{E_i\right\}\right]_{\mathrm{vec}}\right\}. \tag{3-45}$$

The obtained expression allows the use of Lemma A-2.5 followed by Lemma A-2.6, arriving at the following expression,

$$\dot{V}_\delta \leq -\gamma k_{\mathrm{sum}} \mathrm{tr}\left\{\left[E_i\right]_{\mathrm{vec}}^T (L \otimes I) \left[E_i \cos(\theta_i)\right]_{\mathrm{vec}}\right\} \tag{3-46}$$

where θ_i is the angular rotation about the principal axis associated with E_i, that is, it is the attitude angle error between the estimated desired attitude $R_{\mathrm{des},i}$ and the payload attitude R_o. The right hand side in the above equation can be rewritten as,

$$\mathrm{tr}\left\{\left[E_i\right]_{\mathrm{vec}}^T (L \otimes I) \left[E_i \cos(\theta_i)\right]_{\mathrm{vec}}\right\} = \sum_{i=1}^{n_f} \sum_{j=1}^{n_f} \mathrm{tr}\left\{I - E_{ij}\right\} \cos\left(\theta_i\right) \tag{3-47}$$

where $E_{ij} = E_i^T E_j \in SO(3)$. From (A-22) it is known that $\mathrm{tr}\left\{I - E_{ij}\right\} \geq 0$ for any $E_{ij} \in SO(3)$. This shows that as long as $\cos(\theta_i) > 0$ it is certain that $\dot{V}_\delta < 0$. Thus adding the assumption that $-\frac{1}{2}\pi < \theta_i < \frac{1}{2}\pi$ gives (3-46) as

$$\dot{V}_\delta \leq -\gamma k_{\mathrm{sum}} \cos(\theta_{\min}) \mathrm{tr}\left\{\left[E_i\right]_{\mathrm{vec}}^T (L \otimes I) \left[E_i\right]_{\mathrm{vec}}\right\} < 0, \qquad \text{if} \quad -\tfrac{1}{2}\pi < \theta_i < \tfrac{1}{2}\pi \tag{3-48}$$

where $\theta_{\min}$ is the error angle closest to $\pm\frac{1}{2}\pi$, i.e. $\theta_{\min} = \left\{\arg\min_{\theta_i} \cos(\theta_i) : |\theta_i| < \frac{1}{2}\pi\right\}$. The above expression shows that if $|\theta_i| < \frac{1}{2}\pi$, i.e. if the estimation of the attitude tracking error remains within $\pm 90\,\text{deg}$, that the agents converge to the agreement set $\lim_{t\to\infty} E_i \in \mathbb{A}$. Furthermore, note that the above equation can be written in terms of the original Lyapunov equation given in (3-37),

$$\dot{V}_\delta \leq -\gamma k_{\text{sum}} \cos(\theta_{\min}) V_\delta < 0, \qquad \text{if} \quad -\tfrac{1}{2}\pi < \theta_i < \tfrac{1}{2}\pi \tag{3-49}$$

which allows the use of Lemma A-5.3 to show that the convergence rate is bounded by $\alpha \geq \gamma k_{\text{sum}} \cos(\theta_{\min})$ if $|\theta_i| < \frac{1}{2}\pi$.

Proof of Convergence to the Leader Desired Attitude

As previously stated, the proof *depends* on remaining within the region of attraction. Therefore, in the following this is simply assumed to be the case, and posed as an unsolved problem in this work.

If it is assumed that $|\theta_i| < \frac{1}{2}\pi$, and since it holds that all signals remain bounded, we proceed by assuming that the agents are synchronized $E_i \in \mathbb{A}$, where $\mathbb{A}$ is the agreement set. The consensus law (3-28) is then reduced to,

$$\dot{E}_i = E_i \tilde{\Omega}_o - \gamma k_l E_i \left(\mathbb{P}_a\left\{E_i\right\} - \mathbb{P}_a\left\{E_o\right\}\right), \qquad \text{if} \quad E_i \in \mathbb{A} \tag{3-50}$$

where $E_o = R_{\text{des}}^T R_o$ is the leader tracking error. The convergence proof starts by considering the following Lyapunov candidate,

$$V_\Delta = \tfrac{1}{2}\tfrac{1}{\gamma k_{R,l}} \text{tr}\left\{\left(E_o - E_i\right)^T \left(E_o - E_i\right)\right\} = \tfrac{1}{\gamma k_{R,l}} \text{tr}\left\{I - E_o^T E_i\right\} \geq 0 \tag{3-51}$$

Taking the time derivative, and substitution of the leader kinematics (3-25) and the consensus law (3-50), gives

$$\dot{V}_\Delta = \text{tr}\left\{E_o^T E_i \left(\mathbb{P}_a\left\{E_i\right\} - \mathbb{P}_a\left\{E_o\right\}\right)\right\} \tag{3-52}$$

where the payload angular velocity Ω_o has dropped from the equation. Proceed by switching the asymmetric operator to $E_o^T E_i$ using Lemma A-2.2 and subsequently expand the resulting asymmetric operator $\mathbb{P}_a\{R\} = \frac{1}{2}\left(R - R^T\right)$,

$$\dot{V}_\Delta = \text{tr}\left\{\mathbb{P}_a\left\{E_o^T E_i\right\}\left(E_i - E_o\right)\right\} = \tfrac{1}{2}\text{tr}\left\{\left(E_o^T E_i - E_i^T E_o\right)\left(E_i - E_o\right)\right\}. \tag{3-53}$$

Further simplification can be achieved by considering the identity $\left(E_i + E_o\right)^T \left(E_i - E_o\right) = E_o^T E_i - E_i^T E_o$ and substituting this in the above equation, resulting in

$$\dot{V}_\Delta = -\tfrac{1}{2}\text{tr}\left\{\left(E_i - E_o\right)^T \left(E_i + E_o\right)\left(E_i - E_o\right)\right\} \tag{3-54}$$

The trace is invariant to transposing the inner matrix, allowing the above expression to be rewritten as,

$$\dot{V}_\Delta = -\tfrac{1}{2}\text{tr}\left\{\left(E_i - E_l\right)^T \left(\mathbb{P}_s\left\{E_i\right\} + \mathbb{P}_s\left\{E_l\right\}\right)\left(E_i - E_l\right)\right\} \tag{3-55}$$

with $\mathbb{P}_s\{\cdot\}$ given in Definition A-2.2. Additionally assuming that the leader attitude error is restricted to $-\frac{1}{2}\pi < \theta_l < \frac{1}{2}\pi$ allows the use of Lemma A-2.6 stating that $\mathbb{P}_s\{E_i\}, \mathbb{P}_s\{E_l\} > 0$. As the trace of a positive definite matrix is positive the above equation gives,

$$\dot{V}_\Delta < 0 \qquad \text{if} \quad \begin{cases} -\frac{1}{2}\pi < \theta_l < \frac{1}{2}\pi, & \text{and} \\ -\frac{1}{2}\pi < \theta_i < \frac{1}{2}\pi, & \text{and} \\ E_i \in \mathbb{A} \end{cases} \tag{3-56}$$

If the above conditions hold, then all agents converge to the leader $\lim_{t\to\infty} E_i = E_l$. Furthermore, note from (A-19) that $\mathbb{P}_s\{E_i\} = I\cos(\theta_i) + (1-\cos(\theta_i))\,\epsilon\epsilon^T$, such that with angles constrained as above it holds that,

$$\dot{V}_\Delta \leq -\tfrac{1}{2}(\cos(\theta_l) + \cos(\theta_i))\,\mathrm{tr}\left\{(E_i - E_l)^T(E_i - E_l)\right\} \tag{3-57}$$

Comparing the above to the originally posed Lyapunov function (3-51), shows that,

$$\dot{V}_\Delta \leq -\gamma k_{R,l}(\cos(\theta_l) + \cos(\theta_i))\,V_\Delta. \tag{3-58}$$

and the convergence rate follows from Lemma A-5.3 as $\alpha \geq \gamma k_{R,l}(\cos(\theta_l) + \cos(\theta_i))$, assuming that $|\theta_l| < \frac{1}{2}\pi$ and $|\theta_i| < \frac{1}{2}\pi$.

Proof of Convergence of the Payload Attitude Tracking Error

The convergence of the payload tracking error naturally depends on the previous results. Again the assumption is made that $|\theta_i| < \frac{1}{2}\pi$ and $|\theta_l| < \frac{1}{2}\pi$ holds. If so, the attitude dynamics in (3-24) is reduced to,

$$\dot{\Omega}_o = -\zeta_{\text{sum}}\Omega_o - k_{\text{sum}}\mathbb{P}_a\{E_l\}^V, \qquad \text{if} \quad E_i = E_l \forall i \tag{3-59}$$

where $k_{\text{sum}} = k_l + \sum_{i=1}^{n_f} k_i$ is the sum of the control gains of the agents. Convergence of the payload to the desired attitude is then proven using the Lyapunov candidate given as

$$V_e = \tfrac{1}{2}\Omega_o^T\Omega_o + \tfrac{k_{\text{sum}}}{2}\mathrm{tr}\{I - E_l\}. \tag{3-60}$$

Taking the time derivative and substitution of the leader kinematics (3-25) and the payload dynamics (3-59) gives,

$$\dot{V}_e = -\Omega_o^T\zeta_{\text{sum}}\Omega_o - k_{\text{sum}}\Omega_o^T\mathbb{P}_a\{E_l\}^V - \tfrac{1}{2}k_{\text{sum}}\mathrm{tr}\left\{E_l\tilde{\Omega}_o\right\} \tag{3-61}$$

Lemma A-2.3 allows the above to rewritten as

$$\dot{V}_e = -\Omega_o^T\zeta_{\text{sum}}\Omega_o \leq 0, \qquad \text{if} \quad E_i = E_l \forall i \tag{3-62}$$

The proof is completed using LaSalle's invariance principle: If $\Omega_o = 0$ for all time then $\mathbb{P}_a\{E_l\} = 0$ from (3-59). The last equality holds for $\theta_l = c\pi$ for any integer c and where θ_l is the principle angle associated with the attitude tracking error E_l. Although, it is well known that the angle error of $\theta_l = \pm\pi$ is an unstable equilibrium of the system [5], it lies outside the convergence region, and thus the proof of Proposition 3-3.1 is completed.

Evidently, the convergence region forms a restriction for the proof, as it is not shown that the system is invariant to this region. However, before discussing the difficulties of the proof it will be shown that the proposed solution can directly be extended to the underactuated case.

3-4 Extension of the Geometric Consensus Law to the Underactuated Case

This section considers extending the previously proposed solution to the case where the agents can only apply a force at the attachment point, rather than a wrench. Similarly as was done in Section 2-3, the proposed approach is to use the generalized inverse and identical observer gains. This allows the consensus problem to be decoupled from the payload tracking dynamics. In the following it is shown that the proposed geometric consensus law for the fully actuated case can be directly extended to the underactuated case. As such, the proof also relies on the restrictive assumption of $|\theta| < \pm\frac{1}{2}\pi$.

In the following the controlled payload dynamics is given, followed by the extension of the geometric approach to the underactuated case.

3-4-1 Reduced Payload Dynamics

To obtain the payload dynamics the same approach as outlined in Section 2-3 can be followed. To summarize: The leader is still represented as a wrench acting at the payload CoG, applying (3-7). The followers however, make use of the generalized inverse to convert the control law for the desired wrench to a force at the agent's attachment point, using (2-26). Resulting in the reduced system description given as

$$\begin{bmatrix} \dot{\Omega}_o \\ \dot{v}_o \end{bmatrix} = -\begin{bmatrix} \zeta_{\text{sum}}\Omega_o \\ \beta_{\text{sum}} v_o \end{bmatrix} - \begin{bmatrix} k_l \mathbb{P}_a \{E_l\}^V \\ K_l e_{r,l} \end{bmatrix} - \sum_{i=1}^{n_f} W_i(R_o) \begin{bmatrix} k\mathbb{P}_a \{E_i\}^V \\ K e_{r,i} \end{bmatrix} \tag{3-63}$$

where $e_{r,l} \in \mathbb{R}^3$ and $E_l \in SO(3)$ are the leader position and attitude tracking error, $e_{r,i} \in \mathbb{R}^3$ and $E_i \in SO(3)$ are the follower tracking errors, $\zeta_{\text{sum}} = \zeta_l + n_f\zeta \in \mathbb{R}^{3\times3}$ and $\beta_{\text{sum}} = \beta_l + n_f\beta \in \mathbb{R}^{3\times3}$ are the sum of the damping gains, $k_* \in \mathbb{R}$ and $K_* \in \mathbb{R}^{3\times3}$ are positive gains, and $W_i(R_o)$ is given as,

$$W_i(R_o) = n_f M^{-1} J_{p_i}(R_o)^T J_{p_i}(R_o)^\dagger M. \tag{3-64}$$

where $J_{p_i}(R_o)^T$ is the adjoint matrix (2-24), and $J_{p_i}(R_o)^\dagger$ is the generalized inverse of $J_{p_i}(R_o)^T$ (2-25). By assuming identical control gains, as well as observer gains, the disagreement dynamics can be isolated, as a means to eliminate the generalized inverse. It was noted in Subsection 2-3-5 that the assumption on identical actuation gains $k_i = k$ and $K_i = K$ can be relaxed by using a weighted generalized inverse.

3-4-2 Proposed Geometric Consensus Law for the Underactuated Case

Except for the use of the generalized inverse, the control law for the underactuated case is the same as for the fully actuated case, but instead the observer gains γ for both the translation and attitude dynamics are identical for all agents:

Proposition 3-4.1. *Consider the CMP of the payload for the underactuated case, resulting in the reduced payload dynamics given in* (3-63)*. Let the agents update the estimate of the desired payload configuration as*

$$\begin{aligned} \dot{E}_i &= E_i\tilde{\Omega}_o - \gamma E_i \left(k_{sum}\mathbb{P}_a\left\{E_i\right\} - \tilde{y}_R\right) \\ \dot{e}_{r,i} &= v_o - \Gamma\left(K_{sum}e_{r,i} - y_r\right) \end{aligned} \tag{3-65}$$

where the measurements y_R and y_r are as given in Proposition 3-2.1, $\gamma > 0$ and $\Gamma > 0$ are the observer gains, $\{e_{r,i}, E_i\} \in SE(3)$ denotes the estimated configuration tracking error, $k_{sum} = k_l + n_f k$ and $K_{sum} = K_l + n_f K$ are the sum of the control gains in (3-63)*.*

Then, the system state remains bounded. Regarding the attitude dynamics the Objectives 3-3.1, and regarding the translation dynamics the Objectives posed in 2-2.1, are guaranteed to be achieved if $|\theta_i| < \frac{1}{2}\pi$ and $|\theta_l| < \frac{1}{2}\pi$, where θ_* denotes the angle of rotation associated with E_*. Within that region a bound on the convergence rate can be derived.

For the underactuated case it can be seen that if the agreement set is reached that $\sum_{i=1}^{n_f} W_i\left(R_o\right) = n_f I$ in (3-63), such that the dynamics are the same as for the fully actuated case.

For the attitude dynamics the proof of convergence to the agreement set is exactly the same as for the fully actuated case, by starting with the same Lyapunov function given by equation (3-37):

$$V_{\delta,E} = \mathrm{tr}\left\{\left[I - E_i\right]_{\mathrm{vec}}^T \left(L \otimes I\right)\left[I - E_i\right]_{\mathrm{vec}}\right\} \tag{3-66}$$

which results in the same time derivative (3-48). The time derivative which was shown to be negative definite if $|\theta_i| < \frac{1}{2}\pi$. For the translation dynamics the proof of convergence to the agreement set follows from the Lyapunov candidate,

$$V_{\delta,r} = \tfrac{1}{2} e_r^T \left(L \otimes I\right) e_r \quad \rightarrow \quad \dot{V}_{\delta,r} = e_r^T \left(L \otimes \left(\Gamma K_{\mathrm{sum}}\right)\right) e_r \tag{3-67}$$

where $e_r = \begin{bmatrix} e_{r,1}^T & \dots & e_{r,n_f}^T \end{bmatrix}^T$, and the time derivative was obtained following the steps in Subsection 2-3-4. For the translation dynamics global convergence to the agreement set follows.

Since the agreement set is reached, globally for the translation dynamics, and within the convergence region $|\theta_i| < \frac{1}{2}\pi$ for the attitude dynamics, the underactuated system reduces to the fully actuated system. Due to the boundedness of $E_i \in SO(3)$ and the linear nature of the translation dynamics the consensus dynamics and payload tracking dynamics can be separated, without losing stability. The problem of the convergence region remains, preventing global convergence results.

3-5 Discussion on the Dependence of a Convergence Region

In the following it is illustrated what causes the difficulty in proving global convergence, but before doing so, consider what was provided by the proofs, and what is missing: The solutions in this chapter resulted in,

- a global system description,
- almost globally converging autonomous dynamics (synchronization),
- boundedness of all signals,
- and a large exponential convergence region.

The difficulty in proving convergence of the consensus dynamics is related to the coupling with the payload motion, and the evaluation of disagreement on $SO(3)$. These two issues will be illustrated in the following two subsections.

3-5-1 Inability to Decouple the Consensus Dynamics from the Payload Motion

The convergence region of $|\theta_i| < \frac{1}{2}\pi$ is interpreted as the relative attitude error between the agents desired attitude $R_{\text{des},i}$ and the payload's current attitude R_o. This is different from that found in [31], i.e. (3-3), where the convergence region only depends on $R_{\text{des},i}$. The dependence on the payload attitude indicates that the convergence region changes as the payload attitude changes, thus complicating the analysis. In the following it is clarified why this coupling can not be easily eliminated. For ease of exposition, this is illustrated for the synchronization law in Proposition 3-2.1.

The update laws given in (3-11) was given for the attitude tracking error $E_i = R_{\text{des},i}^T R$, rather than for the desired attitude $R_{\text{des},i}$ directly. The control law could however be equivalently represented using the latter, and this clearly shows the effect of the payload on the consensus law. The equivalent consensus law is given as,

$$\dot{R}_{\text{des},i} = \gamma R_{\text{des},i}\left(k_{\text{sum}}\mathbb{P}_a\left\{R_{\text{des},i}^T R_o\right\} - \tilde{y}_R\right) \tag{3-68}$$

and the same measurement applies. Elimination of the measurement y_R gives the consensus law as,

$$\dot{R}_{\text{des},i} = -\gamma R_{\text{des},i}\sum_{j=1}^{n_f} k_j\left(\mathbb{P}_a\left\{R_o^T R_{\text{des},i}\right\} - \mathbb{P}_a\left\{R_o^T R_{\text{des},j}\right\}\right) \tag{3-69}$$

The same could be done for the translation dynamics, and following the same steps, this gives,

$$\dot{r}_{\text{des},i} = -\Gamma\sum_{j=1}^{n_f} K_j\left(r_{\text{des},i} - r_{\text{des},j}\right) \tag{3-70}$$

where the measurement was changed to $y_r = -\dot{v}_o - \beta_{\text{sum}} v_o - K_{\text{sum}} r_o$. Aside from that y_r now requires position measurements, the same Lyapunov function can be used, ans the same stability results follow: The two representations are simply identical. Clearly the position tracking law (3-70) is decoupled from the payload motion. For the attitude the given form

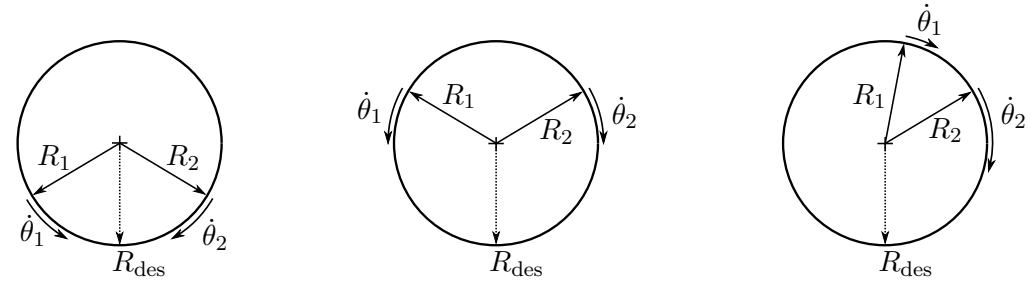

Figure 3-1: Graphical illustration of the convergence region: The three arrows represent three attitudes R_{des}, R_1 and R_2. In each case the attitudes R_1 and R_2 move to align with R_{des} as illustrated by the direction of $\dot{\theta}_1$ and $\dot{\theta}_2$. In case (a) the angle between R_1 and R_2 is decreasing. In cases (b) and (c) the angle between R_1 and R_2 is increasing.

(3-69) shows that the payload attitude, in the form of $R_o \in SO(3)$, couples the consensus dynamics to the payload dynamics. This can be seen by comparison with the consensus law taken from the literature (3-3). It is however, to the best of my knowledge, not possible to remove $R_o \in SO(3)$ from $\mathbb{P}_a \left\{ R_{des,i}^T R_o \right\}^V \in \mathbb{R}^3$, which would allow the consensus problem to be separated. The result is that the convergence region rotates with the payload attitude, as opposed to [34] where the same convergence region is static.

3-5-2 The Challenge With Disagreement Evaluation on $SO(3)$

The convergence region found in Proposition 3-3.1 is a recurring problem in consensus dynamics that are defined in the form of (3-3), see [34], [30], [31], [32], [33]. The interpretation of this effect is shown in Figure 3-1, where the three dimensional rotations are reduced to a single dimensional rotation for ease of exposition. Let the arrows radiating outward represent the attitudes R_1, R_2 and R_{des}, where R_1 and R_2 represent two agents that converge to the desired attitude R_{des}. Considering Figure 3-1a the agent's attitudes R_1 and R_2 move to align their attitude with R_{des} as indicated by the direction of $\dot{\theta}_1$ and $\dot{\theta}_2$. This means that the angle difference between the agents decreases. Considering Figure 3-1b both agents again move to align their attitude with R_{des}. In this case the angle difference between the agents increases, despite that the agents converge to the desired attitude. A similar problem is shown in Figure 3-1c, where again both agents move to align with R_{des}. Since the control action has a magnitude of $\sin(\theta_i)$, the result is that agent 1 moves slower than agent 2, as indicated by the arrow length of $\dot{\theta}$. This again results in that the angle between the agents increases, despite the convergence to the desired attitude. This graphical interpretation shows that the disagreement amongst the agents is difficult to evaluate, even if the agents are exactly behaving as desired. Although the situation considered in this chapter might appear more complicated than depicted in Figure 3-1, the reason for finding this convergence region is at least caused by this effect.

3-6 Simulation Results of the Geometric Control Law for the Underactuated Case

This section presents the simulation results for the underactuated case, i.e. Proposition 3-4.1. The simulation settings are as described in Appendix C providing a detailed listing of all settings. To summarize: The simulation is done with $n_f = 10$ follower agents, applying a force at the attachment points, and a single leader as a wrench at the payload CoG. The system step response is simulated by changing the leader's desired payload configuration at $t = 4$ seconds. The observer gains for the follower agents in Proposition 3-4.1 where taken as $\gamma = 12.64$ and $\Gamma = 6.32 \times I_{3\times 3}$.

The aim is to show via simulations that the convergence region appears to be a limitation of the proof rather than the proposed control and consensus laws. As such the agent's initial estimates and the leader reference signal are such that these are well outside of the convergence region. Half the agent's initial estimates of the desired payload attitude is chosen between $-90\,\text{deg}$ and $-180\,\text{deg}$, with equal interspacing, and the other half of the agent's estimated between $+90\,\text{deg}$ and $+180\,\text{deg}$, again with equal interspacing. All agents are thus initiated outside of the convergence region $|\theta_i| < \pi$. The axes of rotation are chosen randomly. The leader changes the reference attitude after 4 seconds from the origin to $\theta_{\text{des}} = 135\,\text{deg}$ about an axis given as $\epsilon_{\text{des}} = [3 \quad 2 \quad 1]^T$, which is also outside of the convergence region. The desired position changes simultaneously to $r_{\text{des}} = [3 \quad 2 \quad 1]^T$.

Simulation Results for the Translation Dynamics The simulation results for the underactuated case, i.e. Proposition 3-4.1, are shown in Figure 3-2 for the attitude dynamics. The results for the translation dynamics can be found in Appendix D, Figure D-3, as these are very similar to the results obtained using MRPs, and the discussion in Subsection 2-4 equally applies.

Payload Attitude Tracking Error Dynamics The payload angular velocity and MRPs are shown in Figure 3-2a and Figure 3-2b respectively. The payload attitude is purposefully represented in terms of MRPs, rather than plotting all nine elements of the rotation matrix. It can be seen that the payload attitude stabilizes at the desired equilibrium, and the performance is seen to be similar to the case where the leader controls the payload alone (illustrated by the colored dashed lines).

Amplification of the Leader Control Effort Figure 3-2c shows the leader torque, and Figure 3-2d shows the leader attitude tracking error $e_{R,l} = \mathbb{P}_a\{E_l\} = \mathbb{P}_a\left\{R_{\text{des}}^T R_o\right\}$. The colored dashed lines, corresponding to the case where the leader is controlling the payload alone, show that the leader control effort is indeed lowered by a factor of approximately the total number of agents, without a significant loss of performance. Comparison of the leader tracking error with the payload attitude clearly illustrates the difference between the geometric approach, and the use of MRPs. While the MRPs are increasing from $0\,\text{deg}$ to $135\,\text{deg}$, the tracking error $e_{R,l}$ first increases before converging to zero. This is due to the definition of the tracking error $e_{R,l} = \sin(\theta_l)\,\epsilon_l$ which has a maximum at $\theta_l = 90\,\text{deg}$.

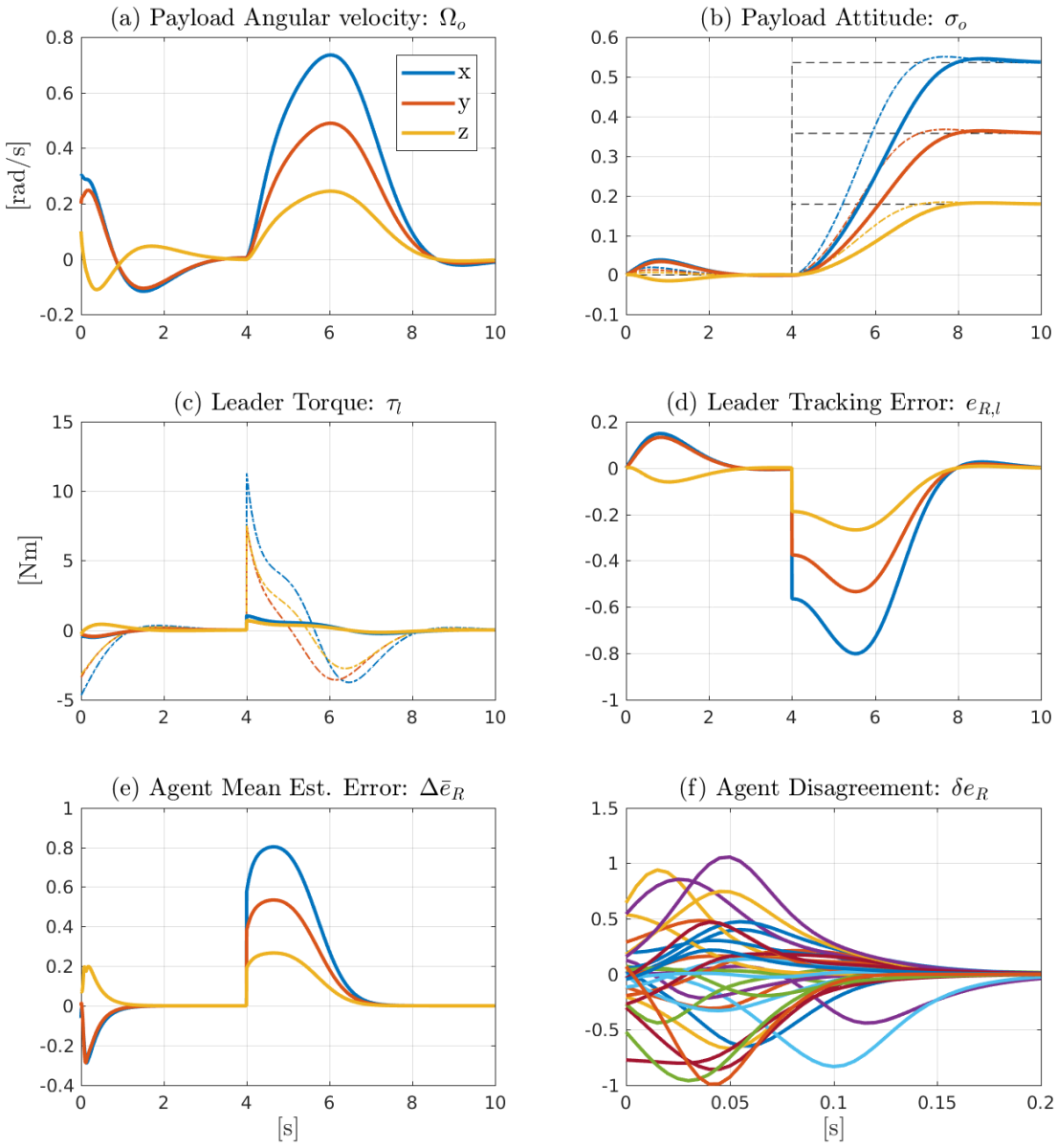

Figure 3-2: Simulation results of the attitude dynamics for the underactuated CMP (Proposition 3-4.1): From left to right and top to bottom the plots show, (a) the payload angular velocity, (b) the payload MRPs, (c) the torque applied by the leader, (d) the leader tracking error, (e) the mean of the agent's estimation errors, and (f) the disagreement of the agent's estimation errors. The three colors, blue red and yellow, represent the x, y and z directions of the corresponding three dimensional vectors. The black dashed line in the attitude plot shows the leader reference MRPs. It can be seen that the leader applies a reference step to the desired payload attitude at $t = 4$[s], corresponding to a $\theta = 135\,\text{deg}$ rotation about the $\epsilon = [3 \quad 2 \quad 1]^T$ axis. The colored dashed lines in the payload attitude and leader torque plot show the simulation result for the case that the leader is controlling the payload alone.

Consensus Dynamics of the Estimation Error Figure 3-2e shows the mean estimation error, defined as

$$\Delta\bar{e}_R = \frac{1}{n_f}\sum_{i=1}^{n_f}\mathbb{P}_a\left\{E_l^T E_i\right\} = \frac{1}{n_f}\sum_{i=1}^{n_f}\mathbb{P}_a\left\{R_{\text{des}}^T R_{\text{des},i}\right\} \tag{3-71}$$

where $R_{\text{des},i}$ denotes the i^{th}-agent's estimate of the desired payload attitude. Figure 3-2f shows the disagreement vectors of the follower agents, defined as

$$\delta e_{R,i} \quad = \quad \mathbb{P}_a\left\{R_{\text{des}}^T R_{\text{des},i}\right\} - \Delta\bar{e}_R \tag{3-72}$$

resulting in many lines of different colors. The difference in tracking performance between the case where the leader is controlling the payload alone, and the CMP can be seen to be caused by the time required for the estimation error to converge. Both the estimation error and disagreement dynamics show the same behavior as the leader tracking error: Since all agents were initialized at angles larger that $\pm 90\,\text{deg}$ it is expected that direct convergence to the desired equilibrium will result in the errors as defined in (3-71) and (3-72) to first increase, before converging to zero. This is again due to the definition of the a-symmetric operator $\mathbb{P}_a\{\cdot\} = \sin(\theta)\,\epsilon$, which has the extrema at $\pm 90\,\text{deg}$. This illustrates the difficulty in assessing the estimation error and disagreement dynamics on $SO(3)$.

Summary of the Simulation Results From the simulation results Figure 3-2 it can be concluded that the consensus law given in Proposition 3-4.1 can recover from large initial estimation errors and allows for large changes in the desired payload configuration. With the observer dynamics chosen to be faster than the payload dynamics it is shown that the leader control effort is amplified. Furthermore, it is shown that the system convergences to the desired equilibrium, even if all signals are chosen outside of the convergence region upon which the proof depended.

3-7 Conclusion

This chapter considered the use of the rotation matrix for the control law design, resulting in a global system description. It was shown that without a leader, an almost globally converging synchronization law could be formulated. With the addition of a leader a proof of global convergence could not be obtained. The convergence could only be proven if the attitude tracking errors remained within $\pm\frac{1}{2}\pi$. Within that region a bound on the convergence rate was derived. The proposed method for the fully actuated case could directly be extended to the underactuated case, but depended on the same region of convergence. From the construction of the consensus law, and the simulations, there is a strong incentive that the system always converges to the desired equilibrium. The challenge in completing the proof was traced back to:

- The inability to decouple the payload motion from the consensus dynamics, which directly obstructed proving invariance of the convergent region.
- The evaluation of the disagreement on $SO(3)$, which can diverge even when the agents are converging to the desired state.

Despite the restriction of the proof, the convergence region is relatively large, much larger than a linear region. In fact, to leave the region of convergence effectively means that the overshoot is more than $\frac{1}{2}\pi$. For all practical considerations, this region should be large enough. Nevertheless, further research is required for a completing the proof.

Chapter 4

Payload State Measurements as a Means of Communication

The aim of this chapter is to relax the assumption of requiring acceleration measurements. The proposed approach is to design a local observer for reconstructing the desired payload configuration. The challenge in reconstructing the desired payload configuration is that this information appears in the payload dynamics in a nonlinear fashion. Geometric observer approaches, such as [35], [36], enable to reconstruct rotation matrices on the nonlinear manifold, and are provided with an elegant proof. These methods show similarity to the geometric approach in Chapter 3, and should be considered as kinematic approaches, requiring direct information exchange. These methods are not trivially extended to the use of arbitrary measurements. Nonlinear Kalman filters in combination with quaternions are considered a powerful tool for attitude reconstruction using arbitrary state measurements [37]. The focus of these methods is to construct locally optimal estimates of the state through linearization. This limits the proof to a local convergence region. For these reasons it is chosen to use the Modified Rodrigues Parameters (MRPs) to represent the attitude of payload. The additive attitude tracking error again resulting in a significant simplification of the problem. With this choice, the results suffer from the same limitations as discussed in Section 2-1 and Assumption 2-1.1 is considered to hold. Finally, no method was found to analytically, and globally, reconstruct the Coriolis terms. As such, the Coriolis terms are canceled from the payload motion, as was done in the previous chapters. In case of velocity measurements the estimation error dynamics result in a second order consensus problem, comparable to that seen in cooperative vehicle control problems. For arbitrary measurements the result is a higher order consensus problem, which gives rise to a simultaneous stabilization problem. A short literature review reveals that the problem of finding stabilizing feedback gains is nonlinear and difficult to solve in general.

As in the previous chapters, the robot dynamics are neglected, and the MRPs are used to represent the payload attitude. The fully actuated case is considered first, leading to a globally converging solution. Similarly to Subsection 2-3 the underactuated case results in a

state dependent Laplacian matrix, and the system is shown to converge only locally. Alternatively, a Nonlinear Dynamic Inversion (NDI) based control law is proposed which allows for a separation of the disagreement, mean estimation error and tracking dynamics. Global convergence could be derived, at the cost of further dependency on model parameters.

The remainder of this chapter is structured as follows. In section 4-1 the fully actuated case is considered, resulting in global convergence. Subsequently, the proposed solution is extended to the underactuated case in Section 4-2 , but results in a restriction of the proof. The effect of assuming position measurements is discussed in Section 4-4. In Section 4-5 the simulation results are presented. This chapter concludes with a discussion on the presented results in Section 4-6.

4-1 Reconstructing the Desired Payload Configuration Assuming Velocity Measurements and Full Actuation

This section considers the fully actuated case, where the agents apply a wrench at the payload Center of Gravity (CoG). It is assumed that the payload velocities, as well as the attitude, are measurable for all agents. A separation of the estimation error dynamics from the payload motion results merely in boundedness of the estimation errors. Similarly as was done in Subsection 2-2, a small coupling gain is introduced to prove global convergence. Although the control- and observer gains can be chosen individually, it is shown that the observer gains must satisfy a constraint related to the control gains of the other agents. The observer gain can always be chosen to satisfy this constraint, and is thus considered to be non-restrictive.

The remainder of this section is structured as follows. The agent control laws, and the reduced payload dynamics are introduced in Subsection 4-1-1. The objectives for the Cooperative Manipulation Problem (CMP) are defined in Subsection 4-1-2, and subsequently the proposed consensus law is given in Subsection 4-1-3. This section concludes with a short discussion on the proposed solution, and a comparison with cooperative vehicle control in Subsection 4-1-4.

4-1-1 Agent Control Laws and Reduced Payload Dynamics

The payload equations of motion are as given in Subsection 2-2-1, and it is assumed that the agents apply a wrench at the payload CoG without loss of generality. The leader control law is as given in Subsection 2-2-2, equation (2-3). The follower agent's control law has the same structure as that of the leader, but partially relies on the estimates obtained from the observer,

$$w_i = \frac{1}{n_f+1}\left(C\left(\nu_o\right)+G\right) - M\left(\zeta_i\hat{\nu}_i + K_i J_o\left(q_o\right)^T \hat{e}_i\right), \qquad i \in \{1,\ldots,n_f\} \tag{4-1}$$

where $\hat{\nu}_i$ and $\hat{e}_i$ are the local estimates of the payload velocity and the leader tracking error, as indicated by the hat[1] , and otherwise the variables are as introduced in Subsection 2-2-2. For the proposed control law in the following, it should hold that $KJ_o\left(q_o\right) = J_o\left(q_o\right)K$, i.e. these

[1]The hat is used in this chapter to explicitly indicate the local estimates. In the previous chapters this was assumed to be clear from context, and the hat was omitted.

matrices must commute, resulting in the structure given in (2-6). Furthermore, it is assumed that the control gains are positive definite, diagonal matrices. Substitution of the leader and follower control laws into the payload dynamics gives the reduced payload equations of motion as,

$$\begin{aligned} \dot{\nu}_o &= -\zeta_l \nu_o - J_o(q_o)^T K_l e_l - \sum_{i=1}^{n_f} \left[\zeta_i \hat{\nu}_i + J_o(q_o)^T K_i \hat{e}_i \right] \\ \dot{e}_l &= J_o(q_o)\, \nu_o \end{aligned} \tag{4-2}$$

where $e_l = q_o - q_l$ is the leader tracking error and all other variables are as defined in Subsection 2-2-2.

4-1-2 Mathematical Objectives for the Cooperative Manipulation Problem

With the introduction of an observer it is chosen to decouple the objective as follows,

Objectives 4-1.1. *Consider the CMP described by the reduced description* (4-2)*. The stability of the system follows if the*

$$\begin{aligned} &\textit{estimation errors:} && \Delta e_i = \hat{e}_i - e_l, \\ & && \Delta \nu_i = \hat{\nu}_i - \nu_o, \\ &\textit{and tracking error:} && e_l = q_o - q_{des} \end{aligned} \tag{4-3}$$

converge to zero.

4-1-3 Proposed Consensus Law Assuming Full Actuation and Velocity Measurements

It is proposed to design an observer for meeting the Objectives 4-1.1. The observer can be constructed as a local copy of the payload dynamics given in (4-2), with an observer correction term. This leads to the following proposed consensus law:

Proposition 4-1.1. *Consider the CMP of the payload using n_f follower agents and a single leader, resulting in the reduced payload dynamics given in (4-2). Assume the agents to have access to measurements of the payload velocities $\nu_o = \begin{bmatrix}\Omega_o^T & v_o^T\end{bmatrix}^T$ and payload attitude σ_o. Let the follower agents locally update the estimates $\hat{\nu}_i$ and $\hat{e}_i$ as*

$$\begin{aligned}\dot{\hat{\nu}}_i &= -\zeta_{sum}\hat{\nu}_i - K_{sum}J_o(q_o)^T\hat{e}_i - \Gamma_{v,i}\Delta\nu_i + \epsilon_{\nu,i}\nu_o \\ \dot{\hat{e}}_i &= J_o(q_o)\hat{\nu}_i + \Gamma_{e,i}J_o(q_o)\Delta\nu_i + \epsilon_{e,i}J_o(q_o)\nu_o\end{aligned} \tag{4-4}$$

where $\Delta\nu_i = \hat{\nu}_i - \nu_o$ is the measurement error, $K_{sum} = K_l + \sum_{i=1}^{n_f} K_i > 0$ is the sum of the control gains, $\epsilon_{e,i} \geq 0$ and $\epsilon_{\nu,i} \geq 0$ are diagonal coupling matrices, and $\Gamma_{e,i}$ is a gain matrix structured as given in (2-6). Furthermore, $\Gamma_{v,i} \in \mathbb{R}^{6\times 6}$ is a diagonal matrix for which the following inequality holds,

$$\Gamma_{v,i} > -\zeta_l - \tfrac{1}{2}\sum_{j=1}^{n_f}\zeta_j + \tfrac{1}{2}K_i^{-1}(\Gamma_{e,i}+I)^{-1}\left(\sum_{j=1}^{n_f}(\Gamma_{e,j}+I)K_j\right)\zeta_i. \tag{4-5}$$

Then, there exist arbitrarily small $\epsilon_{e,i} > 0$ and $\epsilon_{\nu,i} > 0$ such that the Objectives 4-1.1 are globally achieved.

Underlying Consensus Law

The Exchange of local information can be made visible through the estimation error dynamics. Considering the payload dynamics (4-2) and the observer dynamics (4-4) the estimation error dynamics is obtained as

$$\begin{aligned}\Delta\dot{\nu}_i &= -(\zeta_l + \Gamma_{v,i})\Delta\nu_i - K_l J_o(q_o)^T\Delta e_i - \sum_{j=1}^{n_f}\left[\zeta_j(\Delta\nu_i - \Delta\nu_j) + K_j J_o(q_o)^T(\Delta e_i - \Delta e_j)\right] + \epsilon_{\nu,i}\nu_o \\ \Delta\dot{e}_i &= (I_{6\times 6} + \Gamma_{e,i})J_o(q_o)\Delta\nu_i + \epsilon_{e,i}\dot{q}_o\end{aligned} \tag{4-6}$$

with $\Delta\nu_i$ and Δe_i as defined in the Objectives 4-1.1. Setting $\epsilon_{e,i} = 0$ and $\epsilon_{\nu,i} = 0$ reveals a second order consensus problem, where all agents exchange information on Δe_i and $\Delta\nu_i$, and use this to control the acceleration $\Delta\dot{\nu}_i$. The similarities and differences with the literature will be further discussed at the end of this section, after the proof has been completed.

Proof of Convergence

The complete proof of boundedness of the estimation error dynamics in (4-6) is shown in Appendix B-2-1. The proof is constructed via the Lyapunov candidate given as,

$$V_\Delta = V_e + V_\nu \qquad \begin{cases} V_e = \tfrac{1}{2}\Delta e^T\left(L_w^{(e)} + P_e\right)\Delta e \\ V_\nu = \tfrac{1}{2}\sum_{i=1}^{n_f}\Delta\nu_i^T(\Gamma_{e,i} + I_{6\times 6})K_i\Delta\nu_i \end{cases} \tag{4-7}$$

where $P_e \in \mathbb{R}^{6n_f \times 6n_f}$ and $(\Gamma_{e,i} + I_{6\times 6})\, K_i$ are diagonal positive definite matrices, and $L_w^{(e)}$ is the weighted Laplacian matrix for the complete graph as given in Definition A-1.4 by substituting $a_i = K_i$ in the definition. Taking the time derivative of V_Δ with $\epsilon_{e,i} = 0$ and $\epsilon_{\nu,i} = 0$ gives

$$\dot{V}_\Delta = -\Delta\nu^T \left(L_w^{(\nu)} + Q_\nu\right) \Delta\nu \tag{4-8}$$

where $L_w^{(\nu)}$ is a weighted Laplacian matrix associated with the complete graph. If the constraint (4-5) holds it follows that the matrix Q_ν is a diagonal positive definite matrix, see Appendix B-2-1. From V_Δ and $\dot{V}_\Delta$ it merely follows that $\Delta\nu$ is bounded. LaSalle's invariance principle can not be applied due to the dependency of the estimation error dynamics (4-6) on the payload state q_o. Barbalat's Lemma A-5.2 can not be applied, because unbounded q_o leads to unbounded $\ddot{V}$. Similarly as was done in Section 2-2 the consensus dynamics will be coupled to the payload motion through $\epsilon_{e,i}$ and $\epsilon_{\nu,i}$, as a means to guarantee that q_o remains finite. This allows for a global proof of convergence to the desired equilibrium for arbitrarily small $\epsilon_{e,i}$ and $\epsilon_{\nu,i}$. The complete proof is provided in Appendix B-2-2.

4-1-4 Remarks on the Proposed Solution for the Fully Actuated Case

Interpretation of the Coupling Gain As discussed in Chapter 2, the intention was to decouple the consensus dynamics from the payload motion. However, in constructing the proof it was found that the coupling must be reestablished through a small gain ϵ, and the same discussion posed in Subsection 2-2-5 applies.

Interpretation of the Constraint on the Observer Gain The posed inequality constraint (4-5) shows that the observer gain should be chosen such that it captures the dynamics of agents that are faster. This can be seen from the summation over K_j and $\Gamma_{e,j}$ for the i^{th}agent. Furthermore, note from the above expression that if all gains K_i, $\Gamma_{e,i}$, ζ_i are chosen equal for all i, that the observer gain reduces to

$$\Gamma_{v,i} > -\zeta_l \tag{4-9}$$

For the case of all gains chosen equal any positive definite observer gain suffices. The fact that a negative gain is possible is correct, but it would be unwise, as this removes the damping that is injected by the leader.

Comparison with Cooperative Vehicle Control It should be noted that the estimation error dynamics show a great similarity to that considered in general cooperative vehicle control, such as [29] for attitude control of multiple satellites via quaternions. The estimation error dynamics was shown to be given as

$$\begin{aligned} \Delta\dot{\nu}_i &= -\left(\zeta_l + \Gamma_{v,i}\right)\Delta\nu_i - K_l J_o\left(q_o\right)^T \Delta e_i - \sum_{j=1}^{n_f} \left[\zeta_j \left(\Delta\nu_i - \Delta\nu_j\right) + K_j J_o\left(q_o\right)^T \left(\Delta e_i - \Delta e_j\right)\right] \\ \Delta\dot{e}_i &= \left(I_{6\times 6} + \Gamma_{e,i}\right) J_o\left(q_o\right) \Delta\nu_i \end{aligned} \tag{4-10}$$

The interpretation when comparing to [29] is that the local estimation errors take the role of distinct vehicles. The vehicles are then coupled by exchanging their velocities and positions

and using their relative difference directly as the control input to the vehicle. There are two main differences: Firstly, the individual scaling in the kinematics is unusual, here caused by $\Gamma_{e,i}$, since the kinematics are the same for each vehicle. Secondly, the kinematics are seen to be coupled to the payload through $J_o(q_o)$, while the payload motion does not effect the consensus dynamics otherwise. Naturally, in cooperative vehicle control the matrix $J_o(q_o)$ would be replaced by the individual vehicle jacobian matrix.

4-2 Reconstructing the Desired Payload Configuration Assuming Velocity Measurements and Underactuation

This section extends the approach outlined in the previous section to the underactuated case, where the agents can apply forces at the attachment points, rather than a wrench. The proposed approach is identical to that in Section 2-3: The agents use the generalized inverse to compute the desired force at the attachment point, and by taking identical observer gains the disagreement problem can be isolated. It will be shown that, due to the nonlinear system description only local stability can be concluded, forming a restriction of this solution. The method of adding a small coupling gain is not applicable due to the complexity of the Laplacian matrix associated with the consensus dynamics.

The remainder of this section is structured as follows. The reduced payload dynamics is presented in Subsection 4-2-1. The objective for achieving cooperative manipulation of the payload is defined in Subsection 4-2-2, after which a solution is proposed in Subsection 4-2-3.

4-2-1 Reduced Payload Dynamics Assuming Underactuation

The payload dynamics for the underactuated case was given in (2-23), and the design approach follows the same steps as outlined in Section 2-3. To this end, let the followers make use of the generalized inverse to convert the control law for the desired wrench given in (4-1) to a force at the agent's attachment point. Whereas the leader is still represented as a wrench acting at the payload CoG. This results in the reduced payload dynamics given as

$$\begin{aligned} \dot{\nu}_o &= -\zeta_l \nu_o - J_o(q_o)^T K_l e_l - \sum_{i=1}^{n_f} W_i(q_o)\left[\zeta \hat{\nu}_i + J_o(q_o)^T K \hat{e}_i\right] \\ \dot{e}_l &= J_o(q_o)\,\nu_o \end{aligned} \tag{4-11}$$

where

$$W_i(R_o) = n_f M^{-1} J_{p_i}(R_o)^T J_{p_i}(R_o)^{\dagger} M. \tag{4-12}$$

and it is assumed that the follower control gains ζ and K are identical.

4-2-2 Mathematical Objective for the Cooperative Manipulation Problem

Let the objectives for the proposed consensus law be given as,

Objectives 4-2.1. *Consider the CMP with underactuation as described by the reduced description* (4-11)*. Define the payload state and local estimated state as,*

$$x_o = \begin{bmatrix} \nu_o^T & e_l^T \end{bmatrix}^T, \qquad \hat{x}_i = \begin{bmatrix} \hat{\nu}_i^T & \hat{e}_i^T \end{bmatrix}^T \tag{4-13}$$

respectively. The stability of the system follows if the

$$\begin{aligned} &\textit{disagreement:} && \delta x_i = \hat{x}_i - \tfrac{1}{n_f} \sum_{j=1}^{n_f} \hat{x}_j, \\ &\textit{mean estimation error:} && \Delta \bar{x}_i = \tfrac{1}{n_f} \sum_{i=1}^{n_f} \hat{x}_j - x_o, \\ &\textit{and tracking error:} && e_l = q_o - q_{des} \end{aligned} \tag{4-14}$$

all converge to zero.

4-2-3 Proposed Consensus Law Assuming Underactuation and Velocity Measurements

The observer for the underactuated case is similar to the fully actuated case, but instead the observer gains are identical for all agents:

Proposition 4-2.1. *Consider the CMP of the payload using n_f agents with underactuation and a single leader, resulting in the reduced dynamics* (4-11)*. Let the followers apply the proposed observer given in Proposition 4-1.1, but with identical observer gains for all agents:*

$$\begin{aligned} \dot{\hat{\nu}}_i &= -\zeta_{sum}\nu_i - K_{sum} J_o(q_o)^T \hat{e}_i - \Gamma_\nu \Delta\nu_i \\ \dot{\hat{e}}_i &= J_o(q_o)\,\hat{\nu}_i + \Gamma_e J_o(q_o)\,\Delta\nu_i \end{aligned} \tag{4-15}$$

where $\Delta\nu_i = \hat{\nu}_i - \nu_o$ is the measurement error, $K_{sum} = K_l + n_f K > 0$ is the sum of the control gains, $\Gamma_{v,} > 0$ and $\Gamma_{e,} > 0$ are the observer gain matrices, where $\Gamma_{e,} > 0$ is structured as given in (2-6)*. Then, considering the Objectives 4-2.1, local convergence to the desired equilibrium is achieved.*

Underlying Consensus Dynamics The interconnection between the agents is revealed by following the same steps outlined in Subsection 2-3-4. From the payload dynamics (4-11) and the observer dynamics (4-15) the estimation error dynamics is obtained as

$$\begin{aligned} \Delta\dot{\nu}_i &= -(\zeta_l + \Gamma_\nu)\Delta\nu_i - K_l J_o(q_o)^T \Delta e_i - \sum_{j=1}^{n_f} W_j(q_o)\left[\zeta(\Delta\nu_i - \Delta\nu_j) + K J_o(q_o)^T(\Delta e_i - \Delta e_j)\right] \\ \Delta\dot{e}_i &= (I_{6\times 6} + \Gamma_e) J_o(q_o)\,\Delta\nu_i \end{aligned} \tag{4-16}$$

where the matrices $W_i(q_o)$ are defined in (4-12). Similarly to the previous section, the result is a second order consensus problem, where the associated Laplacian matrix would be characterized as a state dependent, weighted non symmetric Laplacian matrix with non-symmetric, rank-deficient matrix weights.

Local Convergence of the Disagreement Dynamics

The disagreement dynamics of the follower agents can be obtained from the local update law (4-15) by left multiplication of the estimation error dynamics with the Laplacian matrix for the complete graph, as was done in Subsection 2-3-4. Since the observer gains were assumed to be identical the measurement ν_o drops from the dynamics, resulting in the following disagreement dynamics for the i^{th}-agent,

$$\begin{aligned} \delta\dot{\nu}_i &= -\left(\zeta_{\text{sum}} + \Gamma_\nu\right)\delta\nu_i - K_{\text{sum}} J_o\left(q_o\right)^T \delta e_i \\ \delta\dot{e}_i &= \left(I_{6\times 6} + \Gamma_e\right) J_o\left(q_o\right)\delta\nu_i \end{aligned} \tag{4-17}$$

Consider the Lyapunov function given as

$$V_{\delta,i} = \tfrac{1}{2}\delta\nu_i^T\delta\nu_i + \tfrac{1}{2}\delta e_i^T P_e \delta e_i \geq 0 \tag{4-18}$$

where $P_e = \left(I_{6\times 6} + \Gamma_e\right)^{-1} K_{\text{sum}}$ which is symmetric positive definite. Taking the time derivative of $V_{\delta,i}$, and substitution of the disagreement dynamics (4-17), gives

$$\dot{V}_{\delta,i} = -\delta\nu_i^T\left(\zeta_{\text{sum}} + \Gamma_\nu\right)\delta\nu_i \leq 0 \tag{4-19}$$

where it was used that $J_o(q_o)$ commutes with K_{sum}, as it abides by the structure given in (2-6). From $\dot{V}_{\delta,i}$ and $V_{\delta,i}$ it can be concluded that $\delta\nu_i$ and δq_i are bounded. However, LaSalle's can not be used, as the payload configuration state form an exogenous signal to the disagreement dynamics (4-17). Linearizing about the equilibrium state given as $\delta x_i = 0$, $\nu_o = 0$ and $q_o = q_{\text{des}}$ allows for the proof of local convergence.

Local Convergence of the Estimation Error Dynamics

Since the system must be linearized to obtain the proof of convergence, the separation theorem for linear systems can be applied. Therefore, in the following the disagreement vectors are simply set to zero. Following the decoupling of the objectives, the mean estimation error dynamics can be obtained from the complete estimation error dynamics (4-16), resulting in

$$\left.\begin{aligned} \Delta\dot{\bar{\nu}} &= -\left(\zeta_l + \Gamma_\nu\right)\Delta\bar{\nu} - K_l J_o\left(q_o\right)^T \Delta\bar{e} \\ \Delta\dot{\bar{e}} &= \left(I_{6\times 6} + \Gamma_e\right) J_o\left(q_o\right)\Delta\bar{\nu} \end{aligned}\right\} \quad \text{if} \quad \{\delta\nu_i, \delta e_i\} = 0 \tag{4-20}$$

Note the similarity between the above dynamics, and the disagreement dynamics (4-17). It thus follows that linearization about the equilibrium state results in local convergence of the mean estimation errors.

Local Convergence of the Payload to the Desired Configuration

It remains to show that the payload reaches the desired configuration, that is, that the leader tracking error converges to zero. From the payload dynamics (4-11), it can be seen that if $e_i = e_l, \forall i$, i.e. all agents have converged to the leader, the payload dynamics reduce to

$$\dot{\nu}_o = -\zeta_{\text{sum}}\nu_o - K_{\text{sum}} J_o(q_o)^T e_l, \qquad \text{if} \quad \begin{cases} \{\delta\nu_i, \delta e_i\} = 0, \\ \\ \{\Delta\nu_i, \Delta e_i\} = 0 \end{cases} \tag{4-21}$$

which is again similar to (4-20) and (4-17). Through similar arguments it can be shown that local convergence of the payload tracking error follows, i.e. $\lim_{t\to\infty} \nu_o = 0$ and $\lim_{t\to\infty} e_l = 0$. This completes the proof of Proposition 4-2.1.

4-3 Nonlinear Dynamic Inversion (NDI) for the Underactuated Case

The previously outlined strategy proposed to separate the consensus dynamics from the payload dynamics. It was found to be difficult to show that the payload state remains bounded during the convergence of the consensus dynamics. With the introduction of the coupling gains this could still be guaranteed. However, for the underactuated system such a coupling gain is not easily introduced. As an alternative, this section considers NDI to remove the kinematics from the problem, and impose linear dynamics onto the configuration state. Although this further simplifies the system dynamics, all the complexity is concentrated in the applied wrench instead. For this reason the proposed method is considered as less favorable to that of the previous section. Nevertheless, it was found to lead to a guarantee of global convergence for the underactuated case. The problem setting is the same as outlined in the previous section.

The agent control laws and the reduced payload dynamics is shown in the following subsection. The objective for the CMP is similar to the Objectives 4-2.1, and the proposed solution is presented in Subsection 4-3-2.

4-3-1 Agent Control Laws and the Reduced Payload Dynamics

The payload equations of motion can be given in terms of the configuration coordinates as

$$\breve{M}_o(q_o)\,\ddot{q}_o = -\breve{C}_o(\dot{q}_o, q_o) - G_o + J_o(q_o)^{-T}\left(w_l + \sum_{i=1}^{n_f} J_{p_i}(q_o)^T F_{p_i}\right) \tag{4-22}$$

with $\breve{M}_o(q_o)$ and $\breve{C}_o(\dot{q}_o, q_o)$ denote the mass tensor and Coriolis terms, which are explicitly given in Appendix A-4-3, $J_o(q_o)$ is given in (A-34), $J_{p_i}(q_o)^T$ is the adjoint matrix given in (A-38), and F_{p_i} is the i^{th}-agent's force at the corresponding attachment point. Let the leader wrench be given as

$$w_l = \tfrac{1}{1+n_f} J_o(q_o)^T\left(\breve{C}_o(\dot{q}_o, q_o) + G_o\right) - J_o(q_o)^T \breve{M}_o(q_o)\left(\zeta_l \dot{q}_o - K_l e_l\right) \tag{4-23}$$

with $e_l = q_o - q_{\text{des}}$ the leader tracking error. The followers compute the force at the i^{th}-attachment point using the generalized inverse (2-25) as,

$$F_{p_i} = n_f J_{p_i}(q_o)^{\dagger} w_i \tag{4-24}$$

where w_i is the i^{th}-agent's estimate of the desired wrench at the payload CoG, and is computed using a similar structure as (4-23). This reduces the underactuated payload dynamics (4-22) to,

$$\begin{aligned} \ddot{q}_o &= -\zeta_l \dot{q}_o - K_l e_l - \sum_{i=1}^{n_f} W_i(q_o)\left(\zeta \dot{\hat{q}}_i + K \hat{e}_i\right) \\ \dot{e}_l &= \dot{q}_o \end{aligned} \tag{4-25}$$

where $\hat{e}_i$ and $\dot{\hat{q}}_i$ are the i^{th}-agent's local estimates of the tracking error and generalized velocities respectively, and the matrices $W_i(q_o)$ are given as

$$W_i(q_o) = n_f \breve{M}_o(q_o)^{-1} J_o(q_o)^{-T} J_{p_i}(q_o)^T J_{p_i}(q_o)^{\dagger} J_o(q_o)^T \breve{M}_o(q_o) \tag{4-26}$$

The expression above is rather unwieldy, but important to note is that $\sum_{i=1}^{n_f} W_i(q_o) = n_f I_{6\times 6}$ and that it is bounded even for unbounded q_o. The boundedness of $W_i(q_o)$ is derived in Appendix B-2-3.

4-3-2 Proposed Consensus Law Assuming Velocity Measurements and NDI

Consider the Objectives 4-2.1 with $x_o = \begin{bmatrix} \dot{q}_o^T & e_l^T \end{bmatrix}^T$, and $\hat{x}_i = \begin{bmatrix} \dot{\hat{q}}_i^T & \hat{e}_i^T \end{bmatrix}^T$. The proposed solution to meet these objectives is then given as:

Proposition 4-3.1. *Consider the CMP of the payload using n_f follower agents and a single leader, resulting in the reduced payload dynamics given in* (4-25)*. Assume the agents to have access to measurements of the payload velocities $\dot{q}_o$ and payload attitude σ_o. Let the follower agents locally update the estimates $\dot{\hat{q}}_i$ and $\hat{e}_i$ as*

$$\begin{aligned} \ddot{\hat{q}}_i &= -\zeta_{sum} \dot{\hat{q}}_i - K_{sum} \hat{e}_i - \Gamma_\nu \Delta \dot{q}_i \\ \dot{\hat{e}}_i &= \dot{\hat{q}}_i + \Gamma_e \Delta \dot{q}_i \end{aligned} \tag{4-27}$$

where $\Delta \dot{q}_i = \dot{\hat{q}}_i - \dot{q}_o$ is the measurement error, Γ_e, Γ_ν, $K_{sum} = K_l + n_f K$ and $\zeta_{sum} = \zeta_l + n_f \zeta$ are diagonal positive definite matrices of dimension 6×6. Then, the Objectives 4-2.1 are globally achieved.

The proof in the following is constructed following the separation of the disagreement, mean estimation error and payload tracking dynamics, as reflected by the Objectives 4-2.1.

Underlying Consensus Dynamics

The consensus dynamics is obtained from the payload dynamics (4-25) and the consensus law (4-27), resulting in the estimation error dynamics given as

$$\begin{aligned} \Delta\ddot{q}_i &= -\left(\zeta_l + \Gamma_\nu\right)\Delta\dot{q}_i - K_l\Delta e_i - \sum_{j=1}^{n_f} W_j\left(q_o\right)\left(\zeta\Delta\dot{q}_j + K\Delta e_j\right) \\ \Delta\dot{e}_i &= \left(I_{6\times 6} + \Gamma_e\right)\Delta\dot{q}_i \end{aligned} \tag{4-28}$$

where $\Delta\dot{q}_i = \hat{\dot{q}}_i - \dot{q}_o$ and $\Delta e_i = \hat{e}_i - e_l$ are the local estimation errors, and $W_i\left(q_o\right)$ is given in (4-26).

Proof of Global Convergence of the Disagreement Dynamics

The disagreement dynamics of the follower agents can be obtained from the local update law (4-27) by left multiplication with the Laplacian matrix for the complete graph, as was done in Subsection 2-3-4. Since the observer gains were assumed to be identical the measurement $\dot{q}_o$ drops from the dynamics, resulting in the following disagreement dynamics for the i^{th}-agent,

$$\begin{aligned} \delta\ddot{q}_i &= -\left(\zeta_{\text{sum}} + \Gamma_\nu\right)\delta\dot{q}_i - K_{\text{sum}}\delta e_i \\ \delta\dot{e}_i &= \left(I_{6\times 6} + \Gamma_e\right)\delta\dot{q}_i \end{aligned} \tag{4-29}$$

The disagreement dynamics given above are linear in $\delta\dot{q}_i$ and δe_i, and all matrices ζ_{sum}, K_{sum}, Γ_ν and Γ_e are assumed to be positive definite diagonal matrices. Considering Objectives 4-2.1, it can thus be concluded that the disagreement dynamics globally converge to the origin.

Proof of Global Convergence of the Estimation Error Dynamics

The estimation error dynamics given in (4-28) can be written in terms of the mean estimation error and the disagreement vectors as defined in the Objectives 4-2.1, resulting in,

$$\begin{aligned} \Delta\ddot{\bar{q}} &= -\left(\zeta_{\text{sum}} + \Gamma_\nu\right)\Delta\dot{\bar{q}} - K_{\text{sum}}\Delta\bar{e} - \sum_{j=1}^{n_f} W_j\left(q_o\right)\left(\zeta\delta\dot{q}_j + K\delta e_j\right) \\ \Delta\dot{\bar{e}} &= \left(I_{6\times 6} + \Gamma_e\right)\Delta\dot{\bar{q}} \end{aligned} \tag{4-30}$$

Consider the Lyapunov candidate given as

$$V_\Delta = \tfrac{1}{2}\Delta\dot{\bar{q}}^T P_1\Delta\dot{\bar{q}} + \tfrac{1}{2}\Delta\bar{e}^T P_2\Delta\bar{e} + \tfrac{1}{2}\left\|\Delta\dot{\bar{q}} + P_3\Delta\bar{e}\right\|^2 \tag{4-31}$$

with P_1, P_2 and P_3 diagonal positive definite matrices, explicitly given in Appendix B-2-4. Taking the time derivative of V_Δ, and substitution of (4-30) gives,

$$\begin{aligned} \dot{V}_\Delta &= -\Delta\dot{\bar{q}}^T Q_1\Delta\dot{\bar{q}} - \left\|\Delta\dot{\bar{q}} + P_3\Delta\bar{e}\right\|_{Q_2}^2 \\ &\quad - \left(P_1\Delta\dot{\bar{q}} + \left(\Delta\dot{\bar{q}} + P_3\Delta\bar{e}\right)\right)^T \times \underbrace{\sum_{j=1}^{n_f} W_j\left(q_o\right)\left(\zeta\delta\dot{q}_j + K\delta e_j\right)}_{\text{bounded}} \end{aligned} \tag{4-32}$$

where $\|\cdot\|^2_{Q_2}$ denotes $(\cdot)^T Q_2(\cdot)$, and Q_1 and Q_2 are positive definite diagonal matrices, explicitly given in Appendix B-2-4. As it was established that $W_j(q_o)$ remains bounded (see Appendix B-2-3), and the disagreement vectors $\delta\dot{q}_i$ and δe_i remain bounded it can be concluded that the braced term in (4-32) indeed remains bounded. It then follows from V_Δ and $\dot{V}_\Delta$ that $\Delta\dot{\bar{q}}$ and $z = \Delta\dot{\bar{q}} + Q_3\Delta\bar{e}$ must remain bounded. This shows that $\Delta\bar{e}$ remains bounded, leading to the conclusion that all signals in the estimation error dynamics (4-30) remain bounded. Since the disagreement vectors converge globally to the origin it holds that $\lim_{t\to\infty} \dot{V}_\Delta \leq 0$. This shows that $\lim_{t\to\infty} \Delta\dot{q}_i = 0$ and $\lim_{t\to\infty} \left(\Delta\dot{\bar{q}} + Q_3\Delta\bar{e}\right) = 0$, and thus $\lim_{t\to\infty} \Delta\bar{e} = 0$. Considering Objectives 4-2.1, the conclusion is that the mean estimation errors globally converge to the origin.

Proof of Global Convergence of the Payload Tracking Dynamics

The convergence of the payload tracking error follows the same steps as for the mean estimation error dynamics. Consider writing the reduced payload dynamics given in (4-25) in terms of the estimation errors,

$$\begin{aligned} \ddot{q}_o &= -\zeta_{\text{sum}}\dot{q}_o - K_{\text{sum}} e_l - \sum_{i=1}^{n_f} W_i(q_o)\left(\zeta\Delta\dot{q}_i + K\Delta e_i\right) \\ \dot{e}_l &= \dot{q}_o \end{aligned} \tag{4-33}$$

where $\Delta\dot{q}_i = \delta\dot{q}_i + \Delta\dot{\bar{q}}$ and $\Delta e_i = \delta e_i + \Delta\bar{e}$, which were previously shown to be bounded. Consider the Lyapunov candidate given as

$$V = \tfrac{1}{2}\dot{q}_o^T P_4 \dot{q}_o + \tfrac{1}{2} e_l^T P_5 e_l + \tfrac{1}{2}\left\|\dot{q}_o + P_6 e_l\right\|^2 \tag{4-34}$$

with P_4, P_5, and P_6 positive definite diagonal matrices given as,

$$P_4 = \zeta_{\text{sum}}^{-2} K_{\text{sum}} + I, \qquad P_5 = K_{\text{sum}}, \qquad P_6 = \zeta_{\text{sum}}^{-1} K_{\text{sum}}. \tag{4-35}$$

Taking the time derivative of V, and substitution of (4-33) gives,

$$\begin{aligned} \dot{V}_\Delta &= -\dot{q}_o^T \zeta_{\text{sum}} \dot{q}_o - \left\|\dot{q}_o + P_6 e_l\right\|^2_{Q_3} \\ &\quad - \left(P_4\dot{q}_o + \left(\dot{q}_o + P_6 e_l\right)\right)^T \times \underbrace{\sum_{i=1}^{n_f} W_i(q_o)\left(\zeta\Delta\dot{q}_i + K\Delta e_i\right)}_{\text{bounded}} \end{aligned} \tag{4-36}$$

where $\|\cdot\|^2_{Q_3}$ denotes $(\cdot)^T Q_3(\cdot)$, and with $Q_3 = \zeta_{\text{sum}}^{-1}$. Note that the obtained equations V and $\dot{V}$ are of the same form as V_Δ and $\dot{V}_\Delta$ given in (4-31) and (4-32) respectively. Following a similar reasoning, the boundedness of the braced term in (4-36) leads to the conclusion that $\lim_{t\to\infty} \dot{q}_o = 0$ and $\lim_{t\to\infty} \left(\dot{q}_o + Q_3 e_l\right) = 0$, and thus $\lim_{t\to\infty} e_l = 0$. Considering the Objectives 4-2.1, this completes the proof.

4-4 The Simultaneous Stabilization Problem for Arbitrary State Measurements

It was shown in Chapter 2 that with acceleration measurements the estimation error dynamics give a first order consensus problem. It is not surprising that with velocity measurements a second order consensus problem arises. Naturally, for arbitrary state measurements a higher order consensus problem is found. However, in the latter case a new problem is encountered. Considering Objectives 4-2.1 it can be shown that the disagreement dynamics and the mean estimation error dynamics give two different systems, which should be simultaneously stabilized by the observer gains. In case of acceleration or velocity measurements any positive definite observer gain suffices, rendering the simultaneous stabilization problem irrelevant. For arbitrary state measurements this is no longer the case, and the observer gain should be chosen to simultaneously stabilize two plants.

The simultaneous stabilization problem received considerable attention in the literature, dating back to the 1980's [38]. From the literature it can be concluded that the simultaneous stabilization problem is in fact nonlinear and difficult to solve in general [39], [40], [41]. Methods that rely on root locus or Nyquist arguments tend to assess stability after the design, rather than present a guarantee before the design. For this reason the main focus is in numerical approaches. These approaches tend to consider a general class of systems, and since the problem is nonlinear and NP-hard [41], these solutions give no guarantee for solving the problem relevant for this thesis. A popular approach is to use a common Lyapunov function, which renders the problem convex [39], [42]. But, again, it is unclear how restrictive the use of a common Lyapunov function is, and whether it exists for an arbitrary system. Additionally these methods consider linear systems, and can not trivially be extended to nonlinear system descriptions. Given these findings, it is chosen not to further investigate global convergence results for the CMP assuming arbitrary state measurements. In Appendix B-2-5 it is shown that the Objectives 4-2.1 give rise to the simultaneous stabilization problem, by considering the linear translation dynamics.

4-5 Simulation Results for the Underactuated Case Assuming Velocity Measurements

This section presents the simulation results of Proposition 4-2.1, i.e. for the underactuated case. The results for Proposition 4-3.1, using the NDI based approach were found to be very similar and can be found in Appendix D.

The CMP is simulated with $n_f = 10$ follower agents applying a force at the attachment points, and a single leader as a wrench at the CoG. The aim of the simulation is to verify that consensus is reached and the leader control effort is amplified. Additionally it is illustrated that the system is able to handle large angles of rotation, despite the local convergence result. To this end, the agents are initialized with large attitude estimation errors ranging ± 180 deg, and the leader applies a large reference step of 60 deg for the desired attitude. The observer gains obtained using Linear Quadratic (LQ)-optimal pole placement, resulting in

$\Gamma_\nu = 2.27 \times I_{6\times6}$ and $\Gamma_e = 9.04 \times I_{6\times6}$. A detailed description of the simulation settings can be found in Appendix C.

Payload Tracking Error Dynamics The simulation results for the attitude dynamics and translation dynamics are presented in Figure 4-1 and Figure 4-2 respectively. It can be seen in Figure 4-1a and Figure 4-2a that the payload velocities converge to zero, and from Figure 4-1b and Figure 4-2b that the configuration converges to the reference. The colored dashed lines show the response of the system were the leader controls the payload alone, serving as a benchmark. The delay with respect to the benchmark can be traced to the time required for the estimation errors to converge.

Amplification of the Leader Control Effort The leader control effort and tracking errors are shown in the second row of plots in Figure 4-1 and Figure 4-2. Comparison of the leader control effort with the benchmark shows that the leader control effort is indeed lowered, with little performance loss.

Consensus Dynamics of the Estimation Error The consensus dynamics is reflected by the mean estimation error dynamics and the disagreement dynamics, shown in plots (e)-(h) in Figure 4-1 and Figure 4-2. The mean estimation error and disagreement for the angular velocity depicted in Figure 4-1e is computed as,

$$\Delta\bar{\Omega} = \tfrac{1}{n_f}\sum_{i=1}^{n_f}\left(\hat{\Omega}_i\right) - \Omega_o, \qquad \delta\Omega_i = \hat{\Omega}_i - \tfrac{1}{n_f}\sum_{j=1}^{n_f}\left(\hat{\Omega}_j\right) \tag{4-37}$$

and a similar definition holds for the estimation error and disagreement of, the attitude tracking error e_σ, the payload linear velocity v and the position tracking error e_r. From the disagreement dynamics it can be seen that the consensus dynamics is indeed of second order. The attitude dynamics show more chaotic behavior in the first few seconds of the simulation. This can be traced to the convergence of the disagreement dynamics, which takes more than a second. Note that, as long as the agents have not reached the agreement set that the attitude and translation dynamics are coupled through a complicated state dependent Laplacian matrix. After the disagreement dynamics have converged, it can be seen that the estimation error dynamics, and the payload state behave much more smoothly.

4-6 Conclusion

This chapter considered the use of state measurements for reaching consensus amongst the agents. It was shown that the use of velocity measurements resulted in a second order consensus problem, closely related to cooperative vehicle control problems. For the fully actuated case a nonlinear Proportional Derivative (PD)-type control law was proposed, and the agents could use individual control and observer gains. With the use of a small coupling gain a global proof of convergence was established. The extension to the underactuated case required identical observer gains and showed a restriction in the proof. It was shown to be difficult to separate the consensus dynamics from the payload motion, leading to a proof of local stability. It was shown that NDI could be used to overcome this problem, allowing for a

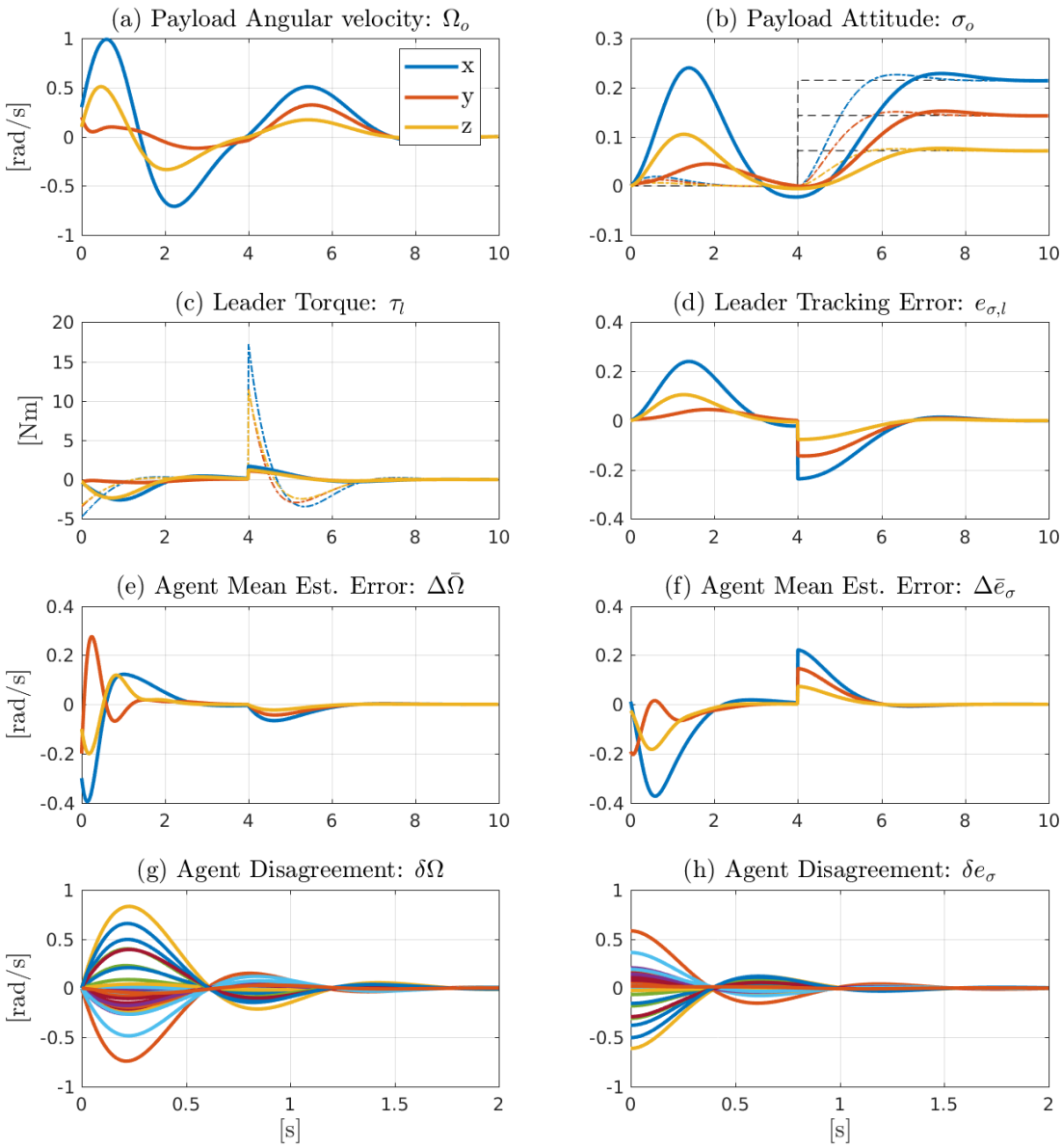

Figure 4-1: Simulation results of the attitude dynamics for the underactuated CMP (Proposition 4-2.1): From left to right and top to bottom the plots show, (a) the payload angular velocity, (b) the payload MRPs, (c) the torque applied by the leader, (d) the leader tracking error, the mean of the agent's estimation errors regarding the (e) angular velocity and the (f) tracking error, and the disagreement of the agent's estimation errors in (g) and (h). The three colors, blue red and yellow, represent the x, y and z directions of the corresponding three dimensional vectors. The black dashed line in the attitude plot shows the leader reference MRPs. The leader applies a reference step to the desired payload attitude at $t = 4$[s], corresponding to a $\theta = 60\,\mathrm{deg}$ rotation about the $\epsilon = [3 \quad 2 \quad 1]^T$ axis. The colored dashed lines in the payload attitude and leader torque plot show the simulation result for the case that the leader is controlling the payload alone.

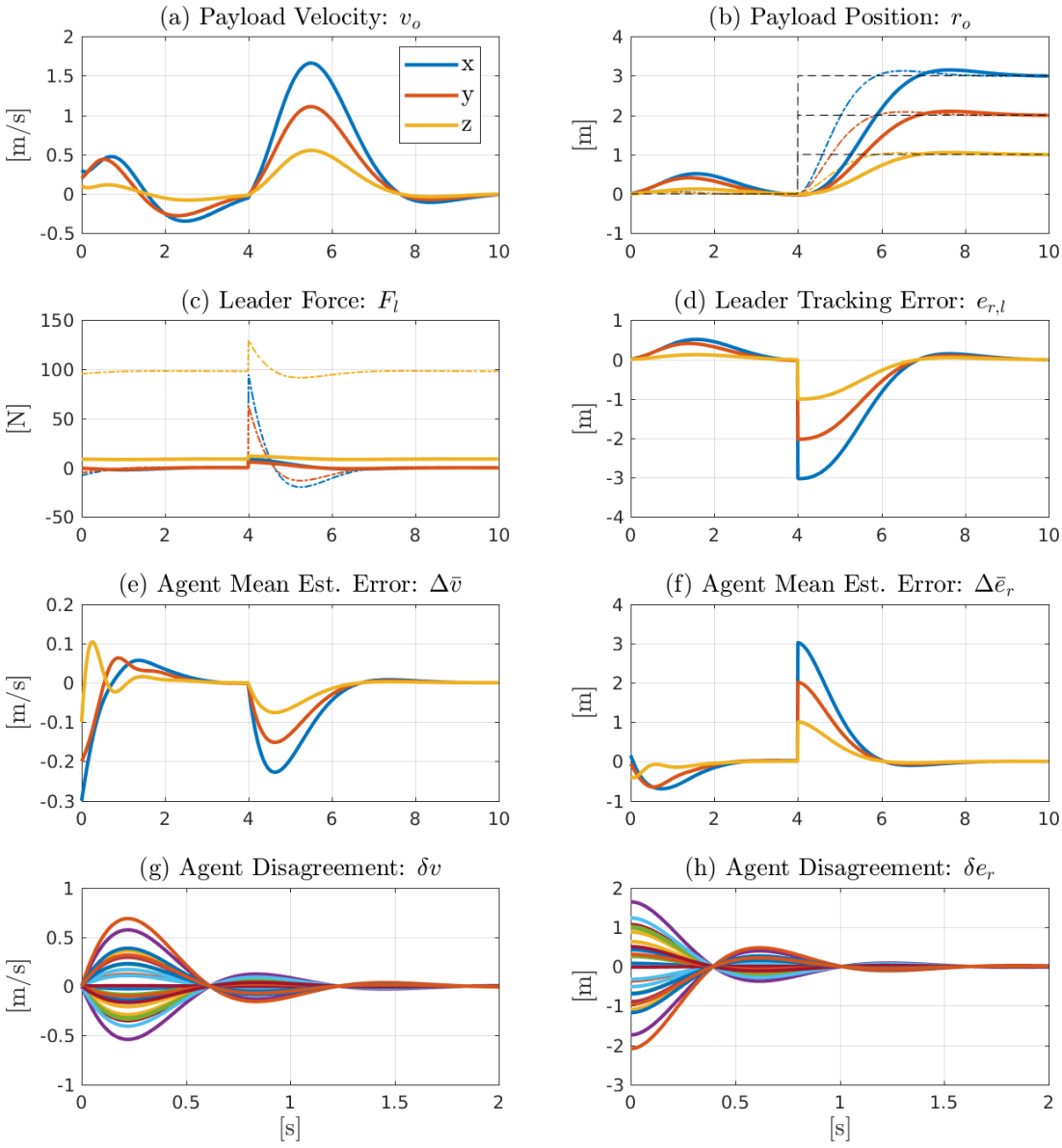

Figure 4-2: Simulation results of the translation dynamics for the underactuated CMP (Proposition 4-2.1): From left to right and top to bottom the plots show, (a) the payload linear velocity, (b) the payload position, (c) the force applied by the leader, (d) the leader tracking error, the mean of the agent's estimation errors regarding (e) the linear velocity and (f) the position tracking error, and the disagreement of the agent's estimation errors in (g) and (h). The three colors, blue red and yellow, represent the x, y and z directions of the corresponding three dimensional vectors. The black dashed line in the position plot shows the leader's desired position, changing from the origin to $r_{\text{des}} = [3 \quad 2 \quad 1]^T$ at $t = 4$[s]. The colored dashed lines in the position and force plot show the simulation result for the case that the leader is controlling the payload alone.

separation of the disagreement, mean estimation error and tracking dynamics. Although the resulting Laplacian matrix is state dependent it could be shown to remain bounded, allowing for the proof to be completed. However, it was argued that the use of NDI further increases the dependency on an accurate model description. Through simulations it was shown that the PD-type control law was able to describe large angles of rotation, and recover from large initial errors, despite the proof of local convergence. The proposed nonlinear PD-type control law is considered preferable over the NDI approach, but global convergence was found difficult to achieve.

Chapter 5

Aerial Cooperative Towing Problem with Multiple Leaders

The aim of this chapter is to relax the assumption of directly controlling the wrench or force acting on the payload. The problem setting is the Aerial Towing Problem (ATP) where multiple Unmanned Aerial Vehicles (UAV) are towing the payload via cables, as depicted in Figure 5-1. The centralized approach, where all agents have access to the desired payload configuration and the complete system state, has been studied in the literature [7], [43]. More specifically, in [44] a control law for the UAV is derived that aims to control the wrench at the payload Center of Gravity (CoG). This approach is reviewed in this chapter by first considering all agents to be a leader, i.e. to have access to the desired configuration. A decentralized approximation is proposed such that the agents no longer require the full system state. The approximate solution is directly extendable to the follower agents, relaxing the assumption of a controlled force acting on the payload. A downside of this approach is that at least three leaders are required to control the payload motion. The solution presented in Chapter 4 is applied to the ATP and the effectiveness is shown via simulation results, rather than an analytic proof. This chapter concludes with a discussion on the results.

This chapter is structured as follows. Section 5-1 reviews the centralized solution for the ATP found in the literature. In section 5-2 an approximation is proposed that allows for a decentralized implementation. In Section 5-3 the approximate solution is extended to the follower agents. Simulation results of the complete system, that is the consensus problem and the ATP combined, are presented in Section 5-4. This chapter concludes with a discussion on the results in Section 5-5.

5-1 Centralized Nonlinear Dynamic Inversion (NDI) for the ATP

This section reviews the UAV tracking law designed in [44] for controlling the wrench at the payload CoG assuming all agents have access to the desired configuration. This design is reviewed extensively for two reasons,

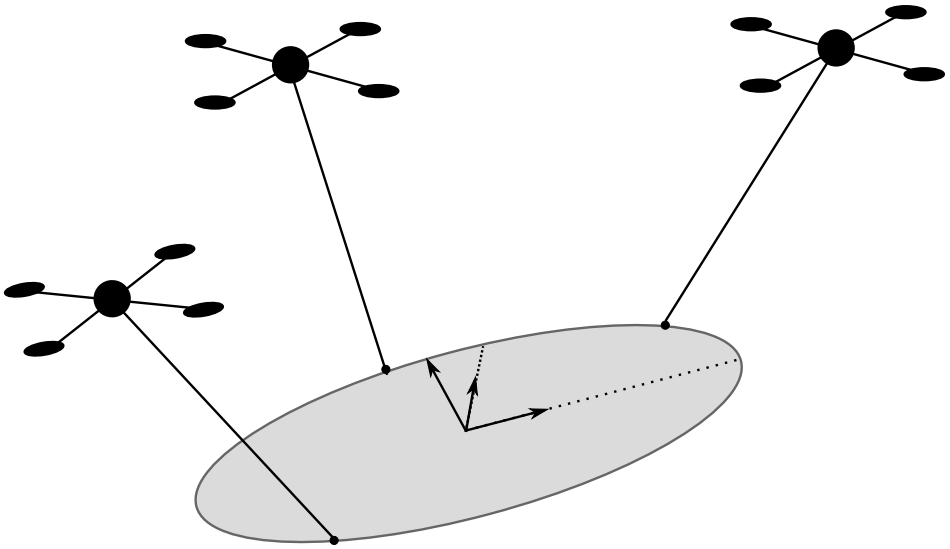

Figure 5-1: Illustration of the ATP: The payload is towed by three UAV, which are attached to the payload via cables.

1. The proposed control law in [44] appears to be less complicated than it actually is. The downside of this approach is made clear by considering what is required to compute the control action.
2. At first glance, the presented control law in [44] appears to be of decentralized design. In this chapter it will be shown that it is in fact a centralized design, i.e. each agent requires knowledge on the payload state as well as the states of all other agents.

This last point follows from a derivation that was not provided in [44], and will be derived in this work. For the system model the following assumptions are made:

1. The cables are modeled as massless rigid links.
2. The cables are attached at the CoG of the corresponding UAV.
3. The UAV are assumed to be fully actuated. This effectively reduces the UAV dynamics to that of a point mass, as it decouples the attitude dynamics from the problem completely. This assumption can be relaxed following [44], without any changes to the overall design, and the same results hold.

It is assumed that the agents have access to acceleration measurements of the payload as well as the individual UAV. Furthermore, the solution posed in [44] is of centralized design, indicating that each agent requires knowledge on the state of the complete system. With these assumptions the proposed tracking law in [44] enables the wrench acting on the payload CoG to asymptotically converge to the desired wrench at the payload CoG.

The remainder of this section is structured as follows. Subsection 5-1-1 gives a description of the system geometry. The equations of motion required for deriving the control law is given in Subsection 5-1-2. The objective of the tracking law is stated in Subsection 5-1-3. In Subsection 5-1-4 the proposed tracking law given in [44] is restated.

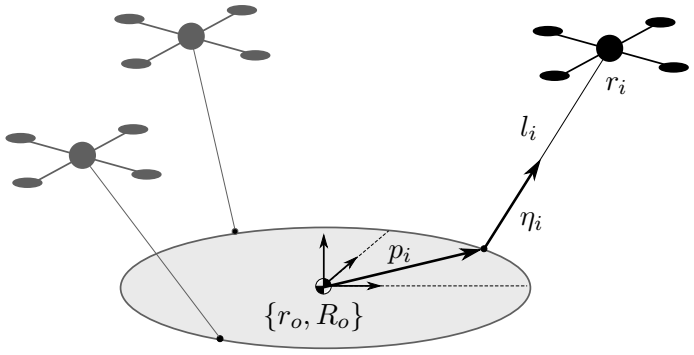

Figure 5-2: Geometry of the payload towed by $n = 3$ UAV: The payload configuration is denoted by $\{r_o, R_o\} \in SE(3)$, the cables are modeled as rigid links with length l_i and direction η_i, the cables are attached to the payload at the relative positions p_i w.r.t. the payload CoG.

5-1-1 Description of the Geometry for the ATP

The system geometry is depicted in Figure 5-2 for $n = 3$ UAV. Let the payload position and attitude, i.e. the configuration, be given by the pair $\{r_o, R_o\} \in SE(3)$. Let the position of the attachment point of the cable on the payload be given by p_i. The i^{th}-cable direction is given by the unit vector η_i and the cable length is given by l_i. The position of the i^{th}-UAV, denoted by r_i, is then given as

$$r_i = r_o + R_o p_i + \eta_i l_i. \tag{5-1}$$

It is assumed that the UAV are fully actuated, i.e. a controlled torque and force act on the UAV body. A direct consequence of this assumption is that the attitude dynamics of the UAV are completely decoupled from the rest of the system. Therefore the UAV are modeled as having point mass dynamics, and are not assigned any attitude dynamics.

5-1-2 Equations of Motion for the ATP

For the control design the unconstrained equations of motion is used in [45], which requires the elimination of the cable tension forces from the description. Although very interesting [46] this is not required. Instead, a simple force and momentum balance of each body suffices, which can be derived using Figure 5-3.

Considering Figure 5-3, the gravitational attraction acts at the payload CoG and at the UAV positions, resulting in the forces $m_o g \bar{b}_3$ and $m_i g \bar{b}_3$ respectively. The cable tensions are scalars denoted by $\lambda_i \in \mathbb{R}$ and the controlled force of the i^{th}-UAV is denoted by $F_i \in \mathbb{R}^3$. Using a force balance for the i^{th}-UAV it must hold that

$$m_i \ddot{r}_i = m_i g \bar{b}_3 - \lambda_i \eta_i + F_i \tag{5-2}$$

where m_i is the mass of the i^{th}-UAV. For the payload the momentum and force balance are given as

$$\begin{aligned} \mathcal{I}_o \dot{\Omega}_o &= -\tilde{\Omega}_o \mathcal{I}_o \Omega_o + \sum_{i=1}^{n} \tilde{p}_i R_o^T \lambda_i \eta_i \\ m_o \ddot{r}_o &= m_o g \bar{b}_3 + \sum_{i=1}^{n} \lambda_i \eta_i \end{aligned} \tag{5-3}$$

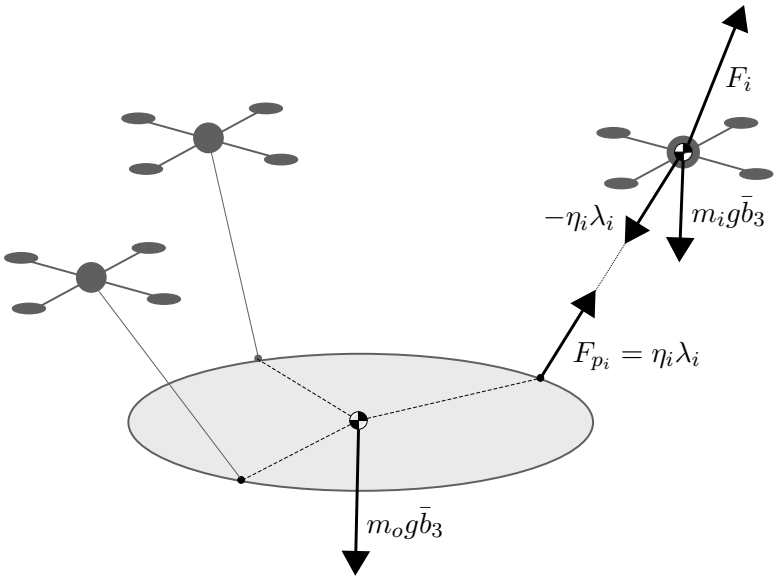

Figure 5-3: Illustration of the forces acting on the ATP system: The gravitational attraction acts on the CoG of the payload and the UAV with magnitudes of $m_o g\bar{b}_3$ and $m_i g\bar{b}_3$ respectively. The force at the attachment point, denoted by F_{p_i}, equals the cable tension λ_i multiplied by the cable direction η_i. The UAV is modeled as a fully actuated point mass, upon which the controlled force F_i acts.

where the mass and inertia of the payload are given by m_o and $\mathcal{I}_o$ respectively. The kinematics of the i^{th}-cable direction η_i is given as,

$$\omega_i \quad = \quad \tilde{\eta}_i\dot{\eta}_i \tag{5-4}$$

where the tilde operator is given in Definition A-2.1, and ω_i denotes the angular velocity of the i^{th}-cable.

5-1-3 Mathematical Objective for the UAV Control Law

As previously stated the control law for the UAV should be designed such that the wrench at the payload CoG can effectively be controlled. The desired wrench at the payload CoG is assumed to be of the form given in (2-3) for the leader, or given by (4-1) in the prospect of adding the followers. From this the corresponding forces at the attachment points can be derived using the generalized inverse as was done in Subsection 2-3-2. This gives the motion inducing component of the force. With the addition of the UAV dynamics the force components resulting in a zero net-wrench at the payload CoG can be used to control the system pose in static equilibrium. The following force at the i^{th}-attachment point is proposed to control the direction of the i^{th}-cable in static equilibrium,

$$F_{\mu,i} = \mu R_o \left(p_i - \tfrac{1}{n} \sum_{j=1}^{n} p_j \right) = \mu R_o p_i^c \tag{5-5}$$

where $\mu \in \mathbb{R}$ can be chosen to design the radial tension and angle of the cables and the superscript c in p_i^c refers to the point as being relative to the geometric center of all points

p_i. Note that a force equal to $F_{\mu,i}$ acting at the i^{th}-attachment point indeed does not induce motion, as can be seen by substituting $F_{\mu,i} = \eta_i \lambda_i$ into the dynamics (5-3) and considering static equilibrium. Combining the desired wrench with the radial component (5-5) gives the desired force at the i^{th}-attachment point as,

$$F_{p_i,\text{des}}(x_o) = \mu R_o p_i^c + J_{p_i}(q_o)^\dagger w_{\text{des}}(x_o) \tag{5-6}$$

where $J_{p_i}(q_o)^\dagger$ denotes the generalized inverse of $J_{p_i}(q_o)^T$ as given in (2-25), $w_{\text{des}}(x_o)$ denotes the desired wrench at the payload CoG, and x_o denotes the payload state. Note that this is the *desired* force at the attachment point, not the *actual* force at the attachment point. The purpose of the UAV control law is to generate $F_{p_i,\text{des}}$ at the attachment point:

Objectives 5-1.1. *Consider the ATP described by equations* (5-1)-(5-4) *and assume all agents to have access to the desired wrench at the payload CoG, denoted by* $w_{des}(x_o)$*. Then, the resultant wrench at the payload CoG converges to the desired wrench if*

$$\lim_{t\to\infty} \eta_i \lambda_i = F_{p_i,des}(x_o) \tag{5-7}$$

where η_i *denotes the cable direction,* λ_i *denotes the cable tension, and* $F_{p_i,des}$ *denotes the desired force at the attachment point given in* (5-6)*.*

5-1-4 N-Leader Nonlinear Dynamic Inversion Control Law

In the previous chapters it was assumed that the forces at the attachment points could be controlled directly by each agent. However, it can be seen from Figure 5-3 that the force at the attachment point is constrained to be in the direction of the cable given by η_i. The control law for the UAV thus attempts to align the cable direction with the force that is currently desired to act at the attachment point, and then to pull along the cable direction with the desired force magnitude. This control strategy is considered in [45], resulting in the following control law:

Theorem 5-1.1 (Leader UAV NDI control law)**.** *Consider the objective of controlling the wrench at the payload CoG by towing the payload via multiple UAV as depicted in Figure 5-1. Assuming that the UAV are fully actuated, let the control law for the force acting on the i^{th}-UAV body be given as*

$$F_i = F_{i,tension} + F_{i,direction} + F_{i,cancel} \tag{5-8}$$

with each component given as,

$$\begin{aligned} F_{i,tension} &= \eta_i \eta_i^T F_{i,des} \\ F_{i,direction} &= -m_i l_i \tilde{\eta}_i \varpi_i \\ F_{i,cancel} &= m_i \left(-g\bar{b}_3 + \ddot{r}_o + R_o \tilde{\Omega}_o^2 p_i - R_o \tilde{p}_i \dot{\Omega}_o - l_i \left\| \omega_i \right\|^2 \eta_i \right) \end{aligned} \tag{5-9}$$

where the cable direction kinematics is controlled through ϖ, which is given as

$$\varpi = \dot{\omega}_{i,des} - k_d \left(\omega_i - \omega_{i,des} \right) - k_p \tilde{\eta}_{i,des} \eta_i + \tilde{\eta}_i \tilde{\omega}_{i,des} \tilde{\omega}_i \eta_i \tag{5-10}$$

where the desired cable direction $\eta_{i,des}$ and desired cable angular velocity $\omega_{i,des}$ are given as

$$\begin{aligned} \eta_{i,des} &= \frac{1}{\left\| F_{p_i,des} \right\|} F_{p_i,des} \\ \omega_{i,des} &= \tilde{\eta}_{i,des} \dot{\eta}_{i,des} \end{aligned} \tag{5-11}$$

and the desired force at the attachment point, denoted as $F_{p_i,des}$ is given as,

$$F_{p_i,des} = \mu R_o p_i^c + J_{p_i} \left(q_o \right)^{\dagger} w_{des} \left(x_o \right) \tag{5-12}$$

where $w_{des}\left(x_o\right)$ is the desired wrench at the payload CoG. Then, the Objective 5-1.1 is globally achieved [45].

The proof of convergence of the cable direction dynamics is given in Appendix B-3-1 as it is not given in [45], and leads to the conclusion that the above control law is of centralized design.

5-2 Decentralized Approximate Computation of the Desired Cable Direction

Considering the Objectives 5-1.1, the control law in Theorem 5-1.1 would appear to be a good choice for relaxing the assumption of having either a controlled force at the attachment point, or a controlled wrench at the CoG. However, in the following it will be shown that this control law requires global state knowledge to compute the expressions for the reference state-trajectories of the cable dynamics, given by $\{\eta_{i,\mathrm{des}}, \omega_{i,\mathrm{des}}, \dot{\omega}_{i,\mathrm{des}}\}$ in (5-10). Subsequently an approximation for computing $\{\eta_{i,\mathrm{des}}, \omega_{i,\mathrm{des}}, \dot{\omega}_{i,\mathrm{des}}\}$ is proposed that allows for local computation of (5-8).

5-2-1 Centralized Computation of the Reference Cable Direction State

The reference cable direction $\eta_{i,\text{des}}$ was given by the direction of the desired force at the attachment point $F_{p_i,\text{des}}$ given in (5-12). To simplify further analysis, let the reference force at the attachment point be represented as a function $h_i(\cdot)$ of the velocities $\nu_o = \begin{bmatrix}\Omega_o^T & v_o^T\end{bmatrix}^T$ and configuration coordinates $q_o = \begin{bmatrix}\sigma_o^T & r_o^T\end{bmatrix}^T$,

$$F_{p_i,\text{des}} = h_i(\nu_o, q_o) = h_i(x_o). \tag{5-13}$$

The reference state for the cable dynamics can then be computed from Proposition 5-1.1, equation (5-12) as,

$$\begin{aligned}\eta_{i,des} &= \tfrac{h_i(x_o)}{\|h_i(x_o)\|} \\ \omega_{i,des} &= \tfrac{\tilde{h}_i \dot{h}_i}{\|h\|^2} \\ \dot{\omega}_{i,des} &= \tfrac{1}{\|h_i\|^2}\left(\tilde{h}_i \ddot{h}_i - 2\left(h_i^T \dot{h}_i\right)\omega_{i,des}\right)\end{aligned} \tag{5-14}$$

where $\eta_{i,\text{des}}$ is the desired cable direction and $\omega_{i,\text{des}}$ is the corresponding cable angular velocity reference. This means that the cable reference state should be computed using the higher-order time derivatives of the function $h_i(\nu_o, q_o)$ given in (5-13). Let the *complete* system state be defined as

$$\chi = \begin{bmatrix}\nu_o^T & q_o^T & \omega_1^T & \eta_1^T & \dots & \omega_n^T & \eta_n^T\end{bmatrix}^T \tag{5-15}$$

Using the equations of motion (5-2) and (5-3) this gives the closed loop dynamics as

$$\dot{\chi} = \begin{bmatrix}\dot{\nu}_o \\ \dot{q}_o \\ \dot{\omega}_1 \\ \dot{\eta}_1 \\ \vdots\end{bmatrix} = \begin{bmatrix}-C_o(\nu_o) - G_o - M^{-1}\sum_{i=1}^{n_{\text{tot}}} J_{p_i}(q_o)^T \tilde{\eta}_i \tilde{\eta}_i^T h_i(\nu_o, q_o) \\ J(q_o)\nu_o \\ \tilde{\eta}_1 \tilde{\eta}_1^T \varpi_1 \\ \tilde{\omega}_1 \eta_1 \\ \vdots\end{bmatrix} = f(\chi) \tag{5-16}$$

where the cable dynamics η_i and ω_i follow from the derivation given in Appendix B-3-1. The higher order derivatives of $h_i(x_o)$ given in (5-13), which are required for computing the reference state (5-14), can thus be computed as

$$\begin{aligned}\dot{h}_i(\chi) &= \tfrac{\partial h_i(x_o)}{\partial \chi} f(\chi) \\ \ddot{h}_i(\chi) &= \tfrac{\partial}{\partial \chi}\left[\tfrac{\partial h_i(x_o)}{\partial \chi} f(\chi)\right] f(\chi)\end{aligned} \tag{5-17}$$

This shows that the proposed control law in Theorem 5-1.1 is of a centralized design, since the computation of the reference state trajectory for the cable direction requires all current cable directions η_i as can be seen from $\dot{\nu}_o$ in (5-16). Note that for computing $\ddot{h}_i(\chi)$ even the time derivatives of all cable directions is required.

5-2-2 Approximate Computation of the Reference Cable Direction State

NDI is often accompanied by an offline computed state trajectory that serves as the reference trajectory for the system. The offline computed trajectory assumes that at each time instant the NDI control was successfully applied with zero tracking error and determines the corresponding state trajectory. A good approximation would thus be to compute the cable reference state while assuming zero cable tracking error. Note that zero cable tracking error means that the desired wrench at the CoG is successfully applied. Successful application of the wrench reduces the payload dynamics significantly. To this end, consider the *desired* state equations,

$$\dot{x}_{o,\text{des}} = \begin{bmatrix} \dot{\nu}_{o,\text{des}} \\ \dot{q}_o \end{bmatrix} = \begin{bmatrix} -\zeta\nu_o - kJ(q_o)^T(q_o - q_{\text{des}}) \\ J(q_o)\nu_o \end{bmatrix} = f_{\text{des}}(x_o) \tag{5-18}$$

which are obtained from the payload dynamics and the desired wrench. Note that $f_{\text{des}}(x_o)$ does not depend on the cable directions η_i of the other agents, and can thus be computed locally by each agent. The desired force at the attachment point is still computed the same way (5-6), but the time derivatives are computed along the desired trajectory,

$$\begin{aligned} h_i(x_o) &= F_{p_i,\text{des}} \\ \dot{h}_{i,\text{des}}(x_o) &\triangleq \tfrac{\partial h_i(x_o)}{\partial x_o} f_{\text{des}}(x_o) \\ \ddot{h}_{i,\text{des}}(x_o) &\triangleq \tfrac{\partial}{\partial x_o}\left[\tfrac{\partial_o h_i(x_o)}{\partial x_o} f_{\text{des}}(x_o)\right] f_{\text{des}}(x_o) \end{aligned} \tag{5-19}$$

with $F_{p_i,\text{des}}$ defined in Theorem 5-1.1, in (5-1.1). The reference state for the cable dynamics $\{\eta_{i,\text{des}}, \omega_{i,\text{des}}, \dot{\omega}_{i,\text{des}}\}$ is then computed using the *desired* time derivatives

$$\begin{aligned} \eta_{i,des}(x_o) &= \tfrac{h_i(x_o)}{\|h_i(x_o)\|} \\ \omega_{i,des}(x_o) &\triangleq \tfrac{\tilde{h}_i \dot{h}_{i,\text{des}}}{\|h\|^2} \\ \dot{\omega}_{i,des}(x_o) &\triangleq \tfrac{1}{\|h_i\|^2}\left(\tilde{h}_i \ddot{h}_{i,\text{des}} - 2\left(h^T \dot{h}_{i,\text{des}}\right)\omega_{i,des}\right). \end{aligned} \tag{5-20}$$

The motivation for this approximation is that the reference state is computed as the desired state, i.e. assuming zero tracking error. Furthermore, the centralized computation of the reference state converges to the approximate computation if the tracking error converges to zero. Although this method allows for a decentralized computation of the desired cable direction, it is still an approximation of the exact solution, and as such it is not guaranteed that the Objectives 5-1.1 are met. The proposed approximation for the UAV control law can be summarized as:

Proposition 5-2.1 (Decentralized Approximate NDI Control Law for the Leader UAV)**.** *Consider the objective of controlling the wrench at the payload CoG by towing the payload via multiple UAV as depicted in 5-1. Let the agents apply the control law as given in Theorem 5-1.1, but let the reference cable trajectory* $\{\eta_{i,des}, \omega_{i,des}, \dot{\omega}_{i,des}\}$ *be computed using equations* (5-18) - (5-20)*, instead of using* (5-11)*.*

Although this approximate computation of the desired cable trajectory is much less computationally expensive than the centralized version, it would still be categorized as very computationally expensive. The equations (5-18) - (5-20) are a short description of a series of computations that have to be executed at each sampling time of the UAV. The complete listing of these computations that have to be made is shown in Appendix B-3-2. Although these computations are not particularly complicated, they illustrate a requirement for accurate knowledge on system parameters, a very fast on-board computer.

5-3 Extension to the Follower UAV Control Law

It is chosen to extend the consensus law derived in Chapter 4, i.e. Proposition 4-2.1 to the ATP. This extension is straightforward: The UAV tracking law aims to cooperatively control the wrench at the payload CoG, while the consensus law aims to reach consensus on the applied wrench. The assumption is then that both succeed.

The followers thus use Proposition 4-2.1 to determine the UAV control action, where the desired wrench in (5-19) is replaced by the i^{th}-agent's local estimate of the desired wrench given in (4-1). The local estimates are then updated using Proposition 5-2.1. For the leaders a similar approach is taken, but without the use of local estimates, as the leaders have direct access to the desired configuration.

5-4 Simulation Results of the ATP

This section presents the simulation results for the ATP where three leader UAV are used to control the payload motion. The construction of the model used in simulation is described in Appendix C-3. The payload parameters are as described in Appendix C-2. It was argued that the pose of the system could be controlled through the parameter μ in (5-5), which sets the desired radial tension. By choosing $\mu = -m_o g \frac{1}{n}$, i.e. equal to the payload weight divided by the number of agents, the cables will be at an approximate angle of 45 deg.

Firstly, the results for the system without follower UAV are presented, after which the followers are added. The followers apply the consensus law given in Proposition 4-2.1, which used Modified Rodrigues Parameters (MRPs) and velocity measurements. In both cases, the system performance is evaluated by changing the desired payload configuration at $t = 4$ seconds to a desired rotation of $\theta_{\text{des}} = 60\,\text{deg}$ about the axis given as $\epsilon_{\text{des}} = [3 \quad 2 \quad 1]^T$, and the desired position to $r_{\text{des}} = [3 \quad 2 \quad 1]^T$ meters. The simulation results show that the decentralized approximation given in Proposition 5-2.1 is well applicable to both cases.

The control gains for the desired payload tracking dynamics are given in Table C-2. Division of these gains by the number of agents gives the i^{th}-agent's control gains. The gains used for the cable dynamics in Theorem 5-1.1, equation (5-11), were taken as $k_p = 100$ and $k_d = 14.14$. The observer gains for the follower agents are as given in Subsection 4-5.

5-4-1 Simulation Results of the ATP: Three Leader UAV and no Followers

The simulation results of Proposition 5-2.1 for the ATP with three leaders, and no followers, is shown in 5-4. This situation will serve as the benchmark for the case where the follower agents are added.

Payload Tracking Error Dynamics From Figure 5-4a and Figure 5-4b it can be seen that the payload attitude and position stabilize at the desired values. The simulation of the ATP was compared to the ideal case where the payload is controlled by a wrench at the CoG directly, without UAV dynamics. The ideal case is shown in the top two plots by the dashed colored lines, but is almost indistinguishable from the ATP results. The reason is that the cable direction dynamics were tuned to be faster than the observer (used in the following), which was tuned to be faster than the payload dynamics.

Figure 5-4c shows the norm of the cable direction error, computed as

$$e_{\text{cable},i} = \left\| \tilde{\eta}_i^2 \eta_{\text{des},i} \right\|. \tag{5-21}$$

Note that the tilde operator is related to the cross-product which shows that $e_{\text{cable},i} = 0$ if $\eta_i = \eta_{\text{des},i}$. The norm of the actuation force of each agent is given in Figure 5-4d. In Figure 5-4e two snap-shots of the system configuration are shown, at $t = 4$ and $t = 10$ seconds. The cable direction error is shown to converge in about 0.6 seconds, after which the UAV behaves as a controlled force at the attachment point.

5-4-2 Simulation Results of the ATP: Three Leader and Ten Follower UAV

The simulation results of the ATP with three leader UAV and ten follower UAV are shown in Figure 5-5, Figure 5-6 and Figure 5-7, where the followers use Proposition 4-2.1 to reach consensus on the desired wrench. The results are compared to the case where three leader UAV are towing the payload, without any followers. The aim is to show that the design requirements 1-3 are met, and that the system is able to achieve large angle deflections, despite the local convergence result of Proposition 4-2.1.

Payload Tracking Error Dynamics The payload attitude and position are shown in Figure 5-5a and Figure 5-5b. The dashed colored lines correspond to the case where the payload is towed by three leaders, as also shown in Figure 5-4, serving as the benchmark. It can be seen that the step response is very similar, where the delay can be explained by the time required to reach consensus on the desired payload configuration. The follower cable direction errors are shown in Figure 5-4c, and are computed using (5-21). The smoothness of these lines, in comparison to Figure 5-4, is due to the fact that the follower agents determine the desired cable direction based on the estimated desired payload configuration. The time required for the cable direction error to converge should thus be comparable to the time required for the estimation errors to converge. A small error in the cable direction indicates that the UAV behaves similar to a controlled force at the attachment point. The system configuration at $t = 4$ and $t = 10$ seconds is shown in Figure 5-5e, where the three colors indicate the leader UAV. It can be concluded that the system is able to achieve tracking of the desired

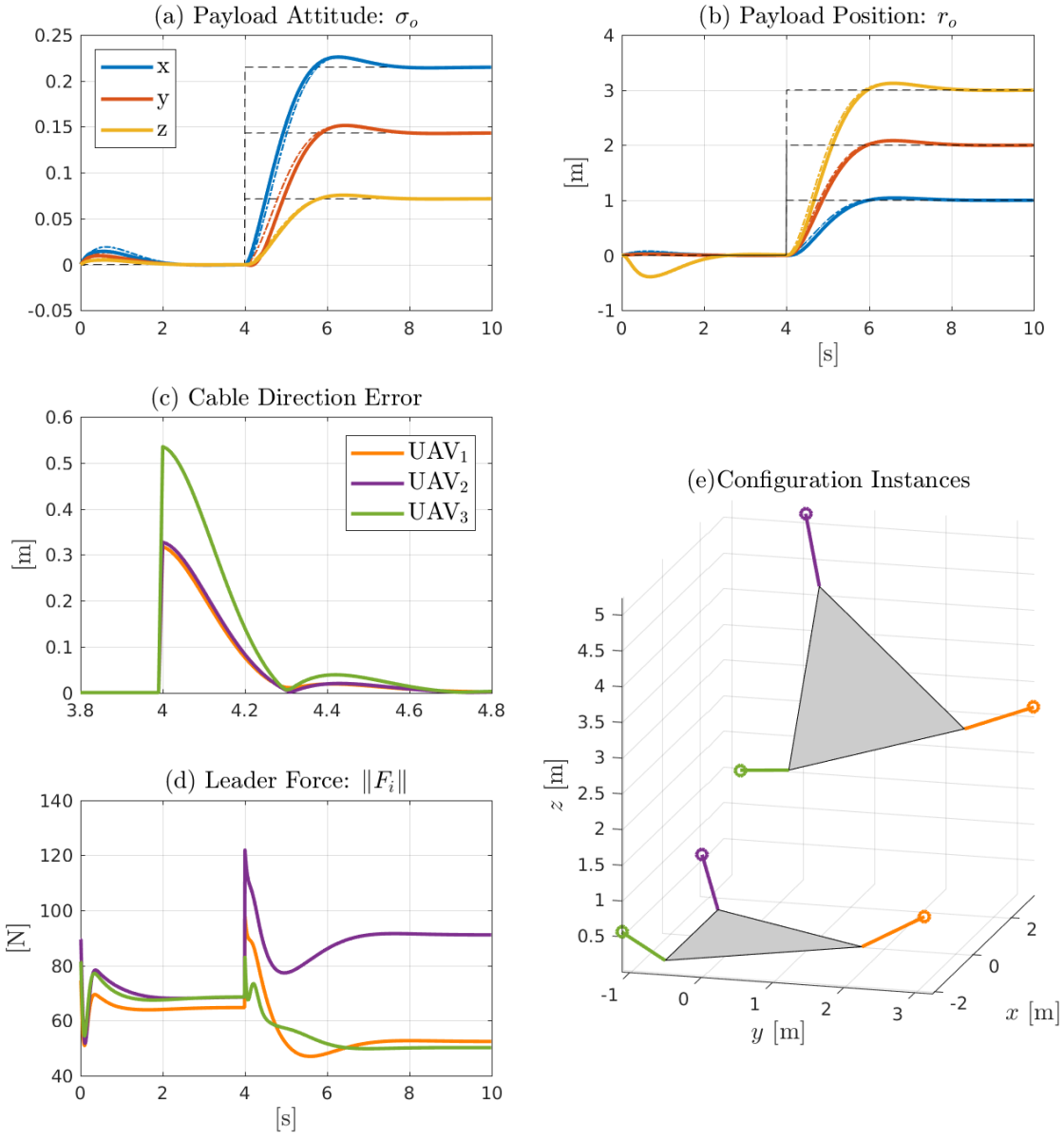

Figure 5-4: Simulation results for the ATP using three leader UAV: Plots (a) and (b) show the payload MRPs and position. The three colors, blue, red and yellow, represent the x, y and z components of the three dimensional vectors. The dashed black line shows the reference signal, which is known to all UAV. Plot (c) shows the norm of the cable tracking error. Plot (d) shows the norm of the force that each agent applies to the UAV body. The three colors, purple, green and orange, refer to one of the agents. Plot (e) illustrates the system configuration at $t = 4$ and $t = 10$ seconds, with corresponding colors for indicating the agents. The payload is illustrated by the grey area and the UAV by the circles.

payload configuration, with comparable performance as shown in Subsection 4, where the UAV dynamics was neglected.

Leader Amplification The norm of the leader UAV actuation effort is shown in 5-5d. With the addition of ten follower UAV the leaders control efforts should be lowered by approximately a factor four, compared to the benchmark. Note that the control effort is more difficult to compare to the case of no followers: The sudden change in the desired payload configuration causes the leader UAV to suddenly change the desired cable direction. The UAV mass prevents this, which causes a peak in the applied force, which is very similar for both cases, as it depends mostly on the UAV mass. Furthermore, the change in the payload configuration causes a change in the distribution of the weight over the three leaders, where the bottom two leaders require a much lower force in static equilibrium. Nevertheless it can be seen that the control effort is lowered for all leaders, with little loss of performance.

Consensus Dynamics The follower agents use the consensus law in Proposition 4-2.1 to estimate the leader's desired payload configuration. The mean estimation errors are shown in Figure 5-6 and the disagreement between the agents is shown in Figure 5-7. It can be seen that the estimation errors for the attitude dynamics are slightly disturbed in comparison to the results found in Subsection 4-5. It can be seen that large cable direction errors cause a disturbance in the estimation dynamics. The interpretation is that, if the cable direction error is large, that the UAV does not behave as a controlled force at the attachment point. This results in a disturbance of the estimation dynamics. The disagreement dynamics shown in Figure 5-7 show similar results as seen in 4-5. This is due to the fact that the measurements drop from the disagreement dynamics, as can be seen from (4-17), with the only coupling to the payload dynamics through the jacobian matrices $J_o(q_o)$.

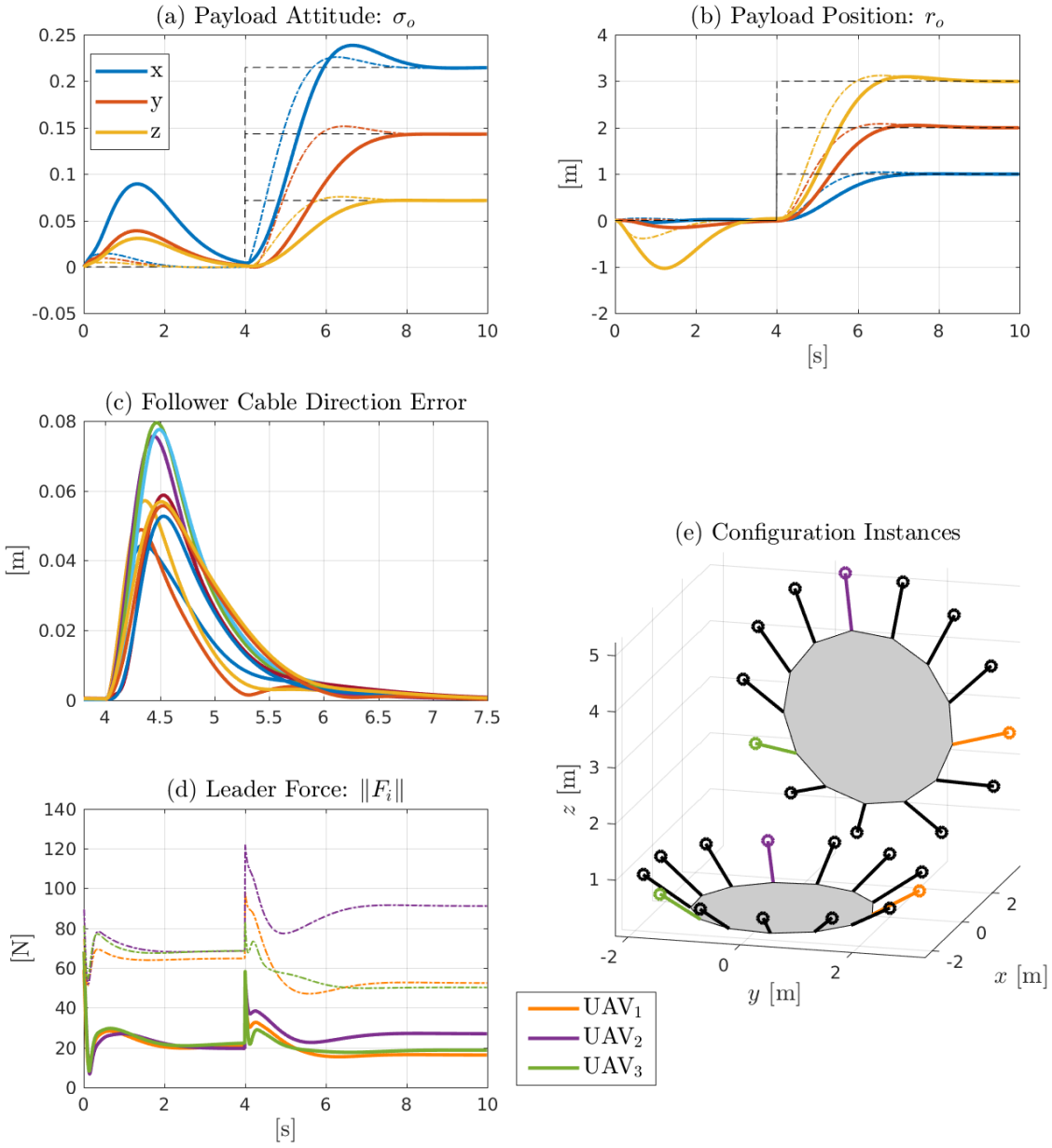

Figure 5-5: Simulation results for the ATP with three leader UAV and ten follower UAV: Plots (a) and (b) show the payload MRPs and position respectively. The black dashed lines show the reference signal known to the leader UAV. Plot (c) shows the norm of the cable direction errors of the follower UAV. Plot (d) shows the norm of the leader UAV forces. The three colors, purple, orange and green correspond to each of the three leader UAV. The colored dashed lines correspond to the case where three leaders are towing the payload without followers, shown in Figure 5-4. Plot (e) depicts the system configuration at $t = 4$ and $t = 10$ seconds. The payload is illustrated by the grey areas, the UAV by the circles, and the cables by the lines connecting the circles to the payload. The leaders are indicated by the corresponding colors.

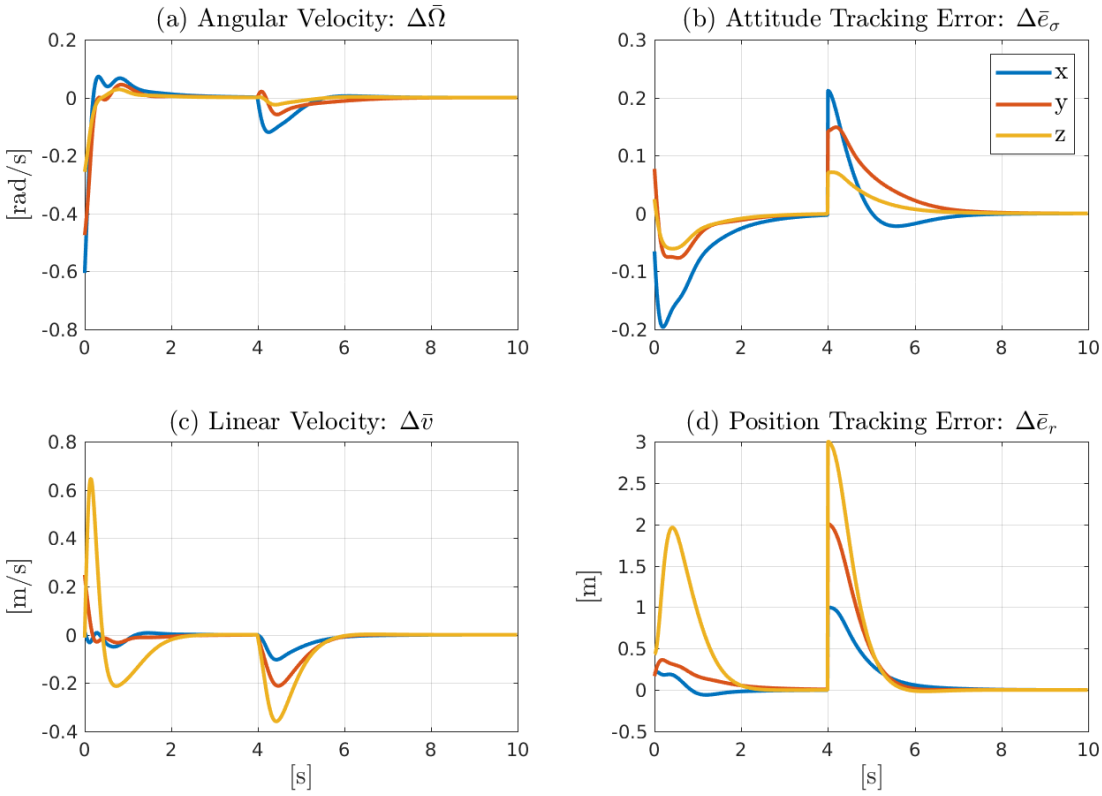

Figure 5-6: The mean estimation errors of the follower UAV during the ATP depicted in Figure 5-5. The mean estimation errors are shown for: (a) the payload angular velocity, (b) the attitude tracking error, (c) the payload linear velocity, and (d) the position tracking error. The three colors, blue, red and yellow correspond to the x, y and z components of the corresponding vectors.

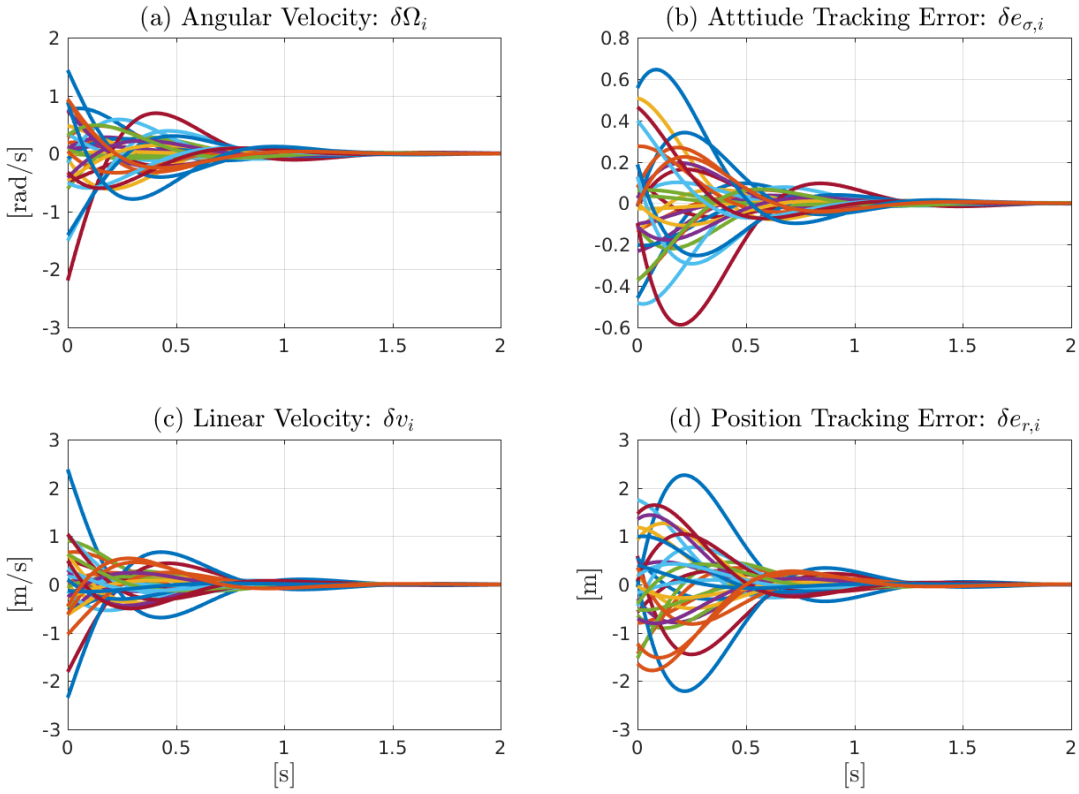

Figure 5-7: The disagreement vectors of the follower UAV during the ATP depicted in Figure 5-5. The disagreement vectors are shown for: The mean estimation errors are shown for: (a) the payload angular velocity, (b) the attitude tracking error, (c) the payload linear velocity, and (d) the position tracking error. The many different colors correspond to the different agents.

5-5 Conclusion

This chapter considered the application of the consensus laws derived in Chapters 2-4 to the ATP using UAV. It was shown that the assumption of a controlled wrench acting at the payload CoG can be relaxed by using multiple UAV. The UAV use a tracking law for the desired force at the attachment point with the aim to cooperatively control the resultant wrench acting on the payload. The solution to this problem as presented in [45] was reviewed, and it was shown to be of centralized design. A decentralized tracking law for the UAV was proposed, which approximated the desired cable trajectory. Simulation results of the ATP using three leader UAV, and no followers, were presented. Comparison to the case where the payload is directly controlled by a wrench at the CoG showed that the decentralized approximation was very effective in controlling the wrench at the payload CoG. The UAV control law was designed such that the UAV behaves as a controlled force at the attachment point. This allows for a straightforward application of the consensus laws presented in Chapters 2-4. The efficacy of the solution presented in Chapter 4 for reaching consensus on the desired payload configuration without communication was shown in simulation. Despite positive results in simulation the presented approach was argued to suffer from several downsides:

- Three leaders are required to control the payload motion.
- The control law is fairly complex, posing as a potential problem for practical implementations.
- The presented solution additionally requires knowledge on all local UAV parameters, and local state measurements.

Although the last two points require further investigation, the requirement of three leaders is inherent to the chosen approach, preventing a small scale experiment.

Chapter 6

Aerial Towing Problem using a Single Leader with Three Extendable Cables

The Aerial Towing Problem (ATP) as described in the previous chapter requires a minimum of three leaders to control the payload motion. This raises the question on how these three (or more) leaders have access to the desired configuration, and whether or not this requires communication. By towing the payload using three extendable cables it is possible to control the configuration using a single leader Unmanned Aerial Vehicles (UAV), see Figure 6-1. With three (scalar) tension forces to control the full motion of the payload, the leader-payload system is underactuated. Consequently, the leader control law is not aimed at controlling the wrench at the payload Center of Gravity (CoG) as was done in the previous chapter. The idea is that the leader UAV will behave similarly enough compared to a controlled wrench, allowing the follower agents to estimate the desired payload configuration.

This chapter is structured as follows. A qualitative description of the control law is given in Section 6-1. For the control law the leader requires the desired cable lengths and desired cable tensions. These can be obtained by solving the Inverse Kinematics Problem (IKP), which will be discussed in Section 6-2. The control law for a single UAV towing the payload is derived in Section 6-3. The follower UAV are added to the description in Section 6-4. The simulation results are presented in Section 6-5. Simulation results for the leader towing the payload alone are shown in Subsection 6-5-1. Subsequently simulation results are shown for the complete ATP including the follower UAV in Subsection 6-5-2. This chapter concludes with a discussion on the results in Section 6-6.

6-1 Control Design Approach for the ATP with a Single Leader

The system, consisting of the payload towed by the leader UAV via three cables, and the follower UAV via a single cable each, is depicted in Figure 6-1. It is assumed that the leader can vary the cable lengths such that the payload's attitude can be changed. Instead of controlling the cable lengths directly, the leader can control the tension forces in the cables and

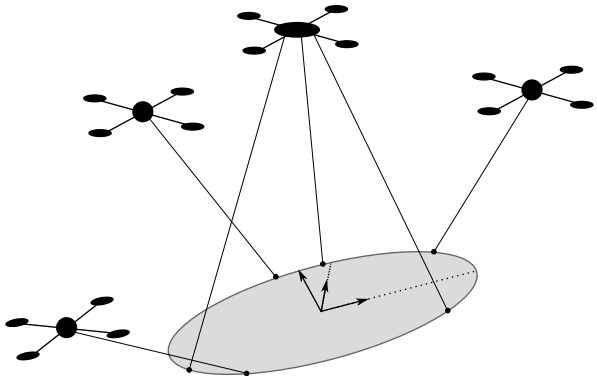

Figure 6-1: Illustration of the ATP with three follower UAV and a single leader UAV: The leader UAV is located in the middle and is attached to the payload via three extendable cables. The follower UAV are attached via a single cable each, along the edge of the payload.

the lengths will vary as a consequence of this.

The control law for the leader UAV is designed without considering the follower UAV. The follower UAV will be added to the system using the tracking law derived in the previous chapter, and Proposition 4-2.1 is used to reach consensus on the desired payload configuration. The performance of the complete system is tested in simulation, rather than proven analytically. The design of the leader control law can be seen to comprise of three parts: The control law for the leader body, the control law for the cable tension forces, and the generation of the reference signals. These will be shortly discussed in the following.

The Control Law for the Leader Body The leader UAV is modeled as a fully actuated rigid body. The leader uses a tracking law for his own body, with the aim to stabilize at a specified static configuration in the inertial reference frame. The relative configuration of the payload is then controlled through the cable tensions. Even though full actuation is assumed it would in reality not be possible to hover at a desired position if the leader body has a nonzero pitch or roll angle. Therefore the attitude of the leader body is controlled such that it remains upright, stabilizing at the desired yaw angle, with zero pitch or roll angles.

The Control Law for the Cable Tension Forces The leader controls the cable lengths indirectly by setting the tension forces in the cables. This requires a conversion of the desired payload attitude to a set of desired cable lengths and pre-tensions. The tension force in the cable is designed such that the cable behaves as a virtual spring-damper, see Figure 6-2, driving the cable length to the reference length. A reference cable tension must be computed such that in static equilibrium the gravitational pull on the payload is canceled and the cable lengths acquire the desired cable lengths. The problem of computing the reference cable length and cable tension given a desired configuration is introduced in the next section.

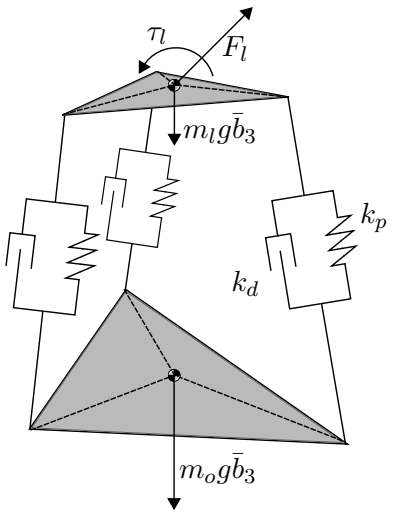

Figure 6-2: Illustration of the applied control for the relative orientation of the two bodies: The leader controls the tension force λ_i in each of the three cables such that the cables behave as virtual spring-damper systems, with spring and damping constants k_p and k_d respectively.

6-2 Computation of the Desired Cable Lengths Given the Desired Payload Attitude

The required reference signals for the leader are obtained by solving the Inverse Kinematics Problem (IKP), which is that of finding the cable lengths that correspond to the desired relative payload configuration with respect to the leader in *static equilibrium*. In this Section the IKP is defined and a method is proposed to solve it. It is assumed that the leader is towing the payload, without any follower UAV. The extension of the IKP to the case with follower UAV can be done by dividing the payload weight by the total number of agents.

The remainder of this section is structured as follows. Subsection 6-2-1 presents the geometry of the system. In Subsection 6-2-2 the IKP is defined, and the conditions for static equilibrium are presented in Subsection 6-2-3. A method for solving the IKP is proposed in Subsection 6-2-4, followed by a numerical example in Subsection 6-2-5. This section concludes with an overview of the reference signals that result from solving the IKP.

6-2-1 Geometry of the Leader and Payload System

In the following the index l and o will be reserved for indicating the leader and payload respectively, as was done throughout this thesis work. As depicted in Figure 6-3 let the configuration of the payload and leader body be denoted by the pair $\{r_o, R_o\} \in SE(3)$ and $\{r_l, R_l\} \in SE(3)$ respectively. The cables are modeled as massless links attached to the payload and leader body at the body fixed positions p_i^o and p_i^l, respectively, for $i = \{1, 2, 3\}$. Let the direction of the cables be denoted by $\bar{\rho}_i = \frac{1}{\|\rho_i\|}\rho_i$ where ρ_i is the vector from the i^{th}-attachment point at the payload to the i^{th}-attachment point at the leader body:

$$\rho_i \;=\; \left(r_l + R_l p_i^l\right) - \left(r_o + R_o p_i^o\right), \qquad i \in \{1, 2, 3\}\,. \tag{6-1}$$

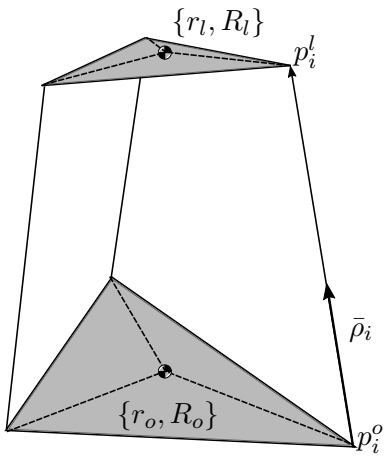

Figure 6-3: Geometry of the payload towed by a single leader via three cables: The cables are attached to the payload at the points p_i^o and p_i^l, for $i \in \{1, 2, 3\}$, on the payload and leader body respectively. The leader and payload configuration is given by the pair $\{r_l, R_l\}$ and $\{r_o, R_o\}$ respectively. The cables have a variable length with a direction given by $\bar{\rho}_i$.

6-2-2 Definition of the Inverse Kinematics Problem (IKP)

In the following the IKP is defined specifically for the system depicted in 6-3. It must be emphasized that the IKP is considered in static equilibrium, because the solution is used as the reference signal for reaching the desired equilibrium. The actual motion is not constrained as described in this section. With this consideration the IKP can be formally stated:

Definition 6-2.1 (Inverse Kinematics Problem)**.** *Consider a given desired payload attitude $R_{o,des} \in SO(3)$, a desired relative vertical distance between the payload and leader body Δz_{des}, and the system geometry depicted in Figure 6-4. The inverse kinematics problem is then defined as finding the relative planar position Δx, Δy, the leader yaw angle ψ and the cable tensions λ_i for $i = \{1, 2, 3\}$ such that the static equilibrium conditions for the payload body are met.*

This definition of the IKP can be derived from Figure 6-4, depicting the relevant configuration coordinates, together with the following observations:

- The payload attitude is constrained to the reference attitude $R_{o,\text{des}}$ for which the problem is to be solved.
- The IKP is independent of the desired inertial position of the payload $r_{o,\text{des}}$, since the leader can always translate the complete system in any direction.
- The relative position between the payload and leader body, denoted as $r_o^l = r_o - r_l$ is clearly relevant to solving the IKP as shown in Figure 6-4. However, the IKP can be solved for any relative vertical distance between the payload and leader body. Therefore

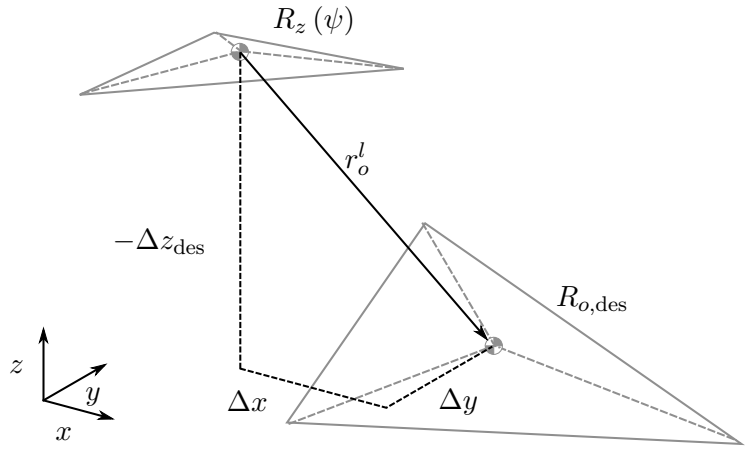

Figure 6-4: Illustration of the important geometric variables for solving the Inverse Kinematics Problem (IKP): The leader body (top triangle) attitude is given by $R_z(\psi)$. The payload (lower triangle) attitude is given by $R_{o,\text{des}}$. The relative position between the two bodies is given by $r_o^l = [\Delta x \quad \Delta y \quad \Delta z_{\text{des}}]^T$.

the desired relative vertical distance between the leader and payload, denoted by Δz_{des}, should be chosen. The relative position is thus given by $r_o^l = \begin{bmatrix}\Delta x & \Delta y & \Delta z_{\text{des}}\end{bmatrix}^T$, with Δz_{des} fixed, and Δx, Δy free variables.

- The leader body represents an UAV and as such it is desired that the leader attitude remains parallel to the horizontal plane in static equilibrium (hovering). Therefore the leader body is only free to rotate about the third body axis, indicated by the yaw angle ψ, and pitch or roll angles are constrained to zero. The rotation matrix for rotations about the yaw angle is denoted by $R_z(\psi)$, as depicted in Figure 6-4.

- The IKP only considers the static equilibrium conditions for the payload, and not for the leader body.

From these considerations it can be concluded that the IKP can be solved by choosing the desired payload attitude and the desired relative vertical distance. The free variables for solving the IKP are then given by the leader yaw angle, the payload planar position, and the cable tensions. This leads to the IKP as given in Definition 6-3.1.

6-2-3 Static Equilibrium Conditions of the Payload Suspended by Three Cables

The problem under consideration is to find the desired cable tensions such that the payload remains in static equilibrium. The equilibrium conditions are given by setting the sum of the forces $\sum F$ and torques $\sum \tau$ acting on the payload to zero, using Figure 6-5 this gives

$$\begin{aligned} \sum F &= \sum_{i=1}^{3} \bar{\rho}_i \lambda_i + m_o g \bar{b}_3 = 0 \\ \sum \tau &= \sum_{i=1}^{3} \tilde{p}_i^o R_{o,\text{des}}^T \bar{\rho}_i \lambda_i = 0 \end{aligned} \tag{6-2}$$

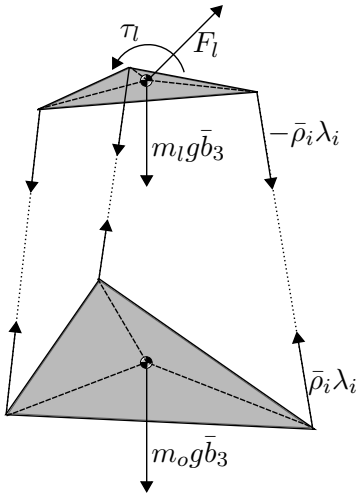

Figure 6-5: Depiction of the forces and torques acting on the leader and payload in static equilibrium: The tension forces λ_i in the cables act along the cable direction $\bar{\rho}_i$ on both the leader and payload body. The gravitational force indicated by $m_l g\bar{b}_3$ and $m_o g\bar{b}_3$ act on the leader and payload body respectively. It is assumed that the leader body is fully actuated through the controlled force F_l and τ_l.

where $\bar{\rho}_i$ is the unit vector in the direction of the i^{th}-cable, λ_i is the tension force in the i^{th}-cable, $m_o g\bar{b}_3$ is the gravitational force acting on the towed payload and p_i^o is the position of the attachment point of the i^{th}-cable on the payload, as depicted in Figure 6-3. The cable directions are given as $\bar{\rho}_i = \rho_i/|\rho_i|$ with ρ_i given as

$$\rho_i = R_l\left(\psi_l\right) p_i^l - R_{des,o} p_i^o - \begin{bmatrix} \Delta x \\ \Delta y \\ \Delta z_{\text{des}} \end{bmatrix}, \qquad i \in \{1,2,3\} \tag{6-3}$$

which can be found from ρ_i as defined in (6-1) and substituting the relative position $r_o - r_l = r_o^l = \begin{bmatrix}\Delta x & \Delta y & \Delta z_{\text{des}}\end{bmatrix}^T$. The rotation matrix $R_z\left(\psi_l\right) \in SO(3)$ is the rotation matrix for the leader body such that it can rotate about the third body axis:

$$R_l\left(\psi_l\right) = R_z\left(\psi_l\right) \triangleq \begin{bmatrix} \cos(\psi_l) & -\sin(\psi_l) & 0 \\ \sin(\psi_l) & \cos(\psi_l) & 0 \\ 0 & 0 & 1 \end{bmatrix}. \tag{6-4}$$

The equilibrium conditions (6-2) with the variables (6-3) and (6-4) substituted form a set of nonlinear equality constraints, depending on constant parameters and free variables. The constant parameters denoted by Θ, are then given as,

$$\Theta = \left\{R_{o,\text{des}}, \Delta z_{\text{des}}, p^l, p^o, m_o\right\} \tag{6-5}$$

where, with slight abuse of notation, p^l denotes $\left\{p_1^l, p_2^l, p_3^l\right\}$ and similarly for p^o. The free variables are collected in X which is given as,

$$X = \{\psi_l, \Delta x, \Delta y, \lambda\} \tag{6-6}$$

where $\lambda = \begin{bmatrix}\lambda_1 & \lambda_2 & \lambda_3\end{bmatrix}^T$. The constraints for static equilibrium can then be written in terms of Θ and X by substitution of (6-3) and (6-4) into the force and momentum balance (6-2),

$$c(\Theta, X) = \begin{bmatrix} \sum_{i=1}^{3} \bar{\rho}_i \lambda_i + m_o g \bar{b}_3 \\ \sum_{i=1}^{3} \tilde{p}_i^o R_{o,\text{des}}^T \bar{\rho}_i \lambda_i \end{bmatrix} = 0 \tag{6-7}$$

The problem is then to find X given Θ such that the above constraint holds, which is a nonlinear root finding problem.

6-2-4 Nonlinear Root Finding Program for Solving the IKP

It is here chosen to solve the nonlinear root finding problem by sequentially solving a quadratic problem multiple times. Starting from an initial guess for X a step δX is chosen as the minimizer of a quadratic problem, which is obtained by approximating the problem as a linear least squares problem in the unknown iteration step δX. To this end define the cost function V as

$$V_k = \tfrac{1}{2} \|c_k + J_k \delta X_k\|^2 \tag{6-8}$$

where the subscript k indicates the k^{th}-iteration, $c_k = c(\Theta, X_k)$ is the constraint (6-7) evaluated at the k^{th}-iteration and J_k is the jacobian of the constraint,

$$J_k = \left.\frac{\partial c(\Theta, X)}{\partial X}\right|_{X=X_k}. \tag{6-9}$$

The solution X_k is then updated as $X_{k+1} = X_k + \delta X_k$ where δX_k is chosen to minimize V_k. The minimum of V_k can be found by setting the gradient of V_k to zero,

$$\frac{\partial V_k(\delta X)}{\partial \delta X} = J_k^T (c_k + J_k \delta X) = 0, \qquad \rightarrow \qquad \delta X_k = -\left(J_k^T J_k\right)^{-1} J_k^T c_k. \tag{6-10}$$

After each iteration the norm of the constraint c_k is used as the stopping criteria. The root finding program can be summarized as follows,

Proposition 6-2.1. *Consider the IKP as given in Definition 6-2.1. Given the system geometry and desired payload attitude, collected in* Θ (6-5)*, and a desired solution precision* $\epsilon > 0$*. Then, the proposed solution to solving the IKP is to follow these steps:*

1. *Initialize the program: Guess* X_k *given in* (6-6) *and set the iteration number* $k = 1$*.*
2. *Evaluate the constraint* c_k *and the jacobian* J_k *using* (6-7) *and* (6-9) *respectively.*
3. *If* $\|c_k\| < \epsilon$ *stop, otherwise go to the next step.*
4. *Determine the minimizing step:* $\delta X_k = -\left(J_k^T J_k\right)^{-1} J_k^T c_k$
5. *Update the solution:* $X_{k+1} = X_k + \delta X_k$
6. *Update the iteration number* $k = k + 1$ *and go to step 2.*

Choosing the Initial Guess For choosing the initial guess a good option is to choose the equilibrium condition for a symmetric geometry and zero attitude angle displacement, i.e. $\lambda_1 = \lambda_2 = \lambda_3$, and all other values in X set to zero. It was found that the algorithm typically converges in 2-3 iterations, for rotations smaller than 90 deg. As the problem is of so little size, and is solved in so few iterations it was concluded that this simple root finding program was sufficient. Suppose that one encounters a choice of Θ for which the program has difficulty finding the solution, then, the parameters can incrementally be changed to the desired parameters. This method is illustrated in the following, where the desired attitude is incrementally changed.

6-2-5 Numerical Example of the IKP

The efficacy of Proposition 6-2.1 for solving the IKP is shown via a numerical example. The payload mass is taken as 10.0[kg], the cables are attached to the payload in a circle of radius 90[cm], and to the leader body in a radius of 50[cm], with equal spacing. The desired vertical distance was set to $\Delta z = 1.5$ meter. The solution precision was set to $\epsilon = 10^{-8}$.

The IKP is solved for different desired payload attitudes. The desired payload attitude is incrementally increased from 0 deg to a desired rotation of $\theta_{\text{des}} = 60$ deg about the axis given as $\epsilon_{\text{des}} = [3 \quad 2 \quad 1]^T$ in ten steps. The IKP is solved for each desired angle of rotation, using the previous solution as the initial estimate. The initial guess for the cable tension at 0 deg is taken as the payload weight divided by three (which is incorrect). A final step is added, which drops the desired angle from 60 deg back to 0 deg in a single step. This illustrates a large error in the initial guess.

The results are shown in Figure 6-6, where Figure 6-6a and Figure 6-6b show the resulting configuration at $\theta_{\text{des}} = 0$ deg and $\theta_{\text{des}} = 60$ deg. Figure 6-6c shows the incremental increase in the desired payload angle. The computed leader yaw angle is shown in Figure 6-6d, and the cable lengths in Figure 6-6e. Note that the cable lengths can be computed using (6-3) if the IKP is solved. The number of iterations that the algorithm requires to solve the IKP is shown in Figure 6-6f. It can be seen that for large desired payload angles the situation becomes more extreme, and the algorithm tends to require an extra iteration. Clearly, the most iterations are required for the large drop from $\theta_{\text{des}} = 60$ deg to $\theta_{\text{des}} = 0$ deg. It can be concluded that for the considered geometry, the proposed algorithm is sufficiently fast and robust to solve the IKP.

6-2-6 Complete Reference Signal Available to the Leader

The algorithm in Proposition 6-2.1 allows the leader to convert a reference signal for a desired payload configuration $\{r_{o,\text{des}}, R_{o,\text{des}}\}$ into the required reference signals for the actual control law. Before deriving the leader control law, the results obtained from solving the IKP are summarized here.

The algorithm in Proposition 6-2.1 returns the optimal solution $X = X^* = \{\psi_l^*, \Delta x^*, \Delta y^*, \lambda^*\}$.

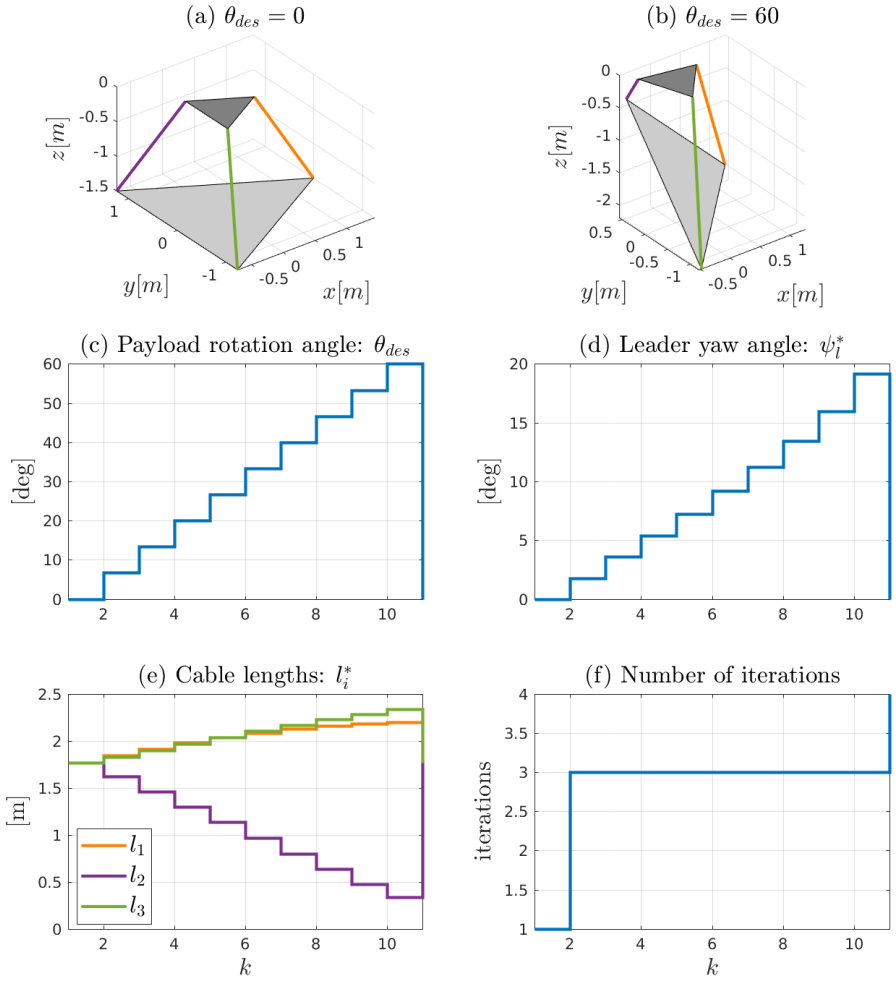

Figure 6-6: Numerical example of Proposition 6-2.1 for solving the IKP: The payload desired attitude is rotated with an angle that increases from $\theta_{\text{des}} = 0\,\text{deg}$ and $\theta_{\text{des}} = 60\,\text{deg}$ in 10 steps. An additional step is added that drops the desired angle back to $0\,\text{deg}$. Plots (a) and (b) illustrate the system configuration at $\theta_{\text{des}} = 0\,\text{deg}$ and $\theta_{\text{des}} = 60\,\text{deg}$. Plot (c) shows the incremental increase in the desired payload attitude. Plots (d) and (e) show the corresponding leader yaw angle and the cable lengths, as computed by the IKP. Plot (f) shows the number of iterations that the algorithm in Proposition 6-2.1 requires for solving the IKP.

This optimal solution contains the following important results:

$$
\begin{aligned}
&\text{Cable tension force:} && \lambda_{\text{des},i} = \lambda_i^* \geq 0 \\
&\text{Cable direction (see (6-3)):} && \bar{\rho}_{i,\text{des}} = \tfrac{1}{\|\rho_i(\Theta, X^*)\|}\rho_i(\Theta, X^*) \\
&\text{Cable length:} && l_{i,\text{des}} = \|\rho_i(\Theta, X^*)\| \\
&\text{Leader yaw angle:} && \psi_{des} = \psi^* \\
&\text{Leader reference position:} && r_{l,\text{des}} = r_{o,\text{des}} + \begin{bmatrix}\Delta x^* & \Delta y^* & \Delta z^*\end{bmatrix}^T \\
&\text{Additional force on the leader body:} && F_l^* = -\sum_{i=1}^{3} \bar{\rho}_{\text{des},i}\lambda_{\text{des},i} = m_o g \bar{b}_3 \\
&\text{Additional torque on the leader body:} && \tau_l^* = -\sum_{i=1}^{3} \tilde{p}_i^l R_z(\psi_{\text{des}})^T \bar{\rho}_{\text{des},i}\lambda_{\text{des},i}
\end{aligned}
\tag{6-11}
$$

The leader control law, as designed in the following subsection, requires the above *constants* as reference signals such that the payload is stabilized at the desired configuration.

6-3 Control Law for a Single UAV Towing the Payload via Three Extendable Cables

In this section the control law is designed for the leader towing the payload alone. The combined payload and leader body system is underactuated: The tension forces give three scalar variables to control the full motion of the payload. Consequently the control law is designed such that the desired cable lengths are achieved. The gravitational attraction then ensures a minimum potential energy at the desired configuration. This would result in a very poorly damped system. Although the follower UAV are not yet added, it is known in advance that these can provide the necessary damping. For this reason it is assumed that an external damping acts on the payload during the design of the leader control law. This external damping is later removed, when considering the follower UAV.

A globally converging control law is designed for the leader UAV. Evaluation of the equilibrium state gives rise to the Direct Kinematics Problem (DKP), which states that given the cable lengths there are multiple configurations possible that satisfy the static equilibrium conditions. For the problem under consideration it is argued that the DKP has little practical value, and it is assumed that the desired equilibrium is the unique system equilibrium.

The remainder of this section is structured as follows. The problem of uniqueness of the equilibrium state is introduced in Subsection 6-3-1. Subsection 6-3-2 states the equations of motion of the system. Subsection 6-3-3 presents the proposed control law and the proof of convergence to the desired equilibrium.

6-3-1 Assumption on Configuration Uniqueness

The control law is designed to set the lengths of the cables to the desired lengths as computed by the IKP. However, even if the cable lengths are stabilized at their desired lengths this does not mean that the system has acquired the desired configuration. This problem is well known in the literature, and referred to as the Direct Kinematics Problem (DKP) [43]:

Definition 6-3.1 (Direct Kinematics Problem)**.** *Given the cable lengths, find all possible configurations of the payload, that satisfy the equilibrium conditions* (6-2)*.*

What can be concluded from studies on parallel manipulators and the towing of payloads is that the solution to the DKP is not unique, see [43] and references therein. This has implications for the convergence proof of the proposed control law: Even though the system can be shown to be stable and converging, it can not be shown that the desired equilibrium is reached, since the DKP does not have a unique solution in general. For practical considerations this problem is less significant as most configurations can not be reached. For example, consider Figure 6-7 which depicts three possible configurations for given cable lengths. The inverted pendulum type configuration in Figure 6-7b can not be achieved since the cables can not push on the payload. The cables can in practice not move through one another, and neither can the payload and leader body. This means that configurations as depicted in Figure 6-7c are difficult to achieve. Lastly, assuming the leader has access to the configuration state of the payload, it is relatively straightforward to determine a reference trajectory that guides the payload to the desired equilibrium state. These considerations lead to the following simplifying assumption:

Assumption 6-3.1 (Uniqueness of the Direct Kinematics Problem)**.** *Suppose that a stabilizing control law is designed for the system depicted in Figure 6-3 for which it can be shown that the system converges to an equilibrium state. If it can be shown that the solution to the IKP is a valid equilibrium state for the controlled system, then, as a simplification, it is assumed that the equilibrium state found from solving the IKP is the unique equilibrium state of the system.*

The above assumption is, simply put, incorrect for an arbitrary system geometry. But for the purpose of this thesis it is not considered to be restrictive.

6-3-2 Equations of Motion for the ATP

Consider Figure 6-5 which illustrates the forces and torques acting on the two bodies. As a simplification the leader is assumed to be fully actuated, i.e. a controllable force F_l and torque τ_l act on the leader body through the CoG. Furthermore the leader is able to control the tension forces in the cables, denoted by $\lambda_i \in \mathbb{R}$. The equations of motion for the leader

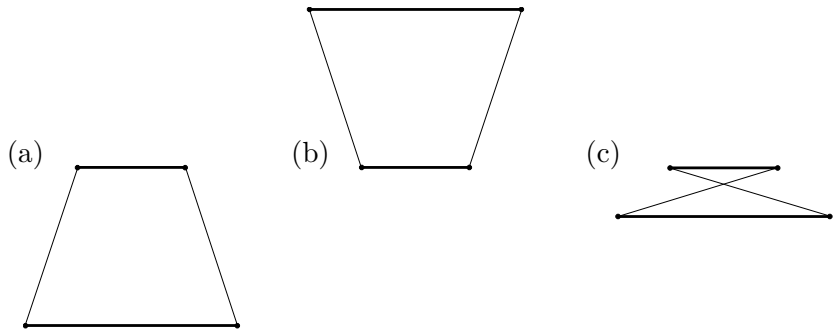

Figure 6-7: Illustration of the Direct Kinematics Problem (DKP): A side-view of three possible equilibrium configurations is shown, where the leader and payload body are represented by the horizontal bars. (a) illustrates the desired configuration. (b) and (c) show two undesired configurations with the same cable lengths.

body are then given as

$$\begin{aligned} \mathcal{I}_l \dot{\Omega}_l &= -\tilde{\Omega}_l \mathcal{I}_l \Omega_l + \tau_l - \sum_{i=1}^{3} \tilde{p}_i^l R_l^T \bar{\rho}_i \lambda_i \\ m_l \dot{v}_l &= m_l g \bar{b}_3 + F_l - \sum_{i=1}^{3} \bar{\rho}_i \lambda_i \end{aligned} \tag{6-12}$$

where the notation is as given in Section 6-2-1 and Appendix A-4. The equations of motion for the payload are given as

$$\begin{aligned} \mathcal{I}_o \dot{\Omega}_o &= -\tilde{\Omega}_o \mathcal{I}_o \Omega_o + \sum_{i=1}^{3} \tilde{p}_i^o R_o^T \bar{\rho}_i \lambda_i - \Lambda_\Omega \Omega_o \\ m_o \dot{v}_o &= m_o g \bar{b}_3 + \sum_{i=1}^{3} \bar{\rho}_i \lambda_i - \Lambda_{\dot{r}} v_o \end{aligned} \tag{6-13}$$

where $\Lambda_{\dot{r}} \in \mathbb{R}^{3\times3}$ and $\Lambda_\Omega \in \mathbb{R}^{3\times3}$ are external damping matrices. These damping matrices are removed when adding the follower UAV in the next section. Without the external damping, or the follower UAV, the system is extremely poorly damped, resulting in almost pendulum-like behavior.

6-3-3 Proposed Control Law for a Single UAV Towing the Payload

The following control law is proposed for the leader towing the payload as depicted in 6-3:

Proposition 6-3.1 (Control Law for the Leader Towing the Payload via Three Cables)**.** *Consider the system depicted in Figure 6-3 and Figure 6-5 with the corresponding equations of motion* (6-12) *and* (6-13)*. Assume that for the system geometry and a desired payload configuration the IKP can be solved using Proposition 6-2.1. Let the cable tension be given as*

$$\lambda_i = k_p \left(\|\rho_i\| - l_{i,des} \right) + \lambda_{i,des} + k_d \dot{\rho}_i^T \bar{\rho}_i \tag{6-14}$$

the leader controlled force be given as

$$F_l = -\left(m_l + m_o\right) g \bar{b}_3 - \beta v_l - K \left(r_l - r_{l,des} \right). \tag{6-15}$$

and the leader controlled torque be given as

$$\tau_l = \sum_{i=1}^{3} \left[\tilde{p}_i^l R_l^T \bar{\rho}_{des,i} \lambda_{des,i} \right] - \zeta \Omega_l - k \mathbb{P}_a \left\{ R_{l,des}^T R_l \right\}^V \tag{6-16}$$

where the scalars $k > 0$ and matrices $K, \zeta, \beta > 0$ are control gains, ρ_{des}, λ_{des} and $R_{l,des}$ are the desired cable vector, tension force and leader attitude respectively, as obtained from solving the IKP. Then, the system is globally stable. If Assumption 6-3.1 is assumed to hold, then, the system globally converges to the desired equilibrium state.

The proof is shown in Appendix B-4-1. The above proposition assumes a geometric control law for the leader torque. The control law using Modified Rodrigues Parameters (MRPs) is very similar, and is given in Appendix B-4-2 for completeness.

6-3-4 Comparison of the Proposed Control Law to Nonlinear Dynamic Inversion (NDI)

Comparison of the proposed control law in this section with that of the previous chapter shows that the implementation is much less dependent on system parameters. The IKP does depend on the geometry of the system, but parameter uncertainty will merely result in other cable lengths than was intended. Integral action could be used to keep the UAV in the upright position, and reduce the effect of parameter uncertainty on the UAV attitude. With these considerations it can be seen that the computation of the leader control law given in Proposition 6-3.1 is much less demanding than the NDI-type control law posed in Proposition 5-1.1, which includes the required computations given in Appendix B-3-2 to be executed at every sampling time.

6-4 Addition of the Follower UAV to the ATP

The consensus problem is added by considering multiple UAV to be attached to the payload as depicted in Figure 6-1. Due to the complexity of the complete system, the consensus dynamics is not evaluated in an analytic fashion, as reflected by the research goals for this thesis, see Section 1-3. The tracking law for the follower UAV is taken as proposed in Subsection 5-3.

Table 6-1: Selected control gains for the leader towing the payload alone (Proposition 6-3.1)

	Symbol	Value
Cable tracking	k_p	31.62
Cable damping	k_d	25.35
Leader tracking	K, k	31.62
Leader damping	ζ, β	2.53
External Payload damping	$\Lambda_\Omega, \Lambda_{\dot{r}}$	25.35

For the leader control law given in Proposition 6-3.1 the only modification is that the payload mass is divided by the total number of participating agents.

6-5 Simulation Results of the ATP

This section presents the simulation results for the ATP where the leader is towing the payload via three cables, i.e. Proposition 6-3.1. The case where a single leader is towing the payload is considered first, and subsequently the follower UAV are added. The follower UAV apply Proposition 4-2.1 for estimating the leader's desired payload configuration, and apply the tracking law introduced in Chapter 5 for determining the actuation force.

The simulation setting is described in Appendix C, with the numerical values of the payload and UAV as given in Appendix C-2. The extendable cables are attached to the payload in a circle of radius 90[cm], and to the leader body in a radius of 50[cm], with equal spacing. The desired vertical distance was set to $\Delta z = 1.5$ meter. The control gains for the case that the leader is towing the payload alone are listed in Table 6-1. Note that the leader damping of the leader body is relatively low, and a high external damping is applied to the payload. Together, these gains were designed for a desired performance. With the addition of the follower UAV the gains listed in Table 6-1 are divided by the total number of agents, except for the damping on the leader body. The control gain selection for the follower UAV is as described in Section 5-4.

6-5-1 Simulation Results of a Single UAV Towing the Payload

In the following the simulation results for the case where the leader is towing the payload alone are presented. It was noted that the proposed control law is not aimed to control the wrench at the payload CoG, and it is expected that certain motions are more difficult to control than others. This was partly resolved by adding external damping to the payload motion. This damping was added such that the performance can be compared to the case where the follower UAV are added. With the addition of the follower UAV this external damping is removed. The motions that are difficult in the current situation are rotations about the third body axis, i.e. a yaw angle, and the sideways motion of the payload. These two motions are considered first in the following, before the complete system step response is shown. The control gains for the leader UAV are given in Table 6-1, with the symbols given in Proposition 6-3.1.

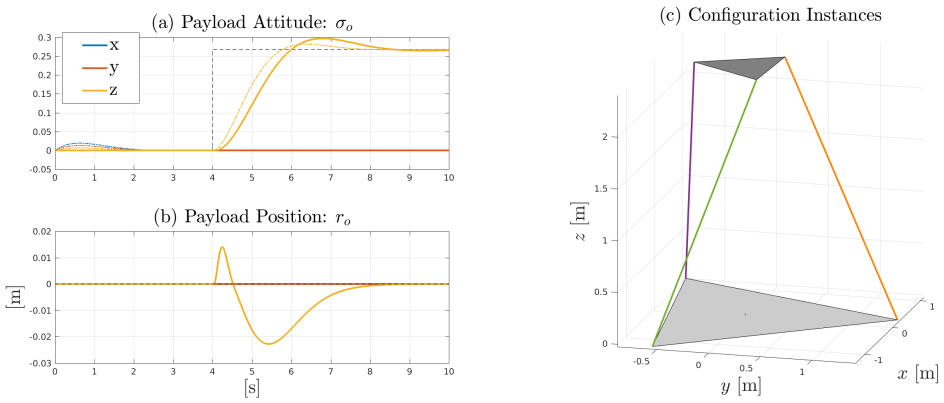

Figure 6-8: Simulation result for a desired payload yaw angle rotation (Proposition 6-3.1): Plots (a) and (b) show the payload MRPs and position respectively. The three colors, blue, red and yellow correspond to the x, y and z components of the presented vector. The black dashed line shows the payload reference signal, which is a reference step to the desired yaw angle of $60\,\mathrm{deg}$. Plot (c) shows a depiction of the system configuration during the motion.

System Response for a Desired Payload Yaw Angle The simulation results for a reference step to the desired payload yaw angle is shown in Figure 6-8. For the purpose of this simulation the desired vertical distance between the payload and leader is set to 2.5 meter. The left plots show the payload attitude and position and on the right the system configuration during motion is depicted. It can be seen that the UAV simply rotates his own body, causing the wires to twist. This causes the payload to rise a few centimeters. The gravitational attraction essentially causes the payload to rotate, such that it has the least potential energy at the desired yaw angle. The speed of the response is determined by the system geometry, rather than the chosen control gains.

System Response for Planar Translation The simulation results for a reference step in the x-direction is shown in 6-9. The desired vertical distance between the payload and leader body is kept at 2.5 meter, to illustrate the disturbances. The left plots show the payload attitude and position, and a depiction of the system configuration during motion is shown on the right. The leader applies a reference step to the desired payload position at $t = 4$ seconds. In reality, this would result in sustained oscillations, but with the external damping the translation of the payload is very well controlled. The problem can be seen in the payload attitude plot. As illustrated by the system configuration in the right hand plot, the sideways motion causes the payload to roll. Although this effect quickly diminishes, due to the added damping, it can be expected that the follower UAV will mistake the disturbance for a desired rotation, and amplify this motion.

Combined System Step Response The simulation results for the ATP for a combined desired translation and rotation is shown in 6-10. The desired vertical distance between the leader and payload body has been decreased to 1.5 meters, to decrease the disturbing effects shown in Figure 6-8 and Figure 6-9. The payload attitude and position are shown in 6-10a and 6-10b respectively. It can be seen that the payload eventually converges to the desired configuration. By comparison, the ideal case where the leader acts as a controlled

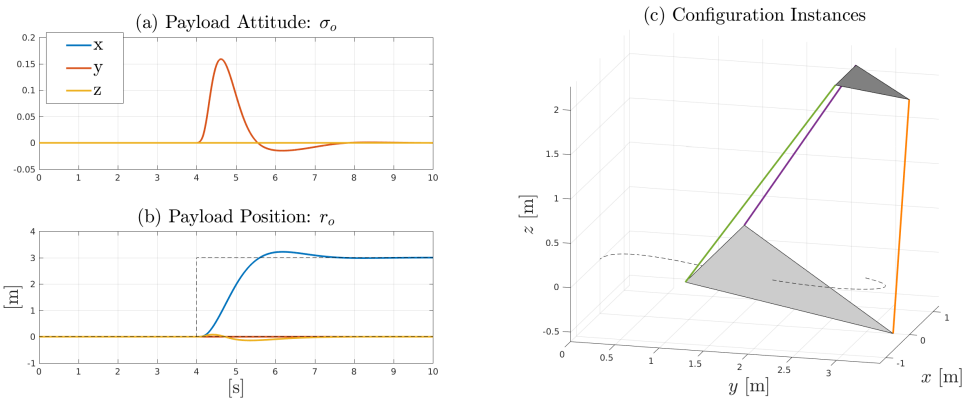

Figure 6-9: Simulation results for a desired payload translation in the x-direction (Proposition 6-3.1): Plots (a) and (b) show the payload MRPs and position respectively. The three colors, blue, red and yellow correspond to the x, y and z components of the presented vector. The black dashed line shows the payload reference signal, which is a reference step to the desired position of 3 meter in the x-direction. Plot (c) shows a depiction of the system configuration during the motion.

wrench at the payload CoG is shown by the colored dashed lines. The payload motion shows several disturbances, which are related to the combined effects of the sideways motion and the desired yaw rotation. These disturbances also effect the torque and force applied to the leader UAV body, as can be seen from 6-10c and 6-10d. From Figure 6-10e it can be seen that the cable lengths converge to the desired lengths without much disturbance. The cable tensions, shown in Figure 6-10(f) show a large spike due to the reference step signal. This spike could potentially be decreased by a simple saturation limit. Note from the depiction of the system configurations that Assumption 6-3.1 can safely be assumed to hold.

6-5-2 Simulations of a Single Leader and Ten Follower UAV

Ten follower UAV are added to the system description, by considering each to be attached to the payload via a single cable. The follower UAV apply the tracking law given in Proposition 5-2.1, and apply the consensus law given in Proposition 4-2.1 for estimating the desired payload configuration. The external damping is removed from the payload, since the follower agents are able to provide this. The simulation results are given in Figure 6-11, Figure 6-12 and Figure 6-13. It is found that the disturbances seen in 6-10 are amplified by the follower agents, resulting in much slower convergence. Nevertheless, eventually, all requirements posed in 1-3 are achieved. Furthermore, it must be noted that the leader towing the payload alone is unable to damp the motion of the payload, without the added external damping. It can thus be argued that the complete system still performs better than nothing at all.

Payload Tracking Dynamics and Leader Amplification From Figure 6-11a and Figure 6-11b it can be seen that the payload eventually stabilizes at the desired configuration. Comparison with the leader towing the payload alone, represented by the colored dashed lines, shows significant disturbances as well as a much slower response. It was found that the disturbances shown in Figure 6-8 and Figure 6-9 have a large impact on the performance. These undesired

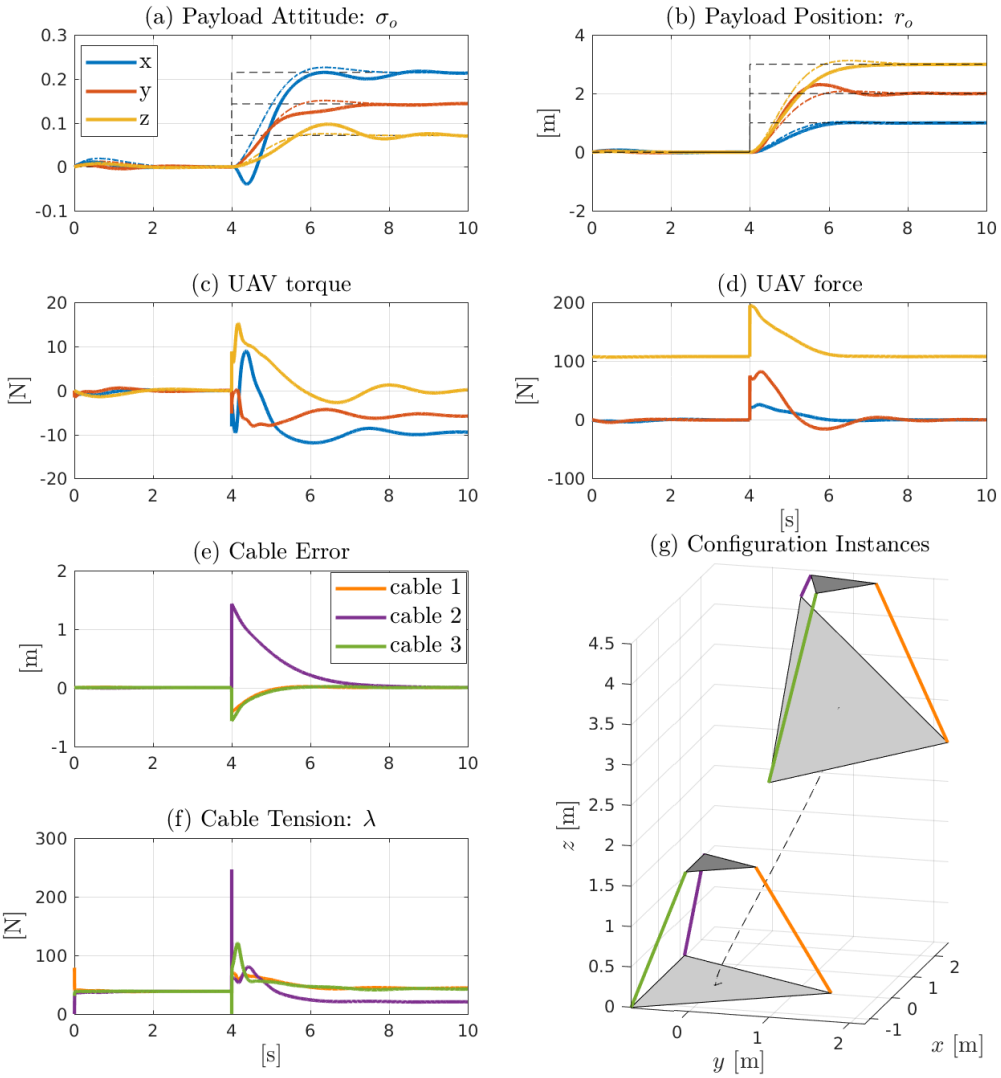

Figure 6-10: Simulation results for the ATP with a single UAV (Proposition 6-3.1: In plots (a) and (b) the payload MRPs and position are shown respectively. The leader leader reference signals are shown by the black dashed lines, corresponding to a $\theta = 60\,\text{deg}$ rotation about the $\epsilon = [3 \quad 2 \quad 1]^T$ axis, and a translation to $r_{\text{des}} = [3 \quad 2 \quad 1]^T$ [m], applied at $t = 4$ seconds. Plots (c) and (d) show the leader torque and force applied to the UAV body. Plots (e) and (f) show the cable length error and the cable tension. The three colors, orange, purple and green, correspond to each of the three cables. Plot (g) shows the system configuration at $t = 4$ and $t = 10$ seconds, where the leader UAV is represented by the small triangle.

motions are amplified by the followers, and require some time to settle down. Nevertheless, it can be seen that the leader control effort is significantly lowered, by comparison with Figure 6-10.

Consensus Dynamics of the Estimation Errors The mean estimation errors of the follower agents are shown in 6-12. The follower agents expect the leader to be a controlled wrench at the CoG, and a significant deviation from that presumption will lead to significant estimation errors. Notably, the disagreement dynamics shown in 6-13 are very similar to the ideal case, shown in Figure 4-1 and Figure 4-1. This is because the disagreement dynamics are still described by (4-17).

6-6 Conclusion

This chapter considered the case where a single leader controls the payload motion via three extendable cables. The control law was designed for the leader towing the payload alone. The three leader cables where controlled to behave as virtual spring dampers, stabilizing the relative configuration of the payload with respect to the leader. This allowed the leader to control the full motion of the payload, despite the underactuation of the system. The IKP was introduced as the problem of finding the desired cable lengths for controlling the relative payload configuration. A method for solving the IKP was proposed, and the efficacy was shown via a numerical example. The control law for the leader towing the payload alone was proposed, and convergence to an equilibrium state was proven via Lyapunov arguments. The existence of multiple equilibrium states was argued to be of little practical relevance, and convergence to the desired equilibrium was assumed to hold. Simulation results of the leader towing the payload alone were presented. It was shown that the system step response deviates significantly from the benchmark, which can be traced back to the underactuation of the system. Nevertheless, the payload was shown to stabilize at the desired configuration, which included an angle of rotation of 60 deg.

The consensus problem was addressed by adding the follower UAV to the system using the approach outlined in the previous chapter. The complete system performance was evaluated via simulation rather than through analytic expressions. From the simulation results it was found that the performance loss is similar to the case where the leader is towing the payload alone. Nevertheless, it was shown that, the payload is stabilized at the desired configuration, the agents converge to the agreement set, and that the leader control effort was amplified.

In comparison to the approach outlined in the previous chapter, which was of NDI-type, the proposed approach was argued to be much less computationally demanding and dependent on an accurate model. Furthermore, the control law is independent of both the payload and leader UAV inertia. The use of a single leader allows for the Cooperative Manipulation Problem (CMP) to be achieved without any communication between the agents. The underactuation results in performance deterioration for rotations about the yaw axis, and for translation in the horizontal plane. Despite these disturbances it was shown that the proposed consensus law does not destabilize the system, showing a certain robustness to unmodelled disturbances.

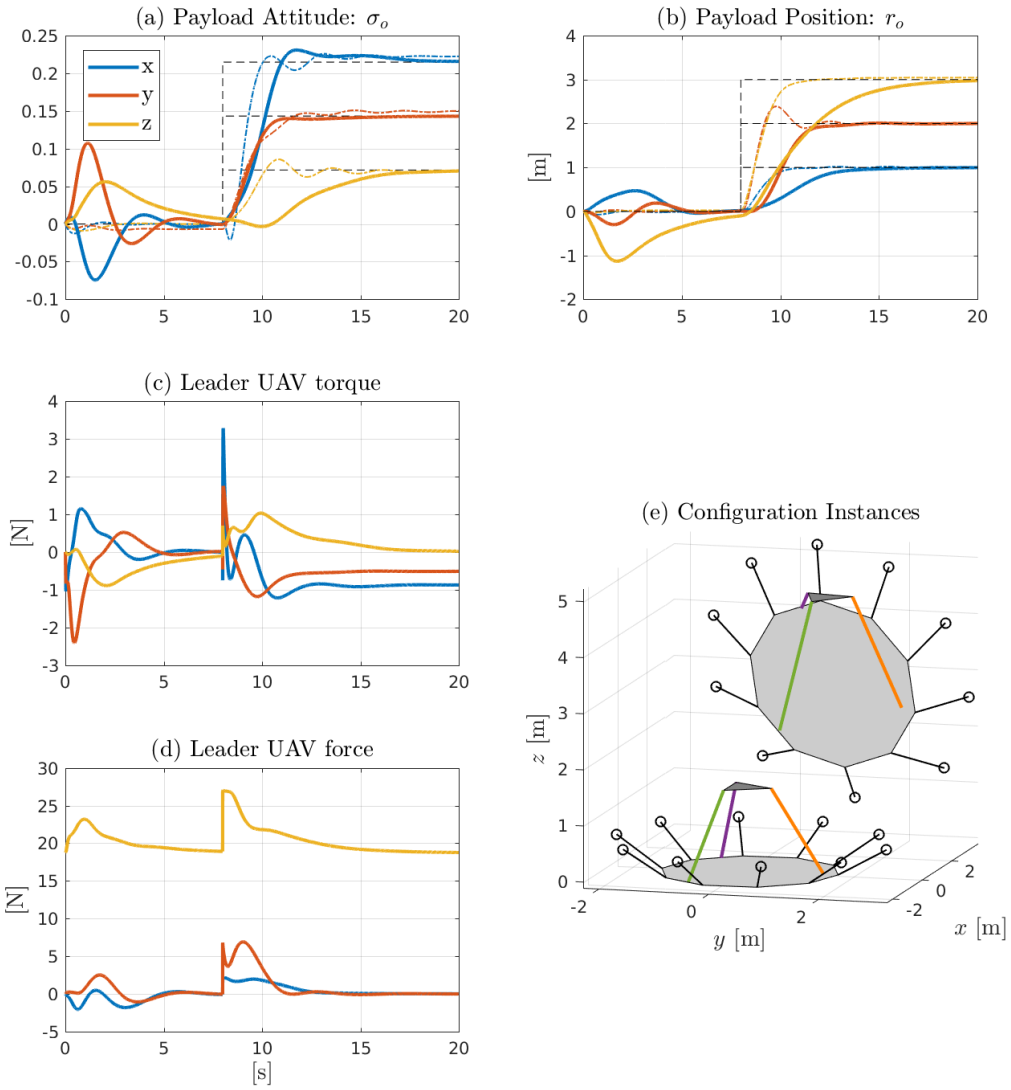

Figure 6-11: Simulation results for the ATP using 10 follower UAV and a single leader: Plot (a) and (b) show the payload attitude and position respectively. The dashed black lines are the reference signals of the leader, corresponding to a $\theta = 60\,\text{deg}$ rotation about the $\epsilon = [3 \quad 2 \quad 1]^T$ axis, and a translation to $r_{\text{des}} = [3 \quad 2 \quad 1]^T$ [m], applied at $t = 8$ seconds. Plot (c) and (d) show the leader torque and force applied to the UAV body. Plot (e) shows the system configuration at $t = 8$ and $t = 20$ seconds, where the follower UAV are represented by the black circles, and the leader UAV by the small triangle.

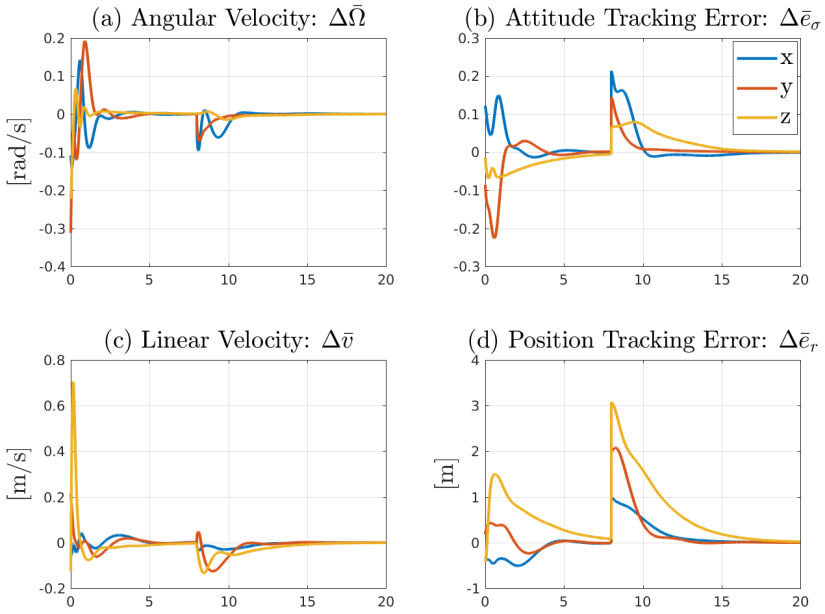

Figure 6-12: Simulation results of the follower mean estimation errors during the ATP as depicted in Figure 6-11: The mean estimation errors are shown for the, (a) payload angular velocity, (b) attitude tracking error, (c) payload linear velocity, and (d) for the position tracking error. The three colors, blue, red and yellow correspond to the x, y and z components.

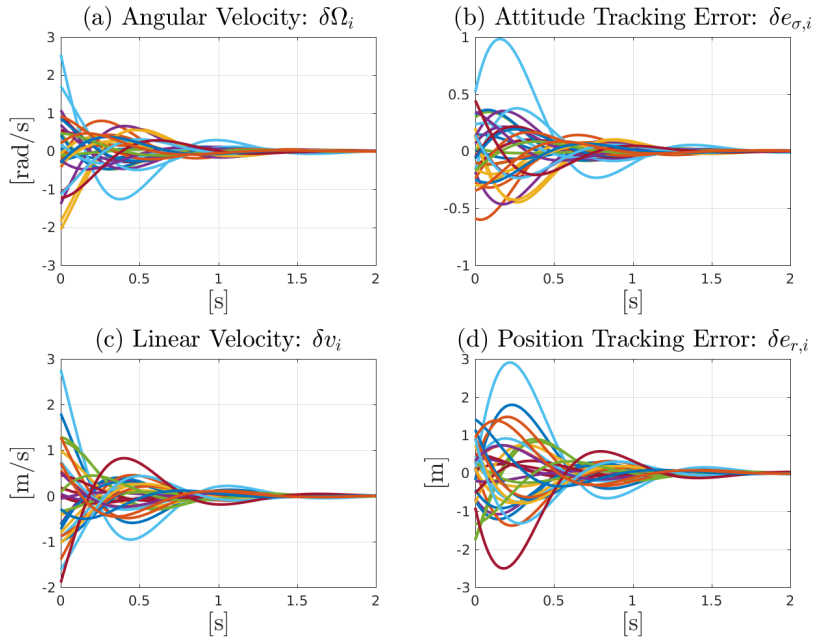

Figure 6-13: Simulation results of the follower disagreement vectors during the ATP as depicted in Figure 6-11: The disagreement vectors are shown for the, (a) payload angular velocity, (b) attitude tracking error, (c) payload linear velocity, and (d) for the position tracking error. The many different colors correspond to the different agents.

Chapter 7

Conclusion and Recommendations

The main goal of this thesis was to investigate the consensus dynamics for the Cooperative Manipulation Problem (CMP) where consensus is reached without using explicit communication. This problem was addressed in a general setting by considering a directly actuated rigid body, and subsequently applied to the Aerial Towing Problem (ATP) where multiple Unmanned Aerial Vehicles (UAV) are towing the payload. A summary of the results is provided next, followed by a conclusion and the contributions of this thesis work. This chapter finalizes with recommendations for future research.

7-1 Summary

Using multiple robots for the CMP of a payload couples the robot dynamics. For a Leader-Follower (LF) based approach, where only some of the agents have knowledge on the desired configuration, this would require a fast type of communication to avoid high tension forces and ensure stability of the system. By using the payload motion as the means of reaching consensus this problem is resolved, leading to all-to-all communication regardless of the number of participating agents. With the decrease in size and cost of commercially available UAV this approach was considered applicable to the ATP. For the control law the following design requirements where set:

1. The leader control effort must be amplified.
2. The agents must reach consensus on the desired payload configuration.
3. The payload must be stabilized at any desired configuration, that is a position and an attitude.

To make this problem more amenable it was chosen to split the problem into two parts: The consensus laws were designed while the robot dynamics were neglected, and subsequently, the resulting consensus laws were applied to the ATP. With the robot dynamics neglected the

design requirements could be investigated for a general rigid body which is directly actuated. This resulted in a more general problem setting such that parallels could be drawn between existing results on cooperative control and the problem at hand.

Even disregarding the consensus problem, it was found that a great number of parameters were required to simply stabilize the payload. In order to cancel the gravitational wrench and the Coriolis terms it was concluded that all payload parameters must be known. This led to the choice of canceling these terms, resulting in a much simplified description of the payload motion. Three subjects were chosen as the topic of investigation, that directly effect the consensus dynamics:

1. The choice of attitude representation.
2. The measurements that are available to the agents.
3. The ability to apply a wrench or a force to the payload, i.e full- or underactuation.

These three problems allowed for a further division of the thesis work.

The simplest combination of these three was identified as the use of Modified Rodrigues Parameters (MRPs), acceleration measurements, and full actuation. The MRPs were chosen as these give a minimal attitude representation allowing for an additive tracking error. A nonlinear Proportional Derivative (PD)-type control law was proposed where each agent uses his local estimate of the payload tracking error. Assuming acceleration measurements this allowed for a direct communication of the local estimates between the agents. A separation approach was considered, with the intent to isolate the consensus problem from the payload dynamics. This allowed for a structured design of the consensus law, and convergence of the consensus dynamics was achieved. Despite global convergence of the estimation errors it was shown that boundedness of the payload state could not be guaranteed. For the fully actuated case this problem could be resolved by adding a small coupling between the consensus dynamics and the payload dynamics. This coupling could be chosen arbitrarily small, such that the performance remains unaffected but the proof could be completed. For the underactuated case it was shown that the associated Laplacian matrix is state dependent, and stability of the payload configuration could only be locally guaranteed. It was illustrated via simulations that the proposed solution is able to describe large rotations, despite the proof of local stability.

The disadvantage of the MRPs is that they become singular at angles of ± 360 deg, preventing arbitrary motion descriptions. Furthermore, an additive tracking error can not be regarded as a proper attitude error metric. For these reasons a geometric control approach was investigated. A globally defined consensus law was proposed through the use of rotation matrices. Acceleration measurements where assumed available to the agents, and the fully actuated case was considered first. It was shown that, without a leader, *almost global* convergence could be derived. With the addition of a leader it was proposed to separate the disagreement, mean estimation error and tracking dynamics. As opposed to the use of MRPs it could be shown that all signals remain bounded, but not that the state reaches a limit. For attitude tracking errors within ± 90 deg of the current payload attitude it was shown that convergence to the desired equilibrium results, and a bound on the convergence rate was provided. Global

convergence could not be derived, and it was graphically illustrated that the disagreement evaluation on $SO(3)$ causes this problem. Through simulations it was illustrated that there is a strong incentive that the proposed geometric control law always reaches the convergent region. A direct extension to the underactuated case was provided, but the same limitation in the proof remained.

The requirement of acceleration measurements was relaxed by designing a nonlinear observer requiring velocity measurements. The MRPs were chosen as a simplification of the problem. A separation of the consensus dynamics from the payload dynamics resulted in a similar problem: While this separation is intuitive for the control law design, it complicates the proof of convergence. For the fully actuated case the problem was similarly resolved by adding a small coupling gain, but for the underactuated case a mere proof of local convergence resulted. Through simulation results it was shown that the decoupling strategy could be advocated for, as the payload configuration state shows no danger of growing unbounded. Alternatively it was shown that a complete Nonlinear Dynamic Inversion (NDI) of the payload dynamics resulted in almost linear consensus dynamics. For the underactuated case this allowed for a separation of the consensus and payload dynamics, leading to global convergence. It was noted that NDI further increases the dependency on an accurate model description, reducing its practical value.

The consensus laws were designed under the assumption that the agents can control the force acting on the payload. To apply these results to the ATP the tracking law for the UAV was designed to approximate this assumption. A centralized approach taken from the literature was modified to allow for a decentralized implementation. This approximation of the centralized approach was proposed such that the consensus laws could be applied to the ATP. It was shown in simulation that this approach indeed allows the consensus laws to be applied to the ATP where the payload is towed via cables attached to the UAV. A downside to this approach is that three or more leaders are required to control the payload motion. Furthermore, it was shown that the tracking law is very dependent on an accurate model description.

As an alternative to the use of three or more leader UAV it was considered to use a single specialized leader UAV. By towing the payload via three extendable cables a single UAV is able to control the payload motion. In this case the leader is not able to completely control the wrench at the payload Center of Gravity (CoG), resulting in a slower convergence to the desired equilibrium state. This loss of performance is complemented by a decrease in control law complexity.

7-2 Discussion and Conclusions

The main research question can be answered as positive: For a general rigid body it can be concluded that a LF based approach to the CMP can be accomplished by communicating through the motion of the payload. This allows for the leader control effort to be amplified, constitutes a fast means of communication, and scales well for an increasing number of participating agents. A nonlinear system description allows for the payload to be stabilized at any

desired configuration. Regarding the posed objectives in Section 1-3 the following conclusions are drawn:

The Effect of Full- Versus Underactuation If the agents can apply only a force to the payload the generalized inverse of the adjoint matrix can be used to control the full payload motion. With the addition of the consensus problem the use of the generalized inverse results in a matrix-weighted graph Laplacian. These matrix weights are rank deficient, state dependent, and non-symmetric, which makes the underactuated case a challenging problem. The rank deficiency would indicate that some of the local information can not be communicated to the other agents. It was however shown that for identical observer gains the disagreement dynamics still show all-to-all communication. This property was used to separate the disagreement problem, removing the state dependent Laplacian matrix from the consensus problem. A final obstacle is then formed by the nonlinear description of the payload dynamics. Even if global convergence of the consensus dynamics can be shown, this can in general not be separated from the payload dynamics. Only through the use of NDI was it found possible to account for both the complicated Laplacian matrix, as well as the payload dynamics.

Minimal versus Global Attitude Description The use of MRPs allows for global convergence properties to be derived, as long as neither the initial condition nor the reference is chosen at the singularity. The absence of a constraint simplifies the control design, and from simulations it can be seen that they are well behaved for large rotations. A disadvantage is that arbitrary motions, such as multiple rotations, can not be described without switching to another set of MRPs. The main challenge when using MRPs is to show boundedness, which is the price for a constraint free representation.

A geometric approach shows many advantages, but simply complicates the mathematical analysis. The proposed solutions are shown to be applicable to both the fully actuated as the underactuated case, and allow for global motions to be described. Boundedness of all signals is more easily shown, as opposed to the use of MRPs, but the difficulty lies in proving the convergence of the state to a limit. Convergence was proven within a region of $\pm 90\,\text{deg}$, for which a bound on the convergence rate can be derived. The provided solutions are limited, firstly due to the assumption of acceleration measurements, and secondly due to the restriction of the convergence region. Nevertheless, this approach showed promising results, motivating further investigation.

Effect of Available Measurements on the Consensus Dynamics The order of the consensus problem was shown to be determined by the available measurements. The information exchange between the agents could be revealed through the estimation error dynamics. For acceleration measurements a first order consensus problem results and any positive gains were found to be stabilizing. In case of velocity measurements a constraint on the observer gain was found, but this was considered to be non-restrictive. For arbitrary measurements a higher order consensus problem arises, where the search for stabilizing control gains gives rise to a simultaneous stabilization problem. This simultaneous stabilization problem is nonlinear, and difficult to solve in general.

Parameter Dependency of the Proposed Solutions The proposed methods were shown to be dependent on all the payload parameters. Proof of convergence could only be obtained by canceling both the gravitational wrench as well as the Coriolis terms. It can be concluded that this is caused by the posed requirements: If it is desired to amplify the leader's control effort, then consensus must be reached during the motion. This indicates an observer problem, which is challenging to solve without a system model. Similarly, the agents require knowledge on all the control gains used by the other agents, in order to reconstruct the estimated state. This can be related to the Laplacian matrix, as a requirement for a zero-row sum.

Application to the ATP The assumption of a controlled force acting on the payload could be relaxed through a proper tracking law for the UAV. It was shown that the exact solution for controlling the force at the attachment point requires centralized knowledge. This solution could be approximated allowing for a decentralized implementation. For simulation purposes it can be concluded that a nonlinear tracking law for the UAV can be used to apply the consensus problem to the ATP. From a practical point of view this method requires many computations and shows a high degree of parameter dependency. Furthermore, for a small-scale experiment the requirement of three or more leaders is restrictive. The use of a single leader with three extendable cables was shown to be a good alternative to reduce the controller complexity and the number of leaders required. The downside of this approach is that the leader-payload system is underactuated, resulting in loss of performance.

7-3 Thesis Contributions

The main contributions of this thesis comprises of two parts, the first considering the CMP of a general rigid body, and the second the application to the ATP:

1. A decentralized control approach for the LF based CMP is presented that requires no communication amongst the agents. The followers reach consensus, and estimate the desired payload configuration through the motion of the payload. This allows the leader's control effort to be amplified, and the payload to be stabilized at any desired configuration.
    (a) The effect of available measurements on the consensus dynamics has been investigated. In case of acceleration or velocity measurements globally converging consensus laws were developed. In case of acceleration measurements the convergence rate was derived.
    (b) The effect of underactuation on the Laplacian matrix has been investigated, leading to several proposed solutions. Control laws for global convergence were developed which assumed accurate knowledge on model parameters. More practical control laws were developed leading to local convergence.
    (c) A geometric control approach is presented that allows for a global system description. Assuming acceleration measurements, the proposed consensus law was shown to have a large region of convergence, and a bound on the convergence rate was derived. This method was shown to be applicable to both the full- and underactuated case.

2. The proposed consensus laws were applied to the ATP, leading to a decentralized cooperative towing of a payload using multiple UAV. A control law for a single UAV towing the payload via three extendable cables was developed. The resulting system is poorly damped. The result is a decentralized control approach for the ATP using an arbitrary number of followers, and a single leader UAV.

7-4 Recommendations

This section provides recommendations for extending this thesis work. Recommendations for a small scale experiment are given next, followed by recommendations for future research.

7-4-1 Recommendations for a Small Scale Experiment

The following contains recommendations for applying the proposed consensus laws to the ATP through a small scale experiment.

Mechanical Considerations One conclusion that could be drawn from the tracking law design for the UAV in Chapter 5 is that this approach is too dependent on system parameters, and too computationally expensive for implementation on UAV. It was initially assumed that the control law could be simplified to the point of a simple PD-type control for the cable direction. This was found to be insufficient, even in simulation. For a small scale experiment the approach in [1], and depicted in Figure 7-1 might provide a much more practical solution. The main simplification is that the robot dynamics can indeed be neglected, and one can consider the rigid body to be directly actuated. This brings several other challenges, but the general approach considered in this thesis work still applies.

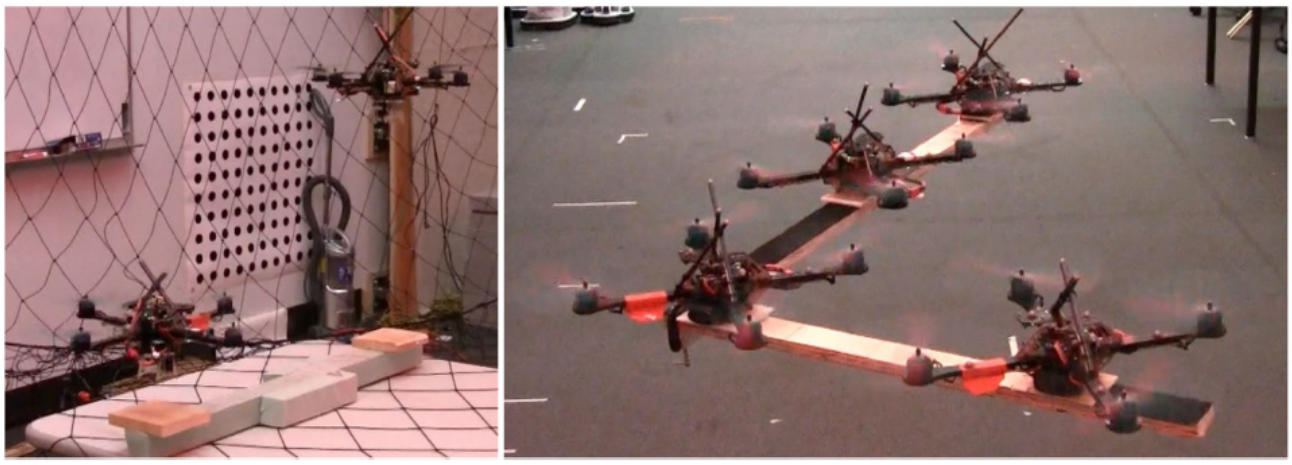

Figure 7-1: Images from an experiment conducted in [1]: Left: shows the quadrotor with the gripping mechanism. Right: Four quadrotors carrying a payload.

Sensing Considerations Considering the ATP as described in Chapter 5, it would be challenging to obtain the payload attitude through forward kinematics. This would require involved rotation sensors to be mounted on both ends of the cable. A simple alternative is to

mount a small Inertial Measurement Unit (IMU) on the payload which transmits the measurements to all follower agents. In [47], [36] a simple filter is shown that allows the reconstruction of the rotation matrix from a gyroscopic, acceleration, and magnetic field sensor. Although provided with a very elegant proof, it is based on the assumption that the acceleration sensor points towards earth on average. This assumption should be incorrect, but claims of successful results in the literature have been reported. This would provide a cheap and simple method of obtaining the payload's attitude, provided it works.

7-4-2 Recommendations for Future Research

The provided solutions in this thesis work can be seen to have several limitations. The limitations, and possible improvements are discussed next:

1. **Decentralized adaptive control:** The dependency on model parameters could potentially be reduced through adaptive control. An additional challenge is to derive a decentralized adaptive control law. See [48] for a decentralized adaptive approach to the CMP using robotic manipulators.

2. **Geometric control approach:** The presented geometric solution in Chapter 3 depended on a region of convergence. Further investigation is required to investigate global convergence.

3. **State Dependent Weighted Laplacian Matrix:** The underactuated case resulted in a complicated state dependent Laplacian matrix, see (4-16) and (4-12). Due to the non-symmetry and state dependency of this matrix it was found to be challenging to relax the assumption of identical observer gains. In case of individual observer gains a method is required for analyzing a Laplacian matrix with non-symmetric state dependent matrix weights. Additionally, it must be applicable to a second order consensus problem where the jacobian of the kinematics in general does not commute with these matrix weights. This is a challenging problem.

4. **Shadow set for MRPs:** The use of shadow parameters is mentioned in the literature, as a means to overcome the singularity problem of the MRPs [49], [50], [51], [25]. The intention is to use two different sets of MRPs and to switch at $\theta = \pm 180$ to the other set. This causes the used MRPs to always remain norm-bounded, and at the switching surface both sets have the same norm. The possible interest for application to the CMP is that all agents can switch to the shadow set simultaneously, since it can be deduced from the payload state. This shows a clear advantage over multi vehicle control scenarios, such as [25], where this would have to be communicated. However, a proper Lyapunov based argument was only provided in [49] for the case where the reference attitude is at the origin. This result can not be directly extended to general reference signals, simply because it must be decided whether or not to also map the reference signal to the shadow set. This must be done via heuristics to prevent injection of energy into the system, and a convincing mathematical support appears to be missing.

5. **Human Operator:** A human operator as the leader of the CMP would make a very strong case, since in that case the leader can not communicate the intended trajectory to the other agents. The proposed control laws are difficult to combine mathematically

with this scenario, since it was assumed that the leader control action fits a certain model. Impedance based control methods pose an interesting approach to human-robot interactions, and shows several similarities to this thesis work. By measuring the payload's motion the interaction to external disturbances can be regulated, see [52], [53].

6. **Effect of Time Delays and Acceleration Measurements:** The acceleration measurements were considered unpractical. However, in [54] use is made of acceleration measurements and a butterworth filter is used to reduce the noise. This introduces a time delay which should be accounted for. The effect of time-delays is a well studied subject in consensus theory, and this would make a great practical case.

7. **Passivity Based Control:** If the requirement that the leader control effort must be amplified is removed this opens a path to the use of Passivity Based Control (PBC). In [13] it is shown that PBC can be used for the CMP, where consensus is reached using the payload motion. This approach is not aimed at amplifying the leader control effort, but allows for compliant behavior. This approach is not considered for the rotational motion, which would make for an interesting subject.

Appendix A

Background Theory

A-1 Graph Theory: The Complete Graph

Graph theory [55] presents a high-level description of the network topology and plays an essential role in the analysis of consensus dynamics. The following contains only the required definitions for analyzing consensus in this thesis work.

The agreement set can be considered as the definition of reaching consensus amongst the follower agents:

Definition A-1.1. *Let the agreement set be defined as*

$$\mathbb{A} = \{x_i | x_i = x_j, \forall i \in \{1, \dots, n_f\}\} \tag{A-1}$$

For multiplications of large matrices with a repetitive structure the Kronecker product allows for a compact notation:

Definition A-1.2 (Kronecker Product)**.** *Consider matrices $A \in \mathbb{R}^{m \times n}$ and $B \in \mathbb{R}^{p \times q}$, the Kronecker product is the defined as*

$$A \otimes B = \begin{bmatrix} a_{11}B & \dots & a_{1n}B \\ \vdots & \ddots & \vdots \\ a_{m1}B & \dots & a_{mn}B \end{bmatrix} \tag{A-2}$$

where a_{ij} denote the elements of A.

For this thesis essentially all communication topologies considered are that of a *complete* graph, which can be represented with the associated Laplacian matrix. Let $\mathbf{1}_n \in \mathbb{R}^n$ denote a vector with elements equal to 1, and consider the Laplacian matrix for the complete graph defined as:

Definition A-1.3. *Let the $n \times n$ Laplacian matrix for the complete graph be defined as*

$$L = nI_{n\times n} - \mathbf{1}_n \mathbf{1}_n^T \tag{A-3}$$

for which it holds that $\mathbf{1}_n \in \mathbf{null}\{L\}$ and the eigenvalues are given by $\lambda = \{0, n, n, \ldots, n\}$.

A specific weighted Laplacian matrix for the complete graph is used various times in this thesis:

Definition A-1.4. *Let the $n \times n$ weighted Laplacian matrix for the complete graph be defined as $L_w\{a_i\}$, where $a_i > 0$ for $i \in \{1, \ldots, n_f\}$ are scalars or diagonal matrices $a_i \in \mathbb{R}^{m\times m}$ specified by the problem. For given a_i the Laplacian matrix $L_w\{a_i\}$ is constructed as,*

$$L_w\{a_i\} \;=\; \mathcal{D}\{a_i\} - \mathcal{A}\{a_i\}, \quad \in \mathbb{R}^{mn_f\times mn_f} \tag{A-4}$$

where $\mathcal{D}\{a_i\}$ and $\mathcal{A}\{a_i\}$ denote the weighted degree and adjacency matrix, given as

$$\begin{aligned} \mathcal{D}\{a_i\} &= [\mathcal{D}_i]_{diag} \in \mathbb{R}^{mn_f\times mn_f}, & \mathcal{D}_i &= a_i \sum_{j=1}^{n_f} a_j \in \mathbb{R}^{m\times m} \\ \mathcal{A}\{a_i\} &= [\mathcal{A}_{ij}] \in \mathbb{R}^{mn_f\times mn_f}, & \mathcal{A}_{ij} &= a_i a_j \in \mathbb{R}^{m\times m} \end{aligned} \tag{A-5}$$

for which it holds that $\mathbf{1}_n$ spans the nullspace of L_w and $L_w = L_w^T \geq 0$.

A-2 Rotation Matrix Properties

For rigid body motions the configuration space is defined on a manifold, which is a curved subspace of the euclidean space. Group theory can be used to define global formulations of the configuration and motion on the manifold [24]. Of special importance is the rotation matrix, denoted by R, which evolves on the special orthogonal group $SO(3)$. Many properties can be found in the excellent books [56] and [24], or the survey on attitude representations [20], of which a selection will be presented in this section.

The Rotation Matrix The space of the rotation matrices R is defined as the special orthogonal group $SO(n)$ [24],

$$SO(n) = \left\{R \in \mathbb{R}^{n\times n} : R^T R = I_{n\times n}, \det R = +1\right\} \tag{A-6}$$

It is assumed throughout this thesis that the rotation matrix maps a vector from the body frame towards the inertial frame, as is the convention in [24]. The position $r \in \mathbb{R}^3$ and

orientation $R \in SO(3)$ of a rigid body gives together the configuration $\{r, R\}$. The space of rigid body motions is the configuration space $SE(3)$, called the special Euclidean group,

$$SE(3) = \{\{r, R\} : r \in \mathbb{R}^3, R \in SO(3)\} = \mathbb{R}^3 \times SO(3) \tag{A-7}$$

The space of skew symmetric matrices S is defined as $so(n)$ [24],

$$so(n) = \left\{S \in \mathbb{R}^{n\times n} : S = -S^T\right\} \tag{A-8}$$

which is related to the angular velocity. Consider the time derivative of the rotation matrix associated with a rigid body,

$$\dot{R} = R\tilde{\Omega} \tag{A-9}$$

where $\Omega \in \mathbb{R}^3$ is the angular velocity, and the tilde operator is defined as:

Definition A-2.1 (Tilde and Untilde Operator)**.** *The tilde operator accepts a vector* $a = \begin{bmatrix} a_1 & a_2 & a_3 \end{bmatrix}^T \in \mathbb{R}^3$ *and returns a skew symmetric matrix*

$$\tilde{a} = \begin{bmatrix} 0 & -a_3 & a_2 \\ a_3 & 0 & -a_1 \\ -a_2 & a_1 & 0 \end{bmatrix} \in so(3) \tag{A-10}$$

The untilde operator $\{\cdot\}^V$ *accepts a skew symmetric matrix* $S \in so(3)$ *and returns a vector* $a \in \mathbb{R}^3$*,*

$$S^V = \tilde{a}^V = a \in \mathbb{R}^3, \qquad S \in so(3) \tag{A-11}$$

Trace Properties The trace of a matrix, denoted as $\mathrm{tr}\{\cdot\}$, plays an important role in the construction of Lyapunov candidates using rotation matrices. The following is a listing of the most important of these properties.

The following operator is useful in deriving the torque applied to a rigid body, and for decomposing a matrix in the symmetric and anti-symmetric part:

Definition A-2.2 (Symmetric and Anti-Symmetric Operator)**.** *Considering any matrix* $A \in \mathbb{R}^{n\times n}$*, define the symmetric and anti symmetric operator,* $\mathbb{P}_s\{A\}$ *and* $\mathbb{P}_a\{A\}$ *respectively, as*

$$\mathbb{P}_s\{A\} = \tfrac{1}{2}\left(A + A^T\right) \qquad \mathbb{P}_a\{A\} = \tfrac{1}{2}\left(A - A^T\right) \tag{A-12}$$

and note that $A = \mathbb{P}_s\{A\} + \mathbb{P}_a\{A\}$*.*

Lemma A-2.1. *Consider a symmetric matrix* $A = A^T \in \mathbb{R}^{3\times 3}$ *and an anti-symmetric matrix* $S = -S^T \in \mathbb{R}^{3\times 3}$*, then*

$$tr\{AS\} = 0. \tag{A-13}$$

This gives the useful lemma:

Lemma A-2.2. *Consider the matrices $A \in \mathbb{R}^{3\times 3}$ and $B \in \mathbb{R}^{3\times 3}$, then*

$$tr\{\mathbb{P}_a\{A\}B\} = tr\{\mathbb{P}_a\{A\}\mathbb{P}_a\{B\}\} = tr\{A\mathbb{P}_a\{B\}\}. \tag{A-14}$$

The trace relates the dot-product and cross-product as,

Lemma A-2.3. *Consider the vectors $a \in \mathbb{R}^3$ and $b \in \mathbb{R}^3$, then*

$$a^T b = \tfrac{1}{2} tr\left\{\tilde{a}^T \tilde{b}\right\}. \tag{A-15}$$

From the above, and the previous lemmas the following useful relation is obtained,

Lemma A-2.4. *Consider any matrix $A \in \mathbb{R}^{3\times 3}$ and any vector $b \in \mathbb{R}^3$, then*

$$\tfrac{1}{2} tr\left\{A\tilde{b}\right\} = -\left(\mathbb{P}_a\{A\}^V\right)^T b. \tag{A-16}$$

The above lemma follows from

$$\begin{aligned} \tfrac{1}{2}\mathrm{tr}\left\{A\tilde{b}\right\} &= \tfrac{1}{2}\mathrm{tr}\left\{\left(\mathbb{P}_a\{A\} + \mathbb{P}_s\{A\}\right)\tilde{b}\right\} \\ &= \tfrac{1}{2}\mathrm{tr}\left\{\mathbb{P}_a\{A\}\tilde{b}\right\} \\ &= -\tfrac{1}{2}\mathrm{tr}\left\{\mathbb{P}_a\{A\}^T\tilde{b}\right\} = -\left(\mathbb{P}_a\{A\}^V\right)^T b \end{aligned} \tag{A-17}$$

The following two lemmas can be used to find bounds on the Lyapunov functions,

Lemma A-2.5. *For any symmetric $A \in \mathbb{R}^{m\times m}$ and any matrix $B \in \mathbb{R}^{m\times m}$ the following holds,*

$$tr\{AB\} \geq \lambda_{\min}\{A\}\, tr\{B\} \tag{A-18}$$

where $\lambda_{\min}\{A\}$ is the minimal eigenvalue of A [34].

Lemma A-2.6 (Minimum Eigenvalue of $R \in SO(3)$)**.** *For any $R \in SO(3)$ the minimal eigenvalue of $\mathbb{P}_s\{R\} = \frac{1}{2}\left(R + R^T\right)$, denoted as $\lambda_{\min}\{\mathbb{P}_s\{R\}\}$ is equal to $\cos\theta$ [34].*

Rodrigues' Rotation Formula Many interesting properties of the rotation matrix can be derived from the Rodrigues formula,

Definition A-2.3 (Rodrigues Formula)**.** *The rotation matrix can be related to the axis ϵ and angle θ of revolution as,*

$$R(\epsilon,\theta) = I + \sin(\theta)\tilde{\epsilon} - (1-\cos(\theta))\tilde{\epsilon}\tilde{\epsilon}^T \tag{A-19}$$

Using the Rodrigues formula and Definition A-2.2 one can directly derive that

$$\mathbb{P}_a\{R\} = \sin\theta\epsilon \tag{A-20}$$

which is often used as the torque to control a rigid body. Considering that $\mathrm{tr}\left\{\tilde{\epsilon}\tilde{\epsilon}^T\right\} = \mathrm{tr}\left\{I - \epsilon\epsilon^T\right\} = 3 - \epsilon^T\epsilon = 2$ gives $\mathrm{tr}\{R\} = 3 - (1-\cos(\theta))2 = 1 + 2\cos(\theta)$. This gives the following basic Lyapunov candidate:

Lemma A-2.7. *Consider the rotation matrix $R(\epsilon,\theta) \in SO(3)$ with the kinematics given as*

$$\dot{R} = R\tilde{\omega} \tag{A-21}$$

Then, the following function is non-negative,

$$\tfrac{1}{2}tr\{I - R\} = 1 - \cos(\theta) \geq 0 \tag{A-22}$$

with a time derivative equal to

$$\tfrac{d}{dt}\left[\tfrac{1}{2}tr\{I-R\}\right] = \left(\mathbb{P}_a\{R\}^V\right)^T\omega = \sin(\theta)\epsilon^T\omega. \tag{A-23}$$

The above lemma forms the basis of most Lyapunov functions using the rotation matrix. The time derivative is derived as

$$\tfrac{d}{dt}\left[\tfrac{1}{2}\mathrm{tr}\{I-R\}\right] = -\tfrac{1}{2}\mathrm{tr}\{R\tilde{\omega}\} \tag{A-24}$$

and application of Lemma A-2.4 gives (A-23).

A-3 Modified Rodrigues Parameters

The Modified Rodrigues Parameters (MRPs) can be used to parameterize the rotation matrix [56]:

Definition A-3.1 (Modified Rodrigues Parameters)**.** *Given the attitude of a frame in terms of MRPs, denoted as σ. The MRPs in terms of the axis and angle of revolution, ϵ and θ respectively, are given as*

$$\sigma = \tan\frac{\theta}{4}\epsilon \tag{A-25}$$

And the rotation matrix in terms of MRPs is given as

$$R(\sigma) = I + \frac{1}{(1+\sigma^T\sigma)^2}\left(8\tilde{\sigma}^2 + 4\left(1-\sigma^T\sigma\right)\tilde{\sigma}\right) \tag{A-26}$$

The MRPs are a minimal and constraint free attitude representation, as can be seen from the attitude kinematics:

Definition A-3.2 (MRPs Kinematics)**.** *Consider the attitude kinematics of a rigid body given as $\dot{R} = R\tilde{\Omega}$ with $R \in SO(3)$, and Ω the angular velocity. The attitude kinematics in terms of MRPs is then given as,*

$$\dot{\sigma} = \Xi(\sigma)\,\Omega \tag{A-27}$$

where $\Xi(\sigma)$ denotes the kinematic matrix given as

$$\Xi(\sigma) = \frac{1}{4}\left(\left(1-\sigma^T\sigma\right)I + 2\tilde{\sigma} + 2\sigma\sigma^T\right). \tag{A-28}$$

The kinematic matrix is almost orthogonal, with the inverse given as,

$$\Xi(\sigma)^{-1} = \frac{16}{(1+\sigma^T\sigma)^2}\Xi(\sigma)^T \tag{A-29}$$

A-4 Rigid Body Dynamics of the Payload

The rigid body dynamics play a central role in this thesis work, as it is used to describe the payload dynamics.

A-4-1 Explicit Rigid Body Dynamics

Let the state of a rigid body be represented in terms of the angular velocity $\Omega \in \mathbb{R}^3$, the linear velocity $v \in \mathbb{R}^3$, the attitude $R \in SO(3)$ and the position $r \in \mathbb{R}^3$. The explicit payload

equations of motion consist of the payload dynamics,

$$\begin{aligned} \mathcal{I}_o \dot{\Omega}_o &= -\tilde{\Omega}_o \mathcal{I}_o \Omega_o + \sum \tau \\ m_o \dot{v}_o &= m_o g \bar{b}_3 + \sum F, \end{aligned} \tag{A-30}$$

and the payload kinematics

$$\begin{aligned} \dot{R}_o &= R_o \tilde{\Omega}_o \\ \dot{r}_o &= v_o, \end{aligned} \tag{A-31}$$

where m and $\mathcal{I}$ represent the mass and inertia respectively, $\sum F$ and $\sum \tau$ respectively represent the sum of the forces and torques acting on the payload Center of Gravity (CoG), g denotes the constant gravitational acceleration, $\bar{b}_3 = \begin{bmatrix} 0 & 0 & 1 \end{bmatrix}^T$ denotes the third basis vector, the tilde operator $\{\tilde{\cdot}\}$ is given in (A-10), and finally the subscript o denotes the reference to the payload.

A-4-2 Compact Rigid Body Dynamics

The use of MRPs allows the payload dynamics to be written in a compact notation. To this end, let the state of a rigid body be represented in terms of the twist $\nu = \begin{bmatrix} \Omega^T & v^T \end{bmatrix}^T \in \mathbb{R}^6$ and the configuration coordinates $q = \begin{bmatrix} \sigma^T & r^T \end{bmatrix}^T \in \mathbb{R}^6$, where σ denotes the MRPs. The compact payload equations of motion are then given as

$$\begin{aligned} M_o \dot{\nu}_o &= -C_o(\nu_o) - G_o + \sum w \\ \dot{q}_o &= J_o(q_o)\, \nu_o \end{aligned} \tag{A-32}$$

where $M_o \in \mathbb{R}^{6\times 6}$ represents the mass tensor, $C_o(\nu_o) \in \mathbb{R}^6$ the Coriolis terms, $G_o \in \mathbb{R}^6$ the (gravitational) potential terms, $J_o(q_o) \in \mathbb{R}^{6\times 6}$ the payload kinematic jacobian, and $w \in \mathbb{R}^6$ denotes a wrench, such that $\sum w$ denotes the total wrench acting at the payload CoG. The expressions for M_o, $C_o(\nu_o)$ and G_o can be related to the explicit notation as,

$$M_o = \begin{bmatrix} \mathcal{I} & 0 \\ 0 & m_o I_{3\times 3} \end{bmatrix}, \quad C_o(\nu_o) = \begin{bmatrix} \tilde{\Omega}_o \mathcal{I}_o \Omega_o \\ 0 \end{bmatrix}, \quad G_o = \begin{bmatrix} 0 \\ -m_o g \bar{b}_3 \end{bmatrix} \tag{A-33}$$

and the kinematics $J_o(q_o)$ as

$$J_o(q_o) = \begin{bmatrix} \Xi(\sigma_o) & 0 \\ 0 & I_{3\times 3} \end{bmatrix} \tag{A-34}$$

where $\Xi(\sigma_o)$ is the kinematic matrix associated with the MRPs as given in (A-28).

A-4-3 Parameterized Rigid Body Dynamics

Finally the rigid body dynamics can be represented completely using the configuration coordinates q_o and higher order derivatives. The equations of motion are then given in a similar form as (A-32), resulting in

$$\breve{M}_o(q_o)\, \ddot{q}_o = -\breve{C}_o(\dot{q}_o, q_o) - G_o + J_o(q_o)^{-T} \sum w \tag{A-35}$$

where G_o is given in (A-33), $J_o(q_o)$ is given in (A-34), and the mass tensor $\breve{M}_o(q_o) \in \mathbb{R}^{6\times 6}$ and Coriolis terms $\breve{C}_o(\dot{q}_o, q_o) \in \mathbb{R}^6$ are given as

$$\begin{aligned} \breve{M}_o(q_o) &= J_o(q_o)^{-T} M_o J_o(q_o) - 1 \\ \breve{C}_o(\dot{q}_o, q_o) &= -J_o(q_o)^{-T} \left(M_o J_o(q_o)^{-1} \dot{J}(q_o) + \tilde{\rho} \right) J_o(q_o)^{-1} \dot{q}_o \end{aligned} \tag{A-36}$$

with $\rho = M_o J_o(q_o)^{-1} \dot{q}_o$.

A-4-4 The Adjoint Matrix for the Underactuated Case

The underactuated case refers to the case where the agents apply a force to the payload. The resulting wrench at the payload CoG due to the i^{th}-agent's force is then given as

$$w_i = J_{p_i}(R_o)^T F_{p_i} \tag{A-37}$$

where F_{p_i} is the force at the attachment point, and $J_{p_i}(R_o)^T \in \mathbb{R}^{6\times 3}$ denotes the adjoint matrix given as

$$J_{p_i}(R_o)^T = \begin{bmatrix} \tilde{p}_i R_o^T \\ I_{3\times 3} \end{bmatrix} \tag{A-38}$$

where p_i represents the position of the i^{th}-attachment point given in the body fixed frame.

A-5 Stability Analysis Tools for Time Varying Systems

The following theorem can be used to show boundedness of the system state.

Theorem A-5.1 (Uniform Boundedness)**.** *Suppose a function $V(x,t)$ is defined on $\|x\| > l > 0$ and $t \in [0, \infty)$ with continuous first order partial derivatives with respect to x and t for which it holds that*

$$\begin{aligned} V(x,t) &> 0 \\ \dot{V}(x, w(t)) &< 0 \end{aligned} \tag{A-39}$$

for all $\|x\| > l$ and $t \in \mathbb{R}_+$ then x is uniformly bounded.

For the purpose of this thesis, the lemma above is made more specific,

Lemma A-5.1. *Consider the non-autonomous system with state $x \in \mathbb{R}^n$ described by the ordinary differential equation,*

$$\dot{x} = f(x) + w(t) \tag{A-40}$$

where $w(t) \in \mathbb{R}^n$ is a bounded signal, i.e. it holds that $\|w(t)\| < l$ for some $l > 0$ and all $t \in \mathbb{R}_+$. Suppose a function $V(x)$ is defined with continuous first order partial derivatives with respect to x for which it holds that

$$\begin{aligned} V(x) &> 0, \quad \forall x \backslash \{0\} \\ V(0) &= 0. \end{aligned} \tag{A-41}$$

Furthermore, suppose that the time derivative gives,

$$\dot{V}(x, w(t)) = -x^T x + x^T w(t) \tag{A-42}$$

then x is uniformly bounded.

The above follows directly from Theorem A-5.1 by noting that $-x^T x + x^T w(t) < 0$ for any $\|x\| > \|w(t)\| < l$. Barbalat's Lemma can be applied to non-autonomous systems proving convergence, rather than boundedness.

Lemma A-5.2 (Barbalat's Lemma)**.** *Let $f : \mathbb{R} \to \mathbb{R}$ be a differentiable function with a finite limit as $t \to \infty$. If $\dot{f}(t)$ is uniformly continuous then $\lim_{t\to\infty} \dot{f}(t) = 0$.*

The following lemma taken from [34] will be useful for deriving a bound on the convergence rate.

Lemma A-5.3. *Let $V : \mathbb{R}_+ \to \mathbb{R}$ be a differentiable function, satisfying $\dot{V}(t) \leq -aV(t)$ for some $a > 0$ and for all $t \in \mathbb{R}_+$. Then, $V(t) \leq V(0)e^{-at}$ holds for all $t \in \mathbb{R}_+$.*

Appendix B

Proofs

B-1 Proofs in Chapter 2

B-1-1 Explicit Expression of the Generalized Inverse

Considering the adjoint matrix given in (A-38), this gives the generalized inverse as

$$J_{p_i}(R_o)^{\dagger} = J_{p_i}(R_o) \times \left(\sum_{i=1}^{n_f} J_{p_i}(R_o)^T J_{p_i}(R_o) \right)^{-1} \tag{B-1}$$

$$J_{p_i}(R_o)^{\dagger} = \begin{bmatrix} R_o \tilde{p}_i^T & I \end{bmatrix} \begin{bmatrix} I & 0 \\ 0 & R_o \end{bmatrix} \left(\sum_{i=1}^{n} \begin{bmatrix} \tilde{p}_i \tilde{p}_i^T & \tilde{p}_i \\ \tilde{p}_i^T & I \end{bmatrix} \right)^{-1} \begin{bmatrix} I & 0 \\ 0 & R_o^T \end{bmatrix} \tag{B-2}$$

Consider defining the following constant matrices,

$$P_i = \begin{bmatrix} P_{i,\tau} & P_{i,F} \end{bmatrix} = \begin{bmatrix} \tilde{p}_i^T & I \end{bmatrix} \left(\sum_{i=1}^{n} \begin{bmatrix} \tilde{p}_i \tilde{p}_i^T & \tilde{p}_i \\ \tilde{p}_i^T & I \end{bmatrix} \right)^{-1} \tag{B-3}$$

this gives the generalized inverse as

$$J_{p_i}(R_o)^{\dagger} = R_o P_{i,\tau} + R_o P_{i,F} R_o^T \tag{B-4}$$

B-2 Proofs in Chapter 4

B-2-1 Proof of Boundedness of the Estimation Errors: Proposition 4-1.1

The estimation error dynamics, as was given in (4-6), is repeated here for convenience,

$$\begin{aligned} \Delta\dot{\nu}_i &= -(\zeta_l + \Gamma_{v,i})\Delta\nu_i - K_l J_o(q_o)^T \Delta e_i - \sum_{j=1}^{n_f} \left[\zeta_j (\Delta\nu_i - \Delta\nu_j) + K_j J_o(q_o)^T (\Delta e_i - \Delta e_j) \right] + \epsilon_{\nu,i}\nu_o \\ \Delta\dot{e}_i &= (I_{6\times 6} + \Gamma_{e,i}) J_o(q_o) \Delta\nu_i + \epsilon_{e,i}\dot{q}_o \end{aligned} \tag{B-5}$$

with $\Delta\nu_i$ and Δe_i as defined in the Objectives 4-1.1. In the following it is derived how to choose the Lyapunov candidate V, such that $\dot{V} \leq 0$. Consider the Lyapunov candidate to be composed as

$$V_\Delta = V_e\left(\Delta e\right) + V_\nu\left(\Delta\nu\right), \tag{B-6}$$

and consider obtaining an expression for V_e and $\dot{V}_e$ first. To this end, define V_e as

$$V_e = \tfrac{1}{2}\Delta e^T\left(L_w^{(e)} + P_e\right)\Delta e \tag{B-7}$$

where $\Delta e = \begin{bmatrix}\Delta e_1^T & \dots & \Delta e_{n_f}^T\end{bmatrix}^T$ denotes the stacking of the estimation errors, P_e is a block diagonal matrix, with diagonal blocks $P_i^{(e)}$ chosen as

$$P_e = \left[P_i^{(e)}\right]_{\text{diag}} \in \mathbb{R}^{6n_f\times 6n_f}, \qquad P_i^{(e)} = K_iK_l \in \mathbb{R}^{6\times 6} \tag{B-8}$$

and $L_w^{(e)}$ is the weighted Laplacian matrix for the complete graph as given in Definition A-1.4 by substituting $a_i = K_i$ in the definition. Note that, since all gains $K_* > 0$ are assumed to be diagonal matrices that $L_w^{(e)}$ and $P_e > 0$ are symmetric matrices. From Definition A-1.4 it follows that $L_w^{(e)}$ is positive semi-definite with the agreement set spanning the null space. Taking the time derivative of V_e, and substitution of (B-5), gives

$$\dot{V}_e = \Delta e^T\left(L_w^{(e)} + P_e\right) \times \left(\left[\Gamma_{e,i}\right]_{\text{diag}} + I_{6n_f\times 6n_f}\right)\left(I_{n_f\times n_f}\otimes J_o\left(q_o\right)\right)\Delta\nu \tag{B-9}$$

where it was assumed that $\epsilon_{e,i} = 0$ and $\epsilon_{\nu,i} = 0$, and $\Delta\nu = \begin{bmatrix}\Delta\nu_1^T & \dots & \Delta\nu_{n_f}^T\end{bmatrix}^T$. Consider that the jacobian matrix $J_o\left(q_o\right)$ commutes with all premultiplied matrices above, because of the structure given in (2-6). This can be used to connect $J_o\left(q_o\right)$ to Δe,

$$\dot{V}_e = \Delta e^T\left(I_{n_f\times n_f}\otimes J_o\left(q_o\right)\right)\left(L_w^{(e)} + P_e\right) \times \left(\left[\Gamma_{e,i}\right]_{\text{diag}} + I_{6n_f\times 6n_f}\right)\Delta\nu. \tag{B-10}$$

With these expressions for V_e and $\dot{V}_e$ obtained the complete Lyapunov candidate can be considered.

Using the expression for V_e defined above (B-7) let the Lyapunov candidate be given as

$$V_\Delta = V_e + V_\nu = V_e + \tfrac{1}{2}\sum_{i=1}^{n_f}\Delta\nu_i^T\left(\Gamma_{e,i} + I_{6\times 6}\right)K_i\Delta\nu_i \tag{B-11}$$

Taking the time derivative gives a rather lengthy expression. For this reason the emerging terms that are quadratic in $\Delta\nu$ will be collected in a single step using the matrices $L_w^{(\nu)}$ and Q_ν, which will be defined after the expression is somewhat simplified. Thus, assuming $\epsilon_{e,i} = 0$ and $\epsilon_{\nu,i} = 0$, taking the time derivative of V_Δ and substitution of the estimation error dynamics (B-5) gives,

$$\begin{aligned}\dot{V}_\Delta \;=\; & \dot{V}_e - \Delta\nu^T\left(L_w^{(\nu)} + Q_\nu\right)\Delta\nu \\ & - \sum_{i=1}^{n_f}\Delta\nu_i^T\left(\Gamma_{e,i} + I_{6\times 6}\right)K_i\left(K_lJ_o\left(q_o\right)^T\Delta e_i + \sum_{j=1}^{n_f}K_jJ_o\left(q_o\right)^T\left(\Delta e_i - \Delta e_j\right)\right)\end{aligned} \tag{B-12}$$

Note that the summation term obtained above is exactly equal to $\dot{V}_e$ as defined in (B-10), which reduces the expression above to

$$\dot{V}_\Delta = -\Delta\nu^T \left(L_w^{(\nu)} + Q_\nu\right) \Delta\nu \tag{B-13}$$

where it remained to define the matrices $L_w^{(\nu)}$ and Q_ν. Consider Q_ν to be a diagonal positive definite matrix. This allows $L_w^{(\nu)}$ to be constructed such that taking the time derivative of V_Δ given in (B-11), results in (B-12). This shows that $L_w^{(\nu)}$ can be constructed as

$$L_w^{(\nu)} = \mathcal{D}^{(\nu)} - \mathcal{A}^{(\nu)}, \quad \in \mathbb{R}^{6n_f \times 6n_f} \tag{B-14}$$

where $\mathcal{D}^{(\nu)} = \left[\mathcal{D}_i^{(\nu)}\right]_{\text{diag}} \in \mathbb{R}^{6n_f \times 6n_f}$ and $\mathcal{A}^{(\nu)} = \left[\mathcal{A}_{ij}^{(\nu)}\right] \in \mathbb{R}^{6n_f \times 6n_f}$ are composed as,

$$\begin{aligned} \mathcal{D}_i^{(\nu)} &= \left(\Gamma_{e,i} + I\right) K_i \left(\zeta_l + \Gamma_{v,i} + \sum_{j=1}^{n_f} \zeta_j\right) - Q_{\nu,i} \\ \mathcal{A}_{ij}^{(\nu)} &= \tfrac{1}{2}\left(\Gamma_{e,i} + I\right) K_i \zeta_j + \tfrac{1}{2}\left(\Gamma_{e,j} + I\right) K_j \zeta_i \end{aligned} \tag{B-15}$$

The intention is for $L_w^{(\nu)}$ to be a symmetric weighted Laplacian matrix, with a zero row sum. For this to hold it must be true that the diagonal elements of the degree matrix equals the row sum of the adjacency matrix. From the above equation this gives

$$\mathcal{D}_i^{(\nu)} = \sum_{j=1}^{n_f} \mathcal{A}_{ij}^{(\nu)} \tag{B-16}$$

Using the expressions given in (B-15) the above equality can be solved for the observer gain $\Gamma_{v,i}$ via algebraic manipulations:

$$\begin{aligned} \left(\Gamma_{e,i} + I\right) K_i \left(\zeta_l + \Gamma_{v,i} + \sum_{j=1}^{n_f} \zeta_j\right) - Q_{\nu,i} &= \sum_{j=1}^{n_f} \left[\tfrac{1}{2}\left(\Gamma_{e,i} + I\right) K_i \zeta_j + \tfrac{1}{2}\left(\Gamma_{e,j} + I\right) K_j \zeta_i\right] \\ \left(\Gamma_{e,i} + I\right) K_i \left(\zeta_l + \Gamma_{v,i} + \tfrac{1}{2}\sum_{j=1}^{n_f} \zeta_j\right) - Q_{\nu,i} &= \sum_{j=1}^{n_f} \tfrac{1}{2}\left(\Gamma_{e,j} + I\right) K_j \zeta_i \\ \zeta_l + \Gamma_{v,i} + \tfrac{1}{2}\sum_{j=1}^{n_f} \zeta_j &= \tfrac{1}{2} K_i^{-1} \left(\Gamma_{e,i} + I\right)^{-1} \left(\sum_{j=1}^{n_f} \left(\Gamma_{e,j} + I\right) K_j \zeta_i + 2Q_{\nu,i}\right) \end{aligned} \tag{B-17}$$

and finally,

$$\Gamma_{v,i} = -\zeta_l - \tfrac{1}{2}\sum_{j=1}^{n_f} \zeta_j + \tfrac{1}{2} K_i^{-1} \left(\Gamma_{e,i} + I\right)^{-1} \left(\sum_{j=1}^{n_f} \left(\Gamma_{e,j} + I\right) K_j \zeta_i + 2Q_{\nu,i}\right) \tag{B-18}$$

From the fact that all matrices above are diagonal and positive definite, the inequality given in (4-5) shows that indeed $Q_{\nu,i} > 0$ and that the matrix $L_w^{(\nu)}$ given in (B-14) is indeed a Laplacian matrix.

To summarize the proof: The Lyapunov candidate was taken as

$$V_\Delta = \tfrac{1}{2}\Delta e^T \left(L_w^{(e)} + P_e\right) \Delta e + \tfrac{1}{2}\sum_{i=1}^{n_f} \Delta\nu_i^T \left(\Gamma_{e,i} + I_{6\times 6}\right) K_i \Delta\nu_i \tag{B-19}$$

and setting $\epsilon_{e,i} = 0$ and $\epsilon_{\nu,i} = 0$, the time derivative was shown to be given as

$$\dot{V}_\Delta = -\Delta\nu^T \left(L_w^{(\nu)} + Q_\nu\right) \Delta\nu \tag{B-20}$$

where $L_w^{(e)}$ and $L_w^{(\nu)}$ are weighted Laplacian matrices associated with the complete graph, and the matrices $P_e > 0$ and $Q_\nu > 0$ are diagonal matrices.

B-2-2 Proof of Global Asymptotic Convergence of the System State: Proposition 4-1.1

The payload dynamics given in (4-2) can be rewritten in terms of the estimation errors as,

$$\begin{aligned} \dot{\nu}_o &= -\zeta_{\text{sum}}\nu_o - K_{\text{sum}} J_o\left(q_o\right)^T e_l - \sum_{i=1}^{n_f} \left(\zeta_i \Delta\nu_i + K_i J_o\left(q_o\right)^T \Delta e_i\right) \\ \dot{e}_l &= J_o\left(q_o\right)\nu_o \end{aligned} \tag{B-21}$$

where $\zeta_{\text{sum}} = \zeta_l + \sum_{i=1}^{n_f} \zeta_i$ and $K_{\text{sum}} = K_l + \sum_{i=1}^{n_f} K_i$. Supposing that the estimation errors have converged, $\lim_{t\to\infty} \Delta e = 0$ and $\lim_{t\to\infty} \Delta\nu = 0$, then the dynamics given above reduce to a stable system, and the leader tracking error e_l can be shown to converge asymptotically to zero. Clearly, the intention was to decouple the estimation dynamics from the payload dynamics given above, but it was previously shown that this only holds if q_o can be assumed to remain bounded. Therefore, the coupling gains will be used to couple the estimation dynamics with the payload dynamics, thus preventing the Modified Rodrigues Parameters (MRPs) from growing unbounded while the observer dynamics converge.

Let the coupling gains $\epsilon_{\nu,i} \in \mathbb{R}^{3\times3}$ and $\epsilon_{e,i} \in \mathbb{R}^{3\times3}$ be taken as

$$\begin{aligned} \left[\epsilon_{e,i}\right]_{\text{vec}} &= \epsilon \left(L_w^{(e)} + P_e\right)^{-1} \left[K_i\right]_{\text{vec}} \quad \in \mathbb{R}^{3n_f\times3} \\ \epsilon_{\nu,i} &= \epsilon \left(\left(\Gamma_{e,i} + I_{6\times6}\right) K_i\right)^{-1} \zeta_i \quad \in \mathbb{R}^{3\times3} \end{aligned} \tag{B-22}$$

where $\epsilon \in \mathbb{R}$ is an arbitrarily small scalar constant, $P_e > 0$ is the diagonal matrix as defined in (B-8), and $L_w^{(e)}$ is the Laplacian matrix appearing in (B-7), which was obtained from Definition A-1.4 by substituting $a_i = K_i$ in the definition. Since the null space of $L_w^{(e)}$ is spanned by the agreement set, and $P_e > 0$ is a diagonal full-rank matrix, it can be concluded that $L_w^{(e)} + P_e$ is indeed invertible. Consider adding to the previously proposed Lyapunov candidate (B-6) a potential and kinetic energy term for the payload,

$$V = V_e + \tfrac{1}{\epsilon}V_\nu + \tfrac{1}{\epsilon}V_o \quad \begin{cases} V_e &= \tfrac{1}{2}\Delta e^T \left(L_w^{(e)} + P_e\right) \Delta e \\ V_\nu &= \tfrac{1}{2}\sum_{i=1}^{n_f} \Delta\nu_i^T \left(\Gamma_{e,i} + I_{6\times6}\right) K_i \Delta\nu_i \\ V_o &= \tfrac{1}{2}\nu_o^T\nu_o + \tfrac{1}{2}e_l^T K_{\text{sum}} e_l \end{cases} \tag{B-23}$$

where (B-7) was used to obtain V_e and V_ν, and $\epsilon \in \mathbb{R}$ is the small positive scalar appearing in (B-22). Taking the time derivative of V gives,

$$\dot{V} = \dot{V}_o + \sum_{i=1}^{n_f} \left(\Delta e_i^T K_i J_o(q_o) \nu_o + \Delta \nu_i^T \zeta_i \nu_o \right) - \tfrac{1}{\epsilon} \Delta \nu^T \left(L_w^{(\nu)} + Q_\nu \right) \Delta \nu \tag{B-24}$$

where (B-20) was used to obtain the last term, and the coupling gains were chosen to obtain the middle term. Using (B-21) to derive $\dot{V}_o$ gives,

$$\dot{V} = -\nu_o^T \zeta_{\text{sum}} \nu_o - \tfrac{1}{\epsilon} \Delta \nu^T \left(L_w^{(\nu)} + Q_\nu \right) \Delta \nu \leq 0 \tag{B-25}$$

By proposing a single Lyapunov candidate it is now allowed to use LaSalle's invariance principle. From V and $\dot{V}$ it can be concluded that $\lim_{t\to\infty} \nu_o = 0$ and $\lim_{t\to\infty} \Delta\nu = 0$. Furthermore Δe and $e_l = q_o - q_{\text{des}}$ are bounded. Since q_{des} is constant this shows that q_o is bounded, and in turn that $J_o(q_o)$ is bounded. From (4-6) follows that $\Delta \dot{e}_i = 0, \forall i$, since $J_o(q_o)$ is invertible. To show that $\lim_{t\to\infty} \Delta e_i = 0 \forall i$, consider the multiplication of all error estimation dynamics (4-6) on the left hand side by a diagonal matrix as follows,

$$\lim_{t\to\infty} \quad [K_i]_{\text{diag}} \times \Delta \dot{\nu} = \left(L_w^{(e)} + P_e \right) \Delta e = 0 \tag{B-26}$$

where the velocities have been set to zero in the limit. Since $L_w^{(e)} + P_e$ is invertible it follows that $\lim_{t\to\infty} \Delta e = 0$, i.e. all agents correctly reconstruct the payload state ν_o and the leader's tracking error e_l. From the payload dynamics (B-21) it finally follows that $\lim_{t\to\infty} e_l = 0$, i.e. the payload tracking error converges to zero. This shows that, if Assumption 2-1.1 holds, the Objectives 4-1.1 are indeed globally achieved, completing the proof.

B-2-3 Proof of Boundedness of the State Dependent Weighting Matrices

In the following it is shown that the weighting matrices in (4-26) are bounded. The weighting matrices are repeated here for convenience,

$$W_i(q_o) = n_f \breve{M}_o(q_o)^{-1} J_o(q_o)^{-T} J_{p_i}(q_o)^T J_{p_i}(q_o)^\dagger J_o(q_o)^T \breve{M}_o(q_o) \tag{B-27}$$

where $\breve{M}_o(q_o)$ is given as,

$$\breve{M}_o(q_o) = J_o(q_o)^{-T} M_o J_o(q_o)^{-1} \tag{B-28}$$

It can be seen from $J_o(q_o)$ that it depends only on the MRPs, denoted as σ_o, rather than $q_o = \begin{bmatrix} \sigma_o^T & r_o^T \end{bmatrix}^T$. The kinematic matrix is almost orthogonal, as the inverse is given as

$$J_o(\sigma_o)^{-1} = \tfrac{16}{(1+\sigma^T\sigma)^2} J_o(\sigma_o)^T \tag{B-29}$$

which can be derived from the definition of $J_o(q_o)$ in (A-34) and the MRPs kinematics (A-28). This allows the weighting matrices to be rewritten as

$$W_i(\sigma_o) = \tfrac{16}{(1+\sigma_o^T\sigma_o)^2} J_o(\sigma_o) \underbrace{n_f M_o^{-1} J_{p_i}(\sigma_o)^T J_{p_i}(\sigma_o)^\dagger M_o}_{\text{bounded}} J_o(\sigma_o)^T \tag{B-30}$$

Note that the braced term is bounded since M_o is constant, see (A-33), and $J_{p_i}(\sigma_o)^T$ and $J_{p_i}(\sigma_o)^\dagger$ are bounded, as derived in Appendix B-1-1. Collecting the braced term in a bounded matrix B,

$$W_i(q_o) = \frac{16}{(1+\sigma^T\sigma)^2} J_o(\sigma_o) B J_o(\sigma_o)^T \tag{B-31}$$

Multiply this equation by $\left(\sigma^T\sigma\right)^2 \times \left(\sigma^T\sigma\right)^{-2} = 1$,

$$W_i(q_o) = \frac{16}{\left(\frac{1}{\sigma^T\sigma}+1\right)^2} \left(\frac{1}{\sigma^T\sigma} J_o(\sigma_o)\right) \times B \times \left(\frac{1}{\sigma^T\sigma} J_o(\sigma_o)\right)^T \tag{B-32}$$

It can be seen from the definition of $J_o(q_o)$ in (A-34) and the MRPs kinematics (A-28) that $\left(\frac{1}{\sigma^T\sigma} J_o(\sigma_o)\right)$ is bounded for any σ_o, completing the proof on boundedness of the weights in (B-27).

B-2-4 Proof of Convergence of the Estimation Error: Proposition 4-3.1

The estimation error dynamics was given as,

$$\begin{aligned} \Delta\ddot{\bar{q}} &= -\left(\zeta_{\text{sum}} + \Gamma_\nu\right)\Delta\dot{\bar{q}} - K_{\text{sum}}\Delta\bar{e} - \sum_{j=1}^{n_f} W_j(q_o)\left(\zeta\delta\dot{q}_j + K\delta e_j\right) \\ \Delta\dot{\bar{e}} &= \left(I_{6\times 6} + \Gamma_e\right)\Delta\dot{\bar{q}} \end{aligned} \tag{B-33}$$

and the Lyapunov candidate was taken as,

$$V_\Delta = \tfrac{1}{2}\Delta\dot{\bar{q}}^T P_1 \Delta\dot{\bar{q}} + \tfrac{1}{2}\Delta\bar{e}^T P_2 \Delta\bar{e} + \tfrac{1}{2}\left\|\Delta\dot{\bar{q}} + P_3\Delta\bar{e}\right\|^2 \tag{B-34}$$

The explicit expressions for P_1, P_2 and P_3 are given as,

$$\begin{aligned} P_1 &= \left(\zeta_{\text{sum}} + \Gamma_\nu\right)^{-2} K_{\text{sum}}\left(I + \Gamma_e\right) + I \\ P_2 &= K_{\text{sum}}\left(I + \Gamma_e\right)^{-1} \\ P_3 &= \left(\zeta_{\text{sum}} + \Gamma_\nu\right)^{-1} K_{\text{sum}}. \end{aligned} \tag{B-35}$$

Taking the time derivative of V_Δ, and substitution of (B-33) and the above matrix definitions, gives

$$\begin{aligned} \dot{V}_\Delta = &-\Delta\dot{\bar{q}}^T Q_1 \Delta\dot{\bar{q}} - \left\|\Delta\dot{\bar{q}} + P_3\Delta\bar{e}\right\|_{Q_2}^2 \\ &- \left(P_1\Delta\dot{\bar{q}} + \left(\Delta\dot{\bar{q}} + P_3\Delta\bar{e}\right)\right)^T \times \sum_{j=1}^{n_f} W_j(q_o)\left(\zeta\delta\dot{q}_j + K\delta e_j\right) \end{aligned} \tag{B-36}$$

where $\|\cdot\|_{Q_2}^2$ denotes $(\cdot)^T Q_2 (\cdot)$, and the matrices Q_1 and Q_2 are given as,

$$\begin{aligned} Q_1 &= \zeta_{\text{sum}} + \Gamma_\nu \\ Q_2 &= \left(\zeta_{\text{sum}} + \Gamma_\nu\right)^{-1} \end{aligned} \tag{B-37}$$

which follows from substitution.

B-2-5 The Simultaneous Stabilization Problem for Arbitrary State Measurements

In the following the simultaneous stabilization problem is illustrated for a simple case, revealing that the disagreement and mean estimation error dynamics must be stabilized by two different plants. This is done by considering full actuation, such that the attitude and translation dynamics can be separated. The simultaneous stabilization problem will then be illustrated for the (linear) translation dynamics. Furthermore, for ease of exposition all agents use identical control and observer gains.

Considering the translation dynamics, define the augmented payload dynamics as

$$\begin{bmatrix} \dot{v}_o \\ \dot{r}_o \\ \dot{r}_{\text{des}} \end{bmatrix} = \begin{bmatrix} 0 \\ v_o \\ 0 \end{bmatrix} + \begin{bmatrix} I \\ 0 \\ 0 \end{bmatrix} \times \left(g\bar{b}_3 + \tfrac{1}{m_o} F_l + \tfrac{1}{m_o} \sum_{i=1}^{n_f} F_{p_i} \right) \tag{B-38}$$

where r_{des} is the desired constant payload position, as known to the leader, and the other variables are as introduced in Appendix A-4. Consider the following matrices,

$$x_o = \begin{bmatrix} v_o \\ r_o \\ r_{\text{des}} \end{bmatrix}, \quad A = \begin{bmatrix} 0 & 0 & 0 \\ I_{3\times 3} & 0 & 0 \\ 0 & 0 & 0 \end{bmatrix}, \quad B = \begin{bmatrix} I_{3\times 3} \\ 0 \\ 0 \end{bmatrix} \tag{B-39}$$

where the zeros are of dimension 3×3, which gives the translation part of the payload dynamics as

$$\begin{aligned} \dot{x}_o &= Ax_o + B\left(g\bar{b}_3 + \tfrac{1}{m_o} F_l + \tfrac{1}{m_o} \sum_{i=1}^{n_f} F_{p_i} \right) \\ y &= Cx_o \end{aligned} \tag{B-40}$$

where C is a matrix of appropriate dimensions, and y is the measurement available to all agents. Let the leader apply a force given as,

$$F_l = -\tfrac{1}{n_f+1} m_o g - m_o K x_o \tag{B-41}$$

and similarly define the force applied by the follower agents as,

$$F_i = -\tfrac{1}{n_f+1} m_o g - m_o K \hat{x}_i \tag{B-42}$$

where $\hat{x}_i$ denotes the i^{th}-agent's local estimate of the augmented payload state,

$$\hat{x}_i = \begin{bmatrix} \hat{v}_i^T & \hat{r}_i^T & \hat{r}_{\text{des},i} \end{bmatrix}^T \tag{B-43}$$

Consider achieving Objectives 4-2.1, that is, convergence of the disagreement, mean estimation error and tracking error dynamics:

Proposition B-2.1. *Consider the Cooperative Manipulation Problem (CMP) for the translation dynamics described by equations* (B-40)-(B-42). *Consider n_f-follower agents and a single leader. Let the follower agents update the estimated state as*

$$\dot{\hat{x}}_i = (A - (1+n_f)BK)\hat{x}_i - \Gamma C \Delta x_i \tag{B-44}$$

with $\Gamma \in \mathbb{R}^{9\times 3}$ chosen such that the following two plants are simultaneously stabilized:

$$\begin{matrix} A - BK - \Gamma C \\ A - (1+n_f)BK - \Gamma C. \end{matrix} \tag{B-45}$$

Then the Objectives 4-2.1 are achieved.

Disagreement Dynamics The disagreement dynamics of the follower agents can be obtained from the local update law (B-44). To this end, consider stacking all the update laws into a single vector,

$$\dot{\hat{x}} = \Big(I_{n_f\times n_f} \otimes (A - (1+n_f)BK - \Gamma C)\Big)\hat{x} + \mathbf{1}_{n_f} \otimes (\Gamma C x_o) \tag{B-46}$$

where $\hat{x} = \begin{bmatrix}\hat{x}_1^T & \hat{x}_2^T & \dots & \hat{x}_{n_f}^T\end{bmatrix}^T \in \mathbb{R}^{9n_f}$. Left multiplication with the Laplacian matrix L gives the disagreement dynamics $\delta\dot{x} = (L \otimes I_{9\times 9})\dot{\hat{x}}$ resulting in

$$\delta\dot{x} = \Big(I_{n_f\times n_f} \otimes (A - (1+n_f)BK - \Gamma C)\Big)\delta x \tag{B-47}$$

where the measurements x_o have dropped, since $\mathbf{1}_{n_f} \in \mathbf{null}\{L\}$ for the complete graph. Noting that the above matrix is block diagonal gives,

$$\delta\dot{x}_i = (A - (1+n_f)BK - \Gamma C)\delta x_i \tag{B-48}$$

which is indeed the plant given in (B-45).

Mean Estimation Error Dynamics The payload translation dynamics can be obtained from the dynamics given in (B-40) and substitution of the leader and follower control laws,

$$\dot{x}_o = (A - BK)x_o - n_f BK\bar{x} \tag{B-49}$$

where $\bar{x} = \frac{1}{n_f}\sum_{i=1}^{n_f} x_i$. Using (B-44) the mean estimation error dynamics are then obtained as,

$$\Delta\dot{\bar{x}} = (A - BK - \Gamma C)\Delta\bar{x} \tag{B-50}$$

which is the plant given in (B-45), and completes the proof.

B-3 Proofs in Chapter 5

B-3-1 Proof of Theorem 5-1.1

The following contains the proof for controlling the cable direction of the Unmanned Aerial Vehicles (UAV).

Cable Direction Kinematics The kinematics of the i^{th}-cable direction η_i is given as

$$\begin{aligned} \omega_i &= \eta_i \times \dot{\eta}_i = \tilde{\eta}_i \dot{\eta}_i \\ \dot{\eta}_i &= \omega_i \times \eta_i = \tilde{\omega}_i \eta_i \end{aligned} \tag{B-51}$$

where ω_i denotes the angular velocity of the i^{th}-cable and the tilde operator is given in Definition A-2.1. Taking the second time derivative of the last expression gives the cable direction acceleration as,

$$\ddot{\eta}_i = \dot{\tilde{\omega}}_i \eta_i + \tilde{\omega}_i \dot{\eta}_i = -\eta_i \times \dot{\omega}_i + \tilde{\omega}_i \tilde{\omega}_i \eta_i \tag{B-52}$$

The last term in the above equation can be further simplified: Using $\tilde{a}\tilde{a}b = \left(aa^T - (a^T a)I\right) b$ and the fact that $\omega_i^T \eta_i = 0$, gives the acceleration of the cable direction η_i as

$$\ddot{\eta}_i = -\tilde{\eta}_i \dot{\omega}_i - \left(\omega_i^T \omega_i\right) \eta_i \tag{B-53}$$

which will be used in the control law derivation.

Inverting the UAV Dynamics for Control of the Cable Direction and Cable Tension The control over the cable direction and tension can be derived using a simple force balance of the i^{th}-UAV body. Consider taking the second time derivative of the i^{th}-UAV position (5-1), and substitution of $\ddot{\eta}_i$ given in (B-53) then gives,

$$\ddot{r}_i = \ddot{r}_o + R_o \tilde{\Omega}_o^2 p_i - R_o \tilde{p}_i \dot{\Omega}_o - l_i \tilde{\eta}_i \dot{\omega}_i - l_i \left\|\omega_i\right\|^2 \eta_i \tag{B-54}$$

Substitution of the above expression into the force balance (5-2) gives

$$m_i \left(\ddot{r}_o + R_o \tilde{\Omega}_o^2 p_i - R_o \tilde{p}_i \dot{\Omega}_o - l_i \tilde{\eta}_i \dot{\omega}_i - l_i \left\|\omega_i\right\|^2 \eta_i\right) = m_i g \bar{b}_3 - \lambda_i \eta_i + F_i \tag{B-55}$$

Substitution of the proposed force F_i given in (5-8) gives

$$\lambda_i \eta_i - \tilde{\eta}_i \dot{\omega}_i = \left(\eta_i^T F_{p_i,des}\right) \eta_i - \tilde{\eta}_i \varpi_i. \tag{B-56}$$

Multiplication on both sides of the equality sign by $\tilde{\eta}_i^T$ gives,

$$\tilde{\eta}_i^T \tilde{\eta}_i \dot{\omega}_i = \tilde{\eta}_i^T \tilde{\eta}_i \varpi_i, \tag{B-57}$$

and on both sides of the equality sign by η_i^T gives,

$$\lambda_i = \eta_i^T F_{i,des} \tag{B-58}$$

where it was used that $\tilde{\eta}_i \eta_i = 0$. The above equation states that if the cable direction η_i is parallel to the desired force $F_{p_i,des}$, that the desired force is applied to the payload. This can be achieved using (B-57), which states that the cable direction dynamics can be controlled via ϖ_i. In the following the expression for ϖ is derived such that the cable becomes parallel to the desired force at the attachment point.

Proof of Controlling the Cable Direction Dynamics The idea is then to control the cable direction such that it is aligned with $F_{p_i,des}$ given in (5-12). To this end consider the following Lyapunov function,

$$V = V_\omega + V_\eta \tag{B-59}$$

where

$$\begin{aligned} V_\omega &= \tfrac{1}{2}\left(\omega_i - \omega_{i,des}\right)^T \tilde{\eta}_i^T \tilde{\eta}_i \left(\omega_i - \omega_{i,des}\right) \\ V_\eta &= \tfrac{k_p}{2}\left\|\eta_i - \eta_{i,des}\right\|^2. \end{aligned} \tag{B-60}$$

where $\eta_{i,des}$ and $\omega_{i,des}$ are desired cable direction and desired cable angular velocity respectively. Taking the time derivative of V_ω and substitution of (B-57) gives

$$\begin{aligned} \dot{V}_\omega &= \left(\omega_i - \omega_{i,des}\right)^T \tilde{\eta}_i^T \left(\tilde{\eta}_i\left(\dot{\omega}_i - \dot{\omega}_{i,des}\right) - \left(\tilde{\omega}_i - \tilde{\omega}_{i,des}\right)\dot{\eta}_i\right) \\ &= \left(\omega_i - \omega_{i,des}\right)^T \tilde{\eta}_i^T \tilde{\eta}_i \left(\varpi_i - \dot{\omega}_{i,des} - \tilde{\eta}_i^T\left(\tilde{\omega}_i - \tilde{\omega}_{i,des}\right)\dot{\eta}_i\right) \\ &= \left(\omega_i - \omega_{i,des}\right)^T \tilde{\eta}_i^T \tilde{\eta}_i \left(\varpi_i - \dot{\omega}_{i,des} - \tilde{\eta}_i^T\left(\tilde{\omega}_i - \tilde{\omega}_{i,des}\right)\tilde{\omega}_i\eta_i\right) \\ &= \left(\omega_i - \omega_{i,des}\right)^T \tilde{\eta}_i^T \tilde{\eta}_i \left(\varpi_i - \dot{\omega}_{i,des} + \tilde{\eta}_i^T\tilde{\omega}_{i,des}\tilde{\omega}_i\eta_i\right) \end{aligned} \tag{B-61}$$

where the cable kinematics given in (B-51) where used, as well as the rules for cross-product multiplications. Taking the time derivative of V_η gives,

$$\begin{aligned} \dot{V}_\eta &= k_p\left(\eta_i - \eta_{i,des}\right)^T\left(\dot{\eta}_i - \dot{\eta}_{i,des}\right) \\ &= k_p\left(\eta_i - \eta_{i,des}\right)^T\left(\tilde{\omega}_i\eta_i - \tilde{\omega}_{i,des}\eta_{i,des}\right) \\ &= k_p\left(\eta_i - \eta_{i,des}\right)^T\left(-\tilde{\eta}_i\omega_i + \tilde{\eta}_{i,des}\omega_{i,des}\right) \\ &= k_p\left(\eta_{i,des}^T\tilde{\eta}_i\omega_i + \eta_i^T\tilde{\eta}_{i,des}\omega_{i,des}\right) \\ &= k_p\eta_{i,des}^T\tilde{\eta}_i\left(\omega_i - \omega_{i,des}\right) \\ &= -k_p\left(\omega_i - \omega_{i,des}\right)^T\tilde{\eta}_i\eta_{i,des} \end{aligned} \tag{B-62}$$

And thus

$$\begin{aligned} \dot{V} &= \dot{V}_\omega + \dot{V}_\eta \\ &= \left(\omega_i - \omega_{i,des}\right)^T\tilde{\eta}_i^T\tilde{\eta}_i\left(\varpi_i - \dot{\omega}_{i,des} - \tilde{\eta}_i\tilde{\omega}_{i,des}\tilde{\omega}_i\eta_i + k_p\tilde{\eta}_{i,des}\eta_i\right) \end{aligned} \tag{B-63}$$

By taking ϖ as

$$\varpi = \dot{\omega}_{i,des} - k_d\left(\omega_i - \omega_{i,des}\right) - k_p\tilde{\eta}_{i,des}\eta_i + \tilde{\eta}_i\tilde{\omega}_{i,des}\tilde{\omega}_i\eta_i \tag{B-64}$$

thus drives the cable direction towards the desired cable direction.

B-3-2 Explicit Computation of the Desired Cable Reference State

In the following it will be shown how to compute the desired cable angular velocity and angular acceleration $\{\omega_{i,des}, \dot{\omega}_{i,des}\}$ if the desired cable direction $\eta_{i,des}$ is given as the direction of the desired force $F^p_{p_i,des}$ at the attachment point:

$$F_{p_i,des} = R_o \lambda p^c_i + n J_i(R)^\dagger \begin{bmatrix} \tau_{i,des} \\ F_{i,des} \end{bmatrix}, \qquad \eta_{i,des} = \tfrac{1}{\|F_{p_i,des}\|} F_{p_i,des} \tag{B-65}$$

where $\tau_{i,\mathrm{des}}$ and $F_{i,\mathrm{des}}$ are the i^{th}-agent's estimate of the desired torque and force at the payload Center of Gravity (CoG). In the derivation it is assumed that only the current state of the payload is known, and the computations that have to be made are given sequentially, rather than substituted to obtain an explicit expression (this was found to be infeasible). The computation of $\{\omega_{i,des}, \dot{\omega}_{i,des}\}$ given the current payload state is divided into 4 steps:

Step 1. Time Derivatives of the Desired Force

Considering the control gains for the translation dynamics, k_v and k_r, define the following,

$$K_F = \begin{bmatrix} k_v & k_r \end{bmatrix} \otimes I_{3\times 3}, \qquad A_F = \begin{bmatrix} -\frac{n}{m}k_v & -\frac{n}{m}k_r \\ 1 & 0 \end{bmatrix} \otimes I_{3\times 3} \tag{B-66}$$

The desired force at the payload CoG is then given as

$$F_{i,\mathrm{des}} \;=\; -\tfrac{1}{n+1} m g \bar{b}_3 - K_F \begin{bmatrix} v \\ e_r \end{bmatrix} \tag{B-67}$$

where $e_r = r - r_{\mathrm{des}}$, and the time derivatives are computed as

$$\dot{F}^o_{i,\mathrm{des}} = -K_F A_F \begin{bmatrix} v \\ e_r \end{bmatrix}, \qquad \ddot{F}_{i,\mathrm{des}} = -K_F A_F^2 \begin{bmatrix} v \\ e_r \end{bmatrix} \tag{B-68}$$

Step 2: Time Derivatives of the Torques

Define, and compute, the following,

$$\begin{aligned} J_\Omega(\Omega) &= \tfrac{\partial}{\partial \Omega}\left[\tilde{\Omega}\mathcal{I}\Omega\right] + (1+n) K_\Omega, & J_\sigma(\Omega,\sigma) &= \tfrac{\partial}{\partial \sigma}\left[\Xi(\sigma)\Omega\right] \\ J_\tau(\sigma,\sigma_{des}) &= \tfrac{\partial}{\partial \sigma}\left[\Xi(\sigma)^T(\sigma-\sigma_{des})\right], & \dot{J}_\tau(\dot{\sigma},\sigma,\sigma_{des}) &= \sum_{i=1}^{3}\left(\tfrac{\partial J_\tau}{\partial \sigma_i}\right)\dot{\sigma}_i \end{aligned} \tag{B-69}$$

Then compute sequentially the angular acceleration and MRPs velocity,

$$\begin{aligned} \dot{\Omega} &= \mathcal{I}^{-1}\left(-\tilde{\Omega}\mathcal{I}\Omega - (n+1)k_\Omega\Omega - (n+1)k_R\Xi(\sigma)^T(\sigma-\sigma_{des})\right) \\ \dot{\sigma} &= \Xi(\sigma)\Omega \end{aligned} \tag{B-70}$$

and their time derivatives,

$$\begin{aligned} \ddot{\Omega} &= -\mathcal{I}^{-1} J_\Omega \dot{\Omega} - (n+1)\, k_R \mathcal{I}^{-1} J_\tau \dot{\sigma} \\ \ddot{\sigma} &= J_\sigma \dot{\sigma} + \Xi(\sigma)\, \dot{\Omega} \end{aligned} \tag{B-71}$$

Which can be used to compute the time derivatives of the desired torque at the payload CoG

$$\begin{aligned} \tau_{i,\text{des}} &= -K_\Omega \Omega - k_R \Xi(\sigma)^T (\sigma - \sigma_{des}) \\ \dot{\tau}_{i,\text{des}} &= -K_\Omega \dot{\Omega} - k_R J_\tau \dot{\sigma} \\ \ddot{\tau}_{i,\text{des}} &= -K_\Omega \ddot{\Omega} - k_R J_\tau \ddot{\sigma} - k_R \dot{J}_\tau \dot{\sigma} \end{aligned} \tag{B-72}$$

Step 3: Force at the attachment point

Consider rewriting (B-65) using (B-4) as

$$h_i = F_{p_i,\text{des}} = R_o \left(n P_{i,\tau} \tau_i + \lambda p_i^c + n P_{i,F} R_o^T F_i \right) \tag{B-73}$$

Compute the current rotation matrix and the higher order derivatives,

$$\dot{R} = R\tilde{\Omega}, \qquad \ddot{R} = R\tilde{\Omega}^2 + R\dot{\tilde{\Omega}} \tag{B-74}$$

Define and compute, for simplicity,

$$\begin{aligned} b &= n P_{i,\tau} \tau_i + \lambda p_i^c + n P_{i,F} R^T F_i \\ \dot{b} &= n P_{i,\tau} \dot{\tau}_i + n P_{i,F} \left(\dot{R}^T F_i + R^T \dot{F}_i \right) \\ \ddot{b} &= n P_{i,\tau} \ddot{\tau}_i + n P_{i,F} \left(\ddot{R}^T F_i + 2\dot{R}^T \dot{F}_i + R^T \ddot{F}_i \right) \end{aligned} \tag{B-75}$$

Compute the time-derivatives of the force at the attachment point

$$\begin{aligned} \dot{h}_i &= \dot{R} b + R \dot{b} \\ \ddot{h}_i &= \ddot{R} b + 2\dot{R}\dot{b} + R\ddot{b} \end{aligned} \tag{B-76}$$

Step 4: Desired Angular Velocity and Acceleration of the Cable

Finally the desired cable direction, velocity and acceleration can be computed,

$$\begin{aligned} \eta_{i,des} &= \tfrac{h_i}{\|h_i\|} \\ \omega_{i,des} &= \tfrac{\tilde{h}_i \dot{h}_i}{\|h_i\|^2} \\ \dot{\omega}_{i,des} &= \tfrac{1}{\|h_i\|^2} \left(\tilde{h}_i \ddot{h}_i - 2 \left(h_i^T \dot{h}_i \right) \omega_{i,des} \right) \end{aligned} \tag{B-77}$$

completing the computation.

B-4 Proofs of Chapter 6

B-4-1 Proof of Proposition 6-3.1

The proof is constructed via Lyapunov arguments. For ease of exposition the proposed Lyapunov function will be constructed as the sum of three Lyapunov functions,

$$V = V_{\text{kin}} + V_e + V_{\text{pot}} \tag{B-78}$$

where V_{kin} contains the kinetic energy terms, V_e contains the tracking error terms, and V_{pot} contains the potential energy terms of the system. In the following the time derivative of each term will be determined after which the complete Lyapunov function given in (B-78) will be constructed.

Kinetic Energy Term Before defining V_{kin} let the definition of the cable-vector ρ_i from (6-1) be restated here, together with the time derivative of this vector,

$$\begin{aligned} \rho_i &= \left(r_l + R_l p_i^l\right) - \left(r_o + R_o p_i^o\right) \\ \dot{\rho}_i &= \left(v_l + R_l \left(\tilde{p}_i^l\right)^T \Omega_l\right) - \left(v_o + R_o \left(\tilde{p}_i^o\right)^T \Omega_o\right). \end{aligned} \tag{B-79}$$

Let V_{kin} be taken as the kinetic energy of the system, that is the leader and payload body,

$$V_{kin} = \tfrac{1}{2}\Omega_l^T \mathcal{I}_l \Omega_l + \tfrac{m_l}{2} v_l^T v_l + \tfrac{1}{2}\Omega_o^T \mathcal{I}_o \Omega_o + \tfrac{m_o}{2} v_o^T v_o. \tag{B-80}$$

Taking the time derivative, and substituting (6-12) and (6-13), gives

$$\begin{aligned} \dot{V}_{kin} &= \sum_{i=1}^{3} \left[\Omega_o^T \tilde{p}_i^o R_o^T \bar{\rho}_i \lambda_i + v_o^T \bar{\rho}_i \lambda_i - \Omega_l^T \tilde{p}_i^l R_l^T \bar{\rho}_i \lambda_i - v_l^T \bar{\rho}_i \lambda_i\right] \\ &\quad + v_o^T m_o g \bar{b}_3 + v_l^T \left(m_l g \bar{b}_3 + F_l\right) + \Omega_l^T \tau_l. \end{aligned} \tag{B-81}$$

Using the time derivative of the cable vector $\dot{\rho}_i$ as defined in (B-79) the above equation can conveniently be written as

$$\dot{V}_{kin} = \sum_{i=1}^{3} \left[-\dot{\rho}_i^T \bar{\rho}_i \lambda_i\right] + v_o^T m_o g \bar{b}_3 + v_l^T \left(m_l g \bar{b}_3 + F_l\right) + \Omega_l^T \tau_l - \Omega_o^T \Lambda_\Omega \Omega_o - v_o^T \Lambda_{\dot{r}} v_o \tag{B-82}$$

The Tracking Error Term The tracking error potential term V_e in (B-78) is given as

$$V_e = \sum_{i=1}^{3} \left[\tfrac{k_p}{2} \left(\|\rho_i\| - l_{i,des}\right)^2\right] + \tfrac{1}{2} e_{r,l}^T K e_{r,l} + \tfrac{k}{2} \text{tr}\left\{I - E_l\right\} \tag{B-83}$$

where $e_{r,l} = r_l - r_{l,des}$ and $E_l = R_{l,\text{des}}^T R_l$ are the leader attitude and position tracking errors, with $r_{l,\text{des}}$ the reference position for the leader body as given in (6-11), and $R_{l,\text{des}}$ is the reference attitude for the leader body. The latter is determined from the desired yaw angle ψ_{des} as $R_{l,\text{des}} = R_z\left(\psi_{\text{des}}\right)$ using (6-4). Taking the time derivative of V_e in (B-83) gives

$$\dot{V}_e = \sum_{i=1}^{3} \left[k_p \dot{\rho}_i^T \bar{\rho}_i \left(\|\rho_i\| - l_{i,des}\right)\right] + v_l^T K e_{r,l} + k \Omega_l^T \mathbb{P}_a \left\{E_l\right\}^V \tag{B-84}$$

where Lemma A-2.7 was used for the attitude tracking error term.

The Potential Energy Term The potential term V_{pot} in (B-78) is taken as

$$V_{\text{pot}} = \sum_{i=1}^{3} \left[\rho_i^T \left(\bar{\rho}_i - \bar{\rho}_{\text{des},i} \right) \lambda_{\text{des},i} - \left(p_i^o \right)^T R_o \bar{\rho}_{\text{des},i} \lambda_{\text{des},i} \right] + c. \tag{B-85}$$

where $c > 0$ is a positive scalar constant. It is not directly clear whether V_{pot} as defined above is a non-negative function. The first term in the above equation, given as $\rho_i^T \left(\bar{\rho}_i - \bar{\rho}_{\text{des},i} \right) \lambda_{\text{des},i}$ is nonnegative since $\lambda_{\text{des},i} > 0$ from (6-11), and the minimum is attained at $\rho_i = \rho_{\text{des},i}$ for which this term reduces to zero. The second term, given as $-\left(p_i^o \right)^T R_o \bar{\rho}_{\text{des},i} \lambda_{\text{des},i}$, depends only on the rotation matrix R_o as a dynamic variable. Since the rotation matrix evolves on $SO(3)$ all the columns of R_o are norm bounded, and it must therefore always be possible to choose the constant $c > 0$ such that

$$c > \sum_{i=1}^{3} \left[\left(p_i^o \right)^T R_o \bar{\rho}_{\text{des},i} \lambda_{\text{des},i} \right], \qquad \forall R_o \in SO(3) \tag{B-86}$$

holds for all $\forall R_o \in SO(3)$, and thus $V_{\text{pot}} > 0$. Before computing the time derivative of V_{pot} consider rewriting it using (B-79), to obtain

$$V_{\text{pot}} = \sum_{i=1}^{3} \left[\|\rho_i\| \lambda_{\text{des},i} - \left(r_l + R_l p_i^l - r_o \right)^T \bar{\rho}_{\text{des},i} \lambda_{\text{des},i} \right] + c. \tag{B-87}$$

The time derivative of V_{pot} is then given as,

$$\dot{V}_{\text{pot}} = \sum_{i=1}^{3} \left[\bar{\rho}_i{}^T \dot{\rho}_i \lambda_{\text{des},i} - \left(v_l - R_l \tilde{p}_i^l \Omega_l - v_o \right)^T \bar{\rho}_{\text{des},i} \lambda_{\text{des},i} \right]. \tag{B-88}$$

The above equation can be further simplified using $\sum_{i=1}^{3} \bar{\rho}_{\text{des},i} \lambda_{\text{des},i} = -m_o g \bar{b}_3$ as stated in (6-11),

$$\dot{V}_{\text{pot}} = \sum_{i=1}^{3} \left[\bar{\rho}_i{}^T \dot{\rho}_i \lambda_{\text{des},i} - \Omega_l^T \tilde{p}_i^l R_l^T \bar{\rho}_{\text{des},i} \lambda_{\text{des},i} \right] + v_l^T m_o g \bar{b}_3 - v_o^T m_o g \bar{b}_3. \tag{B-89}$$

Complete Lyapunov Function The time derivative of the total Lyapunov function (B-78) can be found by adding the separate terms given in (B-82), (B-84) and (B-89), resulting in

$$\begin{aligned} \dot{V} &= \dot{V}_{kin} + \dot{V}_e + \dot{V}_{\text{pot}} \\ &= \sum_{i=1}^{3} \left[-\dot{\rho}_i^T \bar{\rho}_i \lambda_i + k_p \dot{\rho}_i^T \bar{\rho}_i \left(\|\rho_i\| - l_{i,des} \right) + \dot{\rho}_i^T \bar{\rho}_i \lambda_{\text{des},i} \right] \\ &\quad + v_l^T \left(m_l g \bar{b}_3 + m_o g \bar{b}_3 + K e_{r,l} + F_l \right) \\ &\quad + \Omega_l^T \left(k \mathbb{P}_a \left\{ E_l \right\}^V - \sum_{i=1}^{3} \left[\tilde{p}_i^l R_l^T \bar{\rho}_{\text{des},i} \lambda_{\text{des},i} \right] + \tau_l \right) \\ &\quad - \Omega_o^T \Lambda_\Omega \Omega_o - v_o^T \Lambda_{\dot{r}} v_o \end{aligned} \tag{B-90}$$

Substitution of the proposed control laws (6-14), (6-15) and (6-16) into (B-90) reduces $\dot{V}$ to

$$\dot{V} = -\sum_{i=1}^{3} \left[k_d \left(\dot{\rho}_i^T \bar{\rho}_i \right)^2 \right] - v_l^T \beta v_l - \Omega_l^T \zeta \Omega_l - \Omega_o^T \Lambda_\Omega \Omega_o - v_o^T \Lambda_{\dot{r}} v_o \leq 0. \tag{B-91}$$

From the above equation it can be concluded that the system state remains bounded. From this it can be concluded that the leader and payload accelerations given in (6-12) and (6-13) respectively remain bounded. This shows that also the acceleration of the cable vector, $\ddot{\rho}_i$ obtained from (B-79), is bounded. It follows that $\ddot{V}$ remains bounded, since the system configuration, velocities and accelerations are bounded. This allows the use of Barbalat's Lemma A-5.2 to conclude that $\lim_{t\to\infty} \dot{V} = 0$. It can thus be concluded that the system velocities converge asymptotically to zero, and that an equilibrium configuration will be reached.

LaSalle's Invariance Principle for Finding the Equilibrium State As it was established that the system velocities go to zero asymptotically, LaSalle's invariance principle can be used to evaluate the system equilibrium state. However, this brings us to the Direct Kinematics Problem (DKP) given in Definition 6-3.1. The DKP was considered to be outside the scope of this text, and instead Assumption 6-3.1 is assumed to hold. In the following it will thus be shown that the solution of the Inverse Kinematics Problem (IKP) is a valid equilibrium state of the controlled system, and under Assumption 6-3.1, it is considered to be the unique equilibrium.

Consider the system dynamics (6-12) and (6-13), and substitute the controlled force (6-15) and torque (6-16) to obtain

$$\begin{aligned}
\mathcal{I}_o\dot{\Omega}_o &= -\tilde{\Omega}_o\mathcal{I}_o\Omega_o - \Lambda_\Omega\Omega_o + \sum_{i=1}^{3} \tilde{p}_i^o R_o^T \bar{\rho}_i\lambda_i \\
m_o\dot{v}_o &= -\Lambda_{\dot{r}} v_o + m_o g\bar{b}_3 + \sum_{i=1}^{3} \bar{\rho}_i\lambda_i \\
\mathcal{I}_l\dot{\Omega}_l &= -\tilde{\Omega}_l\mathcal{I}_l\Omega_l - \zeta\Omega_l - k\mathbb{P}_a\left\{R_{l,\mathrm{des}}^T R_l\right\}^V - \sum_{i=1}^{3} \tilde{p}_i^l R_l^T\left(\bar{\rho}_i\lambda_i - \bar{\rho}_{\mathrm{des},i}\lambda_{\mathrm{des},i}\right) \\
m_l\dot{v}_l &= -\beta v_l - m_o g\bar{b}_3 - K_r\left(r_l - r_{l,des}\right) - \sum_{i=1}^{3} \bar{\rho}_i\lambda_i
\end{aligned} \tag{B-92}$$

Using LaSalle's invariance principle all velocities and accelerations are set to zero. Furthermore, the control law for the cable tension (6-14) can be substituted, reducing the equations above to,

$$\begin{aligned}
0 &= \sum_{i=1}^{3} \tilde{p}_i^o R_o^T\left(k_p\bar{\rho}_i\left(\|\rho_i\| - l_{i,des}\right) + \bar{\rho}_i\lambda_{\mathrm{des},i}\right) \\
0 &= m_o g\bar{b}_3 + \sum_{i=1}^{3} \bar{\rho}_i\left(k_p\left(\|\rho_i\| - l_{i,des}\right) + \lambda_{\mathrm{des},i}\right) \\
0 &= -k\mathbb{P}_a\left\{R_{l,\mathrm{des}}^T R_l\right\}^V - \sum_{i=1}^{3} \tilde{p}_i^l R_l^T\left(k_p\bar{\rho}_i\left(\|\rho_i\| - l_{i,des}\right) + \left(\bar{\rho}_i - \bar{\rho}_{\mathrm{des},i}\right)\lambda_{\mathrm{des},i}\right) \\
0 &= -m_o g\bar{b}_3 - K_r\left(r_l - r_{l,des}\right) - \sum_{i=1}^{3} \bar{\rho}_i\left(k_p\left(\|\rho_i\| - l_{i,des}\right) + \lambda_{\mathrm{des},i}\right)
\end{aligned} \tag{B-93}$$

The second and last of the above equations can be rewritten using $\sum_{i=1}^{3} \bar{\rho}_{\text{des},i}\lambda_{\text{des},i} = -m_o g \bar{b}_3$ as given in (6-11), which gives the following set of equations

$$\begin{aligned} 0 &= \sum_{i=1}^{3} \tilde{p}_i^o R_o^T \left(k_p \bar{\rho}_i \left(\|\rho_i\| - l_{i,des}\right) + \bar{\rho}_i \lambda_{\text{des},i}\right) \\ 0 &= \sum_{i=1}^{3} \left(k_p \bar{\rho}_i \left(\|\rho_i\| - l_{i,des}\right) + \left(\bar{\rho}_i - \bar{\rho}_{\text{des},i}\right) \lambda_{\text{des},i}\right) \\ 0 &= -k\mathbb{P}_a \left\{R_{l,\text{des}}^T R_l\right\}^V - \sum_{i=1}^{3} \tilde{p}_i^l R_l^T \left(k_p \bar{\rho}_i \left(\|\rho_i\| - l_{i,des}\right) + \left(\bar{\rho}_i - \bar{\rho}_{\text{des},i}\right) \lambda_{\text{des},i}\right) \\ 0 &= -K_r \left(r_l - r_{l,des}\right) - \sum_{i=1}^{3} \left(k_p \bar{\rho}_i \left(\|\rho_i\| - l_{i,des}\right) + \left(\bar{\rho}_i - \bar{\rho}_{\text{des},i}\right) \lambda_{\text{des},i}\right) \end{aligned} \tag{B-94}$$

From the second and last of the above equations it can be concluded that $r_l \to r_{l,\text{des}}$. Application of Assumption 6-3.1, i.e. substitution of the solution of the IKP sets all above equations to zero: The first equation is set to zero since $\sum_{i=1}^{3} \tilde{p}_i^o R_{o,\text{des}}^T \rho_{i,\text{des}} \lambda i, \text{des} = 0$. The second equation is trivially set to zero for $\rho_i = \rho_{i,\text{des}}$. The third equation is set to zero since the solution to the IKP sets $R_l = R_{l,\text{des}}$. This shows that the desired equilibrium as computed from the IKP is a valid equilibrium for the system, and it is for simplicity assumed to be the unique equilibrium. This completes the proof of Proposition 6-3.1.

B-4-2 Proof of Proposition 6-3.1 When Using MRPs

The control law given in Proposition 6-3.1 assumed a geometric control law for the leader torque. If instead MRPss are to be used, then the leader torque given in (6-16) can be taken as

$$\tau_l = -k\Xi\left(\sigma_l\right)^T \left(\sigma_l - \sigma_{l,des}\right) - \zeta\Omega_l + \sum_{i=1}^{3} \left[\tilde{p}_i^l R_l^T \bar{\rho}_{\text{des},i} \lambda_{\text{des},i}\right] \tag{B-95}$$

where σ_l denotes the leader body MRPss and $\Xi\left(\sigma_l\right)$ is given in (A-28). The tracking error potential term V_e in equation (B-78) is then given as

$$V_e = \sum_{i=1}^{3} \left[\frac{k_p}{2} \left(\|\rho_i\| - l_{i,des}\right)^2\right] + \frac{1}{2} e_{r,l}^T K e_{r,l} + \frac{k}{2} e_{\sigma,l}^T e_{\sigma,l} \tag{B-96}$$

where $e_{r,l} = r_l - r_{l,des}$ and $e_{\sigma,l} = \sigma_l - \sigma_{l,des}$ are the leader attitude and position tracking errors, $r_{l,\text{des}}$ is the leader reference position as given in (6-11) and $\sigma_{l,\text{des}}$ is the leader reference attitude. The reference attitude for the leader was found from solving the IKP, resulting in a desired yaw angle ψ_{des}, from which the desired MRPs can be found using (A-25) as

$$\sigma_{l,\text{des}} = \tan\left(\frac{\psi_{\text{des}}}{4}\right) \begin{bmatrix} 0 & 0 & 1 \end{bmatrix}^T \tag{B-97}$$

Taking the time derivative of V_e gives

$$\dot{V}_e = \sum_{i=1}^{3} \left[k_p \dot{\rho}_i^T \bar{\rho}_i \left(\|\rho_i\| - l_{i,des}\right)\right] + v_l^T K e_{r,l} + k\Omega_l^T \Xi\left(\sigma_l\right)^T e_{\sigma,l} \tag{B-98}$$

where it was used that $\frac{d}{dt}\|\rho_i\| = \dot{\rho}_i^T \bar{\rho}_i$ and $\dot{\sigma}_l = \Xi\left(\sigma_l\right)\Omega_l$ with $\Xi\left(\sigma_l\right)$ given in (A-28). Substitution of the above expression into (B-90) clearly results in (B-91) if the torque is taken as (B-95).

Appendix C

Numerical Values used for Simulation

This appendix gives an overview of how the simulation results where obtained. The system parameters where taken the same for all simulations. In C-1 a short description of the simulation setting is presented. In C-2 a detailed listing of the payload properties and initial conditions is given. The model used for simulating the Aerial Towing Problem (ATP) is described in C-3.

C-1 Short Description of the Simulation

The payload is modeled as a thin solid disc with radius 1.59 [m] and mass 10.0 [kg]. The Center of Gravity (CoG) of the payload is placed 0.1 [m] out of the center. The positions of the agent attachment points are placed on the edge of the payload with equal spacing. The payload is given a small initial angular and linear velocity, and the initial configuration is chosen at the origin.

The system is simulated using $n_f = 10$ follower agents, and with the exception of Chapters 5 and 6, a single leader controls a wrench at the payload CoG. The control gains were designed for the centralized case where the leader controls the payload alone, i.e. without any follower agents participating. This situation serves as the benchmark for evaluating the proposed consensus law. The control gains were obtained using Linear Quadratic (LQ)-optimal pole placement for the linearized system. For the Cooperative Manipulation Problem (CMP) the individual control gains of the agents were then obtained by dividing these centralized gains by the total number of agents. The agent observer gains were chosen such that the consensus dynamics is approximately a decade faster than the tracking dynamics.

To show that the system can recover from large initial rotation errors the agent's initial estimates of the desired payload rotation range from $-180\,\text{deg}$ to $+180\,\text{deg}$ with equal spacing. The axis of rotation is generated randomly using a standard normal distribution. The effect is that initially the agent's estimates of the desired attitude are scattered across a

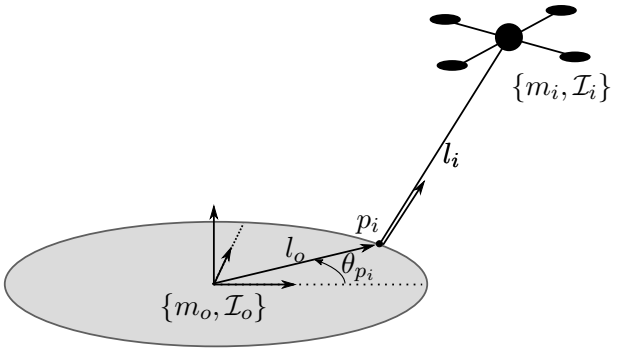

Figure C-1: Geometry of the payload with the variables given in Table C-1.

sphere. All remaining estimation variables are generated randomly.

The step response of the system is simulated by changing the desired configuration of the leader. The leader initially keeps the desired configuration at the origin such that the system stabilizes. After 4 seconds the desired attitude is changed to an angle of $\theta_{\text{des}} = 60\,\text{deg}$ about an axis given as $\epsilon_{\text{des}} = \begin{bmatrix} 3 & 2 & 1 \end{bmatrix}^T$. The corresponding Modified Rodrigues Parameters (MRPs) are given as $\sigma_{\text{des}} = \begin{bmatrix} 0.21 & 0.14 & 0.07 \end{bmatrix}^T$. The desired position changes simultaneously to $r_{\text{des}} = \begin{bmatrix} 3 & 2 & 1 \end{bmatrix}^T$ meters.

C-2 Numerical Values Used in Simulation

Payload Properties The payload properties and their numerical values are given in Table C-1, and are illustrated in Figure C-1. The Unmanned Aerial Vehicles (UAV) properties are relevant to Chapters 5 and 6. Considering Figure C-1 the attachment points of the cables were taken to lie on a circle with equal interspacing, and an offset of $b = [0.1 \quad 0 \quad 0]^T$ from the payload CoG,

$$p_i = \begin{bmatrix} l_o \cos(\theta_{p_i}) & l_o \sin(\theta_{p_i}) & 0 \end{bmatrix}^T + b, \qquad \theta_{p_i} = \tfrac{2\pi}{n_f+1} \times i, \qquad i \in \{1, \ldots, n_f\} \tag{C-1}$$

Payload Initial Conditions The payload initial configuration is chosen at the origin. The initial angular velocity was taken as $\Omega_o(0) = [0.3 \quad 0.2 \quad 0.1]^T$ [rad/s], and the initial linear velocity as $v_o(0) = [0.3 \quad 0.2 \quad 0.1]^T$ [m/s].

C-2-1 Selection of the Control Gains for the Payload Tracking Dynamics

The control gains for the payload tracking error were obtained via LQ-optimal pole placement using the linearized system. All entries on the diagonal of the matrix gains were chosen to be equal. The control gains were designed for the leader controlling the payload alone, such that

Table C-1: Numerical parameters used in simulation. The corresponding variables are illustrated in Figure C-1.

	Symbol	Value	Units
Payload mass	m_o	10.0	kg
Payload radius	l_o	1.59	m
Payload Inertia	$\mathcal{I}_{xx}$	6.333	kgm^2
	$\mathcal{I}_{yy}$	6.333	
	$\mathcal{I}_{zz}$	12.665	
UAV mass	m_i	1.0	kg
UAV Inertia	$\mathcal{I}_{xx}$	0.062	kgm^2
	$\mathcal{I}_{yy}$	0.062	
	$\mathcal{I}_{zz}$	0.125	
Cable length	l_i	1.0	m

Table C-2: Table with the control gains for the payload tracking dynamics: In case of matrix gains the listed value was taken on all diagonal entries.

Description	symbol	value
Configuration tracking	K_{sum}, k_{sum}	2.53
Velocity damping	ζ_{sum}, β_{sum}	3.16

a desired performance was achieved. These values are given by K_{sum} and ζ_{sum} in Table C-2. For MRPs the tracking gain k_σ must be multiplied by a factor of 16, due to the linearization.

With the addition of the follower agents the control effort was evenly distributed over the agents, e.g. if the centralized design gave K_{sum} this gives the i^{th}-agent's control gain as $K_i = K_{\text{sum}}/n$, where n is the total number of agents. The leaders' gain was taken equal to that of the followers, $K_l = K_i = K_{\text{sum}}/n$.

C-3 Simulation Model of the Payload Towed by UAV

This section describes the construction of the model used to simulate the ATP, where the UAV are connected to the payload via cables. It is here chosen to use a constrained representation, where the system is modeled as multiple unconstrained bodies, and the constraints are added via Lagrange multipliers. For the interested reader, the constraint free model is derived in [15]. The aim is to obtain a set of ordinary differential equations that can be numerically integrated to obtain the system motion.

Unconstrained Equations of Motion Consider the payload and UAV as depicted in Figure 5-2 and Figure 5-3. The unconstrained equations of motion consist of the rigid body motion of the payload, and the point mass dynamics of the n_f-UAV. This gives autonomous unconstrained motion as,

$$\mathcal{M}\dot{\mathcal{X}} = \mathcal{F} \tag{C-2}$$

where $\mathcal{M}$, $\mathcal{X}$ and $\mathcal{F}$ are defined as

$$\mathcal{M} = \begin{bmatrix} \mathcal{I}_o & 0 & \dots & & & & & \dots & 0 \\ 0 & m_o I & & & & & & & \vdots \\ \vdots & & m_1 I & & & & & & \\ & & & \ddots & & & & & \\ & & & & m_{n_f} I & & & & \\ & & & & & I & & & \\ & & & & & & I & & \\ & & & & & & & I & \vdots \\ \vdots & & & & & & & \ddots & 0 \\ 0 & \dots & & & & & \dots & 0 & I \end{bmatrix}, \quad \mathcal{X} = \begin{bmatrix} \Omega_o \\ v_o \\ v_1 \\ \vdots \\ v_{n_f} \\ \sigma_o \\ r_o \\ r_1 \\ \vdots \\ r_{n_f} \end{bmatrix}, \quad \mathcal{F} = \begin{bmatrix} -\tilde{\Omega}_o \mathcal{I}_o \Omega_o \\ m_o g \bar{b}_3 \\ m_1 g \bar{b}_3 \\ \vdots \\ m_{n_f} g \bar{b}_3 \\ \Xi(\sigma_o)\, \Omega_o \\ v_o \\ v_1 \\ \vdots \\ v_{n_f} \end{bmatrix} \tag{C-3}$$

where $I = I_{3\times 3}$ and the zeros are of appropriate dimension.

Addition of the Cable Constraints The UAV are connected to the payload via the cables, for the geometry see 5-2. This gives the constraint connecting the i^{th}-UAV to the payload as,

$$\mathcal{D}_i = \tfrac{1}{2} \left\| r_o + R_o p_i - r_i \right\|^2 - \tfrac{1}{2} l_i^2 = 0 \tag{C-4}$$

The jacobian of the above constraint to the state $\mathcal{X}$ is given as,

$$\mathcal{J}_i(\mathcal{X}) = (r_o + R_o p_i - r_i)^T \begin{bmatrix} -R\tilde{p}_i & I & 0 & \dots & 0 & -I & 0 & \dots & 0 \end{bmatrix} \tag{C-5}$$

where the left-most identity matrix above selects the velocity v_i of the i^{th}-UAV. The time derivative of the jacobian is given as,

$$\begin{aligned} \dot{\mathcal{J}}_i(\mathcal{X}) = {} & (v_o - R_o \tilde{p}_i \Omega_o - v_i)^T \begin{bmatrix} -R\tilde{p}_i & I & 0 & \dots & 0 & -I & 0 & \dots & 0 \end{bmatrix} \\ & + (r_o + R_o p_i - r_i)^T \begin{bmatrix} -R\tilde{\Omega}_o \tilde{p}_i & 0 & 0 & \dots & 0 & 0 & 0 & 0 & 0 \end{bmatrix} \end{aligned} \tag{C-6}$$

The acceleration of the constraints can then be represented as,

$$\ddot{\mathcal{D}} = \mathcal{J}(\mathcal{X})\, \dot{\mathcal{X}} + \dot{\mathcal{J}}(\mathcal{X})\, \mathcal{X} = 0 \tag{C-7}$$

Constrained Equations of Motion The constraints are added to the unconstrained equations of motion using Lagrange multipliers. Adding the constraints to the equations of motion gives,

$$\begin{bmatrix} \mathcal{M} & \mathcal{J}(\mathcal{X})^T \\ \mathcal{J}(\mathcal{X}) & 0 \end{bmatrix} \begin{bmatrix} \dot{\mathcal{X}} \\ \lambda \end{bmatrix} = \begin{bmatrix} \mathcal{F}(\mathcal{X}) \\ -\dot{\mathcal{J}}(\mathcal{X})\, \mathcal{X} \end{bmatrix} + \begin{bmatrix} \mathcal{U}_{\text{ext}} \\ 0 \end{bmatrix} \tag{C-8}$$

where the Lagrangian multipliers λ_i will equal the tension forces in the cable, and the vector $\mathcal{U}_{\text{ext}}$ allows for external forces and torque to be applied to the system.

Numerical Integration For the numerical integration of (C-8) consider bypassing the computation of λ by computing the inverse of the left hand matrix as,

$$\begin{bmatrix} \mathcal{A}_{11} & \mathcal{A}_{12} \\ \mathcal{A}_{21} & \mathcal{A}_{22} \end{bmatrix} \begin{bmatrix} \mathcal{M} & \mathcal{J}^T \\ \mathcal{J} & 0 \end{bmatrix} = \begin{bmatrix} I & 0 \\ 0 & I \end{bmatrix} \tag{C-9}$$

where the dependency on $\mathcal{X}$ is omitted for ease of exposition. Solving the above for $\mathcal{A}$ gives

$$\begin{aligned} \mathcal{A}_{11} &= \mathcal{M}^{-1} - \mathcal{M}^{-1}\mathcal{J}^T \left(\mathcal{J}\mathcal{M}^{-1}\mathcal{J}^T\right)^{-1} \mathcal{J}\mathcal{M}^{-1}, & \mathcal{A}_{12} &= \mathcal{M}^{-1}\mathcal{J}^T \left(\mathcal{J}\mathcal{M}^{-1}\mathcal{J}^T\right)^{-1} \\ \mathcal{A}_{21} &= \left(\mathcal{J}\mathcal{M}^{-1}\mathcal{J}^T\right)^{-1} \mathcal{J}\mathcal{M}^{-1}, & \mathcal{A}_{22} &= -\left(\mathcal{J}\mathcal{M}^{-1}\mathcal{J}^T\right)^{-1} \end{aligned} \tag{C-10}$$

The motion of the aerial towing system is then described by the following ordinary differential equations,

$$\dot{\mathcal{X}} = \mathcal{A}_{11}\left(\mathcal{F} + \mathcal{U}_{\text{ext}}\right) - \mathcal{A}_{12}\dot{\mathcal{J}}\mathcal{X} \tag{C-11}$$

Equation (C-11) is integrated numerically using the Runge and Kutta 4 scheme.

Coordinate Projection The numerical integration is not perfect and will result in the buildup of integration errors. This will cause the bodies to drift away from one another. To prevent this the system state is projected back to the constrained surface after each integration step. Using linear least squares the point on the surface that is closest to the current state can be found. Since the constraints are nonlinear this linear projection is iterated until the error is sufficiently small. For the velocities the problem is linear, and thus a single linear least squares step suffices.

Appendix D

Additional Simulation Results

This appendix shows additional simulation results. These results were found to be comparable to the results already presented, but are added for completeness. In D-3 the translation dynamics for the underactuated geometric appraoch is shown. These results are comparable to those discussed in Section 2-4. In D-1 and D-2 the simulation results for the Nonlinear Dynamic Inversion (NDI) based approach in Proposition 4-3.1 are shown. Again, these results are similar to those discussed in Section 4-5, and the same conclusion follows.

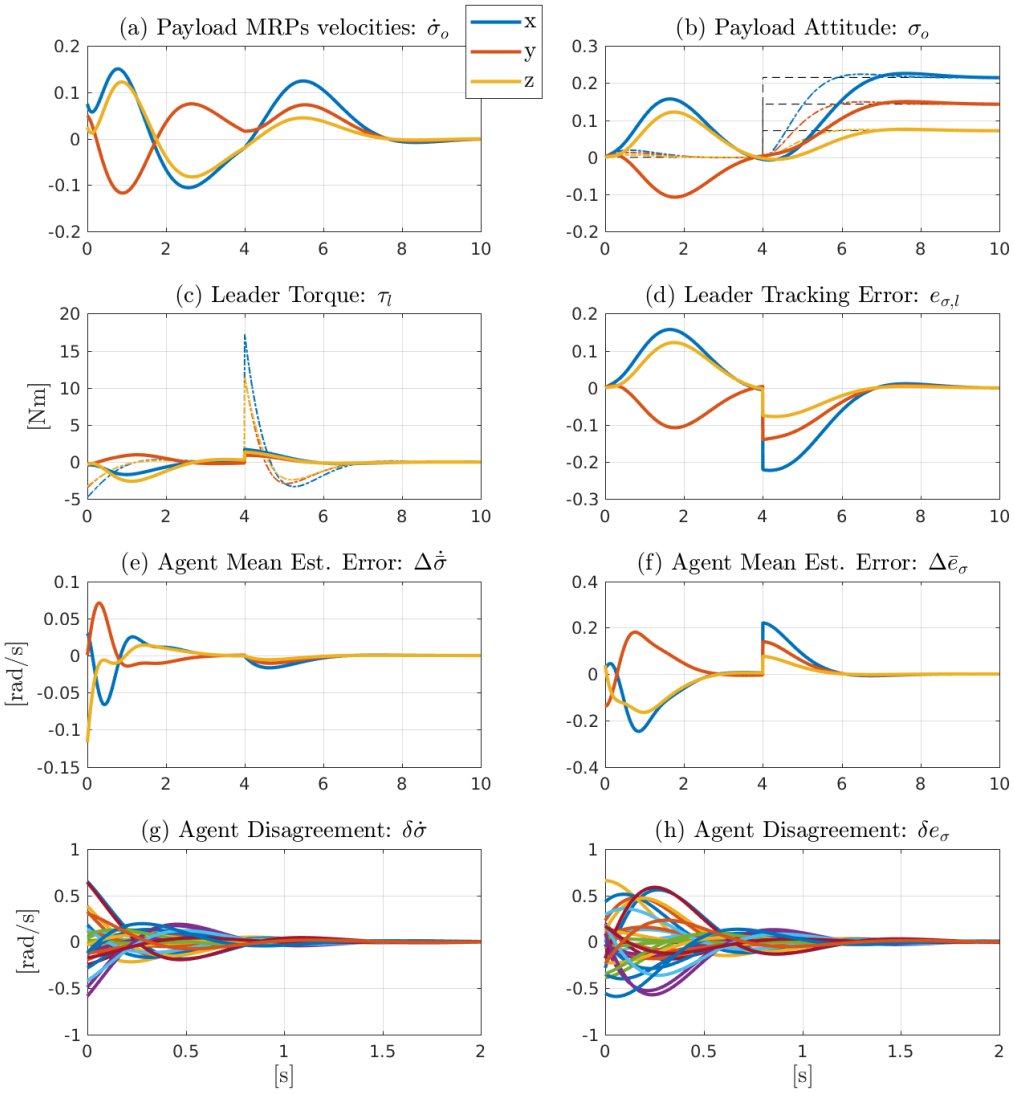

Figure D-1: Simulation results of the attitude dynamics for the under actuated CMP with NDI (Proposition 4-3.1): From left to right and top to bottom the plots show, (a) the payload MRPs velocity, (b) the payload MRPs, (c) the torque applied by the leader, (d) the leader tracking error, (e) and (f) the mean of the agent's estimation errors regarding the angular velocity and the tracking error, and (g) and (h) the disagreement of the agent's estimation errors. The three colors, blue red and yellow, represent the x, y and z directions of the corresponding three dimensional vectors. The black dashed line in the attitude plot shows the leader reference MRPs. The leader applies a reference step to the desired payload attitude at $t = 4$[s], corresponding to a $\theta = 60\,\text{deg}$ rotation about the $\epsilon = [3 \quad 2 \quad 1]^T$ axis. The colored dashed lines in the payload attitude and leader torque plot show the simulation result for the case that the leader is controlling the payload alone.

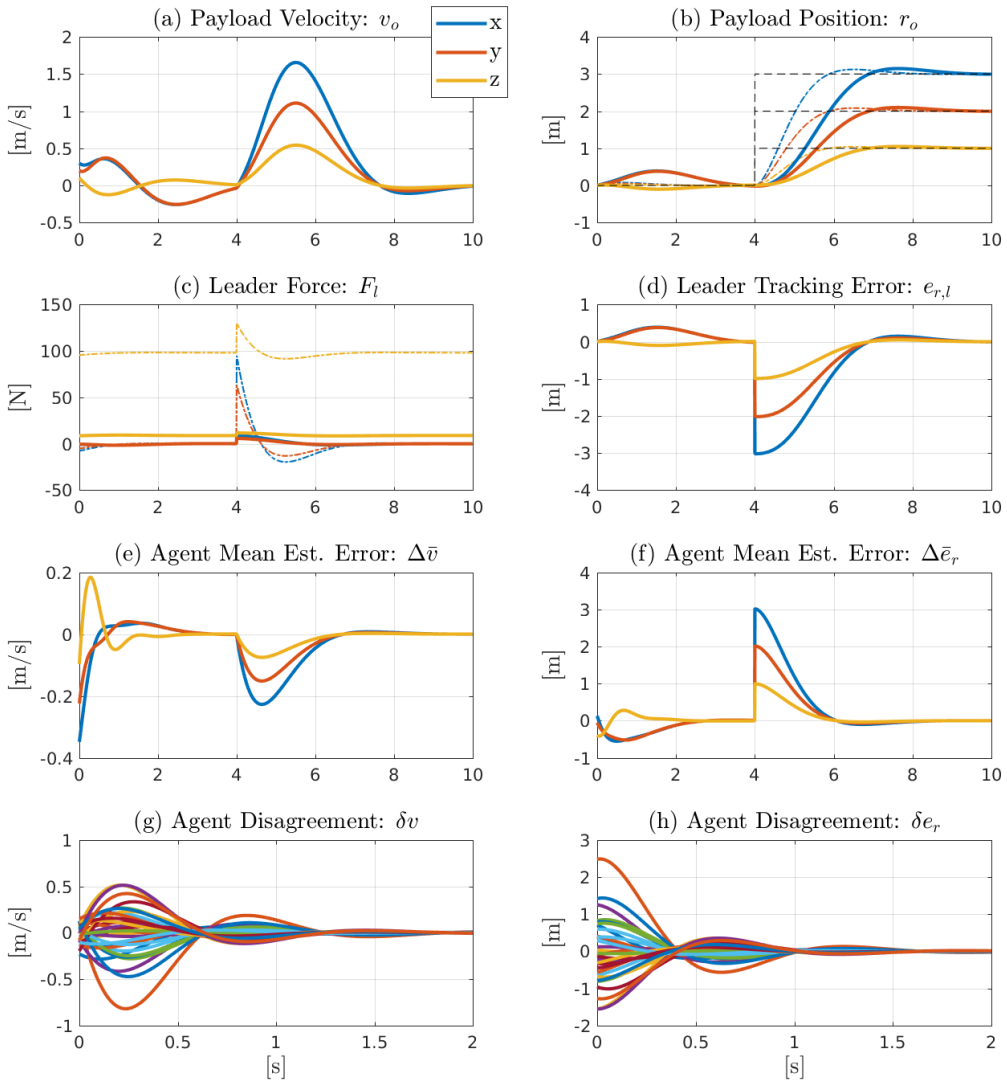

Figure D-2: Simulation results of the translation dynamics for the under actuated CMP with NDI (Proposition 4-3.1): From left to right and top to bottom the plots show, (a) the payload linear velocity, (b) the payload position, (c) the force applied by the leader, (d) the leader tracking error, (e) and (f) the mean of the agent's estimation errors, and (g) and (h) the disagreement of the agent's estimation errors. The three colors, blue red and yellow, represent the x, y and z directions of the corresponding three dimensional vectors. The black dashed line in the position plot shows the leader's desired position, changing from the origin to $r_{\text{des}} = [3 \quad 2 \quad 1]^T$ at $t = 4$[s]. The colored dashed lines in the position and force plot show the simulation result for the case that the leader is controlling the payload alone.

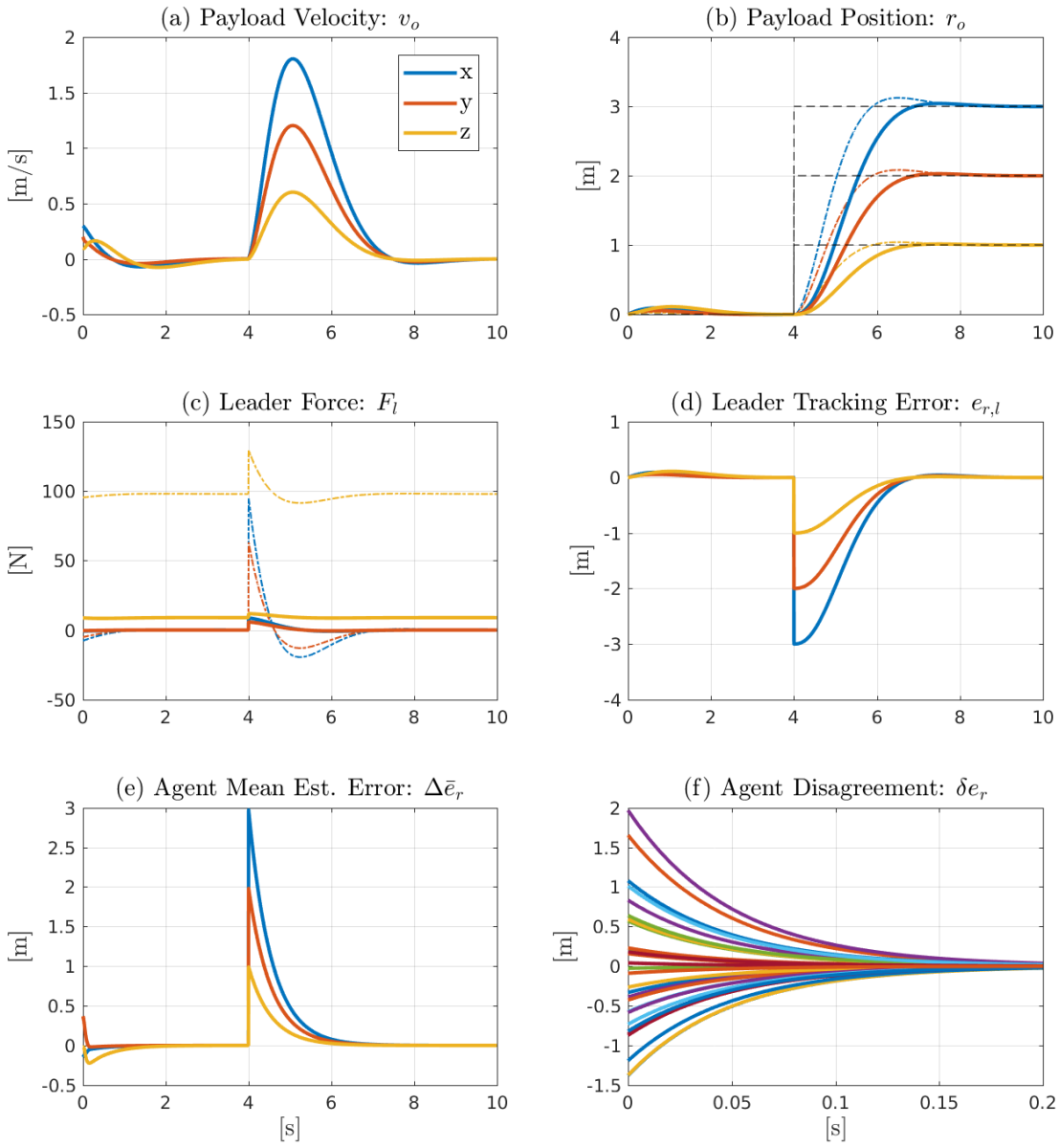

Figure D-3: Simulation results of the translation dynamics for the underactuated CMP using the geometric control law (Proposition 3-4.1): From left to right and top to bottom the plots show, (a) the payload linear velocity, (b) the payload position, (c) the force applied by the leader, (d) the leader tracking error, (e) the mean of the agent's estimation errors, and (f) the disagreement of the agent's estimation errors. The three colors, blue red and yellow, represent the x, y and z directions of the corresponding three dimensional vectors. The black dashed line in the position plot shows the leader's desired position, changing from the origin to $r_{\text{des}} = [3 \quad 2 \quad 1]^T$ at $t = 4$[s]. The colored dashed lines in the position and force plot show the simulation result for the case that the leader is controlling the payload alone.

Bibliography

[1] D. Mellinger, M. Shomin, N. Michael, and V. Kumar, "Cooperative grasping and transport using multiple quadrotors," in *Springer Tracts in Advanced Robotics*, vol. 83 STAR, pp. 545–558, 2012.

[2] Z. Wang and M. Schwager, "Multi-robot manipulation without communication," in *Springer Tracts in Advanced Robotics*, vol. 112, pp. 135–149, 2016.

[3] S. Berman, Q. Lindsey, M. Sakar, V. Kumar, and S. Pratt, "Study of group food retrieval by ants as a model for multi-robot collective transport strategies," in *International Conference on Robotics Science and Systems*, pp. 259–266, 2011.

[4] V. Kumar and N. Michael, "Opportunities and challenges with autonomous micro aerial vehicles," *The International Journal of Robotics Research*, vol. 31, no. 11, pp. 1279–1291, 2012.

[5] T. Lee, M. Leok, and N. H. Mcclamroch, "Geometric Tracking Control of a Quadrotor UAV on SE (3)," *49th IEEE Conference on Decision and Control*, no. 3, pp. 5420–5425, 2010.

[6] K. Sreenath, T. Lee, and V. Kumar, "Geometric control and differential flatness of a quadrotor UAV with a cable-suspended load," in *Proceedings of the IEEE Conference on Decision and Control*, pp. 2269–2274, 2013.

[7] N. Michael, J. Fink, and V. Kumar, "Cooperative manipulation and transportation with aerial robots," *Autonomous Robots*, no. September 2010, pp. 1–14, 2010.

[8] G. Wu and K. Sreenath, "Geometric control of multiple quadrotors transporting a rigid-body load," in *Proceedings of the IEEE Conference on Decision and Control*, vol. 2015, pp. 6141–6148, 2014.

[9] H. Lee, H. Kim, and H. J. Kim, "Path planning and control of multiple aerial manipulators for a cooperative transportation," in *IEEE International Conference on Intelligent Robots and Systems*, vol. 2015-Decem, pp. 2386–2391, 2015.

[10] C. Meissen, K. Klausen, M. Arcak, T. I. Fossen, and A. Packard, "Passivity-based Formation Control for UAVs with a Suspended Load," in *The International Federation of Automatic Control*, 2017.

[11] Z. Wang and M. Schwager, "Force-Amplifying N-robot Transport System (Force-ANTS) for cooperative planar manipulation without communication," *The International Journal of Robotics Research*, vol. 35, no. 13, pp. 1564–1586, 2016.

[12] Z. Wang and M. Schwager, "Force-Amplifying N-robot Transport System (Force-ANTS) for cooperative planar manipulation without communication," *The International Journal of Robotics Research*, vol. 35, no. 13, pp. 1564–1586, 2016.

[13] H. Bai, M. Arcak, and J. Wen, *Cooperative Control Design, A Systematic Passivity-Based Approach.* Springer-Verlag New York Inc., 2011.

[14] K. Sreenath and V. Kumar, "Dynamics, Control and Planning for Cooperative Manipulation of Payloads Suspended by Cables from Multiple Quadrotor Robots," in *Robotics: Science and Systems IX*, 2013.

[15] F. A. Goodarzi and L. Taeyoung, "Stabilization of a Rigid Body Payload With Multiple Cooperative Quadrotors," *Journal of Dynamic Systems, Measurement, and Control*, vol. 138, no. 12, pp. 121001–12018, 2016.

[16] R. Mahony, V. Kumar, and P. Corke, "Multirotor Aerial Vehicles: Modeling, Estimation, and Control of Quadrotor," *IEEE Robotics & Automation Magazine*, vol. 19, no. 3, pp. 20–32, 2012.

[17] Z. Wang and M. Schwager, "Kinematic multi-robot manipulation with no communication using force feedback," in *Proceedings - IEEE International Conference on Robotics and Automation*, vol. 2016-June, pp. 427–432, 2016.

[18] D. V. Dimarogonas, P. Tsiotras, and K. J. Kyriakopoulos, "Leader-follower cooperative attitude control of multiple rigid bodies," *Systems and Control Letters*, vol. 58, no. 6, pp. 429–435, 2009.

[19] Z. Meng, W. Ren, and Z. You, "Decentralised cooperative attitude tracking using modified Rodriguez parameters based on relative attitude information," *International Journal of Control*, vol. 83, no. 12, pp. 2427–2439, 2010.

[20] M. D. Shuster, "A Survey of attitude representations," *The Journal of the Astronautical Sciences*, vol. 1, no. 4, pp. 439–517, 1993.

[21] P. Tsiotras, "Stabilization and optimality results for the attitude control problem," *Journal of Guidance, Control, and Dynamics*, vol. 19, no. 4, pp. 772–779, 1996.

[22] J. M. Esposito, "Decentralized cooperative manipulation with a swarm of mobile robots," in *2009 IEEE/RSJ International Conference on Intelligent Robots and Systems, IROS 2009*, pp. 5333–5338, 2009.

[23] S. A. Vakhrameev and A. V. Sarychev, "Geometric control theory," *Journal of Soviet Mathematics*, vol. 40, no. 3, pp. 384–447, 1988.

[24] R. M. Murray, Z. Li, and S. S. Sastry, *A Mathematical Introduction to Robotic Manipulation*, vol. 29. CRC Press, 1994, 1994.

[25] W. Ren, "Distributed cooperative attitude synchronization and tracking for multiple rigid bodies," *IEEE Transactions on Control Systems Technology*, vol. 18, no. 2, pp. 383–392, 2010.

[26] Z. Meng, Z. You, G. Li, and C. Fan, "Cooperative attitude control of multiple rigid bodies with multiple time-varying delays and dynamically changing topologies," *Mathematical Problems in Engineering*, vol. 2010, 2010.

[27] W. Ren, "Distributed attitude alignment in spacecraft formation flying," *International Journal of Adaptive Control and Signal Processing*, vol. 21, no. 2-3, pp. 95–113, 2007.

[28] W. Ren, "Synchronized multiple spacecraft rotations: A revisit in the context of consensus building," in *Proceedings of the American Control Conference*, pp. 3174–3179, 2007.

[29] W. Ren, *Distributed Consensus in Multivehicle Cooperative Control: Theory and Applications*. Springer, 2008.

[30] Y. Igarashi, T. Hatanaka, M. Fujita, and M. W. Spong, "Passivity-based attitude synchronization in SE(3)," *IEEE Transactions on Control Systems Technology*, vol. 17, no. 5, pp. 1119–1134, 2009.

[31] T. Hatanaka, Y. Igarashi, M. Fujita, and M. W. Spong, "Passivity-based pose synchronization in three dimensions," *IEEE Transactions on Automatic Control*, vol. 57, no. 2, pp. 360–375, 2012.

[32] T. Ibuki, T. Hatanaka, and M. Fujita, "Passivity-based pose synchronization using only relative pose information under general digraphs," in *Proceedings of the IEEE Conference on Decision and Control*, pp. 4709–4714, 2012.

[33] T. Ibuki, T. Hatanaka, and M. Fujita, "Passivity-based visual pose regulation for a moving target object in three dimensions: Structure design and convergence analysis," in *Proceedings of the IEEE Conference on Decision and Control*, pp. 5655–5660, 2012.

[34] T. Hatanaka, N. Chopra, M. Fujita, and M. W. Spong, *Passivity-Based Control and Estimation in Networked Robotics*. Springer International Publishing, 2015.

[35] R. Mahony, T. Hamel, and J. M. Pflimlin, "Nonlinear complementary filters on the special orthogonal group," *IEEE Transactions on Automatic Control*, vol. 53, no. 5, pp. 1203–1218, 2008.

[36] M. Euston, P. Coote, R. Mahony, J. Kim, and T. Hamel, "A complementary filter for attitude estimation of a fixed-wing UAV," in *2008 IEEE/RSJ International Conference on Intelligent Robots and Systems, IROS*, pp. 340–345, 2008.

[37] J. L. Crassidis, F. L. Markley, and Y. Cheng, "Survey of Nonlinear Attitude Estimation Methods," *Journal of Guidance, Control, and Dynamics*, vol. 30, no. 1, pp. 12–28, 2007.

[38] R. Saeks and J. Murray, "Fractional Representation, Algebraic Geometry, and the Simultaneous Stabilization Problem," *IEEE Transactions on Automatic Control*, vol. 27, no. 4, pp. 895–903, 1982.

[39] C. Abdallah, R. Luke, and P. Dorato, "A Survey Of State-Feedback Simultaneous Stabilization Techniques," pp. 1–8, 2012.

[40] G. D. Howitt and R. Luus, "Simultaneous stabilization of linear single-input systems by linear state feedback control," *Internat. J. Control*, vol. 54, no. 4, pp. 1015–1030, 1991.

[41] F. Saadatjoo, V. Derhami, and S. M. Karbassi, "Simultaneous control of linear systems by state feedback," *Computers and Mathematics with Applications*, vol. 58, no. 1, pp. 154–160, 2009.

[42] R. A. Luke, P. Dorato, and C. T. Abdallah, "Linear-quadratic simultaneous performance design," *Proc. American Control Conf.*, no. June, pp. 3602–3605, 1997.

[43] Q. Jiang and V. Kumar, "The inverse kinematics of cooperative transport with multiple aerial robots," *IEEE Transactions on Robotics*, vol. 29, no. 1, pp. 136–145, 2013.

[44] T. Lee, "Geometric control of multiple quadrotor UAVs transporting a cable-suspended rigid body," *Proceedings of the IEEE Conference on Decision and Control*, vol. 2015-Febru, no. February, pp. 6155–6160, 2014.

[45] T. Lee, "Geometric control of multiple quadrotor UAVs transporting a cable-suspended rigid body," in *Proceedings of the IEEE Conference on Decision and Control*, vol. 2015-Febru, pp. 6155–6160, 2014.

[46] T. Lee, M. Leok, and N. H. McClamroch, "Lagrangian and hamiltonian dynamics on manifolds," in *Interaction of Mechanics and Mathematics*, no. 9783319569512, pp. 347–398, Springer Verlag, 2018.

[47] R. Mahony, T. Hamel, P. Morin, and E. Malis, "Nonlinear complementary filters on the special linear group," *International Journal of Control*, vol. 85, no. 10, pp. 1557–1573, 2012.

[48] C. K. Verginis, M. Mastellaro, and D. V. Dimarogonas, "Robust Cooperative Manipulation without Force/Torque Measurements: Control Design and Experiments," in *Conference on Robotics and Automation (ICRA)*, pp. 4086–4091, 2003.

[49] H. Schaub and J. L. Junkins, "Stereographic orientation parameters for attitude dynamics: a generalization of the Rodrigues parameters," *J. Astronaut. Sci.*, vol. 44, no. 1, pp. 1–19, 1996.

[50] S. A. O'Keefe and H. Schaub, "Shadow set considerations for modified rodrigues parameter attitude filtering," *Advances in the Astronautical Sciences*, vol. 150, no. 6, pp. 2777–2786, 2014.

[51] H. Schaub and J. L. Junkins, *Analytical Mechanis of Aerospace Systems*. Reston ,VA: American Institute of Aeronautics and Astronautics, second edi ed., 2002.

[52] S. Erhart, D. Sieber, and S. Hirche, "An impedance-based control architecture for multi-robot cooperative dual-arm mobile manipulation," in *IEEE International Conference on Intelligent Robots and Systems*, pp. 315–322, 2013.

[53] C. Ott, R. Mukherjee, and Y. Nakamura, "Unified impedance and admittance control," in *Proceedings - IEEE International Conference on Robotics and Automation*, pp. 554–561, 2010.

[54] E. J. Smeur, Q. P. Chu, and G. C. de Croon, "Adaptive Incremental Nonlinear Dynamic Inversion for Attitude Control of Micro Aerial Vehicles," *AIAA Guidance, Navigation, and Control Conference*, no. January, pp. 1–16, 2016.

[55] M. Mesbahi and M. Egerstedt, *Graph theoretic methods in multiagent networks*. Princeton University Press, 2010.

[56] H. Schaub and J. L. Junkins, "Analytical mechanics of space systems," *AIAA Education Series*, 2003.

Glossary

List of Acronyms

CoG	Center of Gravity
CMP	Cooperative Manipulation Problem
ATP	Aerial Towing Problem
UAV	Unmanned Aerial Vehicles
Force-ANTS	Force-Amplifying N-robot Transport System
PBC	Passivity Based Control
MRPs	Modified Rodrigues Parameters
CRPs	Classical Rodrigues Parameters
NDI	Nonlinear Dynamic Inversion
LQ	Linear Quadratic
IKP	Inverse Kinematics Problem
DKP	Direct Kinematics Problem
IMU	Inertial Measurement Unit
LF	Leader-Follower
PD	Proportional Derivative